

**THE MORPHODYNAMICS OF SEDIMENT MOVEMENT
THROUGH A RESERVOIR DURING DAM REMOVAL**

John Christopher Bromley, BSc., MSc.

**Thesis submitted to the University of Nottingham
for the degree of Doctor of Philosophy**

September 2007

Abstract

Dam removal has recently emerged as a growing trend in river rehabilitation in the United States. The rate of dam removal has been increasing rapidly since 2000, but is doing so with large gaps in our understanding of how the fluvial system will respond to this disturbance. Most of the structures removed to date have been relatively small and, in the vast majority of cases, have not received any pre- or post-removal monitoring. Very few large structures have been removed but, when such removals occur or are proposed, they tend to attract more monitoring activity because of the generally larger volumes of water and sediment involved. It is thus important to understand the form-process-response interactions that occur during the removal of large dams and the extent to which these may be applicable to other removals of varying sizes.

The proposed removal of the Glines Canyon Dam from the Elwha River in Washington, USA provides such an opportunity. The 67-m high dam is due to be incrementally removed in 2011 but its reservoir, Lake Mills, contains 80 years-worth of uncontaminated sediment that has the potential to adversely impact the aquatic and human environment once released into the channel downstream from the dam. In order to better understand the dynamics that control how sediment might be transported into the downstream channel, a series of scaled physical model experiments was performed in which the principle variable investigated was the magnitude of the drop in reservoir water surface elevation.

Four main findings emerged from the research. First, the hypothesised relationship between increasing magnitudes of baselevel drop and increasing delta erosion volumes is only weakly developed. Furthermore, the small increases in additional erosion volume for very large increases in magnitude of drop suggest that there may be an upper limit beyond which the volume of sediment eroded does not increase substantially, irrespective of the magnitude of drop. The reasons for this are explored.

Second, the volume of delta sediment eroded was greatly affected by the channel's position on the delta surface at the start of each experimental run. The erosion volumes were greatly modulated when the channel was close to the basin boundary (marginal runs), because the boundary inhibited lateral channel movements

and the formation of meander bends. When the channel ran through the middle of the delta surface (central runs) the erosion volumes were much larger, because meander bends were able to more fully develop and the channel had a greater overall freedom to adjust laterally over the entire delta surface. In contrast, the marginal runs generally incised slightly more along the full length of the delta than the central runs, despite a more extensively developed armour layer.

Related to the channel's starting position, a strong element of topographical steering of the incising channel in the original delta area was observed during the marginal runs. When the channels started close to the left basin boundary (left marginal runs), the left hand curvature of this boundary tended to direct the majority of the flow's erosive power away from the main body of the delta. In contrast, during the right marginal runs, the cross-basin downwards slope from basin right to basin left allowed the incising channel to move downslope and into the main body of the delta, particularly during the post-dam removal flood flows.

Third, the armour layer in the central runs generally extended less far downstream through the original delta area than during the marginal runs and this may be because of a frequently observed mobility reversal in sediment transport, which meant that gravels were more effectively flushed out of the original delta area than during the marginal runs.

Finally, a phenomenon hitherto unreported in the literature was observed on many occasions over the course of the experimental runs. Bed Elevation Lowering Without Armour Layer Break-up (BELWALB) occurred when the finer sub-armour sediment was eroded, thus undermining the armour layer and allowing the coarser grains to roll forward by a distance equivalent to a few grain diameters. This undermining action was able to migrate a certain distance upstream, either at the onset or end point of more extensive armour layer disturbance, thus causing subtle changes to bed morphology which are important in understanding how the system approached thresholds of stability and how it responded once these thresholds were exceeded.

Acknowledgements

I am indebted to a great many people and organizations for the help that they have given to me over the course of my study. To Professor Colin Thorne and Dr. Gordon Grant for giving me the opportunity to undertake a PhD, to work on the topic of dam removal, to live and work in a different country, and for supporting me throughout. To Timothy Randle, who provided endless support, encouragement and many insightful suggestions throughout the course of this study. To the U.S. Forest Service and Colorado State University for jointly funding the first phase of the research. Subsequent funding was kindly provided by the U.S. Department of the Interior (Bureau of Reclamation), the National Centre for Earth-surface Dynamics (NCED) through the STC Program of the National Science Foundation under Agreement Number EAR-0120914, and the National Park Service. Funding for the writing of the report came from the US Bureau of Reclamation Science and Technology Program under contract No. 05PG810011.

While in Oregon I was the beneficiary of much good advice and support from Gordon Grant and Gregory Stewart. Greg also provided me with the ArcINFO AML for the cut-fill analysis that has been especially useful throughout the study. Also while in Oregon, someone introduced me to roasted espresso beans covered in dark chocolate. Thank you, whoever you are!

I was privileged to spend over a year at the St. Anthony Falls Laboratory and I wish to thank all the staff and students there for creating such a wonderful working environment. In particular, I would like to thank Dr. Alessandro Cantelli and Professor Gary Parker for advice and encouragement throughout; Brett Otteson for the superb model instrumentation; Dianna K. Smith and Jason Lundheim for taking the lead on model construction; Ben Friesen for help with all manner of tasks; Michal Tal for help in setting up the photographic recording equipment; and Kris Nelson, James Tucker, Benjamin Erickson, Matt Lueker, Jeremy Schultz, Mike Plante and Dick Christopher for help with all manner of construction, sedimentological and hydraulic tasks. In particular, I am very grateful to Corey Markfort who put a huge amount of time and effort into performing model runs 3xC and 21xC, at often ungodly hours, in addition to working on his own Master's research. I am also grateful to Professor Chris Paola and Dr. Omid Mohseni for agreeing to provide the funding for Corey's

time.

Finally, mum and dad, thanks for your unconditional support throughout and sorry for putting you through the agony of wondering if I would ever finish this damn PhD and become gainfully employed. I must offer you the same apology Dianna. And thank you, from the bottom of my heart, for your unyielding patience, support and encouragement. Words will never adequately express my gratitude to you for this.

Contents

Abstract	i
Acknowledgements	iii
Contents	v
List of Figures	ix
List of Tables	xiii
Chapter 1 Introduction	1
1.1 A brief history of dams	1
1.2 Dam removal in the United States	5
1.2.1 Factors driving dam removal in the United States	5
1.3 The impacts of dam construction and dam removal	8
1.3.1 Environmental impacts	8
1.3.1.1 Hydrological impacts	9
1.3.1.2 Geomorphological impacts	10
1.3.1.3 Biological impacts	15
1.3.2 Socio-economical and cultural impacts	19
1.3.2.1 Dam construction	19
1.3.2.2 Dam removal	20
1.4 Unresolved issues in dam removal	21
1.5 Structure and scope of the thesis	24
Chapter 2 The Elwha River System	29
2.1 Physiography of the Elwha River Basin	29
2.2 Human activity in the basin	32
2.2.1 Introduction	32
2.2.2 The Elwha River dams and their effects on the Elwha River System	33
2.2.2.1 Cultural and socio-economical effects	33
2.2.2.2 Geomorphological and hydrological effects	34
2.2.2.3 Biological effects	41
2.3 Objectives of the proposed dam removals	44
2.3.1 Overall project objectives and anticipated benefits	44
2.3.2 Dam removal methodology	48
2.3.3 Issues of concern	48
2.3.3.1 Biological issues	48
2.3.3.2 Physical issues	51
2.3.4 Sediment management and channel restoration objectives	53
2.3.5 Research performed to date	55
Chapter 3 Research Hypotheses	59
3.1 Equilibrium	59
3.2 The nature of the disturbance caused by dam removal	60
3.3 The nature of the response to the disturbance	62
3.3.1 Cross-sectional and longitudinal adjustments	66
3.3.1.1 Vertical adjustments	69
3.3.1.2 Lateral adjustments	71
3.3.1.3 Long profile adjustments	76
3.3.2 Planform adjustments	80
3.3.2.1 Planform definitions and controls	80
3.3.2.2 Meandering channels	82
3.3.2.3 Braided channels	86
3.4 Working hypotheses	90

Chapter 4	Scaled Physical Model Design.....	93
4.1	Introduction to physical modelling	94
4.2	Principles of scaled physical modelling.....	97
4.2.1	Fixed-boundary models	97
4.2.2	Mobile-boundary models.....	101
4.3	Design of the Lake Mills – Glines Canyon Dam model.....	105
4.3.1	Hydraulic equations and prototype calculations	106
4.3.2	Scaling calculations	108
4.3.3	Model sediment.....	112
Chapter 5	Model Construction, Operation and Data Collection	117
5.1	Model construction	117
5.2	Experimental runs	118
5.2.1	Introduction.....	118
5.2.2	Experimental overview	121
5.3	Experimental preparation.....	123
5.3.1	Model calibration	123
5.3.2	Growing the model delta.....	127
5.4	Experimental procedure	130
5.4.1	Baselevel control.....	130
5.4.2	Discharge control	131
5.4.3	Flood flows	132
5.5	Data acquisition	134
5.5.1	Laser profiling and sediment collection at the model’s outlet.....	134
5.5.2	Time lapse photography.....	136
5.5.3	Sediment sampling.....	137
5.5.3.1	Delta growth mixture and sediment coring.....	137
5.5.3.2	Armour and sub-armour sampling.....	137
5.5.4	Particle Tracking Velocimetry	138
Chapter 6	Data Reduction.....	141
6.1	Volumetric analysis	141
6.1.1	Overview of volumetric analysis	141
6.1.2	Assessment of DEM quality and reduction of DEM errors.....	142
6.1.2.1	The quality of individual data points	143
6.1.2.2	The quality of the surface fitted to the data points.....	145
6.1.2.3	The overall quality of the topographic representation	147
6.1.2.4	The quality of the algorithm used to perform the cut-fill calculations 157	
6.1.3	Calculating original delta and full reservoir erosion volumes	158
6.2	Analysis of channel form adjustments.....	161
6.2.1	Measurement of channel form from the time lapse photographs	161
6.2.1.1	Developing algorithms for correcting photographic errors	161
6.2.1.2	Calibrating the photographic measurements.....	162
6.2.1.3	Measurements from Run 1-3 photographs versus measurements from Run 4-9 photographs	164
6.2.2	Planform and longitudinal adjustments	167
6.2.2.1	Thalweg extraction macro.....	167
6.2.2.2	Choice of photographs	168
6.2.2.3	Downstream extent of the armour layer.....	168
6.2.2.4	Channel planform.....	168
6.2.3	Lateral adjustments	169

6.2.3.1	Active channel width	169
6.2.3.2	Top terrace width	169
6.2.3.3	Delta surface width	170
Chapter 7	Analysis and Results	171
7.1	Grain size analysis	171
7.2	Volumetric analysis	173
7.2.1	Erosion of the original delta during dam removal	173
7.2.2	Original delta volumes eroded by flood flows.....	189
7.2.3	Sediment transport through the dam site	191
7.2.4	Summary of volumetric analysis	193
7.3	Delta morphodynamics	195
7.3.1	Right marginal runs.....	198
7.3.2	Left marginal runs.....	200
7.3.3	Central runs.....	207
7.4	Adjustments to channel bed elevations and the longitudinal profile	216
7.5	Cross-sectional adjustments.....	223
7.5.1	Top terrace widths.....	223
7.5.2	Active channel widths.....	223
7.6	Adjustments of channel planform.....	227
7.7	Summary.....	233
Chapter 8	Discussion.....	235
8.1	Experimental limitations and scale effects	235
8.1.1	Experimental limitations.....	235
8.1.2	Scale effects	236
8.2	Volumetric response to baselevel fall.....	239
8.2.1	The role of the magnitude and rate of baselevel drop.....	239
8.2.2	The role of armour layer dynamics.....	245
8.2.2.1	Bed Elevation Lowering Without Armour Layer Break-up (BELWALB).....	245
8.2.2.2	Mobility reversal.....	246
8.2.3	The role of basin geometry and flood flows.....	251
8.3	Implications of the model results for removal of the prototype Glines Canyon Dam	255
Chapter 9	Conclusions.....	259
9.1	Summary of experimental results	259
9.2	Wider implications.....	263
9.3	Further research	264
9.4	Concluding thoughts	265
References	267
Appendix A	A Chronology of Dams.....	285
Appendix B	Arc Macro Language (AML) Script for the Cut-fill Analysis.....	297
Appendix C	Thalweg Extraction Macros.....	309

List of Figures

Figure 1.1. Number of large dams (>15 m high) constructed worldwide during the 20 th century.....	6
Figure 1.2. Dams built and removed from rivers in the United States during the 20 th century.....	6
Figure 2.1. Site location. Modified from United States Geological Survey (2000).	30
Figure 2.2. Study area. Modified from National Park Service (2005).....	31
Figure 2.3. Aerial view of the two Elwha River dams and reservoirs.	35
Figure 2.4. Elwha Dam site.....	36
Figure 2.5. Glines Canyon Dam site.	37
Figure 2.6. Elwha River mouth.....	42
Figure 2.7. Historical spawning ranges of some of the Elwha River basin's anadromous fish species.	45
Figure 2.8. Proposed notch removal scheme for Glines Canyon Dam. Image courtesy of Bureau of Reclamation.	49
Figure 2.9. Proposed expansion of federal levees (National Park Service, 2005).	52
Figure 2.10. Location of main channels and transects during the 1994 drawdown experiment.....	56
Figure 3.1. Energy changes over the Lake Mills delta topset during dam removal.	63
Figure 3.2. Longitudinal patterns of sediment deposition in reservoirs..	63
Figure 3.3. Channel Evolution Models.	68
Figure 3.4. The Lake Mills delta during the April 1994 drawdown experiment.	78
Figure 3.5. Schematic diagram of the timescales of adjustment of various channel form components with given length dimensions in a hypothetical basin of intermediate size.	78
Figure 3.6. Channel planform and stream power.....	81
Figure 3.7. The role of hydraulics in meandering channel formation.	84
Figure 3.8. Increase in the <i>N</i> -row configurations as increasing bed friction effects (increasing width-depth ratios or relative roughness) reduces the maximum size of the horizontal macro-turbulent eddies.	89
Figure 4.1. Different classes of physical model.....	96
Figure 4.2. The Shields diagram shows the approximate point of incipient motion for a range of grain sizes (a) from ASCE (2000); (b) from Yalin (1971).	105
Figure 4.3. Prototype and model grain size distributions.	114
Figure 4.4. (a & b) Armour layer on abandoned channel bed surfaces. (c) Standing waves on the surface indicate the presence of upper regime bedforms (antidunes) on the incising channel bed.....	116

Figure 5.1. Contour map of pre-dam Elwha River valley showing location of model construction cross-sections.	118
Figure 5.2. Stages of model construction.....	120
Figure 5.3. Comparisons of the model delta with the prototype during the 1994 drawdown experiment.....	128
Figure 5.4. (a) Long profile of the dissected delta showing the essentially horizontal contact plane of fine sediment between the Stage 1 and 2 growth surfaces. (b) Close up of the contact plane.	130
Figure 5.5. Pattern of baselevel fall for each experimental run.	131
Figure 5.6. Model discharge control.	132
Figure 5.7. Balanced hydrographs for the McDonald Bridge gauge (ELWP), the temporary gauge (ELWW) and the Lake Mills model.	135
Figure 5.8. (a) Schematic and (b) photograph of the Keyence LK-503 laser and instrument carriage.....	136
Figure 5.9. (a) Model delta coring (white circles) and approximate prototype delta borehole (grey circles) locations. (b) Example of one of the delta sediment cores.	137
Figure 5.10. (a) Armour and sub-armour sampling. (b) Cardboard sampling square for delineating armour and sub-armour sample area.	138
Figure 6.1. (a) Photograph and (b) DEM of the original delta area in run 3xC after 2,550 minutes.	149
Figure 6.2. The gain in fill volume information as point density is progressively increased.	152
Figure 6.3. Regression curves for volume information lost as a function of cross-sectional point spacing.	152
Figure 6.4. Cross-sectional spacing required to produce absolutely accurate sediment volume measurements.....	153
Figure 6.5. The effect of overhanging banks and terraces on laser data collection. ..	155
Figure 6.6. Example of photo target used to develop algorithms to correct for lens distortion and perspective errors.	162
Figure 6.7. Measuring lines for the cameras in their two different positions.	166
Figure 6.8. Thalweg extraction.	168
Figure 7.1. D ₅₀ (mm) of prototype delta borehole sediment samples.....	175
Figure 7.2. D ₅₀ (mm) of delta cores for Run 2 (3xR).	176
Figure 7.3. D ₅₀ (mm) of delta cores for Run 3 (1xL).....	177
Figure 7.4. D ₅₀ (mm) of delta cores for Run 4 (3xL).....	178
Figure 7.5. D ₅₀ (mm) of delta cores for Run 5 (3xL A).....	179
Figure 7.6. D ₅₀ (mm) of delta cores for Run 8 (3xC).	180
Figure 7.7. D ₅₀ (mm) of delta cores for Run 6 (6xC).	181

Figure 7.8. D_{50} (mm) of delta cores for Run 6 (6xC).	182
Figure 7.9. D_{50} (mm) of delta cores for Run 9 (21xC).	183
Figure 7.10. Mean values of D_{50} , D_{84} and D_{90} for each coring cross-section.	184
Figure 7.11. Extent of armour layer formation following complete dam removal and flood flows.	185
Figure 7.12. Proportion of the original delta eroded under different dam removal scenarios.	187
Figure 7.13. Original delta erosion volumes per time step and armour layer evolution.	191
Figure 7.14. Original delta erosion rates per time step and armour layer evolution.	193
Figure 7.15. Total reservoir sediment passing downstream.	194
Figure 7.16. Delta surface zones.	196
Figure 7.17. Erosive activity in the original delta represented by corrected and uncorrected erosion data.	196
Figure 7.18. Dimensionless cut volumes, active channel widths, cumulative top terrace widths and cumulative thalweg elevation change from 0 – 50 cm in the original delta area.	203
Figure 7.19. Dimensionless cut volumes, active channel widths, cumulative top terrace widths and cumulative thalweg elevation change from 50 – 100 cm in the original delta area.	205
Figure 7.20. Dimensionless cut volumes, active channel widths, cumulative top terrace widths and cumulative thalweg elevation change from 100 – 150 cm in the original delta area.	207
Figure 7.21. Dimensionless cut volumes, active channel widths, cumulative top terrace widths and cumulative thalweg elevation change from 150 – 200 cm in the original delta area.	209
Figure 7.22. Dimensionless cut volumes, active channel widths, cumulative top terrace widths and cumulative thalweg elevation change from 200 – 250 cm in the original delta area.	211
Figure 7.23. Dimensionless cut volumes, active channel widths, cumulative top terrace widths and cumulative thalweg elevation change from 250 – 300 cm in the original delta area.	213
Figure 7.24. Cumulative change in dimensionless thalweg lowering in the original delta area.	219
Figure 7.25. Longitudinal profiles at equivalent static equilibrium positions during dam removal.	222
Figure 7.26. Dimensionless top terrace widths after equal amounts of baselevel drop.	224
Figure 7.27. Dimensionless active channel widths.	226

Figure 7.28. Distribution over the delta surface of armoured and unarmoured planform types as a function of mean thalweg slope for each 50-cm section of the delta surface.	231
Figure 7.29. Frequency of occurrence of planform types.	233
Figure 8.1. View looking upstream towards the end of run 3xC.	237
Figure 8.2. Model sediment mixture for run 6xC exemplifying lack of bimodality of the modelling sediment mixture.	249
Figure 8.3. Distribution of bed slopes above and below the threshold for mobility reversal.	250
Figure 8.4. Original delta area in (a-d) run 1xL and (e-f) run 3xR at static equilibriums after (a & e) complete dam removal; (b & f) 1 st two-year flow; (c & g) 2 nd two-year flow; (d & h) five-year flow.	254
Figure 8.5. (a) View looking upstream at the empty basin in the original delta area. (b) Graphical representation of the original delta area, whose downstream extent is delimited by the arrows A and B in (a).	255

List of Tables

Table 1.1. Countries currently building the most large dams.	6
Table 1.2. Dam classification according to reservoir size.	22
Table 4.1. Summary of prototype and model geometrical hydraulic variables.	113
Table 4.2. Truncated prototype delta grain size distribution and model values.	113
Table 4.3. List of lower density modelling material used in hydraulic modelling practice around the world.	115
Table 5.1. Experimental parameters.	120
Table 5.2. Hydraulic parameters in model delivery channel before and after channel roughening.	124
Table 5.3. Model hydraulic and sedimentary variables used to calculate values in Table 5.2.	124
Table 5.4. Parameter values required to obtain the calculated value of the Shields number in a roughened delivery channel.	125
Table 5.5. Balanced flood hydrograph data.	134
Table 6.1. Summary of mean error statistics used to assess the magnitude of systematic errors.	145
Table 6.2. Progression of laser-based volume data to estimate absolute sediment volumes.	153
Table 6.3. Correction of starting sediment (fill) volumes due to basin shape errors.	154
Table 6.4. Calibration factors for the channel lengths measured from the photographs.	164
Table 6.5. Calibration factors for cross-sectional feature measurements (channel, top terrace and delta surface widths).	165
Table 6.6. Comparison of total channel lengths from calibrated and uncalibrated photo measurements with those from DEMs.	165
Table 7.1. Relative abundance of armour layer D_{50} at each coring cross-section.	185
Table 7.2. Summary of original delta erosion volumes during dam removal.	187
Table 7.3. (a) Original delta erosion during flood flows. (b) Sediment volumes passing through the dam site.	194
Table 7.4. Summary of downstream extents of armoured 50-cm delta surface sections.	228
Table 8.1. Reynolds and grain Reynolds numbers in one of the channels incising the Lake Mills delta surface during the 1994 drawdown experiment.	237
Table 8.2. Estimated values of the Reynolds and grain Reynolds numbers during the experimental runs.	237
Table 8.3. Dimensionless parameters used to assess cause of mobility reversal.	249

Chapter 1 Introduction

Humans have abstracted water from and altered the flow and form of river channels for thousands of years. As the planet's population has grown and as our technology has developed, so these intrusions have become more widespread and invasive, to the point now that there remain very few rivers that exist in a completely natural condition. Dams provide a good example of this encroachment. They have been used for thousands of years and have undoubtedly brought many benefits to human society (World Commission on Dams, 2000). Indeed, many of the earlier civilisations would not have been able to survive without them because of their crucial role in helping to deliver water for irrigation and domestic supply. But at the same time they have wrought an increasingly destructive environmental toll, especially since the start of the 20th century, as their sheer number and size has increased enormously (Appendix A) and because of the barriers that they represent to the flows of water, sediment, nutrients and organisms. Now, however, at the start of the 21st century, a new chapter in the history of dams is being written. In 2000, for the first time, more dams were removed from rivers in the United States than were built and this trend appears to be gathering pace. While this is undoubtedly an environmentally beneficial development, caution must nevertheless be exercised because, just as dam construction represents a disturbance to the fluvial system, so too does dam removal (Stanley and Doyle, 2003). Care must therefore be taken to ensure that this undertaking does not unduly damage the systems it is designed to benefit.

1.1 A brief history of dams

The history of the earliest known dams is intimately linked to the needs of domestic water supply, flood control and soil and water conservation. It was only in the second millennium B.C. that dams and weirs were built to guide water through irrigation networks. Without these systems, many of these early societies would not have been able to grow and flourish, or survive at all in some cases, owing to the aridity of the climates in which they existed. By the first millennium B.C. dams were being built throughout Asia and the Americas (Schnitter, 1994). The following is a brief global history of dams, for which a more detailed chronology is provided in Appendix A.

The world's oldest dams for which there is definite supporting evidence were built about 100 km north of what is now the Jordanian capital of Amman. Ten dams were built in around 3,000 B.C. to divert water from the River Rajil to provide the domestic water supply to the town of Jawa (Schnitter, 1994). The world's oldest known large dam was built by the Egyptians. The Sadd-al-Kafara (Dam of the Pagans) was built sometime between 2,950 B.C. and 2,750 B.C. according to Smith (1971), while Schnitter (1994) cites a date of about 2,600 B.C. Smith (1971) suggests that it was used to supply a quarry with water, while Schnitter (1994) states that it was used to retain rare flash floods. There is no evidence to suggest that dams were a significant feature of Egyptian society, however (Smith, 1971). The Mesopotamians were the first regular dam builders, with one of their first structures dating from about 2,140 B.C. and maybe even earlier. The diversion dams of the Mesopotamian civilisations and, during the first millennium B.C., those of several Arabian cultures, were all integral components of extensive systems of irrigation canals and were absolutely crucial to the existence of these civilisations (Smith, 1971). Common to all the structures of antiquity is that they were all either embankment or gravity dams built to resist the pressure of the water they impounded through only their weight (Schnitter, 1994).

The Romans built many dams throughout their empire, from the Middle-East, to North Africa and throughout Europe, largely because of their ability to design and execute large-scale engineering works. In addition to absorbing the irrigation technology of the aforementioned civilizations, they made several important innovations. They were the first dam builders to use concrete in any significant quantities, a practice that was abandoned following the disintegration of their empire and not resumed until 1872 (Schnitter, 1994). They also built the first buttress dams, the first multiple-arch buttress dam and the first true arch dam, although it appears that they only built at most two of the latter. Using this technology, they built dams for water supply, irrigation, flood control, soil and water conservation (Schnitter, 1994) and for controlling canal systems (Smith, 1971). These applications were continued by the Byzantines¹ following the collapse of the Roman Empire in Western Europe. Roman dam-building knowledge was also absorbed by the Persians², who

¹ Byzantine is the name given to the continuation of the Eastern Roman Empire following the collapse of the Roman Empire in Western Europe (Halsall, 2004)

² Persia is the area now occupied by modern-day Iran.

from the middle of the first millennium B.C. onwards had continued the dam building activities of the earlier Mesopotamian civilisations (Smith, 1971).

Within a century of the foundation of Islam in 622 A.D., Muslim rule extended from the Indus River valley to the Atlantic coast of North Africa and into Spain, and with it the accumulated dam building knowledge of the Romans, Mesopotamians and Persians. Smith (1971) considers the history of dams in Spain to be of pivotal importance because of the length and continuity of the dam building record there – about 2,000 years in all, and the technological innovations that occurred. These included linking the irrigation technology imported by the Muslims with the idea of large storage reservoirs; building several arch dams; and building the first big buttress dam (Smith, 1971).

While dam building first developed in the Middle East and subsequently spread throughout North Africa and Europe, it also developed independently in the Far East, perhaps firstly in China. While the Chinese were sophisticated hydraulic engineers, dam building is not thought to have been amongst the first such endeavours that they undertook. The oldest known Chinese dam is the Anfengtang Dam and Reservoir on the Huai River, which was completed in 581 B.C. to impound 100 million m³ of water and is still in use today (Schnitter, 1994). It is unlikely that such a large reservoir would have been the first ever built by the Chinese, but no evidence of earlier dams and reservoirs is known. The Sri Lankans were also builders of large storage dams as early as 370 B.C. and these are in addition to many much smaller village reservoirs that were already being built to store winter runoff (Schnitter, 1994). Dam building continued in these countries into the first millennium A.D., when they were joined by Japan following its unification in about 300 A.D., Cambodia and India, the latter of which enjoyed an increase in dam building starting in 1037 that progressed independently until the arrival of the first Europeans in the 16th century (Schnitter, 1994).

Prior to the Spanish conquest of the Americas in the early years of the 16th century, dams had been built in Latin America since at least 700 B.C. by farming communities that pre-dated the more famous civilizations of the Zapotecs, Mayas, Toltecs and Aztecs. These civilizations began building dams from about the 3rd century A.D. onwards (Schnitter, 1994), while in North America, Native Americans began building small dams for irrigation and domestic water supply no earlier than

about 800 A.D (Smith, 1971). When the Conquistadors arrived, they brought with them the combined dam building knowledge of the Mesopotamians, Romans, Persians and Muslims, which they added to the existing indigenous knowledge. Spanish missionaries moved into North America in about 1700 and established missions in the southwest and along the Pacific coast, for which they built small dams for water supply and irrigation reservoirs (Smith, 1971).

In tandem with Spanish expansion in the southwest, Northern European settlers in New England began building small dams to provide water power for mills from about the 1620s onwards. This reflected the use for which many dams had been built in the settlers' home countries since at least the start of the second millennium A.D. and, in some countries, *e.g.* France, even earlier due to the Roman presence (Smith, 1971). In addition, the construction of ponds for pisciculture was widely practised throughout many countries in northern Europe from the early to middle centuries of the 2nd millennium A.D. From the 17th century onwards, France and Britain in particular built water supply reservoirs to enable river and canal navigation, while dams for flood control began to be built in Italy at about the same time (Schnitter, 1994; Smith, 1971).

Following the onset and acceleration of the industrial revolution in the late 18th century, the focus of world dam building, development and research switched to the industrialising countries of Europe and North America during the first half of the 19th century. With the mass migrations of people from the countryside to the cities, large water supply reservoirs were built for the first time, such as those at Whinhill in 1796 (Smith, 1971) and Glencourse in 1824 (Schnitter, 1994), both in Scotland.

From 1547 onwards, books describing dam-building techniques began to be written, while in Britain and France engineering schools and societies were formed, all of which enabled dam building knowledge and experience to be slowly disseminated (Schnitter, 1994). In the 18th and 19th centuries, empirical and theoretical developments in France lead to a greater understanding of some of the engineering properties of soils, thus paving the way for the design of more stable earth embankments that were very common in northern Europe. In 1853, the publication of the first stress-analysis of masonry dams showed that a gravity dam with a triangular cross-section was the most stable (Schnitter, 1994). All dams built to this point had been designed and built on a trial and error basis, or based on the

experience and intuition of the engineers involved. The application of this and subsequent rational design methods, together with detailed dam performance data, now allowed dams to be built more safely, using relatively less material and therefore more economically. Between 1853 and 1940, the methods for rationally designing gravity, earth, and arch dams were all worked out, with the result that the number of dam failures dropped sharply after 1930 (Schnitter, 1994; Smith, 1971). In addition, the sizes of all types of dam increased dramatically (Schnitter, 1994), thus increasing the magnitude of their environmental impacts.

In 1882, dam-building, water-turbine, and electric-generator technology combined to create the world's first hydro-electric facility on the Fox River at Appleton in Wisconsin, while in 1889 the San Mateo Dam was the first to be built entirely out of concrete, in order to supply water to San Francisco (Smith, 1971). These developments in dam building and usage paved the way for the explosion in their number worldwide during the 20th century (Figures 1.1, 1.2; Table 1.1).

1.2 Dam removal in the United States

While dam removal as a tool for rehabilitating degraded river systems is being applied most vigorously in the United States, it is increasingly being used or pursued in several other countries. Since the 1990s, France has removed a small number of dams in the River Loire basin, mostly to allow the passage of Atlantic salmon (*Salmo salar*), with several more removals planned (Epple, 2000), while a number of dam removal projects are also being considered in Canada (River Alliance of Wisconsin, 2006) and Scotland (Jeffries, Personal Communication, 2007). France may be on the verge of a paradigm shift in thinking with regards to considering dam removal as a valid management option (Epple, 2000), but it has not yet progressed to the same extent as in the United States. The increasing trend for dam removal in the United States is in stark contrast to the rest of the world, however, where large dams are still being built on every continent (Table 1.1), albeit at a decreasing rate (Figure 1.1) (World Commission on Dams, 2000), and especially in China and India.

1.2.1 Factors driving dam removal in the United States

Why is dam removal now occurring in the United States? In the post World War II period, there was an explosion of dam building that peaked in the 1960s and 1970s with the construction of 22,070 and 14,750 dams per decade. The 1980s and

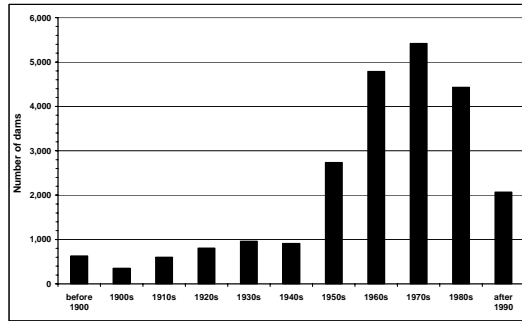


Figure 1.1. Number of large dams (>15 m high) constructed worldwide during the 20th century (World Commission on Dams, 2000). Data exclude over 90% of large dams in China.

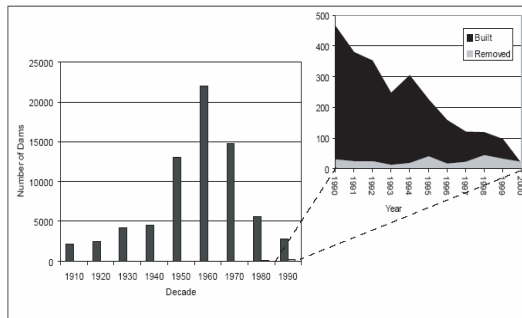


Figure 1.2. Dams built and removed from rivers in the United States during the 20th century. (Source: American Rivers *et al.*, 1999; USACE NID, 2000). Graphic courtesy of Dr. Greg Stewart.

Country	Number of dams under construction
India	695-960*
China	280
Turkey	209
South Korea	132
Japan	90
Iran	48
Spain	10
Italy	9
Romania	8
Algeria	7
Brazil	6
Venezuela	5
Russian Federation	5

Table 1.1. Countries currently building the most large dams (World Commission on Dams, 2000). *Number varies according to sources.

1990s saw a sharp decline in the number built (5,610 and 2,800 per decade respectively) (Figure 1.2) due to increasingly prohibitive costs (Dietz, 1993; Long, 1993; Mann, 1993; Steinberg, 1993), a lack of suitable sites for further dam construction (Morris and Fan, 1998), and an increasing awareness of the deleterious

impacts of dam construction on the physical, biological and chemical integrity of river systems (section 1.3). At the same time, in the 1980s and 1990s, the number of dams being removed began very slowly to increase and, in 2000, for the first time ever, the number of dams removed exceeded the number that were built³ (Figure 1.2), and it is expected that this trend will continue over the coming decades.

The trend of dam construction during the 20th century in the United States mirrors very closely that of large dams throughout the rest of the world (Figure 1.1), although the two sets of data must be compared with caution. The global data only describe structures >15 m high or from 5-15 m high with a reservoir of at least 3 million m³ (World Commission on Dams, 2000). The data for the United States are taken from the National Inventory of Dams (NID), maintained jointly by the Federal Emergency Management Agency (FEMA) and the United States Army Corps of Engineers (USACE), and show that there are more than 79,000 dams in the United States, although this only includes structures that pose a threat to life and property should they collapse; are greater than 1.83 m (6 feet) tall with an impoundment of 61,000 m³ (50 acre-feet); or are ≥ 7.62 m (25 feet) tall with an impoundment of 18,500 m³ (15 acre-feet) (Heinz Center, 2002). There are many more dams that do not meet the criteria for inclusion in the database, however, and their number is estimated to range from over two million (Graf, 1999; National Research Council, 1992) to as much as eight to nine million (Renwick *et al.*, 2005). A significant number of these small structures may be beaver dams (Butler and Malanson, 2005).

Dam removal is occurring in the United States and is being increasingly discussed by professionals in a wide number of fields for a number of reasons (Grant, 2001). First, America's dam infrastructure is aging rapidly (Natural Resources Conservation Service, 2000). Many structures in the NID were built with a design life of about 50 years; 22,000 (30%) of these are already over 50 years old and in 2020, 60,000 (80%) will be over 50 years old (Heinz Center, 2002). If the same percentages are assumed applicable to the aforementioned lower estimate of two million dams, this suggests about 600,000 structures now and 1.6 million structures in 2020 over 50 years old. Such an aging infrastructure results in problems of economic and structural obsolescence, safety considerations, and the associated legal and financial burdens to

³ Only one large dam is currently under construction in the United States, in Puerto Rico (World Commission on Dams, 2000).

the owners (Heinz Center, 2002). Second, changes to the Federal Energy Regulatory Commission's (FERC) relicensing procedure along with the requirements of the Endangered Species Act mean that fish passage, along with other aquatic and riparian considerations need to be addressed during the relicensing of federal dams (Pejchar and Warner, 2001) and this frequently results in dam removal becoming the most economically viable option. Third, it will improve water quality and quantity for instream users. Finally, it will open up many river miles to flowing-water recreation (Heinz Center, 2002).

Dam removal is not a recent phenomenon – removals are documented for as far back as 1922 (Pohl, 2002), but the accelerating rate of removals is without precedent. A recent count identified 579 documented removals having occurred by 2003 (American Rivers *et al.*, 1999), with 60 more removals proposed for 2004 (American Rivers, 2004). Dams are being removed for a variety of reasons and Pohl (2002) has ranked these in order of decreasing influence as environmental, safety and economic, although since the end of the 1990s these and other factors are increasingly combining to drive forward a proposed removal (Pohl, 2002).

1.3 The impacts of dam construction and dam removal

Together with information from the small number of documented dam removals, from situations whose process-form interactions may be analogous to those that occur during dam removal (Doyle *et al.*, 2002), and from laboratory experiments, the changes that occur during dam construction may shed some light on the possible responses to dam removal (Heinz Centre, 2002).

1.3.1 Environmental impacts

Rivers are the principle arteries along which fluxes of water, sediment, nutrients, and many organisms move throughout the landscape. Whenever a dam of any size is built, these flows are partially or completely blocked and the physical and biological continuity of the catchment system is disturbed. The extent of this fragmentation will vary with the number of dams, their size and their operational regimes. Most rivers in the economically developed countries of the world are moderately to severely disturbed by dams (Dynesius and Nilsson, 1994; Graf, 1999), while those in many of the countries of Asia, the Middle-East and South America are

rapidly becoming so (World Commission on Dams, 2000). The physical and biological impacts of this fragmentation are becoming increasingly well understood, as are the implications for the sustainability of many elements of the fluvial system.

In addition to this fragmentation, and of great importance given the serious consequences associated with climate change, some reservoirs are significant sources of sustained methane production, a highly potent greenhouse gas, due to the decomposition of organic material that is delivered to and produced within the reservoir. Where hydroelectricity is generated in tropical and sub-tropical areas, the methane CO₂ equivalent⁴ per kilowatt hour generated can be many times greater than that of coal-fired power stations (McCully, 2001; St. Louis *et al.*, 2000).

1.3.1.1 Hydrological impacts

i) Dam construction

All natural rivers have patterns of flow that vary throughout the year and, in the case of those where the freezing and thawing of snow and ice is a factor, diurnally also (Ward and Robinson, 1990). The natural flow regime has been called a ‘master variable’ that regulates all biotic interactions in a fluvial ecosystem (Poff *et al.*, 1997). Together with sediment supply, it also regulates all physical interactions and its alteration can thus have profound implications for both the geomorphology and ecology of the fluvial system.

The natural flow regime for all rivers is composed of five elements: the magnitude, frequency, duration, timing and rate of change of flow (Poff *et al.*, 1997). All dams alter all of these elements in the channel downstream from the dam to a greater or lesser extent, the precise amount being dependent on the dam’s design and operational regime (Petts, 1984b; Petts and Lewin, 1979; Williams and Wolman, 1984). Generally, however, they tend to reduce flood flows; augment low flows; alter the timing and duration of high and low flow events both throughout the year, for example for irrigation and navigation, and during the day, for example for hydroelectric power generation; and alter the rate at which changes occur between low and high flows (Assani and Petit, 2004; Gore *et al.*, 1994; Magilligan and Nislow,

⁴ The CO₂ equivalent of methane is the number of molecules of CO₂ that would be required to generate the same amount of atmospheric warming as one molecule of methane.

2001; 2005; Magilligan *et al.*, 2003; Petts, 1984b; Petts and Lewin, 1979; Williams and Wolman, 1984).

Equally profound changes occur immediately upstream from the dam in the area occupied by the impoundment, as a free flowing (lotic) environment is changed into one with a very low flow velocity (lentic). Besides flooding part of the valley, the water table will rise locally around the reservoir (Bureau of Reclamation, 1997), potentially leading to flood and hillslope stability problems where none existed previously, especially if the water level in the reservoir drops suddenly. These changes also have significant implications for the geomorphological (section 1.3.1.2) and biological (section 1.3.1.3) components of the fluvial system in this area.

ii) Dam removal

If the reservoir still had some capacity to regulate inflows, *i.e.* was not full of sediment, the removal of the dam should restore the five elements that compose the natural flow regime (Poff *et al.*, 1997). The extent to which the flow regime will resemble that of the pre-impoundment regime, however, will depend on the age of the dam and the extent to which the catchment land use has changed since dam construction. If the dam was very old, it is possible that natural and anthropogenic climate changes will have altered the precipitation and air temperature regimes to the extent that they have appreciable effects on the stream flow. More significant changes to stream flow, however, will probably arise from any land use changes that have occurred and from any surface water and groundwater abstractions for irrigation, industrial and domestic uses (Hogg and Norris, 1991). These changes will not all be relevant to every dam removal situation and they could act together in a number of different ways to either enhance or reduce the differences between the pre- and post-removal hydrograph.

1.3.1.2 Geomorphological impacts

i) Dam construction

The geomorphological changes experienced by river channels following dam construction are directly attributable to the altered hydrological (section 1.3.1.1) and sediment supply regimes. Perhaps the most immediate physical impact of dam construction is on the bed load and suspended sediment load. Reservoirs are extremely efficient sediment traps and may retain the entire bed load and virtually the

entire suspended sediment load, although trap efficiency depends on the shape of the reservoir and the operating regime and design of the structure and in any case declines as the reservoir fills with sediment (Morris and Fan, 1998). The nature and morphology of the reservoir deposit will vary according to reservoir geometry, discharge, the calibre of sediment being deposited and the reservoir's operational regime. Four principal, longitudinal morphologies have been identified (Figure 3.2): the delta deposit, in which coarse sediment is deposited in the upstream reaches of the reservoir and finer bottomsets surfaces are deposited downstream from this; a tapering deposit, which becomes thinner moving downstream through the reservoir; a wedge deposit, which is thickest near the dam; and a uniform deposit that is evenly distributed through the reservoir. Laterally, deposition generally occurs in the deepest part of the reservoir, thus creating a nearly horizontal reservoir bed. These morphologies are a function of both the reservoir's operational regime and the grain size distribution of the inflowing sediment load (Morris and Fan, 1998).

Sediment loads can remain depressed for hundreds of kilometres downstream from dams and in some cases will never regain their pre-impoundment levels (Williams and Wolman, 1984). These reduced loads and the generally muted hydrological regime initiate a series of morphological changes in the downstream channel. The usual response is for the channel to incise its bed and for this incision to migrate downstream through time (Galay, 1983), with the greatest amount of total incision generally occurring in the downstream vicinity of the dam and decreasing towards the downstream end of the 'degraded zone' (Williams and Wolman, 1984). This incision can be accompanied by an increase, a decrease, or no change in channel width, depending on the extent to which flows have been regulated and on the nature of the bank material. Finally, as the channel incises, the surface bed material may coarsen and lead to the formation of an armour layer. The extent of the coarsening is generally greatest close to the dam and decreases downstream (Petts, 1984b; Williams and Wolman, 1984).

Within the degraded zone, these relatively straightforward general tendencies are frequently compounded by variations in the nature of the boundary material and its resistance to erosion, such that the greatest amount of channel bed degradation will not necessarily occur closest to the dam, nor exhibit a smooth decrease downstream,

and channel width adjustments will frequently display a random distribution (Petts, 1984b; Williams and Wolman, 1984).

It is increasingly being realised that, in many cases, degradation may only be the initial response to impoundment and that it may be followed by a period of aggradation as the channel seeks to establish a new equilibrium morphology that is adjusted to the reduced flows of water and sediment. Furthermore, different sections of the adjusting system will display markedly different directions of adjustment: zones of aggradation and degradation will migrate through the system in both space and time and will be modulated by the operation of positive and negative feedbacks (Petts, 1979), as well as by the nature of the flow and sediment transport regimes and boundary material (Assani and Petit, 2004; Petts, 1979), the sediment supply from tributaries (Grams and Schmidt, 2005; Lyons *et al.*, 1992; Petts, 1984a; Schmidt *et al.*, 1995), channel morphology (Petts and Pratts, 1983), channel planform prior to the disturbance (Friedman *et al.*, 1998; Shields Jr. *et al.*, 2000), and the effects of riparian vegetation (Petts, 1982). Such a fluctuation towards a new equilibrium morphology, albeit somewhat more simply, has been conceptualized by Hey (1979). Eventually, the channel will attain a new equilibrium morphology, but with a channel capacity that is reduced compared to the pre-impoundment capacities (Petts, 1979). In rare instances, these variables can interact in ways that essentially cancel out any geomorphological adjustments (Phillips, 2003).

While each river will respond in a unique fashion to upstream impoundment due to the large number of variables, attempts have nevertheless been made to conceptualise and present at least a first-order prediction of this behaviour. Petts (1982) notes that, despite the complexity of response, all variables generally adjust uni-directionally to either enlarge or reduce channel capacity. From this, four possible responses are distilled: two end-member cases represent a clear trend towards either channel aggradation or degradation. Between these, there is the case where a general tendency to erode is resisted by a sufficient supply of sediment, albeit with a good deal of variation, and the case where a general tendency to aggrade is resisted by a sufficient number of scouring flows, but again with much variation. Petts (1982) presents a second model that conceptualises the stabilising effect of vegetation downstream from a tributary sediment source on a river that still experiences periodic flushing flows. Brandt (2000a) developed a nine-case classification of the possible

impacts to downstream channel cross-sectional morphology, based on the post-dam discharge and sediment load regimes. Post-dam discharges will either be less than, equal to, or greater than pre-dam discharges and, for each case, post-dam sediment loads will either be less than, equal to or greater than post-dam transport capacity, as calculated using a sediment transport relation and the dominant discharge. Common to the models of Petts and Brandt is that both can be applied in a space-for-time fashion. More recently, Phillips *et al.* (2005) compared Brandt's (2000a) model to the unstable hydraulic geometry model and found that, while it correctly predicted the general channel changes downstream from a run-of-river water supply reservoir (channel widening and incision), it was unable to predict the increases, decreases and lack of change in channel width, depth, slope and bed roughness that occurred irregularly at the individual cross-sections in the same reach. The unstable hydraulic geometry model was able to do this. Brandt (2000b) presents a method for quantitatively estimating downstream channel shape using dimensionless regime relationships to obtain cross-sectional width and depth, together with an extremal hypothesis (minimal cross-sectional stream power) and sediment transport equation to calculate slope. The method is reliant on knowing the post dam water and sediment supply regime, together with the appropriate choice of equations, but no example is provided of application to a channel downstream from a dam.

ii) Dam removal

The specific effects of dam removal will vary according to the way in which the dam is removed (all at once or in stages, sections 7.2 & 8.2); the unregulated (by the dam) characteristics of the hydrograph; the volume (section 8.2.1) and grain size distribution of the reservoir sediment (sections 7.2 & 8.2.2); and the geometry of the river channel, the reservoir basin, and the sediment deposit (sections 7.3 & 8.2.3). These characteristics will determine the magnitude and rate of erosion of sediment from the reservoir area and hence the magnitude of downstream physical, biological and human impacts. Since a number of these variables are the focus of the current investigation, they will be discussed further in later chapters.

Essentially, dam removal will potentially make available a large volume of sediment for transport into the downstream river system. In reservoirs containing a range of sediment size from clays and silts to cobbles and boulders, there will be a rapid differentiation of the rate at which the different size fractions are eroded into

and transported through the downstream channel. Some of the finer sediments travelling in suspension will be flushed straight through the system, but some will be retained for longer periods. Grant *et al.* (2002) estimated that about 42 million kilograms of fine sediment were flushed out of Cougar Reservoir on the South Fork McKenzie River in the Oregon Cascades, USA, during a reservoir drawdown of 45.7 m (150 feet). Of this mass, about two-thirds was estimated to have been flushed out of the McKenzie River system and about one-third to have been deposited on and probably within the channel bed (Stewart *et al.*, 2002). Following the removal of a low-head, run-of-river dam from the Baraboo River in Wisconsin, most of the sand eroded from the reservoir was observed to be deposited within the interstices of the river's gravel bed (Stanley *et al.*, 2002).

The way in which fines are deposited within the channel bed and sediment of all sizes deposits on the bed will be affected by the nature of the downstream channel prior to the influx of sediment (Rathburn and Wohl, 2003a). Deposition of fines within the hyporheic zone of rivers occurs even over a plane bed, but it is exacerbated by the presence of convexities and concavities on the channel bed due to pressure differentials that develop between the surface and sub-surface. These differences increase the volume of flow through the hyporheic zone (Harvey and Bencala, 1993) and thus increase the amount of fine sediment that can potentially be delivered into the bed. In sand-bed rivers, preferential deposition of fines may occur near the surface of the channel bed, thus limiting hyporheic exchange with deeper sub-surface locations and adversely affecting ecological processes (Packman and MacKay, 2003). The deposition of gravel and cobble fractions, on the other hand, may enhance hyporheic exchange by increasing bed porosity (Packman and Salehin, 2003).

Sediments of all calibres can deposit in areas of reduced flow velocity, but fines and sand are preferentially transported into, and thus dominate, the deposits in these areas. Following the release of about 7,000 m³ of silt- to gravel-sized sediment from Halligan Reservoir on the North Fork Cache la Poudre River in Colorado, the volume of the pools and the calibre of sediment that was filling them both decreased with increasing distance from the reservoir. After a subsequent high flow, the location of the most-filled pool moved downstream (Wohl and Cenderelli, 2000). Attempts to simulate these dynamics using one-dimensional models were moderately successful (Rathburn and Wohl, 2001), but the existence of a conceptual model improved the

interpretation of the numerical model output (Rathburn and Wohl, 2003b). Similar pool filling and sediment movement from pool to pool has also been observed following the influx of sediment from large floods (Lisle, 1982; Lisle and Hilton, 1999) and the replacement of a culvert at a new and lower baselevel (Bromley, 2003). When the supply of sediment is sufficiently large, it can cover the entire channel bed. Waves of sediment have been observed to move downstream, predominantly by dispersion (Lisle, Submitted; Lisle *et al.*, 2001); following large floods and logging activity (Madej and Ozaki, 1996); dam removal (Simons and Li, 1982); and mining activity (Knighton, 1991).

The importance of pool filling and downstream wave migration is that it greatly reduces the form roughness of the bed and, if the sediment influx is finer than the original bed material, the grain roughness also. The reduction in friction allows flow velocities and boundary shear stresses to increase, thus increasing the rate of sediment transport and the rate at which the channel recovers from the disturbance in a process of positive feedback (Hayes *et al.*, 2001; Janda *et al.*, 1984).

Aggradation can also promote bank erosion and channel widening (Lisle, 1982) due to the mass wasting and direct entrainment of non-cohesive materials (Simon and Thorne, 1996) or due to a more frequent change in bank pore water pressures within more cohesive materials that reduces bank shear strength (Simon *et al.*, 2000). It can also change channel planform from single-thread to braided or cause channels to avulse (Ashworth *et al.*, 2004).

1.3.1.3 Biological impacts

i) Dam construction

The biological impacts of dam construction will manifest themselves over a number of time scales ranging from days to decades. Organisms that move along the stream channel will be affected by the barrier effect of the dam, while all organisms will respond to the altered fluxes of water (section 1.3.1.1), sediments (section 1.3.1.2) and nutrients, and will continue to do so for at least one year as the dam and reservoir affect the full annual cycles of these fluxes. They will also respond over the course of years to decades to the adjustments that the altered fluxes of water and sediment bring about to the channel morphology. In addition, there may be an intermediate time scale of response in which organisms at higher trophic levels, *e.g.*

fishes, respond to the changes that occur to their food sources at lower trophic levels (Petts, 1984b).

Energy is introduced into the aquatic food web from autochthonous (within-channel) and allochthonous (riparian zone) sources. The autochthonous primary producers tend to be dominated by attached algae in steeper gradient streams and by angiosperms (higher plants) in middle reaches⁵. Both can benefit from dam construction due to the more regular flow regime, higher winter water temperatures, reduced turbidity (more light for photosynthesis), more nutrient-rich water from hypolimnial⁶ releases, and more stable substrate. The latter allows angiosperms to encroach into former channel areas, thus helping to stabilise the channel boundary. Excessive algal growth can reduce interstitial flow and thus the supply of oxygen to and the flushing of waste products away from buried salmonid eggs. It can also reduce the flow's dissolved oxygen content when it decays. The rapid flow variations associated with hydropower or irrigation releases, however, can be very destructive to algae and angiosperms if they mobilise the channel substrate (Petts, 1984b). A reduced frequency of flows greater than bankfull isolates floodplain channels from their floodplain, thus reducing the availability of allochthonous organic matter and nutrients and adversely affecting system productivity (Junk *et al.*, 1989).

Native species of macroinvertebrates and fishes are adapted to the five components (section 1.3.1.1) that characterise the natural flow regime of any stream (Palmer *et al.*, 1997; Peckarsky *et al.*, 1997; Petts, 1984b; Poff *et al.*, 1997; Poff and Ward, 1989). Alterations to any of these components, for example rapidly fluctuating flows and unnaturally sustained high flows due to hydropower generation, can adversely affect the respiration, physiology and feeding ability of macroinvertebrates, thus reducing the taxonomic richness and relative abundance of certain species by inducing catastrophic downstream drift (Camargo and Voelz, 1998; Petts, 1984b). They can also erode the spawning gravels used by fish species, reduce their access to food (macroinvertebrates), sweep juveniles downstream and strand them in isolated pools. A reduction in peak flows can partially or completely sever the floodplain from the channel, thus reducing the inputs of nutrients to the channel (Gregory *et al.*, 1991;

⁵ Periphyton is the name given to plants such as algae and angiosperms that are attached to the channel substrate.

⁶ The hypolimnion is the lowest and coldest layer of water found in deep (> ~10 m) reservoirs. The epilimnion is the warmest surface layer of the reservoir.

Thoms *et al.*, 2005), reducing the availability of food sources and spawning grounds, particularly in large tropical rivers (Petts, 1984b), disturbing predator-prey interactions by removing access to within-channel or floodplain refugia for prey species (Power *et al.*, 1996) and altering the competitive advantage of native species (Meffe, 1984).

The altered thermal and chemical regime is also of great importance to downstream biota. Where the formation and destruction of thermal strata occurs in larger reservoirs, the release of warmer and nutrient-enriched waters during winter can increase the downstream algal cover, thus boosting primary productivity (Petts, 1984b). On the other hand, thermal cues are important for the regulation of macroinvertebrate hatching, growth and emergence, and so will be disrupted by the warmer winter and cooler summer water temperatures, thus reducing the taxonomic richness and relative abundance of certain species (Camargo and Voelz, 1998; Vinson, 2001), while anadromous fish may hatch too early (United States Army Corps of Engineers, 1999b) or expend greater amounts of energy, resulting in increases in energy-related mortality (Berg *et al.*, 2006).

ii) Dam removal

The most immediate effect of dam removal will be the removal of the barrier to the upstream aerial migration of adult macroinvertebrates and to the downstream drift of macroinvertebrate nymphs and larvae (Petts, 1984b). In addition, anadromous species of fish, such as salmonids (*Salmonidae*) and sturgeon (*Acipenseridae*), will be able to migrate upstream to spawn (National Research Council, 1996), while juveniles will be able to migrate downstream without having to negotiate hazards such as increased predation in the reservoir and dam tailwaters, gas supersaturation in the tailwaters, and hydroelectric turbines (National Research Council, 1996; Wik, 1995). Both migratory and non-migratory species will no longer be subjected to anoxic or toxic reservoir releases (Petts, 1984b).

Assuming that dam removal results in a more natural hydrograph (section 1.3.1.1i), the downstream macroinvertebrate community may see an increase in taxonomic richness as more hydraulic niches become available and a reduction in total biomass and numbers of individuals per species (Townsend *et al.*, 1997). If the hydrograph remains significantly affected by changes in catchment land use, however, the taxonomic richness may not return to pre-dam levels.

While macroinvertebrate taxonomic richness benefits from the moderate levels of hydraulic and sedimentary disturbance associated with a natural hydrograph (Townsend *et al.*, 1997), these benefits may be far outweighed if significant volumes of sediment are released from the reservoir area, at least in the short-term. The deposition of sediment of any calibre on the channel bed may smother periphyton, thus reducing macroinvertebrate habitat and food sources. Sediment deposition and suspended sediment and turbidity can also induce catastrophic drift and/or mortality amongst the species intolerant of these conditions, while other species will see an increase in abundance. Overall, however, there is likely to be a reduction in taxonomic richness and density of individuals following sediment release (Cline *et al.*, 1982; Culp *et al.*, 1986; Doeg and Koehn, 1994; Gray and Ward, 1982; McClelland and Brusven, 1980; Nuttall, 1972; Nuttall and Bielby, 1973; Richards and Bacon, 1994). The ability of macroinvertebrates to recolonise following such disturbance will depend on the amount of refugia available within the channel boundary (Matthaei *et al.*, 1999), or on the availability of individuals to drift from refugia further upstream (Gayraud *et al.*, 2000). Doyle *et al.* (2005) synthesised observations from a number of small dam removal studies in Wisconsin and found that different components of the ecosystem recovered at different rates. Macroinvertebrates recovered most quickly, while riparian vegetation took longer and mussel communities did not recover at all.

Sediment releases can also negatively impact fish, both directly and indirectly. The infiltration of fines into gravel beds can eliminate salmonid spawning areas or smother eggs that have already been fertilised by reducing the hyporheic circulation that is needed to oxygenate the eggs and flush out metabolic waste products (National Research Council, 1996). Sediments of all calibres can fill in hydraulic refugia such as pools and channel margins (section 1.3.1.2ii), which are crucial resting areas for juveniles, thus giving them no respite from higher flows. On the other hand, the deposition of gravels can replenish spawning habitat that was eroded by the release of sediment-free flows from the reservoir, while the introduction of coarser sediments can generate habitat complexity and shelter (National Research Council, 1996). Even low levels of suspended sediment can damage fish gills, while higher levels of sediment can damage fins and the skin (Bergstedt and Bergersen, 1997; Petz-Glechner *et al.*, 2001; Servizi and Martens, 1992). Elevated levels of turbidity have been shown

to reduce the ability of brook trout to locate macroinvertebrate prey (Sweka and Hartman, 2001), while the adverse impacts to autochthonous primary production and macroinvertebrates (see above) may also adversely affect the ability of fish to find sufficient food.

1.3.2 Socio-economical and cultural impacts

1.3.2.1 Dam construction

Humans throughout the ages have undoubtedly benefited from the construction of dams. Perhaps most fundamentally, the earliest civilizations could not have developed and flourished without the use of diversion dams in their irrigation systems (Smith, 1971). Even today, certain sections of many societies throughout the world benefit to some extent from the construction of dams and reservoirs because of the economic activity they support through water supply to agriculture and industry, power generation, navigation and flood control; increased security of domestic water and power supply; and the opportunities that they provide for recreational activity (Dietz, 1993; Petts, 1984b; World Commission on Dams, 2000).

Because of the sheer number of dams that have been built since 1900 and the enormous size of so many of these structures and their reservoirs, however, the magnitude of the deleterious environmental and socio-cultural impacts has increased drastically and, it can be argued, now frequently outweighs the benefits (McCully, 2001; World Commission on Dams, 2000). Particularly in many developing countries, where an explosion in large dam construction is currently occurring (Table 1.1), it is frequently the indigenous and the poorest people that suffer these impacts the most and benefit the least due to relocation, inequitable or missing compensation, loss of traditional ways of life and subsequent mental and physical health problems (McCully, 2001; Petts, 1984b; World Commission on Dams, 2000). The economical justification for many of these projects is also questionable, since the true economical costs to all sections of society and nature are rarely if ever considered and are frequently distorted by subsidies or inaccurate cost-benefit analyses (Mann, 1993; Taxpayers for Common Sense *et al.*, 2006; Whitelaw and MacMullan, 2002; World Commission on Dams, 2000), while some may represent the continued operation of ‘pork-barrel’ politics (Reisner, 1993). Many of them also fail to deliver on their stated design objectives, *e.g.* on area irrigated, agricultural productivity boosted, kilowatt

hours generated, *etc.*, with the performance of multi-purpose projects being particularly poor in this respect (McCully, 2001; World Commission on Dams, 2000).

1.3.2.2 Dam removal

While there are a great many scientific unknowns associated with dam removal, some of the most intractable problems are associated with subjective, value-laden judgements. For example, when a dam removal is proposed, some stakeholders will oppose it because they prefer the aesthetic and recreational benefits afforded by a reservoir (boating, fishing), while others will support it because they would rather have a view of a river and opportunities for white water rafting and fishing for lotic species (Born *et al.*, 1998; Sarakinos and Johnson, 2003). Other stakeholder conflicts cannot be predicted due to a lack of data. For example, how will property prices be affected if a lake-side residence is changed into a river-side residence? There is some evidence that it will not change significantly because it is proximity to water of any kind that adds value to a property (Sarakinos and Johnson, 2003), but many more data are required. Yet other stakeholder conflicts arise from a simple lack of knowledge about what will happen following dam removal. For example, it should not take too much effort to explain to people that the river will not disappear if their dam is removed, nor will the area remain for ever more a stinking mudflat (Sarakinos and Johnson, 2003). Techniques such as social marketing are beginning to be applied to such problems in an effort to appraise communities of the range of benefits that could accrue to them if their dam was to be removed (Johnson and Graber, 2002).

Given the number of dams that may be removed in the United States, never mind globally, in the future, these and other problems must be addressed in a structured fashion. It is no surprise that the States with the most dam removals (Wisconsin, Pennsylvania, Ohio and California) are those in which the legislative process has been streamlined to facilitate and speed up dam removal (Born *et al.*, 1998; Heinz Centre, 2002). Frequently, many different agencies from federal, state and local government may be involved in the dam removal permitting process (Bowman, 2002) and this can greatly increase the length of time, and therefore the cost, of a proposed dam removal. Indeed, current legislation such as the Endangered Species Act can actually make it more difficult to remove a dam in the USA because it contains no provision for the specific circumstances created by dam removal (Bowman, 2002).

1.4 Unresolved issues in dam removal

A major disconnect currently exists between the size of dams that are generally studied and the size of those that are currently being removed. The majority of dams that have been removed, and will continue to be removed in the future, are small structures with relatively small impoundments (see below for definitions), while most of the research into the downstream effects of dam construction – which may be informative of potential responses to dam removal – has focused on the effects of large and very large impoundments (Heinz Centre, 2002). This disconnect may persist for some time as dam removals are studied because, while all large dam removals are likely to be closely monitored due to the potential for adverse downstream impacts, the same will probably not be true for small dam removals. The body of case studies may thus become disproportionately weighted towards the effects of large dam removals. Alternately, however, even if only a small proportion of small dam removals are studied, this may still amount to a greater body of case study material than the study of 100% of large dam removals (Grant, Personal Communication, 2007). Whichever proves to be the case, it will be beneficial to understand how applicable the results of large dam removal studies are to small dam removals and *vice versa*. In order to make these comparisons, it will be necessary to select a suite of adjustment variables and to normalise them in some appropriate fashion so that comparisons can be made across several orders of magnitude.

There is a number of different ways of measuring dam size. The International Commission On Large Dams (ICOLD) defines a large dam as a structure >15 m high, or from 5-15 m high with a reservoir of at least three million m³ storage capacity (World Commission on Dams, 2000). In fact, the size of the dam is fairly meaningless for assessing the magnitude of the impacts of dam construction or removal, because it provides no information about the size of the reservoir, which is a more important indicator of impact magnitudes. Accordingly, the Heinz Centre Panel on Dam Removal (2002) classify dams according to reservoir size, as shown in Table 1.2. This measure is not ideal either, however, because it presents the size of the impoundment in isolation from the ‘size’ of the river system on which it is located. Two ratios can be used to describe the size of a reservoir relative to its river and thus to gauge the potential magnitude of the impacts that dam removal may have. The first is a measure of the reservoir’s hydrological size and is the ratio of the reservoir’s total storage

capacity to the mean annual flow⁷ of the river (Morris and Fan, 1998; Petts, 1984b). A ratio of 1.0 indicates that the reservoir can store, on average, exactly the amount of water that flows through the river channel each year. The second can be considered a measure of the reservoir's sedimentological size and is the ratio of the volume of reservoir sediment storage to the mean annual sediment load transported by the river (Randle, 2003).

Reservoir Size	Size (acre-feet)	Size (m³)
Small	1 – 100	$1.233 \times 10^3 - 1.233 \times 10^5$
Medium	100 – 10,000	$1.233 \times 10^5 - 1.233 \times 10^7$
Large	10,000 – 1,000,000	$1.233 \times 10^7 - 1.233 \times 10^9$
Very large	>1,000,000	$>1.233 \times 10^9$

Table 1.2. Dam classification according to reservoir size (after Heinz Centre, 2002).

The two ratios present a measure of the extent to which the presence of a dam may have disrupted the fluxes of water and sediment along the channel. They may therefore provide some indication of the extent to which the removal of the structures will impact the channel. If it is assumed, for the time being, that large ratios have resulted in extensive changes to the channel morphology and ecosystem and, further, that these systems will seek to return to their pre-impoundment condition following dam removal, then, theoretically, the larger the ratios, the greater the magnitude of the adjustments that will potentially take place following dam removal. The magnitude of adjustments of morphological and biological variables can be scaled according to pre-impoundment values but, as yet, no attempt has been made to relate these adjustments to the values of the two ratios for a population of dams. For any given variable, it is not known whether there will be a gradual increase in the magnitude of the impact as the ratios increase, or whether the impact will remain roughly the same for a range of ratios and will only change significantly once some threshold values of the ratios have been crossed. Given the uniqueness of each river and the effects that a dam will have had on its functioning, it is possible that there will be no general trend. Alternately, trends may only be apparent in rivers from the same physiographic regions.

⁷ The mean annual flow is the average total volume of water that flows past a fixed point in the river channel each year.

While the absence of small dam removal case studies is slowly being rectified as more such removals are studied, the research community is still quite a way from having a sufficient number of case studies to enable conceptual models to be developed that describe the fluvial processes and morphological responses that occur during dam removal (Pizzuto, 2002). Situations analogous to dam removal, some of which are discussed in section 1.3, may provide useful additional information in this respect. Conceptual models are required in order to help develop suitable predictive tools to aid in the design and execution of dam removal projects and to assist with the interpretation of output from numerical models that may be applied to the problem (Rathburn and Wohl, 2003b) (see also Chapter 4).

Information from dam removals and analogues will also help to determine the extent to which the physical and biological adjustments to dam construction can be reversed during dam removal. In this context, a series of questions arise. Will dam removal in fact result in a complete reversal of the effects of dam construction? If so, how long will it take? At what rate will it proceed? Will the reversal simply retrace the trajectory of change or will it take place along a different trajectory? And if the reversal is incomplete, what will be the new equilibrium condition of the physical and biological components of the fluvial system?

While dam removal has the potential to successfully rehabilitate many miles of degraded river channel by re-establishing hydrological, sedimentological and biological connectivity, it is nevertheless a disturbance to the fluvial system (Stanley and Doyle, 2003) and, as such, it also has the potential to cause a great deal of physical and biological damage to the riparian ecosystem and to human users of the river and its floodplain. The nature of the disturbance will be very different in the area occupied by the reservoir and in the downstream channel. In the former, a lentic ecosystem (if the reservoir is not full of sediment) will be replaced by a lotic ecosystem, while a depositional environment will be replaced by an erosional one. Downstream from the dam, a lotic ecosystem will still persist, although its composition is may change significantly, while what may have been a predominantly degradational zone may be replaced by one that alternates between periods of aggradation and degradation in response to the influx of sediment from the reservoir area.

Dam removal is thus a coupled upstream-downstream problem and, in order to understand the nature of the downstream impacts, it is necessary to understand the nature of the adjustments that take place in the reservoir area. The focus of this study will thus deliberately only be on the dynamics of sediment movement through and out of the reservoir during and immediately after dam removal, despite the recognition that system responses will occur over much broader spatial and temporal scales in reality. This degree of specificity is merited in view of the relationships that are hypothesised (Chapter 3) and subsequently shown to exist (Chapters 7 and 8), and because of the importance of understanding these interactions for subsequent system evolution at larger spatial and temporal scales. The vehicle for this investigation is a scaled physical modelling investigation of a proposed large dam removal in the United States. This will deliver both site specific knowledge and, for the reasons explained in section 2.1, an understanding of reservoir sediment dynamics that is more generally applicable.

1.5 Structure and scope of the thesis

Many more research questions and areas of uncertainty have been identified in the preceding sections than can be addressed by the current study. The purpose of this section is thus to outline and provide a rationale for the scope, aims and objectives of the research presented herein.

As discussed in the preceding section, the research community's understanding of system response to dam removal is currently limited. In view of this, the proposed removal of two large dams from the Elwha River in Washington, United States, provides an excellent opportunity to test hypotheses generated from a combination of existing fluvial geomorphological knowledge and site-specific observations.

Chapter 2 thus presents an introduction to the Elwha River Basin. This provides a brief overview of the socio-economical and cultural factors that lead to the construction of the two dams and that, in conjunction with biological factors, are now driving the proposed removals. The physical and biological fabric of the basin and its response to dam construction is described, thus providing case-specific examples of many of the physical, biological and socio-cultural and economical responses to dam removal described in more general terms in the literature review in Chapter 1. The

description of the areas currently occupied by the reservoirs – that they are wider than the channels that flow through them - also provides a physical explanation for some of the reasoning that underlies the research hypotheses, *i.e.* that lateral channel movements will be a significant factor in the response to dam removal (Chapter 3).

The volume of sediment stored in Lake Mills is the key concern during the removals, so Chapter 2 outlines the sediment management objectives as well as the incremental lowering that will be used to remove Glines Canyon Dam. Thus, while the inspiration for the key variable to be investigated during the experiments - the magnitude of drop in reservoir water surface elevation (baselevel) – comes from practical requirements, these requirements lead to the production of a body of information that is of broader scientific value; namely, that channel dynamics within the reservoir area are influenced by both the magnitude of drawdown and the length of the relaxation period between incremental drawdowns. The description of the Elwha River as a typical mountain river demonstrates that the observations collected during the experiments reported herein should be more widely applicable.

For the case of a high dam that impounds a reservoir with a delta deposit that either partially or completely fills the reservoir, the transition from a lotic to a lentic system means that channel incision and lateral adjustments will be the principle response over the delta surface. Chapter 3 thus presents a review of the relevant literature, which is used to provide the rationale for the formulation of two testable hypotheses. Hypothesis 1 states, amongst other things, that the greater the magnitude of the incremental baselevel drop, the greater the volume of delta sediment that will be eroded from its initial position. Hypothesis 2 states that the shorter the relaxation times between each incremental baselevel drop, the greater the volume of delta sediment that will be eroded from its initial position. This formulation of these two hypotheses was deliberately simple because, while the 1994 drawdown experiment provided some evidence to suggest that null hypotheses might be inappropriate – namely that lateral channel movements might be able to introduce differences into the delta erosion volumes, it was not clear what precise form a positive relationship between baselevel drop and erosion volume might take. The results presented and discussed in Chapters 7 and 8 suggest that this caution is well founded.

In order to test the hypotheses developed in Chapter 3, a series of experiments was designed and performed in a scaled physical model of Lake Mills. Chapter 4

presents the necessary principles and theory that underlie the design of movable-bed models and explains that a lack of real-world (prototype) data constrained the application of the scaling calculations to the model's delivery channel. It then works through the scaling calculations that were performed, explaining how the difficulties of fitting such a large prototype site into a relatively small laboratory space were overcome by distorting the model and by relaxing some of the requirements demanded by the scaling calculations. The implications of doing so for the model's representativeness are considered earlier in the chapter, in a discussion of the different classes of physical models that are used in laboratory research, and are returned to in Chapter 8 when considering the role of scale effects when interpreting the model's results.

The introduction to Chapter 4 presents a more philosophically-oriented discussion of the relative strengths and weaknesses of the three approaches to modelling; conceptual, numerical and physical, and is used to justify the choice of a physical model study on the grounds that this is the only one capable of revealing some of the unknown form-process-response interactions that may occur during dam removal and thus contribute to the development of more detailed conceptual models, as called for by Pizzuto (2002). It is therefore important to note that, while much of the laboratory work currently being performed by the research community is focused on understanding physical processes, the aim of this study is to understand the response of alluvial forms to two key driving variables. The results presented and discussed in Chapters 7 and 8 respectively validate this approach.

Chapter 5 explains the methods used to build and operate the model and to collect data. The chapter firstly explains how the model was built and calibrated to ensure that the key Froude and Shields parameters were accurately recreated in the delivery channel. Next, the way in which the experiments were set up and run is detailed. In order to try and recreate the downstream fining and upwards coarsening that occurs naturally in the prototype delta, the model delta was hydraulically grown at an accelerated rate until it matched the dimensions of the prototype as measured in 2002. This is termed the original delta, to distinguish it from the delta that subsequently prograded into the reservoir during the experiments. The hydraulic sorting was generally unsuccessful except for grain sizes coarser than about the D_{90} and it is hypothesised that this was due to the irregular rate of sediment feed that was

employed. Each experiment was performed by running a constant discharge through the model while the dam was removed one section at a time. Following the removal of one section the model was run until the system equilibrated, but with stoppages in the flow to allow the delta surface to be scanned using a laser along closely spaced cross-sections. These delta surface elevation measurements were the principle data collected during the experiments, but other data were obtained from the sediment transported out of the model at the dam site; cores of the original delta prior to dam removal; armour layer and sub-armour layer samples at the end of dam removal; time lapse photography; and Particle Tracking Velocimetry (PTV).

Chapter 6 provides a detailed explanation of how the data were reduced and the steps taken to ensure that the information was as accurate as possible. The principle data used to test the research hypotheses were the delta erosion volumes obtained by Digital Elevation Model (DEM) differencing. The quality of the information obtained from differencing is affected by four sources of error: the individual data points that represent the surface; the surface fitted to the data points; the degree to which the DEM represents the real topography of the surface and its changes through time; and the algorithm used to perform the cut-fill analysis. The steps taken to minimise the size of these errors are described in detail.

In order to explain the differences in erosion volumes from run to run, a series of quantitative data, such as channel width, top terrace width, bed elevation change and longitudinal slope were obtained from both the DEMs and the time lapse photographs. The steps taken to obtain these data and to ensure their accuracy are also described.

The results of the data reduction described in Chapter 6 are presented in six main sections in Chapter 7. The first considers the distribution within the original delta of sediment grains of an armour-forming calibre at the start of each experiment and shows that there is a downstream fining amongst the coarsest of these grains. This has important implications for the morphodynamics of delta surface evolution that are presented qualitatively in the third main section. These are based mainly on the observations from the time lapse movies, but are cross-referenced to the quantitative changes in erosion volume and channel geometry for discrete 50-cm long sections of the delta surface. In particular, observations are presented that describe a disturbance to the armour layer that has not previously been reported in the literature, but which is

referred to herein as Bed Elevation Lowering Without Armour Layer Break-up (BELWALB). The adjustments to channel bed elevations, longitudinal profiles, channel and terrace widths, and planforms are presented in the final three sections of the chapter. The second section presents the results of the volumetric erosion analysis and shows that there is a significant difference in erosion volumes between the experiments in which the channel lies close to the basin boundary and those in which it lies along the centre of the delta surface at the onset of dam removal. These differences are shown to be due to several aspects of the irregular basin boundary shape in the original delta area.

A detailed consideration of experimental limitations and possible scale effects is presented at the start of Chapter 8, which is important as it ensures that the correct degree of confidence is attached to the interpretation of the significance of the results. These limitations notwithstanding, four principle findings emerge from the results. First, topographical steering has a significant impact on the volumes of original delta sediment eroded. Second, the erosion volumes are positively affected by both the magnitude of baselevel lowering and the length of the relaxation interval between intervals of lowering, although in a slightly more complicated way than presented in the two research hypotheses and which necessitates both hypotheses being modified. Third, mobility reversal may be an important phenomenon during dam removal, although its occurrence during the experiments may have been a scale effect. Finally, a previously unreported phenomenon termed BELWALB exists, which appears to operate at the threshold between armour layer stability and instability.

A summary of the findings is presented in Chapter 9, together with suggestions for research to further investigate the phenomena reported herein. Finally, it is noted that while the current research is of utility to the understanding of reservoir sediment dynamics during dam removal, it may also be useful to the understanding of these dynamics as they apply to the recovery of lost reservoir storage capacity during reservoir flushing.

Chapter 2 The Elwha River System

2.1 *Physiography of the Elwha River Basin*

The Elwha River is located on the Olympic Peninsula of north western Washington, in the United States (Figure 2.1). Its drainage basin is in Clallam County and covers 842 km² (325 mi²), 83% of which is within Olympic National Park. The basin contains over 161 km (100 miles) of tributary streams, while the main stem Elwha River rises at an elevation of about 1,370 m (4,500 ft) and flows northwards 72 km (45 miles) from the base of Mount Olympus to the Strait of Juan de Fuca (Bureau of Reclamation, 1996b).

The Olympic Peninsula has a maritime climate with mild, wet winters and cool, dry summers. Precipitation in the Elwha River basin ranges from 5,588 mm (220 inches) in the headwaters to 1,422 mm (56 inches) at the mouth (Bureau of Reclamation, 1996a). The climate in the valley is also transitional between the drier conditions that are characteristic of the eastern half of the Peninsula and the wetter conditions more characteristic of the western half. Most of the Elwha Basin is composed of upland and riparian forest communities that include stands of conifers (*coniferae*) (mostly Douglas fir (*Pseudotsuga menziesii*)), mixed conifers and hardwoods, and hardwoods (red alder (*Alnus rubra*), big-leaf maple (*Acer macrophyllum*), black cottonwood (*Populus balsamifera trichocarpa*) and willow (*Salicaceae*). Wetland vegetation consists of forest (willow and red alder), shrub and scrub, and emergent communities (National Park Service, 2005).

Geologically, the Olympic Peninsula is composed mostly of marine sedimentary and igneous rocks from the Tertiary (2 to 65 million years old) that have been slightly metamorphosed and subjected to intense folding and faulting. Glaciers that extended from the Olympic Mountains during the last ice age carved the U-shaped valleys that contain all the major rivers draining the Peninsula, including the Elwha, while the large continental ice sheet that extended from the north also covered part of the peninsula. In the lowlands between the Olympics and the Strait of Juan de Fuca, till was deposited during the last glacial maximum. These tills were subsequently overlain by glacial outwash deposits from the retreating alpine glaciers and the Juan de Fuca lobe of the Cordilleran ice sheet. Subsequently, the Elwha

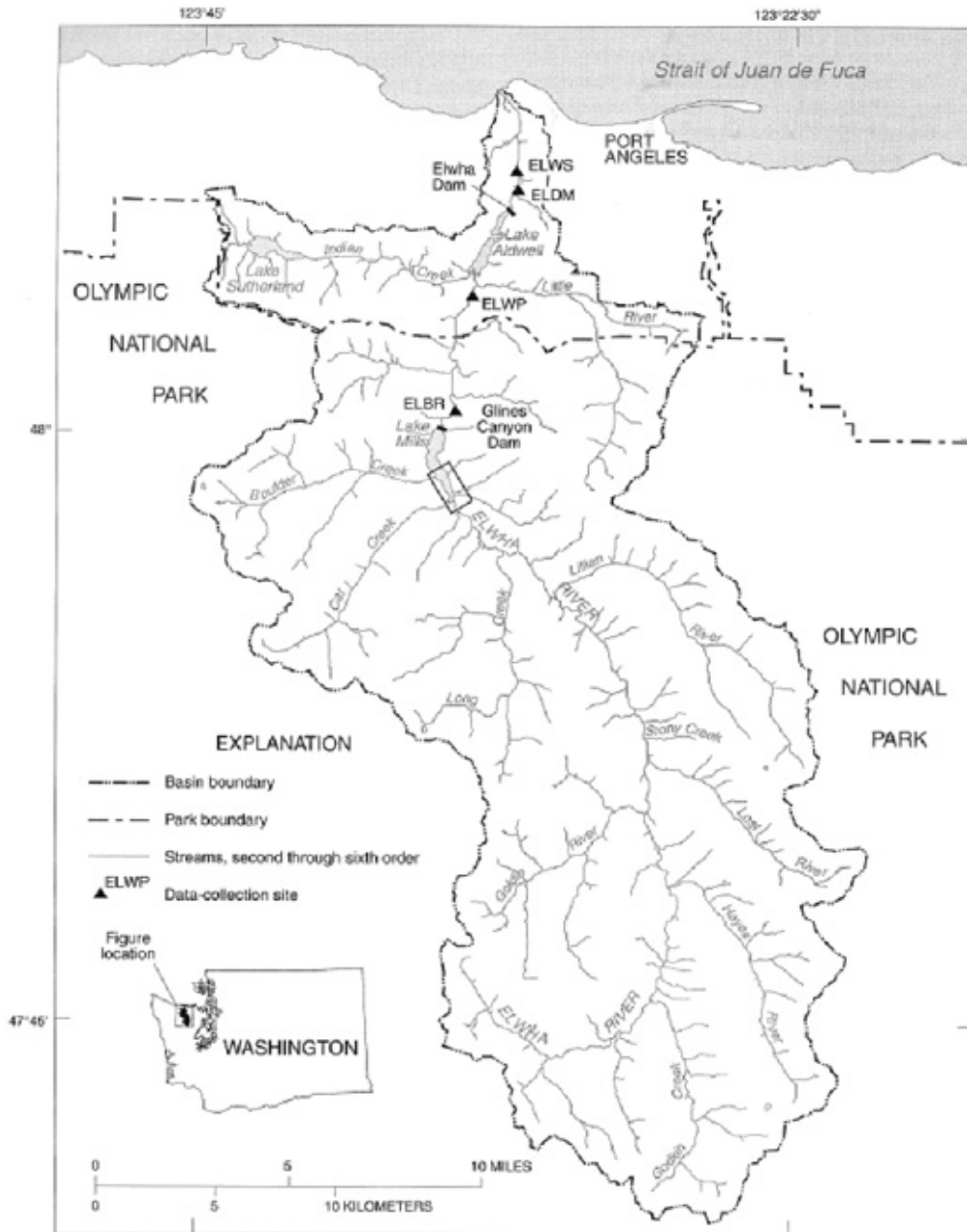


Figure 2.1. Site location. Modified from United States Geological Survey (2000).

incised through them, leaving the glacial and outwash deposits perched high on the sides of the Elwha Valley and creating the high terraces that flank the downstream-most reaches of the river (Figure 2.6b). These glacial deposits, together with material from landslides and post-glacial alluvial material, are the principal sources of sediment transported by the river (Bureau of Reclamation, 1997; Hosey and Associates, 1988). This geological history results in very deep, excessively drained

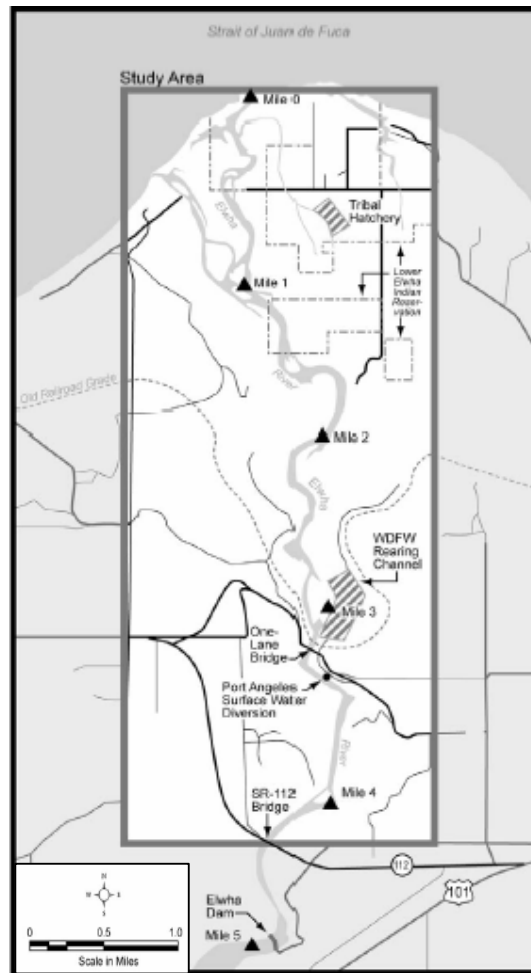


Figure 2.2. Study area. Modified from National Park Service (2005).

soils at lower elevations, transitioning to moderately deep and moderately well drained soils at higher elevations (Clallam gravely sandy loam) (National Park Service, 2005).

The Elwha is a steep, coarse-bedded mountain river along much of its course, with a mean gradient of 1.9% (Bureau of Reclamation, 1996a). Mean gradients in the headwaters, upstream from river kilometre (RK) 69 (river mile (RM) 43), average 16%. The river flows through a series of steep, narrow, bedrock canyons whose parent material was able to resist the scouring action of the alpine glaciers. Between the canyons, where the underlying geology was more easily scoured by the glaciers, channel slope decreases and the floodplain widens considerably. Deltas of coarser sediment and woody material have been deposited where the river leaves a constricting canyon and diverges onto a broader floodplain area (Bureau of

Reclamation, 1996a; Foster Wheeler Environmental Corporation, 2000; National Park Service, 2005). In the alluvial reaches upstream from Lake Mills, the channel displays an actively migrating, meandering planform with pool-riffle sequences and eroding banks. In places, the river undercuts the alluvial and glacial terrace deposits at the margins of the floodplain, which contribute additional material to the sediment load.

These large longitudinal variations in valley and channel morphology are typical of mountain rivers around the world that drain catchments ranging across many orders of magnitude in area, as is the transport of mostly non-cohesive and coarse sediments (Wohl, 2000). Furthermore, many dams are built on mountain rivers in narrow, bedrock-dominated, sections that frequently impound the wider valley sections upstream, since this maximises the storage volume for a given dam height (Graf, 1999). Finally, the removal of any dam will result in dramatic changes to local system energy levels associated with the generally rapid and large drop in baselevel. These factors are important because they suggest that where lateral channel adjustments are able to occur over a prograding alluvial surface that is significantly wider than the equilibrium channel width and that is capable of generating an armour layer, then phenomena such as those reported in Chapters 7 and 8 are likely to occur in locations other than the Lake Mills model. This transferability of form-based results is identical to that associated with, for example, the widespread occurrence of self-propagating knick points (those that maintain their form as they migrate upstream), which occur where there is a drop in baselevel in cohesive sediments or where more erosion-resistant alluvium overlays less erosion-resistant material, or to the occurrence of braided channel planforms, which occur where the volume of bed load and stream power are sufficiently high. Both these morphological expressions are found in many different environments and across many orders of magnitude.

2.2 Human activity in the basin

2.2.1 Introduction

Humans first crossed from Asia into the Pacific Northwest of North America more than 12,500 years ago (Eshleman *et al.*, 2003) and the Lower Elwha Klallam people, a hunter-gatherer tribe, have lived in the Elwha River Valley for several

thousands of years (National Park Service, 2005). Europeans first explored the Olympic Peninsula in the late 1700s, but European-Americans did not settle in the Elwha Valley until the 1860s and 1880s in the lower and upper valleys respectively. In 1855, the Lower Elwha Klallam Tribe signed the Treaty of Point No Point, which allowed them to fish at their 'usual and accustomed' fishing places, but not to reside near these places. Citizens of the United States, or foreigners who intended to become citizens, who settled in the Elwha Valley, were able to acquire land from the government in order to develop homesteads. Native Americans, who were considered neither citizens nor foreigners, were unable to obtain the right to set up homesteads in their own lands. This situation persisted until 1884 and the passage of an effective Native American homestead law. By 1894 the Tribe had obtained legal title to 5.26 km² (1,300 acres) of land in the lower Elwha Valley where they were able to farm and raise livestock, but it was not until 1968 that they were officially allowed to create a reservation for themselves (National Park Service, 1996; 2005).

2.2.2 The Elwha River dams and their effects on the Elwha River System

2.2.2.1 Cultural and socio-economical effects

The climate on the peninsula limited the agricultural activity of European-American settlers to not much more than a subsistence level, while opportunities for logging and mining in the valley disappeared when the land was set aside for the Olympic Forest Reserve in 1897, the Mount Olympus National Monument in 1909 and Olympic National Park in 1938. In 1894, Thomas T. Aldwell began buying land on which to build a hydroelectric facility and, in 1910, with George A. Glines, he formed the Olympic Power and Development Company to build the structure itself (National Park Service, 1996). Elwha Dam was built from 1911 to 1913 at RK 7.9 (RM 4.9) and impounds Lake Aldwell, a 10 million-m³ (8,100 acre-feet) reservoir (Figure 2.3a; Figure 2.4a&c). It is a 32.9-m (108-ft) high concrete gravity structure. Glines Canyon Dam was built from 1925 to 1927 at RK 21.6 (RM 13.4) and is a 64-m (210-ft) high, variable radius, concrete, thin-arch structure (Figure 2.3b; Figure 2.5a&c). Its reservoir, Lake Mills, has a volume of 50 million m³ (40,500 acre-feet) (Bureau of Reclamation, 1996b). Despite state laws that required them, neither dam was built with fish passage facilities (National Park Service, 1996).

The dams provided a reliable source of electricity to Port Angeles, a number of other towns on the Peninsula and to lumber mills and military facilities, thus helping the peninsula's economy to develop (National Park Service, 1996), but their effects were disastrous for the Lower Elwha Klallam Tribe. With the completion of Elwha Dam, the 10 runs of salmon and trout were completely eliminated from all but the downstream-most 7.9 km (4.9 miles) of the river (section 2.2.2.3), thus directly contravening the rights promised to the Tribe under the Point No Point Treaty. While the tribal homesteaders were able to grow a few crops and raise some livestock to sell to the settlers, the fishery was, and continues to be considered as, the Tribe's most important economic asset. Given the almost complete absence of any other significant sources of revenue, the loss of this fishery has had a very negative impact on the Tribe's economic position (National Park Service, 1996), which has created problems of low self-esteem and stress-related health issues for some tribal members (Bachtold, 1982, cited in National Park Service, 2005). In addition, the dams and their reservoirs have buried or flooded tribal villages, fishing camps, homesteads, sites for gathering plants used for medicinal, food and food preparation purposes and, possibly, ancient burial sites. They have also made a number of the Tribe's most important spiritual sites inaccessible. In particular, Elwha Dam and Lake Aldwell have buried the site where the Tribe believes that the Creator made their ancestors. Tribal members used to visit this site to receive spiritual guidance and information about their future life (National Park Service, 1996; 2005). The importance of the river and its salmon runs is perhaps best and most simply summarised by the Tribe's River Restoration Director, who states, "The Tribe has lived along the banks of the Elwha River since time immemorial. Our ties to the river and salmon have deep spiritual and cultural significance. They are at the very heart of the Lower Elwha Klallam people" (www.elwha.org/rrdearreader.htm).

2.2.2.2 Geomorphological and hydrological effects

Because Lake Aldwell and Lake Mills are both hydrologically small reservoirs, with a ratio of storage capacity to mean annual flow of about 0.007 and 0.037 respectively (section 1.4), and have been operated as run-of-river since 1983 and 1975 respectively, they have relatively little impact on the annual runoff hydrograph and particularly little effect on storm flood hydrographs (section 1.3.1.1). Mean annual flow at the McDonald Bridge stream gauge (Figure 2.1) is about 42 m³/s



Figure 2.3. Aerial view of the two Elwha River dams and reservoirs. (a) Aerial view of Elwha Dam and Lake Aldwell (Source: <http://www.nps.gov/archive/olym/elwha/photos/aeriallwr.htm>). (b) Aerial view of Glines Canyon Dam (Source: <http://www.nps.gov/archive/olym/elwha/photos/aerialglines.htm>).

(1,500 cfs), rising to $47 \text{ m}^3/\text{s}$ (1,650 cfs) at the river mouth, while summer low flows range from 8 to $14 \text{ m}^3/\text{s}$ (300 to 500 cfs). High flows occur during winter and spring

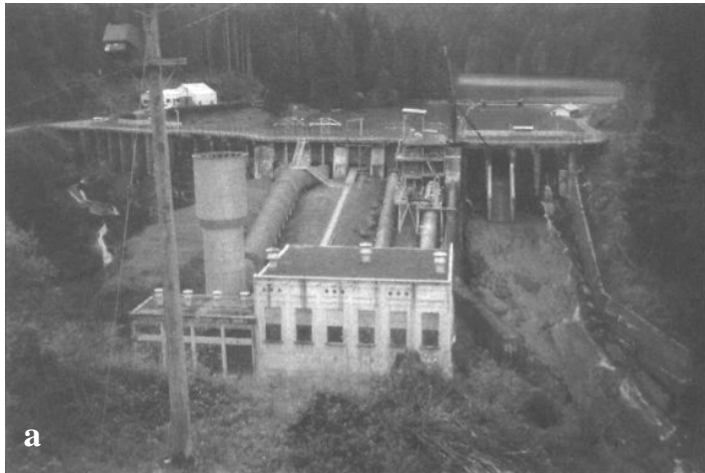


Figure 2.4. Elwha Dam site. **(a)** Elwha Dam. **(b)** Artists impression of the Elwha River in the area currently occupied by Elwha Dam following channel recovery after dam removal. (Source: http://www.nps.gov/archive/olym/elwha/docs/eis0496/figure23_24.jpg). **(c)** Lake Aldwell. **(d)** Artists impression of the Elwha River floodplain in the area currently occupied by Lake Aldwell following channel recovery after dam removal. (Source: http://www.nps.gov/archive/olym/elwha/docs/eis0496/figure25_26.jpg).

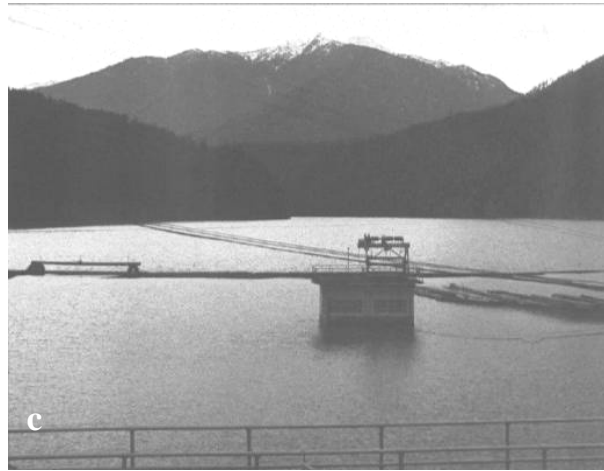
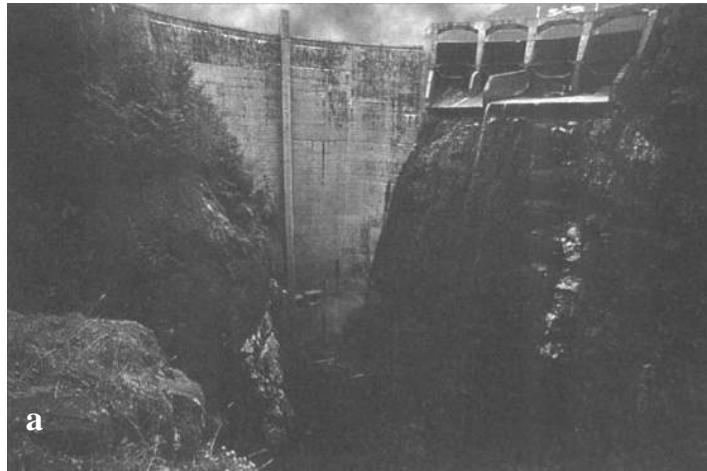


Figure 2.5. Glines Canyon Dam site (a) Glines Canyon Dam. (b) Artists impression of Glines Canyon following channel recovery after dam removal. (Source: http://www.nps.gov/archive/olym/elwha/docs/eis0496/figure27_28.jpg). (c) Lake Mills. (d) Artists impression of the Elwha River floodplain in the area currently occupied by Lake Mills following channel recovery after dam removal. (Source: http://www.nps.gov/archive/olym/elwha/docs/eis0496/figure29_30.jpg).

snowmelt periods. The two-year flood is 368 m³/s (13,000 cfs), while the 100-year flood is 1,212 m³/s (42,800 cfs) (Bureau of Reclamation, 1996a). The two reservoirs operate as efficient sediment traps, however, and channel morphology from Rica Canyon (immediately upstream from Lake Mills) to the mouth of the river has been altered significantly by their impacts on longstream sediment transport and connectivity in the fluvial system.

In total, the two reservoirs have flooded 8.5 km (5.3 miles) of the river and 2.77 km² (684 acres) of valley bottom land. Lake Mills is 4 km long (2.5 miles) and floods what was formally a 274 to 457 m-wide (900 to 1,500 ft) valley bottom. The pre-impoundment channel through this reach had a mean slope of about 1%, with a sinuous planform (Figure 2.5d) and gravel and cobble bars that were fairly active during flood flows, although less so than those in the alluvial reach upstream from Rica Canyon are at present (Hosey and Associates, 1988). In the 9.2-km (5.7-miles) reach between Glines Canyon Dam and the upstream limit of Lake Aldwell, the channel ranges from 61 to 122 m wide (200 to 400 ft) (Foster Wheeler Environmental Corporation, 2000). Comparison of recent aerial photographs with the 1926 survey reveals that there has been little channel migration, while the pre- and post-dam slopes have remained at about 0.7% due to bedrock control. This evidence indicates that there has been no channel incision downstream of Glines Canyon Dam (Bureau of Reclamation, 1996a; Foster Wheeler Environmental Corporation, 2000). Instead, the sediment-free releases have winnowed significant quantities of sand and gravel from the channel bed, leaving behind a heavily armoured, laterally stable channel dominated by cobbles, boulders and bedrock. The remaining channel bars are now covered with trees, indicating that they have been stable for some time, probably due to coarsening and reduced mobility of the bar surface material. This is in contrast to the unvegetated gravel bars in the alluvial reaches upstream from Rica Canyon, which remain active during floods. The armour layer downstream from Glines Canyon Dam is composed of about 40% boulder, 50% cobble and 10% gravel with traces of sand (Bureau of Reclamation, 1996a; Hosey and Associates, 1988). The channel is thus relatively immobile during the two- and 10-year floods and its morphological complexity has been reduced due to the erosion of gravel bars and low alluvial terraces (Pohl, 2004). The small volumes of sand and gravel that are transported through the reach are supplied by tributaries during flood flows and through

occasional reworking of the remaining active channel bars (Foster Wheeler Environmental Corporation, 2000).

Conditions in the area currently occupied by Lake Aldwell prior to the construction of Elwha Dam were very similar to those in the area now occupied by Lake Mills. The channel was meandering, with gravel and cobble bars. In the upstream two-thirds of Lake Aldwell the river flowed through a 305 m-wide valley (1,000 ft), while in the downstream third of the reservoir the valley was only a few tens of metres wide. Between the two valley sections is a narrow bedrock canyon (Hosey and Associates, 1988).

Downstream from Elwha Dam, from RK 6.4 to 4.0 (RM 4.0 to 2.5), there is a reach that is transitional between the bedrock-controlled upper reaches and the alluvial reaches of the river downstream. While bedrock in the upper reaches prevented channel incision in response to the construction of Glines Canyon Dam, some incision has occurred in the alluvial reach downstream of Elwha Dam, from RK 4.0 to 0.0 (RM 2.5 to 0.0) where geological control is absent. The composition of the armour layer in the transitional reach is about 10% boulder, 75% cobble and 15% gravel with traces of sand (Bureau of Reclamation, 1996c). Downstream from RK 4.7 (RM 2.9) the floodplain widens considerably into a wedge shape (in plan view) and the channel is incised into glacial outwash sediments, while the floodplain is flanked by 50 m-high cliffs of glacial outwash material that are, in places, being undermined by the actively migrating channel (Figure 2.6b). Within the channel, active gravel bars become increasingly common in the downstream direction, while evidence from historical air photos establishes that the channel has continued to migrate across its floodplain since the closure of Elwha Dam (Hosey and Associates, 1988). Active meandering has been accompanied by a net increase in channel length of about 1.1 km (0.7 miles), which corresponds to a decrease in mean slope from 0.39% to 0.33% (Hosey and Associates, 1988). The channel appears to be reducing its slope, and therefore its sediment transport capacity, in order to compensate for the essentially sediment-free water being released from Lake Aldwell (see '(i) Dam construction' in section 1.3.1.2). The availability of large amounts of sediment in the floodplain means that armouring is less well developed and less coarse grained than further upstream,

being about 55% cobble and 45% gravel with some sand (Bureau of Reclamation, 1996c).

Four sets of fluvial terraces lie adjacent to the river in the reach between Glines Canyon Dam and the Strait, although they are not all present along the full length of this reach. They range from 0.9 to 1.2 m (3-4 ft), 1.5 to 2.1 m (5-7 ft), 3.0 to 3.7 m (10-12 ft), and 4.6 to 5.5 m (15-18 ft) above the channel bed. It has been hypothesised that the two lowest terraces may be related to channel incision following the closure of the two dams (Bureau of Reclamation, 1996c), although this can only be the case downstream from RK 6.4 (RM 4.0), since the reach upstream from this point is controlled by bedrock.

The sediment-trapping effects of reservoirs can result in adverse coastal impacts if the river is unable to replace its lost sediment load from other sources. Beach erosion of the Elwha River delta occurred between the 1960s and 1980s, but this cannot be categorically ascribed in part or whole to the presence of the dams. The onset of this erosion occurred several decades after the two dams were closed and coincided with the construction of a riprap jetty across the river's mouth (Figure 2.6a) in the mid-1960s to stop the mouth's westward migration. The jetty may have caused beach loss by preventing the eastward longshore drift of sediment along the southern shore of the Strait. Furthermore, much, although not all, of this erosion has been reversed by subsequent aggradation, due to the large volumes of sediment being eroded from the cliffs of glacial outwash material near the river mouth (Hosey and Associates, 1988) (Figure 2.6b). However, the reduction in sediment entering the estuarine area has degraded the habitat. This area is important for out-migrating juvenile salmonids, since it is here that they adapt physiologically for life in salt water, in a process known as smoltification.

About 7.2 km (4.5 miles) east of the delta is Ediz Hook (Figure 2.1), whose rate of growth has been slowing since the 1930s. This is due mostly to the construction of a pipeline and protecting riprap at the base of the cliffs in 1930, immediately to the west of the Hook, which reduced the rate of sediment supply from the eroding cliffs from 198,800 to 30,600 m³/yr (7.02 million to 1.08 million ft³/yr) (Hosey and Associates, 1988). The reduction of sediment from this source accounts for over 70% of the material formerly supplied to Ediz Hook (Triangle Associates, 2004). The reduction in sediment supplied from the Elwha River may therefore be a

smaller contributing factor to the reduced growth rate of the Hook, especially since the river has begun eroding the glacial outwash cliffs near its mouth. The sediment in these cliffs and the adjacent floodplain area is a finite source, however, and would ultimately be exhausted by river reworking and without the annual influx of sediment from the terrestrial catchment. This point may be reached sooner rather than later, given that the need to protect the levees and other infrastructure will mean that the river will not be allowed to rework the full width of its floodplain and delta (Figures 2.2 & 2.9).

2.2.2.3 Biological effects

Both dams were built without fish passage facilities, so the completion of Elwha Dam blocked the upstream migratory routes for 10 runs of salmon and trout at RK 7.9 (RM 4.9). As a result, the estimated annual spawning population of 392,000 fishes prior to dam closure has been reduced to about 3,000 naturally spawning individuals at present. The 10 runs are summer/fall and spring chinook (*Oncorhynchus tshawytscha*); coho (*O. kisutch*); pink (*O. gorbusa*), chum (*O. keta*) and sockeye (*O. nerka*) (all salmon); cutthroat trout (*O. clarki*); winter and summer steelhead trout (*O. mykiss irideus*); Dolly Varden (*Salvelinus malma*); and bull trout (*S. confluentus*) (all trout). Of these, the chinook and bull trout have been listed as Federally threatened⁸ species under the Endangered Species Act, while the coho salmon is a candidate for listing. In addition, the pink, chum, and sockeye salmon, sea-run cutthroat trout and Dolly Varden have all been listed as Washington State species of concern (National Park Service, 2005). The biggest single factor contributing to these declines is undoubtedly the fact that Elwha Dam blocks off so much of these species' historical ranges (Figure 2.7). In summary, up to RK 69.2 (RM 43) out of the 72.4 RKs (45 RMs) of total mainstem river and about 113 RKs (~70 RMs) in total of the Elwha's drainage network is inaccessible to these runs (National Park Service, 2005). In addition, the habitat that does remain downstream from Elwha Dam is of markedly reduced quality and quantity due to the erosion of spawning-size gravels and the lack

⁸ A species listed as 'threatened' under the Endangered Species Act (ESA) is defined as "any species which is likely to become an endangered species within the foreseeable future throughout all or a significant portion of its range." A species listed as 'endangered' under the ESA is defined as "any species which is in danger of extinction throughout all or a significant portion of its range." (<http://www.nmfs.noaa.gov/pr/species/esa.htm>).

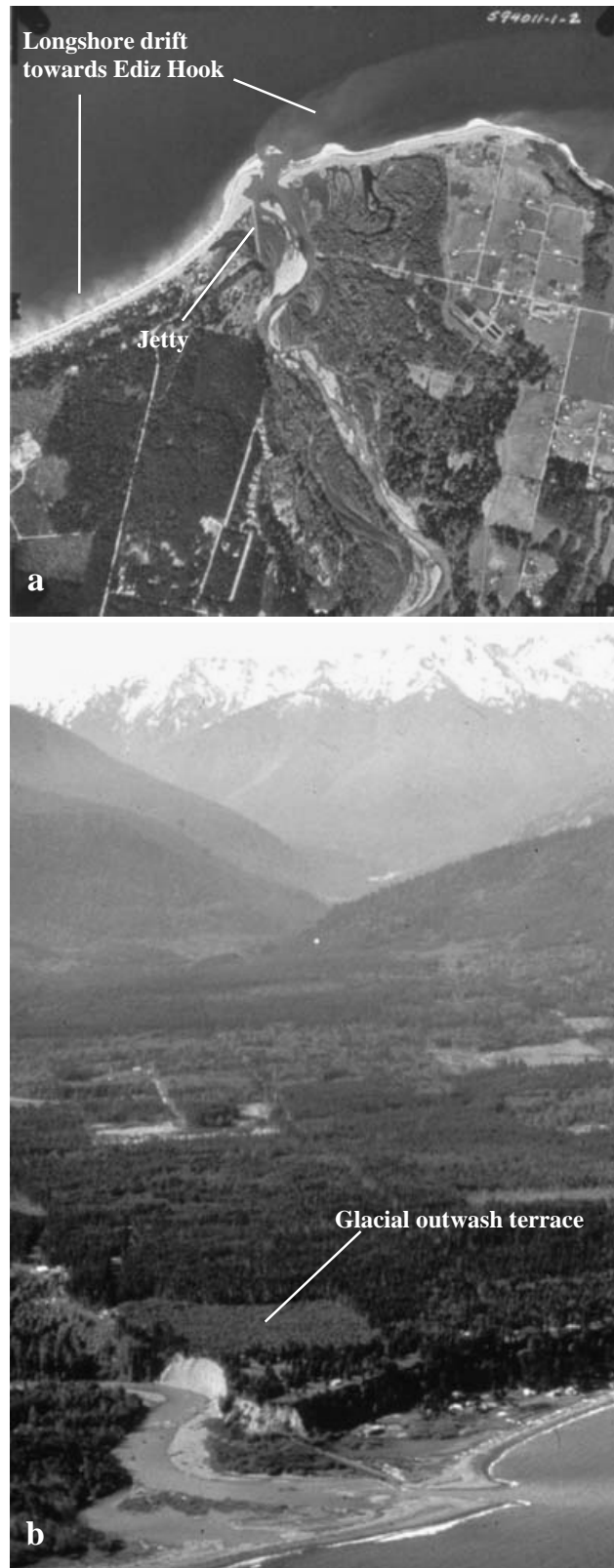


Figure 2.6. (Previous page). Elwha River mouth. (a) Overhead aerial view of the mouth of the Elwha River. (Source: <http://www.nps.gov/archive/olym/elwha/photos/elwhamouth.htm>). (b) Oblique aerial view of the mouth of the Elwha River. (Source: <http://www.nps.gov/archive/olym/elwha/photos/mouthmountain.htm>).

of replenishment from upstream (section 1.3.1.2i); overcrowding that facilitates the spread of disease; water temperatures that are 4°C to 8° C too warm during summer and autumn; water that is insufficiently oxygenated and excessively nitrogenated during spillway releases; a reduced flow of nutrients that impacts primary productivity and thus the availability of macroinvertebrates for food; a reduced supply of large woody material that provides shelter during winter and increases the quantity of instream habitat; and a degraded estuary environment (National Park Service, 1995; 2005) (section 1.3.1).

The decline in fish numbers may have also had more widespread adverse biological effects. Anadromous fish that return to spawn are important sources of marine-derived nutrients for the freshwater aquatic and terrestrial ecosystem, such as nitrogen, phosphorus and carbon, which they deliver to the ecosystem through excretion, gametes, their carcasses, and newly-hatched juveniles (fry). These nutrients benefit the entire ecosystem, including macroinvertebrates, other fish, and riparian vegetation (Bilby *et al.*, 1996; Gregory *et al.*, 2002; Winter *et al.*, 2000). They may be particularly important in streams where the primary and secondary productivity is poor due to a combination of shading, low water temperatures and frequent high flows (which prevent periphyton establishing on the substrate), which is the case in many streams in the Pacific Northwest (Bilby *et al.*, 1996; Winter *et al.*, 2000). The Elwha River appears to be such a stream in that its neutral to slightly alkaline waters indicate oligotrophic (low biological productivity) conditions (National Park Service, 2005). The nutrients supplied by spawning salmon have been shown to increase the size and growth rate of juveniles, thus increasing their over-winter and marine survival rates and therefore the number that return to spawn (Bilby *et al.*, 1996). In streams where autochthonous and allochthonous inputs of energy are poor, the loss of spawning anadromids may therefore contribute to a steady decrease in the quantity of nutrients available for recycling, and thus the ecosystem's ability to support fish, through a process of positive feedback (Bilby *et al.*, 1996; Winter *et al.*, 2000). The reduction in spawning salmon may also affect numerous other species that prey on them or scavenge their carcasses (Winter *et al.*, 2000). In the case of the Elwha, there are 22 such species of birds and mammals, including the black bear (*Ursus americanus*),

mink (*Mustela vison*), mountain lion (*Felis concolor*), bobcat (*Lynx rufus*), and river otter (*Lutra canadensis*) (National Park Service, 2005).

2.3 Objectives of the proposed dam removals

2.3.1 Overall project objectives and anticipated benefits

In view of the massively deleterious impacts that the two dams have had on the physical, biological and socio-cultural fabric of the Elwha River system and those who traditionally depended on it, the two structures are due to be removed in a collaborative venture between the United States National Park Service (NPS); Bureau of Reclamation (BoR); Fish and Wildlife Service; Bureau of Indian Affairs; US Army Corps of Engineers; and the Lower Elwha Klallam Tribe (Bureau of Reclamation, 1996b; United States Geological Survey, 2000). The goal of the removal is to allow the 10 runs of fish to access their historical spawning grounds in order that their numbers might return to healthy levels and to allow the Elwha River and ecosystem as a whole to recover its natural, self-regulating state. Five alternatives were considered to achieve this aim: no action; installation of fish passage facilities at both dams; removal of only Elwha Dam; removal of only Glines Canyon Dam; and complete removal of both dams while allowing the river to naturally erode the impounded sediment (the proposed action) (Figure 2.4b&d; Figure 2.5b&d). It was determined that only the proposed action would achieve the “full restoration of the Elwha River ecosystem and native anadromous fisheries” (National Park Service, 1995) called for and authorized by the Elwha River Ecosystem and Fisheries Restoration Act (the Act) (PL 102-495, Section 4(a)(1)) (United States Congress, 1992).

The Elwha’s water quality has been rated as Class AA (of “extraordinary” quality) by Washington State (National Park Service, 1996) and the Elwha River watershed is in pristine condition (Bureau of Reclamation, 1997), so it is thought that the stated restoration goals have a very good chance of being achieved. Nine of the 10 anadromous species have a ‘good’ or ‘excellent’ restoration potential, but sockeye salmon are only rated as ‘poor/fair’. This is because they require a lake habitat to fulfil part of their life cycle and the quality of Lake Sutherland, the only accessible lake in the Elwha Basin (Figure 2.7), has been degraded by development along its shoreline (National Park Service, 1995). It is estimated that under the proposed action,

close to 400,000 individual fish would return each year and that they would contribute about 363,600 kg (800,000 lb) and about 5,900 kg (13,000 lb) of nitrogen and phosphorus respectively to the ecosystem (National Park Service, 1995) (section 2.2.2.3).

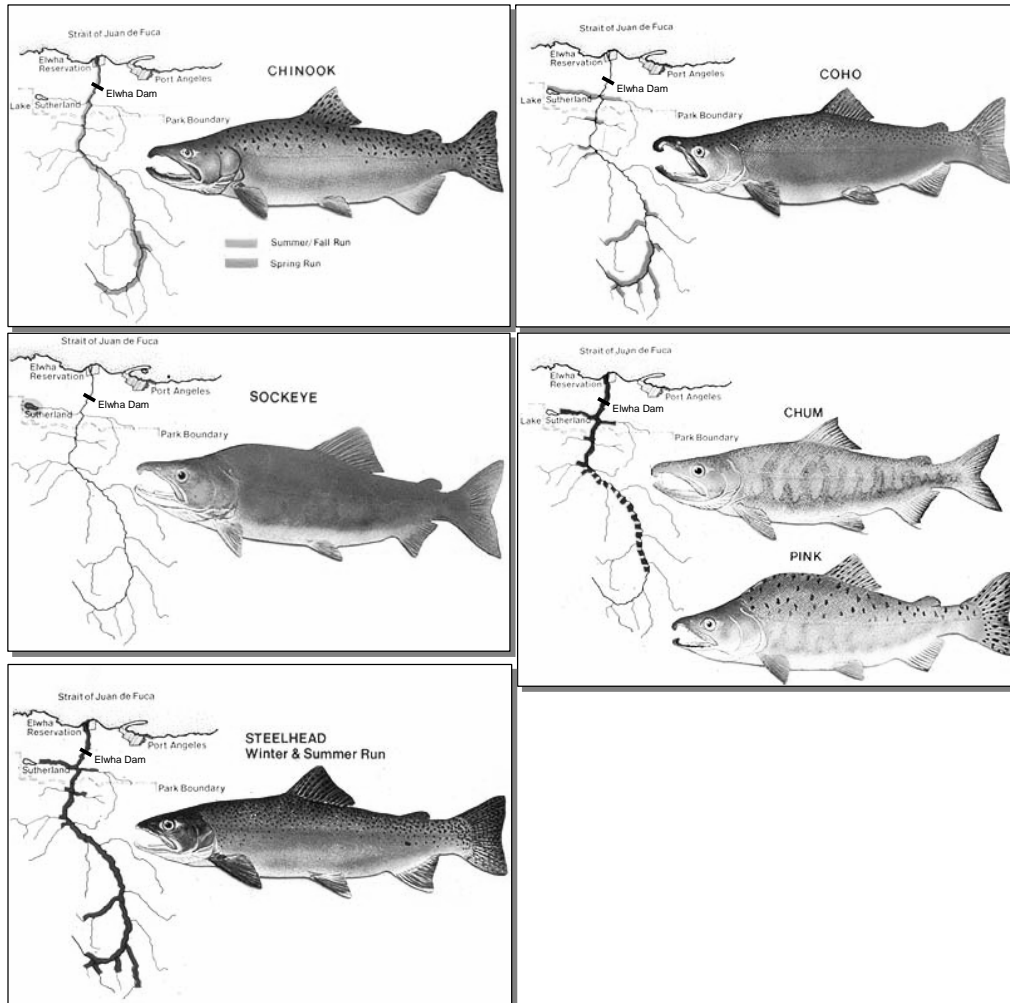


Figure 2.7. Historical spawning ranges of some of the Elwha River basin's anadromous fish species. The location of Elwha Dam is shown for reference (Modified from Source: <http://www.nps.gov/archive/olym/elwha/documents.htm>).

Achieving the restoration goals will have major benefits. Firstly, the Elwha's ecosystem will return to its natural, self-sustaining condition. In turn, this will benefit the Tribe's economy and that of Clallam County as a whole. The total cost of the 10-year restoration programme is estimated at \$182.5 million (£101.4 million), while the total benefits over a 100-year period with a 3% discount rate are estimated at \$365.6 million (£197.4 million): tribal and non-tribal commercial fishing \$36.7 million (£20.4 million); sports fishing \$10.3 million (£5.7 million); savings on maintenance of

Ediz Hook \$1.0 million (£0.55 million); and tourism and recreation \$317.6 million (£176.4 million) (National Park Service, 2005). This results in a benefit to cost ratio of 1.95:1, making the proposed alternative the only one in which the economic benefits will exceed costs (Meyer *et al.*, 1995). Also, the cultural integrity of the Lower Elwha Klallam Tribe will be restored to a condition closer to that which existed prior to the arrival of European-American settlers. A number of other objectives must be met while achieving the restoration objectives: the quality and quantity of water supply to municipal and industrial users must be preserved; flood protection for properties and infrastructure must be maintained at existing levels; any adverse impacts to septic tanks must be mitigated; and chinook and bull trout must be protected as much as possible during dam removal (National Park Service, 2005).

It will only be possible to assess the extent to which the proposed action achieves the goal of full ecosystem restoration a number of years after the two dams have been removed and only if a comprehensive programme of post-project appraisal monitoring has been implemented and sustained. On a purely academic note, however, there must be some doubt as to whether the project will constitute a true river ‘restoration’, which has been defined by Sear (1994, p.170) as ‘The act of restoring (a river) to a former or original condition’ and, perhaps most comprehensively and unambiguously by Cairns (1991) as ‘the complete structural and functional return to a pre-disturbance condition’. In addition, Berger (1990, cited in Brookes, 1996, p.571) notes that:

‘It is axiomatic that no restoration can ever be perfect; it is impossible to replicate the biogeochemical and climatological sequence of events over geological time that led to the creation and placement of even one particle of soil, much less to exactly reproduce an entire ecosystem. Therefore all restorations are exercises in approximation and in the reconstruction of naturalistic rather than natural assemblages of plants and animals within their physical environment.’

A number of factors may be operative that are unrelated to dam removal and that may prevent restoration (*censu* Cairns) from being realised. First, there is the aforementioned problem associated with the complete recovery of sockeye salmon due to development around Lake Sutherland. Second, the health of anadromous populations is highly dependent on oceanic conditions (food supply) (National Research Council, 1996), which varies naturally, but which may be adversely affect

over the coming decades by anthropogenic climate change. Third, as the coarse sediment fraction in particular is released from the reservoirs, this will increase the channel's lateral mobility, particularly on the Elwha River Delta, but this increased channel movement will not be allowed to compromise the human infrastructure and levees that have been built downstream from Elwha Dam (Figures 2.2 & 2.9). The channel will thus be partially constrained in this area, which will therefore impact process-form interactions to a certain extent. Whether this will have any measurable impacts on the biological components of the ecosystem is currently unknown. Finally, it is unlikely that all post-dam sediment will be eroded from the reservoir area in the medium term following dam removal, if at all, which will clearly not represent a 'return to a pre-disturbance condition', since the valley in the Lake Mills and Lake Aldwell areas cannot recover its pre-impoundment topography. On the other hand, if these deposits are left behind as terraces on the valley sides that are inaccessible to floods, then for all practical purposes they could not be said to be interfering with or otherwise preventing a complete structural and functional return of the river to pre-disturbance conditions.

In addition to 'restoration', the terms rehabilitation, enhancement and creation are also used when describing management interventions (Brookes, 1996). 'Rehabilitation' concentrates only on some structural or functional elements of the fluvial system, with respect to a pre-disturbance condition, while 'enhancement' is considered to be an improvement to functional or structural elements, but without reference to a pre-disturbance condition. 'Creation' is considered to be the creation of a new ecosystem that did not exist prior to the disturbance (Brookes, 1996). If a gradation of management interventions ranging from creation, as the least ideologically desirable option, through enhancement and rehabilitation to restoration as the most ideologically desirable option, is constructed, however, then the Elwha River Project should be located very close to what can be considered a true restoration (*censu* Cairns) and certainly closer than the vast majority of other river management projects. The catchment land use upstream from Elwha Dam is pristine and unchanged from pre-dam conditions and, together with the imposed geology and climate, completely determines the water and sediment regimes in the catchment. Once fluvial and riparian form-process interactions have adjusted to the removal of the two dams, then the structural and functional components of the Elwha River

Catchment, at least as far downstream as the floodplain infrastructure downstream from Elwha Dam, will be essentially exactly as they would otherwise have been had the dams never existed.

2.3.2 Dam removal methodology

The dams will be removed concurrently over a two-year period, the details of which are provided in National Park Service (2005). Only the details of the removal of Glines Canyon Dam are outlined here because of their relevance to the physical modelling investigation. Lake Mills will be drawn down from elevation 173.8 m to 163.1 m (570.3 to 535 ft) using the spillway and penstocks. The dam will then be cut down to the elevation of the base of the penstocks in blocks each about 2.29 m high (7.5 ft) and weighing about 35.75 metric tons (35 U.S. tons). Below this elevation, draining the reservoir will continue by blasting notches 7.6 m wide by 4.6 m deep (25 ft by 15 ft) on alternating sides of the dam at about two week intervals (except during ‘fish window’ periods - see section 2.3.3.1. These notches will overlap by 2.29 m (7.5 feet), so the reservoir’s water surface elevation will drop by 2.29 m every two weeks. In between the blasting of each notch, the uppermost 2.29-m of the dam will be removed (Figure 2.8). This process will continue until the entire structure has been removed to the elevation of the pre-dam channel bed (National Park Service, 2005).

2.3.3 Issues of concern

The proposed restoration programme is not without its difficulties, however, most of which are related to the large volumes of sediment stored in the two reservoirs. Lake Aldwell impounds about 3 million m³ (3.92 million yd³) of sediment (out of a total storage capacity of 10 million m³ / 13.08 million yd³), while Lake Mills impounds about 11.85 million m³ (15.5 million yd³) (out of a total storage capacity of 50 million m³ / 65.4 million yd³) (Bureau of Reclamation, 1996a), which together represent the products of 92 years of river sediment transport. The release of such large volumes of sediment has the potential to adversely affect the ecosystem and human infrastructure downstream from the two dams, at least in the short term.

2.3.3.1 Biological issues

The biological impacts of releasing large volumes of sediment have already been discussed (section 1.3.1.3ii) and many will occur during dam removal. During a

1994 drawdown experiment (section 2.3.5), maximum suspended sediment concentrations of 6,110 mg/L were recorded at the downstream end of the incising

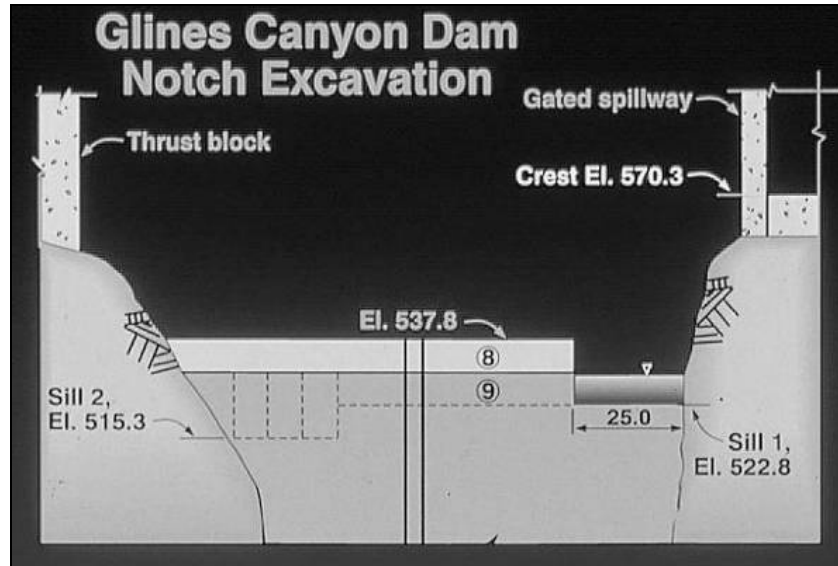


Figure 2.8. Proposed notch removal scheme for Glines Canyon Dam. Image courtesy of Bureau of Reclamation.

delta (United States Geological Survey, 2000), and levels downstream from the dams are expected to exceed 50,000 mg/L for short periods of time (Bureau of Reclamation, 1997) as silts and clays in the reservoir bottomset deposits are eroded. The worst case scenario is that such concentrations will induce catastrophic macroinvertebrate drift and mortality, while also killing fish directly (*e.g.* Wohl and Cenderelli, 2000) and stressing many others. In addition, the high concentrations and turbidity levels at the mouth of the river may discourage returning spawners from entering the Elwha in the first place, thus causing them to seek other rivers (Elwha River Fish Restoration Plan, 2003; National Park Service, 1995).

At worst, then, several year classes of fish could be seriously and/or permanently impaired. In practice, however, a number of measures will be employed to ensure that no year class of any species is damaged or lost. These include relocating the Tribal fish hatchery (Figure 2.2) and supplying it with water from the new water treatment plant; supplying the Washington Department of Fish and Wildlife (WDFW) chinook-rearing channel (Figure 2.2) with water from the new treatment plant during periods when the Elwha is affected by high suspended sediment levels; creating a new chinook-rearing pond on Morse Creek; rearing the individuals of certain species in the streams of nearby river basins; and transporting juvenile anadromids to a number of

sites in the watershed upstream from Lake Mills. In addition, from 2009 to 2011 no reservoir drawdown that would introduce extra (primarily fine) sediment into the channel will be allowed during the 'fish window' periods from May 1st to June 30th, August 1st to September 14th, and November 1st to December 31st. This will maximise the success of juvenile downstream migration, adult upstream migration and spawning, and egg incubation. The success of these measures will be continuously monitored during and after dam removal and any necessary changes will be made (Elwha River Fish Restoration Plan, 2003; National Park Service, 2005). Stocks of summer steelhead, coastal cutthroat trout, bull trout, Dolly Varden trout and sockeye salmon will be allowed to rebuild naturally, while Chinook, coho, chum and pink salmon, and winter steelhead will utilise both natural stock recovery and hatchery breeding to build up numbers. Estimates of stock recovery times for the 10 species range from 15-25 years (Elwha River Fish Restoration Plan, 2003).

Even if some of the fish are exposed to elevated levels of sediment, though, their natural resilience should not be underestimated. In May 1980, Mount St. Helens erupted and deposited about 2.3 billion m³ (3 billion yd³) of sediment on the North Fork Toutle River and about 38.2 million m³ (50 million yd³) on the South Fork Toutle River. In effect, large sections of these stream networks ceased to exist, yet within three months the networks had reformed and adult steelhead were observed in the North Fork Toutle. Steelhead redds were observed in a number of North and South Fork tributaries and, shortly after, fry were captured in these streams indicating that adults had successfully spawned. In one South Fork tributary, the number of steelhead increased ten-fold from 1981 to 1984. This level of sediment-related devastation is far, far in excess of the worst case scenario that could occur on the Elwha and so it should be expected that the salmon and trout runs will recover well and rapidly (National Park Service, 1995). Two cautionary notes should be sounded, however. First, the sediment-related stress that the fishes will be exposed to during dam removal will come on top of the stresses that the few remaining wild fishes are exposed to because of the degraded habitat quality downstream from Elwha Dam (section 2.2.2.3). In addition, hatchery fish have less natural resilience than wild fish (National Research Council, 1996). Both wild and hatchery fish will therefore be resisting the adverse sediment-related impacts of dam removal from a weaker physiological condition than would be the case for healthy, wild runs of fish, thus

potentially compromising the ability of some individuals to do so effectively. Second, ocean conditions will also have a major, perhaps overriding, impact on how many juveniles develop into healthy adults and on how many return to spawn (National Research Council, 1996).

2.3.3.2 Physical issues

Of particular concern is the impact that rapid and large influxes of coarse sediment, the great majority of which is sand and gravel, will have on the risk of flooding. Once coarse sediment begins to pass through the dam sites, it will be deposited on the channel bed, thus promoting lateral channel movement and bank erosion (Bureau of Reclamation, 1996a). Deposition will occur firstly in pools and other lower velocity areas (section 1.3.1.2ii). This will decrease the channel's capacity, but it will not necessarily increase the local flood stage (Bureau of Reclamation, 1996a), because the loss of capacity will be at least partially compensated for by the overall smoothing of the channel bed and the reduction of form drag (section 1.3.1.2ii). Of greater concern is if deposition occurs on riffles, since the local water surface elevation is controlled by the elevation of the downstream riffle (Bureau of Reclamation, 1996a; Richards, 1978). Riffles are higher velocity environments where no significant deposition is expected to occur unless adjacent, lower velocity storage areas are full. Monitoring of riffle elevations and adaptive sediment management will be used to temporarily halt dam removal if it appears that deposition may become problematical in this respect. Nevertheless, once a section of the dam has been removed, the volume of coarse sediment released downstream cannot be controlled and will be determined by the discharge entering the reservoir and the dynamics of sediment transport and channel adjustment within the reservoir. As a precaution, the 2,134 m-long (7,000 ft) federal levees on the east side of the river that protect human infrastructure will be increased in height by one metre (3.3 ft) on average to maintain the existing level of flood protection, with the northern end of the levee being extended by 137 m (450 ft) and the preferred option for the southern end being a 503-m (1,650 ft) extension (Figure 2.9). The 274 m-long (900 ft) private levee on the west side of the river will also be raised to maintain the existing level of flood protection (National Park Service, 2005).

The flood risk associated with dam removal has important implications for water quality issues. One requirement of the Elwha River Ecosystem and Fisheries

Restoration Act is that all reasonable actions necessary ‘to maintain and protect existing water quality for the City of Port Angeles, Dry Creek Water Association, and

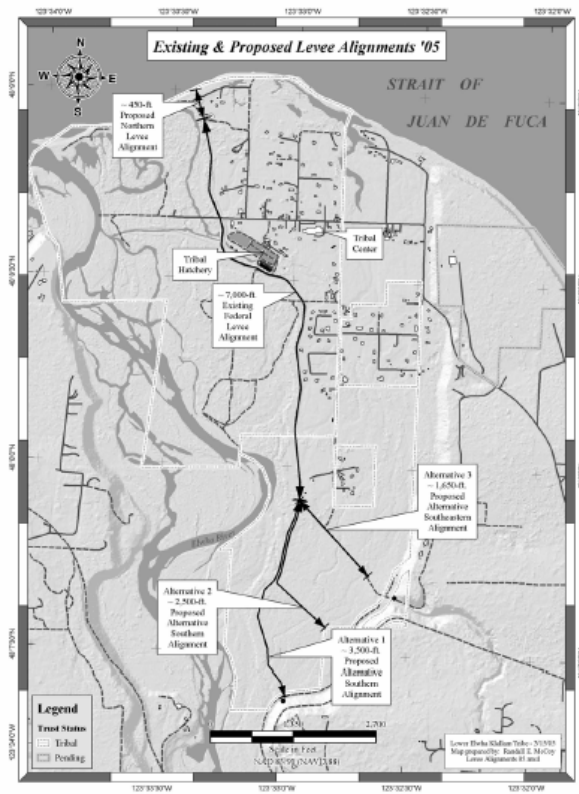


Figure 2.9. Proposed expansion of federal levees (National Park Service, 2005).

the industrial users of Elwha River water against adverse impacts of dam removal’ (United States Congress, 1992, Section 4(b)) must be taken. The coarse-grained (sand and gravel) glacial and alluvial deposits in the Elwha River Valley form an aquifer from which a variety of domestic, industrial and commercial users draw their water supply through wells. Water levels in the river channel and the aquifer are generally the same, indicating that the two systems are hydraulically connected. Because of the pristine nature of Olympic National Park and the lack of industrial and agricultural sources of pollution within the basin, this water is currently of very high quality, while the levels of suspended sediment in the Elwha are also very low due to the sediment trapping effect of the reservoirs (Bureau of Reclamation, 1995d). In both the upper and lower Elwha Valley, several wells are located near to the river channel and an increased flood risk increases the possibility that these wells might become contaminated with suspended sediment during flood events (Bureau of Reclamation,

1997). The Elwha also provides the town of Port Angeles with its water supply and a new water treatment facility has recently been completed that is capable of dealing with the much higher levels of suspended sediment that will occur during and after dam removal. Furthermore, all homes in the lower valley use septic systems for sewage disposal. These systems are already very close to the existing groundwater level and any increase in river stage due to channel aggradation is likely to raise the groundwater level to the point that it floods some of the septic systems, thus creating numerous point sources of pollution (Bureau of Reclamation, 1995d; 1997). This problem will be avoided by replacing the individual septic systems with connections to a municipal sewage treatment facility (National Park Service, 2005).

2.3.4 Sediment management and channel restoration objectives

For any dam removal project, a number of sediment management options exist (ASCE, 1997): (i) the mechanical removal of the entire reservoir sediment deposit; (ii) the mechanical removal of the fine (and sand) component(s) of the deposit, together with either natural fluvial erosion of and/or the construction of a stable channel through the remaining coarse deposit; (iii) construction of a stable channel through the entire deposit, with stabilisation of the ‘floodplain’ sediments; (iv) allow the river to naturally recreate its own channel as the dam is removed (*e.g.* this study).

Which option is chosen should reflect project-specific conditions and issues, as well as the available budget. For example, if reservoir sediments are heavily contaminated, then they may have to be removed entirely or very effectively stabilised in place (options i & iii) in order to prevent the pollutants dispersing and creating a wide-spread pollution problem. Mechanical sediment removal is very expensive, however, and can add very substantially to the overall project budget. If financial constraints preclude mechanical sediment removal of the entire deposit, if large volumes of sediment cannot be allowed to flush downstream, or if nearby infrastructure must be protected, then the construction of a stable channel through some or all of the deposit may be a viable alternative (options ii & iii) since potentially only the volume of sediment equivalent to the volume of the new channel must be removed and disposed of. Structural intervention, such as sheet piling or riprap, will be required to keep the channel stable and ‘locked’ in position and this

may be quite expensive. It may also require periodic maintenance, which will further add to the whole life project costs.

By far the cheapest and easiest approach is to allow the river to recreate its channel naturally through the deposit as, or after, the dam is removed (option iv). For channels with sufficient stream power this has the major added benefit of allowing the river to recreate for itself, over a short- to medium-term time scale, a form that is in equilibrium with the discharge and sediment load supplied to it from the catchment. This ensures that form and process are linked and therefore that the new channel is self-sustaining in the long-term. Natural channel recreation is by far the easiest way of achieving this objective (see Soar and Thorne (2001) for a comprehensive review of other approaches) and is also the one that ensures the highest quality outcome. It also provides an excellent example of the more general river restoration principle of working *with* nature rather than against it (Soar and Thorne, 2001).

From the discussion in the preceding sections, it is clear that there is a range of interconnected issues related to the release of the coarse and fine sediment fractions from the two reservoirs. Adaptive management monitoring will be employed to prevent suspended sediment levels from overwhelming water treatment and supply facilities and to prevent them from hindering the migration of fish into and out of the Elwha River during the fish windows. It will also be used to ensure that coarse sediment deposition on the channel bed does not occur to the extent that the flood risk exceeds the design limits of the new flood-protection measures (National Park Service, 2005). It is nevertheless desirable to understand as much as possible about how the reservoir sediments are likely to behave during removal prior to actually starting the removals. This way, some information will be available to help guide the timing and rate of reservoir drawdown to achieve the sediment management objectives and, importantly, to raise awareness of any unexpected events that may lead to uncontrolled releases of sediment. These could be particularly damaging if they exceeded the design limitations of the flood protection, the water quality protection, and the water supply infrastructure (National Park Service, 2005).

The sediment management objectives are as follows. First, as much sediment as possible should be eroded naturally from the two reservoirs during and after the dam removal process. This will help to achieve the second objective of leaving the remaining reservoir sediments distributed throughout the reservoir basin with as

natural as possible a topography (Randle, Personal Communication 2005). These two objectives will maximise the volume of remaining sediment that lies within the root zone of recolonizing vegetation, thus accelerating the rate at which vegetation can recolonise and stabilise the remaining sediments. Furthermore, avoiding the creation of high terraces with steep, essentially unvegetated faces is more in keeping with the aesthetics required in a national park (National Park Service, 1996) and will reduce the legal liability for the National Park Service with respect to unstable surfaces that could collapse when walked upon.

The key to successfully achieving this sediment management objective is to develop a good understanding of the morphodynamical response of the impounded sediment to the chosen dam removal methodology. In view of the complex, three-dimensional nature of these dynamics, a physical modelling approach is an excellent way of developing this understanding.

2.3.5 Research performed to date

A number of studies of the physical characteristics of the Elwha River System have been performed over the last two decades in preparation for the planned removals of the dams, many of which have been referred to in preceding sections. Because of their relevance to the current study, only those relating to the Lake Mills delta sediments will be discussed further here.

Lake Mills has been drawn down three times since the late 1980s. In 1987 it was drawn down about 3 m (10 ft) from September 8th to October 8th in order to provide extra water for downstream fisheries resources. Several photographs were taken, but no physical measurements were collected. The drawdown completely exposed the delta topset and parts of the foreset surface, allowing a network of channels to develop and erode part of the topset surface, particularly the downstream half (Hosey and Associates Engineering Company, 1990).

In 1989 the reservoir was drawn down 5.4 m (17.6 ft) from September 6th to October 13th (37 days at about 0.2 m (0.5 ft) per day), then held at this lower elevation until October 22nd, before being allowed to refill. Eight cross-sections were established over the downstream two-thirds of the Lake Mills delta and suspended sediment and bedload sediment samples were collected. As in the 1987 drawdown, most of the erosion was concentrated in the downstream half of the delta topset, but

the channel was able to incise about two-thirds of the way upstream along the topset surface before the headcut stalled. Following a five-fold increase in mean discharge from 10 m³/s to 55 m³/s (367 to 1,937 cfs), the channel was able to incise to the very upstream end of the topset (Hosey and Associates Engineering Company, 1990).

The most recent drawdown experiment was performed in April 1994. The water surface elevation was lowered 5.5 m (18 ft) over a one-week period from the 9th to the 16th April, held constant for a further week from the 16th to the 23rd and then allowed to rise naturally. The level was lowered at a rate of 0.9 m (3 ft) per day for the first five days of the drawdown, with the remaining 0.9 m being spread over the last two days. The following samples and data were collected during the experiment: water stage and discharge; suspended sediment and bedload samples; water quality samples; daily resurveys of cross-sections established across the delta surface (Figure 2.10); surface and subsurface sediment samples; and aerial and oblique-angle photographs (United States Geological Survey, 2000).

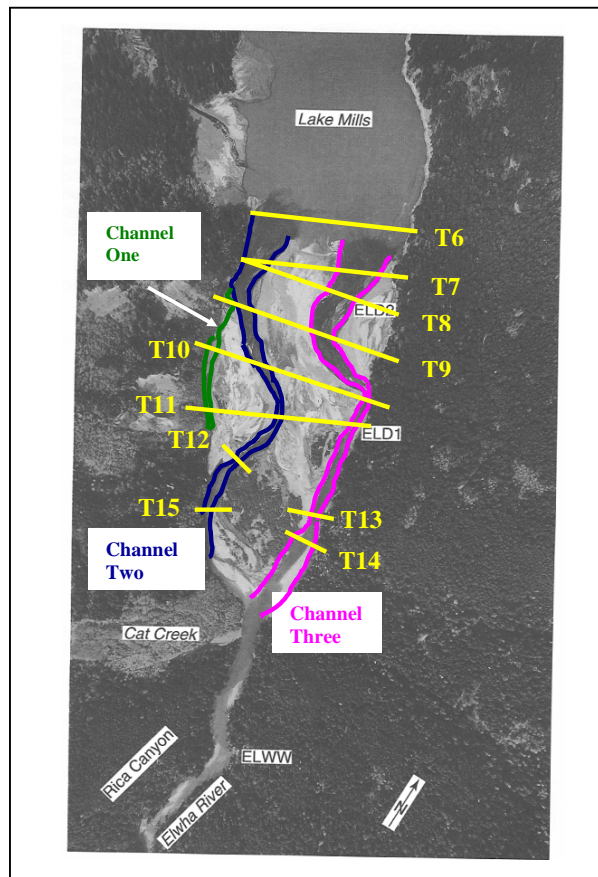


Figure 2.10. Location of main channels and transects during the 1994 drawdown experiment.

Using data from this drawdown experiment together with: an empirically-based model to estimate erosion channel widths over the prograding reservoir deltas; a mass balance model to estimate the elevation at which reservoir sediment would overtop the remaining Glines Canyon Dam structure; together with HEC-6 and STARS sediment transport modelling, the United States Bureau of Reclamation was able to produce an estimate of the likely impact of dam removal on sediment concentrations, channel bed elevations and the likely flood risk in the channel reaches downstream from the two dams (Bureau of Reclamation, 1996a).

While the 1994 drawdown experiment provided much useful information to help understand how the Lake Mills Delta might respond to dam removal, the limited vertical extent of the drawdown did not necessarily reveal the full range of morphodynamical interactions that may occur during the actual removal. The nature of such adjustments is now discussed in the following chapter.

Chapter 3 Research Hypotheses

The purpose of this chapter is to present a discussion of theoretical considerations and empirical observations that are relevant to the adjustments of river channels in the reservoir area responding to dam removal. In so doing, a rational basis is provided for the formulation of two working research hypotheses that will guide the course of the experimental programme detailed later.

3.1 *Equilibrium*

River channels are open systems through which energy and matter flow (Leopold and Langbein, 1962). The three-dimensional form of an alluvial channel adjusts continuously to the flow regime and sediment load supplied by the catchment, in attempting to match the sediment transport capacity for the available discharge to the sediment supply, so that sediment neither erodes or accumulates indefinitely (Knighton, 1998). In situations where the flow and sediment regimes are unchanging, the result is an equilibrium channel form that is arrived at and maintained through the simultaneous adjustment of a large number of hydraulic, geometrical and sedimentary variables.

The type of equilibrium attained depends on the time frame over which the fluvial system is being viewed (Schumm, 1977). In an early account, Schumm and Lichty (1965) suggested that time could be classified, in order of decreasing length, as cyclic, graded and steady. Cyclic time corresponds to dynamic equilibrium, since the fluvial system is continually adjusting in one general direction to the stimulus provided by external variables such as climate and tectonics. Graded time represents a short period of cyclic time and corresponds to steady-state equilibrium, because the fluvial system is not moving in any direction but is fluctuating about an average condition. Steady time represents a short period of graded time during which a static equilibrium condition can exist, because the fluvial system, or the component of interest, exhibits no change whatsoever (Schumm and Lichty, 1965). This model reflects Davis' (1899) model of progressive denudation and, therefore, does not consider the concepts of geomorphological thresholds and episodic behaviour or complex response (Schumm, 1973), which are known to operate in fluvial systems. Accordingly, Schumm (1976) proposed that dynamic metastable equilibrium should

replace dynamic equilibrium at the cyclic time scale, since this allows both progressive erosion and episodic erosion related to the exceedance of thresholds to be accounted for.

The absolute length of time associated with each type of equilibrium described above will vary depending on the ratio of the forces driving and opposing the change in the fluvial system (Richards, 1982). Following the passage of a certain period of time following the completion of dam removal, the prototype⁹ Elwha River may attain a steady-state equilibrium with respect to the discharge supplied by the catchment and with the sediment supplied by the catchment and the terrace deposits in the reservoir area. The maximum prototype time scale of interest is therefore graded time, which may operate at the scale of several decades to over 100 years (section 3.3.1.3), although its absolute value is currently unknown. Similarly, following the removal of each increment of the prototype Glines Canyon Dam, the fluvial system in the reservoir area will try to adjust towards a steady-state equilibrium but, because the removal of successive increments of the dam will take place at about two-week intervals, the prototype fluvial system will exist in a state of disequilibrium (Renwick, 1992) for the duration of the dam removal period because the relaxation time required for recovery will be less than the recurrence interval of the disturbance. Because the objective of the current modelling investigation is to isolate the effect of each drop in baselevel and because the experiments will be performed with a constant discharge and without a sediment feed, the model fluvial system in the reservoir area will be allowed to recover completely from each disturbance, thus reaching a position of static equilibrium, before imposing the next baselevel drop. The model time scale of interest therefore ranges from graded time to steady time.

3.2 The nature of the disturbance caused by dam removal

Many different factors can disturb a river system and move it away from its equilibrium condition, such as catchment urbanization (Doyle *et al.*, 2000; Gregory *et al.*, 1992); reforestation (Gomez *et al.*, 2003; Xu *et al.*, 2006); mining (Gilbert, 1917; Higgins *et al.*, 1987; James, 1991; Knighton, 1989; Knuuti, 2001); road construction (Montgomery, 1994; Wemple *et al.*, 1996; Wemple *et al.*, 2001); channel straightening and/or resectioning (Simon, 1989; Simon and Rinaldi, 2006; Simon and

⁹ The term ‘prototype’ in modelling parlance refers to the real-world object. The term ‘model’ refers to the simplified laboratory version of the real-world object.

Thomas, 2002); and volcanic activity (Hayes *et al.*, 2001; Janda *et al.*, 1984; Montgomery *et al.*, 1999; Simon and Thorne, 1996). Each of these factors can trigger adjustments to a range of different variables that interact non-linearly through the operation of positive and negative feedbacks (Hey, 1979; Simon and Darby, 1999; Simon and Thorne, 1996). These adjustments will generally involve channel bed degradation and bank erosion initially, but as these adjustments migrate upstream through the fluvial system, they can trigger further adjustment at and around the site of the initial disturbance, partially reversing some of the earlier degradational activities in a process of complex response (Schumm, 1973). Many of these adjustments will be relevant to the creation of a new channel through the reservoir whose dam has been removed and they are discussed in more detail in subsequent sections.

Within the reservoir area during dam removal, the most basic change is from a low energy, predominantly depositional environment with the dam still in place, to a much higher energy, predominantly erosional environment during dam removal and for a certain period of time thereafter. The large increase in energy slope results from progressive reduction in base level for the stream in the reservoir area as the dam is removed and is explained as follows (Figure 3.1). Assuming that the water surface elevation has been drawn down to the lip between the delta topset and foreset surfaces, z_2 , and that an equilibrium channel has developed over the topset surface under conditions of constant water inflow, Q , and zero sediment influx, the potential energy, PE , of a mass of water entering the upstream end of the reservoir basin is given by

$$PE = mgz_1 \quad (3.1)$$

Where, m = mass of the water (kg); g = gravitational acceleration (m/s^2); and z_1 = elevation above base level (m) at the upstream end of the basin (Richards, 1982). In the case of a reservoir, base level is the elevation of the thalweg of the bed of the pre-dam channel at the dam site. Because mass is the product of water density, ρ_w (kg/m^3) and water volume, V (m^3), Equation 3.1 can be re-written as

$$PE = \rho_w Vgz_1 \quad (3.2)$$

As the mass of water flows along the equilibrium channel over the delta topset, some of the potential energy is converted to kinetic energy, which performs work in

overcoming the frictional resistance of the channel boundary, transporting sediment, and generating heat (Richards, 1982) and sound energy due to the turbulence within the flow. Kinetic energy, KE , is given by (Richards, 1982)

$$KE = \frac{1}{2} mu^2 \quad (3.3)$$

Where, u = mean velocity (m/s). Assuming that flow approaching the reservoir basin is steady, the supply of potential energy per unit time at the upstream end of the basin is given by (Richards, 1982)

$$PE = \rho_w g Q z_1 \quad (3.4)$$

since discharge, Q , is the volume of water arriving at the upstream end of the delta per unit time. At time T_0 the rate of potential energy expenditure per unit length of channel, which here is between the upstream and downstream ends of the topset surface, is therefore given by (Richards, 1982)

$$\rho_w g Q z_1 - \rho_w g Q z_2 = \rho_w g Q (z_1 - z_2) = \rho_w g Q S_e \quad (3.5)$$

where, S_e = energy slope. Equation 3.5 describes the rate at which energy is expended doing work through water flow and sediment transport, which is the stream power per unit channel length. If the water surface elevation is now lowered such that at time T_1 it is at elevation z_3 above the datum and assuming that the elevation z_1 remains the same, the slope, and therefore the stream power per unit channel length, in the reach flowing across the topset surface must increase. This means that more energy is available to drive the flow of water, overcome friction and transport sediment. It should be noted, however, that once frictional resistance has been overcome, as little as 4% of the potential energy may remain to be used to transport sediment (Rubey, 1933).

3.3 The nature of the response to the disturbance

The nature of the fluvial responses generated by this change in stream energy regime and the channel changes that result are partially dependent on the volume of sediment stored within the reservoir and the disposition of the deposit (Figure 3.2). The other controlling variable is the rate at which the base level is lowered. At one extreme, draw down is effectively instantaneous for the removal of a dam whose reservoir is completely full of sediment, *or* whose reservoir is only partially filled by

sediment, but which is removed *all at once*. In this type of removal sediment delivery downstream of the dam begins more or less immediately once the dam is removed.

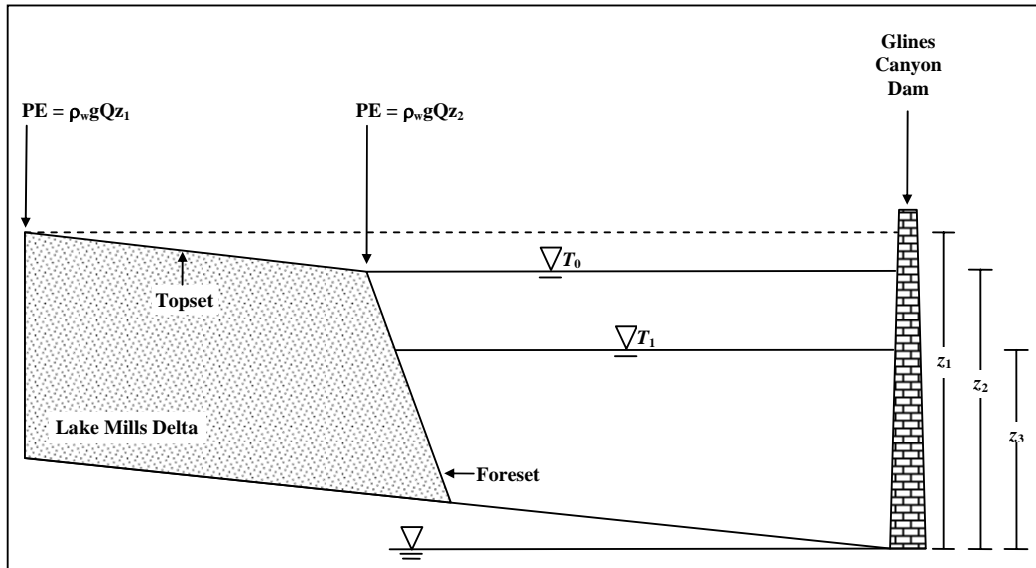


Figure 3.1. Energy changes over the Lake Mills delta topset during dam removal.

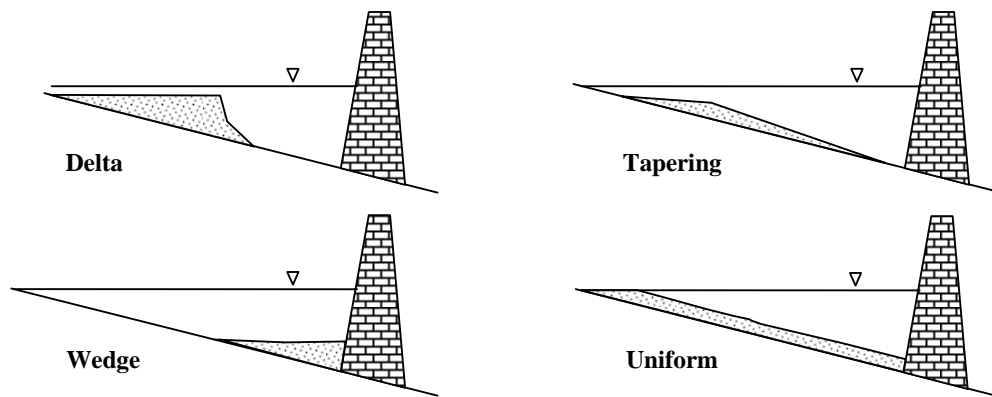


Figure 3.2. Longitudinal patterns of sediment deposition in reservoirs. Modified from Morris and Fan (1998).

Here, this is termed an RSF (Reservoir Sediment-Full) removal. At the other end of the scale, dam removal may be slow and *incremental* or the reservoir completely empty of sediment. Here, this is termed an RPSF (Reservoir Partially Sediment-Full) removal. In this type of removal sediment will only be delivered downstream of the dam site some time after removal commences, if at all. In reality, very few reservoirs on rivers are completely devoid of sediment and, in practise, an RPSF removal

describes the incremental removal of a dam whose reservoir is partially full of sediment, as is the case for the two Elwha River dams (section 2.3.3).

The significance of this distinction is that, in RPSF removals, the dynamics of erosional and depositional responses within the reservoir area will have significant impacts on the subsequent evolution of the fluvial system as it responds to the removal of the dam. This is the case because, while the finer fraction of the sediment will immediately be flushed downstream, the volume leaving the reservoir is likely to be small, both relative to that being eroded and redeposited within the reservoir footprint and also in relation to the volume being flushed downstream during an RSF removal. In an RSF removal, significant volumes of sediment may be flushed downstream immediately following the onset of dam removal, because the effects of the drop in baselevel will be felt first at the downstream limit of the deposit. As the effects of the drop in baselevel migrate upstream some of the eroded sediment may be temporarily deposited in the eroding channel, but these volumes are likely to be small relative to that being flushed downstream and also relative to the volumes being deposited as a prograding delta in an RPSF removal. Once the prograding delta front in an RPSF removal has reached the upstream face of the dam, the response process will transition to an RSF, because more, perhaps most, of the eroded sediment will be flushed downstream (Cantelli, Pers. Comm., 2004). Once the reservoir water surface elevation falls below the elevation of the proximal extent of the reservoir, deposits with deltaic, tapering and uniform sediment dispositions (Figure 3.2) will certainly respond through RPSF behaviour, the extent and length of time over which they do so depending on the capacity of the reservoir foot print to store redeposited sediment. In contrast, while a wedge shaped deposit may exhibit some RPSF behaviour, the nature of which will be dependent on the thickness of the proximal portion of the deposit, it is more likely to respond through predominantly RSF behaviour from the onset of sediment mobilisation.

Within the broad classification into RSF and RPSF responses, the details of sediment morphodynamics will vary widely from case to case owing to the large number of degrees of freedom through which the eroding channel can adjust, and because of the wide ranges that the parameters defining the channel can adopt. For example, Hey (1975; 1988) identified that to define the bankfull channel form uniquely it is necessary to specify no less than nine parameters: mean width, depth

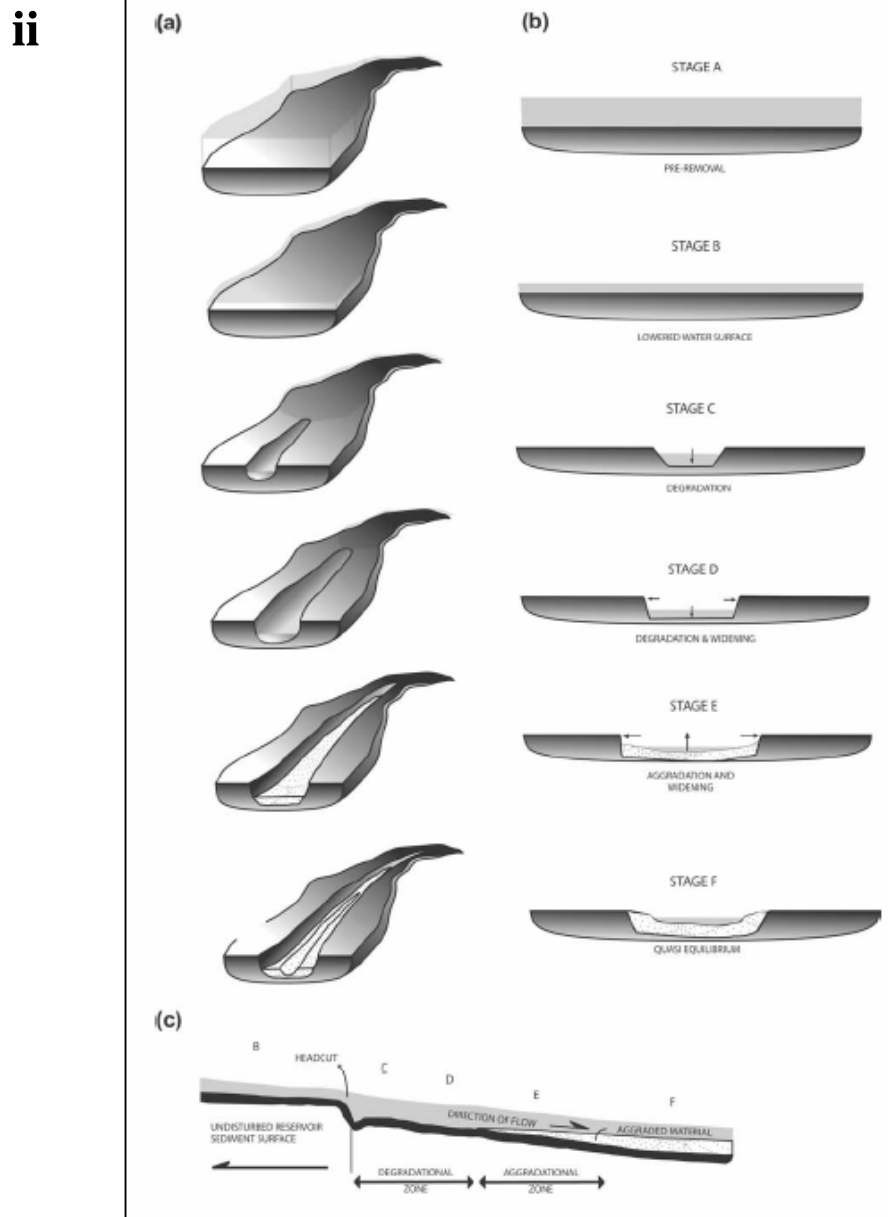
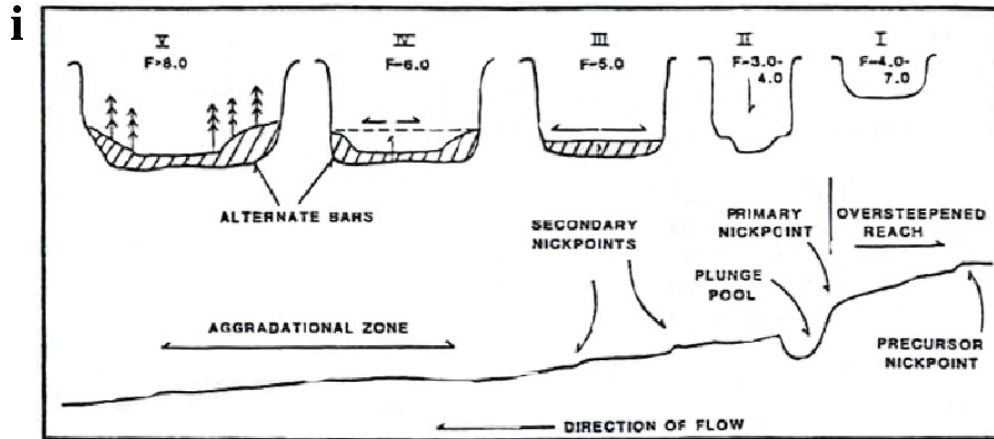
and velocity, maximum depth, bedform height and wavelength, slope, sinuosity, and meander arc length. Analytical prediction of the equilibrium channel form for a given set of controlling variables requires that a process equation be specified for each degree of freedom. However, as only three physically-based equations exist to define the processes responsible for equilibrium channel geometry (continuity, flow resistance and sediment transport) the morphology of a stable, alluvial channel remains analytically indeterminate (Richards, 1982). Analytical solutions are possible for simple channels, which can be represented with fewer degrees of freedom. For example, the geometry of a straight channel can be predicted using a one-dimensional, hydrodynamic, numerical model based on simultaneous solution of the continuity, energy and momentum equations. However, the adjustments of naturally evolving, alluvial channels are distributed between all available degrees of freedom and this is certainly the case for channels formed during dam removal. Three-dimensional, finite difference, element or volume modelling may eventually offer more capability to deal with more complex channels, but available models cannot be used for large systems or long-term simulations due to the excessive run times involved, while their heavy data requirements preclude applications beyond the most intensively studied research sites. Similarly, while the motion of water along a channel with fixed boundaries can be simulated precisely using computational fluid mechanics, the current generation of CFD models cannot account for the evolution of an alluvial channel with a free surface and in which both the bed and banks are deformable. In summary, the complexities of channel evolution to an equilibrium form in the context of dam removal preclude computer modelling using the tools currently available. Conversely, the problem is readily amenable to treatment using a physical modelling approach.

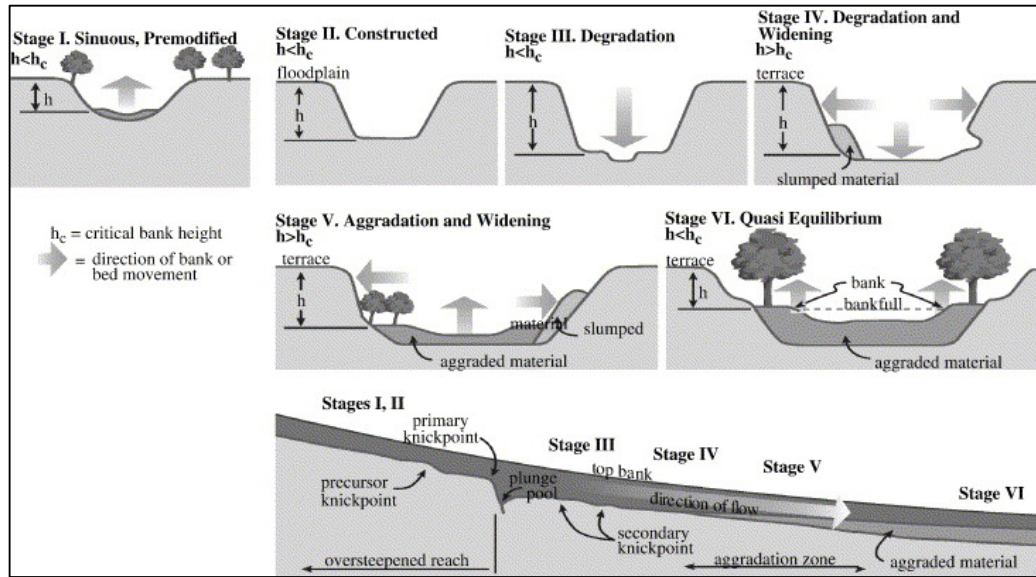
Given the focus of this project, the conceptual discussion of sediment and morphological responses to dam decommissioning presented here will concentrate on the RPSF removal of Glines Canyon Dam, as simplified for this modelling investigation: *i.e.* a deltaic deposit composed mostly of sand but with some gravel occupying the upstream portion of the reservoir basin, with no bottomset deposits.

3.3.1 Cross-sectional and longitudinal adjustments

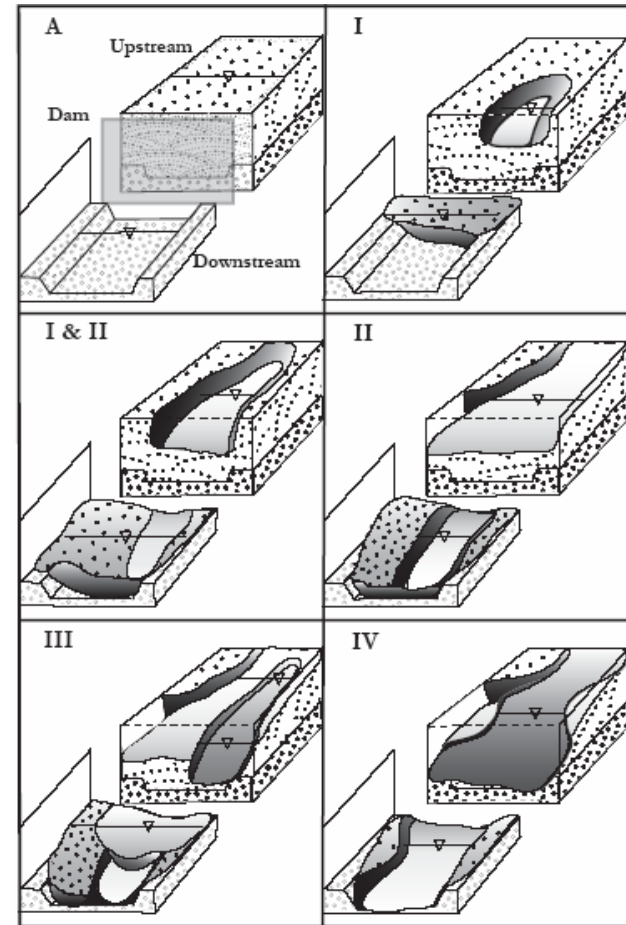
In alluvial channels with erodible boundary materials, an increase in stream power will usually initiate a series of vertical and lateral channel changes as the stream adjusts to the new hydraulic regime. Morphological responses triggered by stream power increases and involving both vertical and lateral instability have been documented to result from land use change in the drainage basin (Doyle *et al.*, 2000; Gregory *et al.*, 1992), channel straightening and/or resectioning of meandering rivers (Simon, 1989; Simon and Rinaldi, 2006; Simon and Thomas, 2002). Lowering the base level of an alluvial reach has been observed to be particularly effective in promoting system-wide instability (Gregory, 1983; Harvey, 2002; Hassan and Klein, 2002; Schumm *et al.*, 1984). In the specific case of dam operations and decommissioning, base level lowering may result from dam removal (Doyle *et al.*, 2003); reservoir drawdown (Grant *et al.*, 2002; Hosey and Associates Engineering Company, 1990; United States Geological Survey, 2000); reservoir flushing (Atkinson, 1996); or artificial channel bed lowering for culvert maintenance purposes (Bromley, 2003; Florsheim *et al.*, 2001).

Vertical instability associated with base level lowering is usually initiated through channel incision and, regardless of the triggering mechanism, the sequence of adjustments that results is generally similar and has been described conceptually in the form of Channel Evolution Models (CEMs) (Harvey and Watson, 1986) (Figure 3.3). These models suggest that an initial period of degradation is followed by rapid widening when increased bank heights and angles trigger bank instability. Lowering of the bed slope, coupled with increased sediment input from degrading reaches upstream and failing banks then leads to aggradation and a degree of recovery in bed elevations. Aggradation, coupled with reductions in sediment input due to upstream migration of the oversteepened zone and stabilisation of the banks may lead to a second wave of incision and aggradation. The bed elevation displays a damped oscillation (Hey, 1979) until, eventually, channel equilibrium is achieved. While the existing CEMs provide a useful first step in characterising the response of an incising channel system, however, they are relatively simplistic and do not address the large number of process-form interactions that occur in an incising channel system. Of particular relevance to this study is that they are all fairly similar and do not have the capacity to address the different suites of process-form interactions that are likely to





iii



iv

Figure 3.3. Channel Evolution Models after (i) Schumm *et al.*(1984); (ii) Doyle *et al.* (2003); (iii) Modified from Simon & Hupp (1986) (after Simon & Rinaldi (2006)); and (iv) Wooster *et al.* (Submitted).

occur as dams and reservoirs of widely different sizes in very different physiographical regions are removed (Pizzuto, 2002).

3.3.1.1 Vertical adjustments

In the context of a reservoir in which sediment has accumulated as an alluvial fan, the initial response to drawdown and effective lowering of the base level for the stream entering the reservoir will be increases in stream power and flow velocities at the distal end of the delta. In the context of CEMs, this location has been referred to as the ‘area of maximum disturbance’ (AMD) by Simon (1989; 1992) as it is here that the effects of the change in energy regime are strongest. Provided that the increase in stream power is sufficient to entrain bed sediments, the channel bed will begin lowering in the zone where the slope is oversteepened. The resulting incision then migrates upstream by a process of headward erosion as a knickpoint or knickzone. These features may be identified as a step in the long profile or a localised zone of oversteepened bed slope relative to the bed slope upstream and downstream, respectively (Schumm *et al.*, 1984).

Supercritical flow has been found to occur just upstream of the, or at the point of, knickpoint development (Bennett, 1999; Bennett *et al.*, 2000; Bryan, 1990; Slattery and Bryan, 1992), while Savat (1976, cited in Bryan, 1990) and Bryan (1990) observed that a series of knickpoints in an incising channel were spaced according to the distance required for the flow leaving the scour pool of the upstream knickpoint to regain its pre-knickpoint, *i.e.* supercritical, velocity. The onset of supercritical flow results in large shear stresses on the bed (Robinson and Cook, 1998), thus increasing the likelihood that the bed can be locally eroded, which then provides the break in the bed profile that can allow a knickpoint or knickzone to form. Based on the results of experiments in homogenous and non-cohesive sands, Brush and Wolman (1960) hypothesised that, once formed, in order for a knickpoint to persist as it migrates upstream, a more erosion-resistant layer would have to overlay a less erosion-resistant layer. This has subsequently been confirmed by many independent laboratory investigations (*e.g.* Bennett, 1999; Bennett *et al.*, 2000; Bennett and Casali, 2001; Holland and Pickup, 1976; LaTray and Stein, 1997; Robinson and Hanson, 1995). Such features are termed self-propagating knickpoints (Begin *et al.*, 1980).

The presence of an erosion-resistant layer at the bed surface allows a submerged or aerated jet to form a scour pool immediately downstream of the knickpoint that undermines the base of the knickpoint's leeward face, maintaining its vertical or near vertical profile (Bennett *et al.*, 2000; Stein *et al.*, 1993; Stein and Julien, 1993). Under these circumstances, the knickpoint migrates through slab-type or cantilever failures of the erosion-resistant layer (Bennett *et al.*, 2000; LaTray and Stein, 1997; Zhang, 1995). However, in the absence of a cohesive, erosion-resistant layer the leeward face of the knickpoint is unable to maintain its near-vertical profile as it migrates upstream. Instead the slope progressively flattens through time and is therefore termed a 'rotating knickpoint' (Begin *et al.*, 1980). Consequently, the slope of the oversteepened face decreases as it migrates upstream, while the bed slope immediately upstream of the knickpoint lip or brink point increases, until the feature degrades to form a knickzone. Eventually, with increasing distance from the area of maximum disturbance, the slope in the knickzone relaxes until it grades into the pre-lowering bed slope. This occurs because the flow is able to erode sediment more rapidly from the channel bed upstream from the lip than the jet in the downstream scour hole is able to erode sediment from the base of the oversteepened face (Stein and Julien, 1993). A rotating knickpoint is thus likely to evolve into a knickzone which will, in due course, grade into the pre-disturbance bed slope as it migrates upstream away from the area of maximum disturbance.

In Lake Mills the deltaic deposits are sand and gravel. As these deposits are both heterogeneous and non-cohesive it is unlikely that incision will encounter any layers that are notably more erosion resistant than the underlying sediments. This will also be the situation in the model, where the delta is formed in mixed sands and gravels. Consequently, degradation triggered by base level lowering due to lake drawdown is likely to be accomplished through upstream migration of rotating knickpoints that evolve into knickzones through time as they move away from the AMD. The steepness, persistence, upstream migration rate and upstream migration distance of these features are all likely to increase generally with the magnitude of the fall in base level, especially if the fall is sufficient to generate locally supercritical flow approaching the knickpoint or within the knickzone. This follows because a larger knickpoint/zone should (all else being equal), migrate further upstream, as a greater length of channel is required for the oversteepened slope to grade back to the

pre-disturbance channel slope. In addition, the greater increases in stream power associated with larger drops in base level increase the capability of the flow downstream of the knickpoint/zone to transport eroded bed sediment more rapidly from the base of the knickzone, thus maintaining the elevation difference between the top and bottom of the oversteepened face for longer and prolonging the distance it can migrate upstream away from the AMD (Bennett and Casali, 2001), therefore increasing the volume of sediment eroded. Evacuation of the scoured sediment has been shown to correlate positively with the rate of knickpoint migration (Bennett, 1999) and to determine whether a knickpoint continues to self-propagate or starts to rotate (Holland and Pickup, 1976). Based on these arguments, it is logical to conclude that the volume of sediment eroded due to adjustment of the long profile of the channel bed will be directly proportional to the degree of reservoir drawdown. Similarly, as the process-form interactions occurring in the oversteepened zone are akin to those occurring in the basal zone of retreating channel banks (section 3.3.1.2), it follows that the volume of bank sediment eroded through lateral channel adjustments driven by bed lowering will also be directly proportional to the degree of reservoir drawdown.

Relatively small magnitudes of drawdown may be insufficient to generate a clearly distinguishable knick point or knickzone that can be traced through time and space. Even so, local increases in stream power and sediment transport capacity associated with small drops in base level are likely to generate bed lowering provided that flows are competent to breach the bed armour. In such cases, the volume of bed and bank sediments eroded is still likely to increase with increasing drawdown magnitude as the greater the increase in stream power and scour potential the further upstream can armour breaching occur.

3.3.1.2 Lateral adjustments

As bed lowering occurs along the longitudinal profile in response to the reductions in base level, lateral adjustments to the channel morphology will occur in response to the vertical adjustments. Existing CEMs indicate that bed lowering leads to rapid widening through mass wasting of the banks once the bank heights and angles exceed the threshold for instability with respect to gravitational failure (Figure 3.3). It should however be noted that widening due to bank instability does not figure in the initial response of the channel to base level lowering, being delayed until stage 3 of

Schumm *et al.*'s CEM and stage 4 in Simon and Hupp's model. In fact, in the initial stages of CEMs, water surface width initially *decreases* as the flow erodes a slot into the pre-disturbance bed. Identification of this lateral response pre-dates the development of CEMs. For example, Brush and Wolman (1960) observed flow narrowing immediately upstream of migrating knick points formed in well sorted sands while Gardner (1983) reported the same phenomenon in cohesive, homogenous material.

This stage of channel evolution is particularly marked in situations where the banks are erosion-resistant and gravitationally stable, or where a large degree of base level lowering occurs instantaneously. For example, in flume experiments simulating *instantaneous* removal of an entire dam, Cantelli *et al.* (2004) observed a phenomenon that they termed 'erosional narrowing', in which the initial lateral adjustment of the incising channel is a narrowing of the wetted channel width. A similar observation was recently made by Wooster *et al.* (Submitted), although the degree of narrowing was less marked.

Erosional narrowing occurs because boundary shear stresses are highest along the centreline of the channel and decrease towards the banks. Consequently, initial incision is concentrated at the channel centre, while the channel margins are less affected. This deepens the channel and causes a streamwise convergence of streamlines towards the deepening thalweg. Flow concentration increases the rate of incision around the thalweg through a process of positive feedback. Eventually, incision of the thalweg increases the side slopes of the inner channel promoting downslope creep of bedload moving along the channel, thus delivering more sediment to the thalweg. The resulting increase in lateral sediment input first slows and then halts flow narrowing through a process of negative feedback (Cantelli *et al.*, 2004). A prerequisite for erosional narrowing therefore appears to be a very marked increase in bed shear stress as a result of a large and instantaneous fall in baselevel. The morphodynamical significance of erosional narrowing is that, although it is only a short-lived phenomenon, it has the potential to erode a large volume of bed material while leaving bank material *in situ*. Further, as the bed material is removed from only a proportion of the bed width, incision can occur very rapidly, with eroded sediment delivered quickly to the prograding delta front in the reservoir area or beyond into the river channel downstream from the dam (Cantelli *et al.*, 2004). In addition, rapid and

efficient removal of bed material downstream of the knickpoint or knickzone promotes upstream migration that is both more rapid and more extensive than would be expected if bed lowering occurred across the full width of the channel.

The experiments of Cantelli *et al.* (2004) and Wooster *et al.* (Submitted) reveal more about the process-response controls that govern erosional narrowing. These experiments differed in that those of Cantelli *et al.* were performed in a sand channel with a $D_{50} = 0.8$ mm, while the three experimental runs of Wooster *et al.* were performed using sand ($D_{50} = 0.6$ mm) and gravel ($D_{50} = 4.2$ mm) mixtures with sand contents of 73% (run S73), 80% (run S80) and 89% (run S89), respectively. The results suggest that the degree of erosional narrowing decreases as the proportion of coarse sediment in the deposit increases. This reflects the potential for the coarser sediments to form an armour layer (through vertical and downstream winnowing of finer grains) that limits incision and upstream propagation of the knickzone in the thalweg (Bromley *et al.*, Accepted for publication). The effect of armouring in reducing the degree of incision and extent of upstream migration in the zone of erosional narrowing is additional to a more general decrease in the minimum width achieved by erosional narrowing with increasing distance from the AMD that was observed in sand bed channels (Cantelli *et al.*, 2004). The minimum width produced by erosional narrowing increases with distance upstream from the AMD, probably because of the phenomenon mentioned earlier that the rate at which eroded sediment can be transported away from migrating knick points and zones decreases as the zone of incision migrates upstream. For example, Bennett (1999) found that the migration rate for a self-propagating knickpoint and the sediment yield were governed by the downstream transport capacity. In the case of channels experiencing erosional narrowing, this limits the degree of positive feedback responsible for thalweg deepening and flow narrowing.

In the later stages of experimental runs in both studies, channel widening occurred, as expected from the relevant CEMs. However, the presence of coarser sediments in Wooster *et al.*'s runs S73 and S80 was observed to produce a decrease in the extent to which the channel widened with increasing distance upstream. Conversely, in their run S89 and in all the runs of Cantelli *et al.* (2004) with uniform sand, the channel widened to the same extent along the entire length of the deposit. The same observation was made by Wolman and Brush (1961) in their experiments in

uniform sands with $D_{50} = 0.67$ mm and 2 mm. In these experiments, the alluvial deposits were built up by feeding sediment into a reservoir full of water in order that sediment sizes should be as close as possible to being naturally sorted. As expected, this produced a greater concentration of coarser sediments at the upstream end of the deposit (Morris and Fan, 1998). Subsequent bed armouring during incision limited the extent to which channels incised and then widened, the effect becoming more pronounced with increasing distance upstream. Similar reductions in channel widening, due to increasing resistance to erosion at the channel bed have been observed in the field as well as the flume in both cohesive (Bromley, 2003; Doyle *et al.*, 2003; Simon, 1994) and non-cohesive deposits (United States Geological Survey, 2000) (Figure 3.4).

As well as being observed in physical models, erosional narrowing has also been modelled in a one dimensional, hydrodynamic, numerical model by Wong *et al.* (Wong *et al.*, 2004) and, less dynamically in Cui *et al.*'s (2006a; 2006b) DREAM model (Cantelli *et al.*, 2004).

Bank retreat in alluvial channels is the result of erosion (fluvial entrainment of material directly from the bank surface) and/or bank failure due to mass instability (Thorne, 1982). Fluvial processes often predominate in graded and aggrading channels where flow either parallel to the bank or impinging against it generates boundary shear stresses that exceed the threshold of erosion for the bank material. Erosion then occurs either through the entrainment of individual grains (in the case of non-cohesive materials or by removal of aggregates or crumbs in the case of cohesive bank materials (ASCE Task Committee on Hydraulics Bank Mechanics and Modelling of River Width Adjustment, 1998; Thorne, 1982; 1998). Fluvial erosion can also trigger mass instability by over-steepening or under mining the bank. For example, under mining generates cantilevers in composite banks (where a layer of cohesive material overlays non-cohesive sediments) that fail by shear, beam or tensile mechanisms when they reach a limiting overhang width (Thorne and Tovey, 1981).

Mass instability is often the mechanism responsible for high rates of bank retreat and rapid widening in incising channels with cohesive banks. This is the case because the cohesive forces generated by the electro-chemical bonding between clay-sized particles (Grissinger, 1982; Kandiah, 1974), or tight packing and mechanical interlocking of non-cohesive sediments (Thorne, 1982) initially resist erosion

effectively, preventing the channel from widening and allowing steep and high banks to develop as the bed lowers. However, as the banks heighten and steepen, they approach the limiting values of height and angle for mass stability. Once the bank stability threshold is crossed, the banks cannot remain stable and they collapse under gravity. Typically, failure mechanisms include planar slips, deep seated rotational failures and slab-type failures (Thorne, 1982; 1998).

Mass failures of potentially unstable banks are often actually triggered by adverse drainage conditions in the bank during excessive precipitation and/or rapid drawdown in the channel which lead to positive pore water pressures in the absence of support for the bank by the hydrostatic confining pressures that occur during high river stages (Casagli *et al.*, 1999; Simon *et al.*, 2000). Common mechanisms of failure associated with bank hydrology include pop-out failures, wet earth flows, sapping and piping (ASCE Task Committee on Hydraulics Bank Mechanics and Modelling of River Width Adjustment, 1998; Thorne, 1998).

Despite the fact that rapid widening is usually associated with bank retreat due to mass instability, it is still the capacity of flow in the near-bank region of the channel that is the main factor governing the rate of bank retreat as this determines the rate at which eroded material and failure debris is removed from the bank toe. This phenomenon has been termed 'basal endpoint control' (Thorne and Tovey, 1981).

For banks retreating due to fluvial erosion, basal endpoint control governs the rate at which eroded material is carried away from the bank, and hence the rate at which further material can be entrained from the intact bank. For banks retreating predominantly by mass wasting, basal endpoint control determines the rate at which failed blocks of bank material are entrained at the bank toe. While in place, these blocks tend to reduce the intensity of fluvial attack on intact material at the base of the bank, thus limiting toe scour and under cutting that would otherwise increase bank height or steepness (Simon *et al.*, 2000; Thorne and Tovey, 1981). The cohesive strength of failed blocks (which are often also root bound), together with their propensity to adhere to the channel bed and lower bank around the toe (Wood *et al.*, 2001) make it progressively more difficult to remove blocks as the time that they have been resting at the toe increases. Hence, basal clean out of failed debris is often limited by the rate of block weathering and break down rather than near-bank hydraulics. Conversely, in channels with weakly cohesive or non-cohesive banks

basal clean out of eroded material can occur much more quickly, particularly in high energy, incising reaches, leading to extremely high rates of bank erosion that drive very rapid widening and a switch from vertical to lateral adjustment in the later stages of channel evolution following base level lowering (e.g. Simon and Thorne, 1996; Thorne *et al.*, 1993) (Figure 3.4).

Wolman and Brush (1961) found that the absolute, percentage and rate of increase in mean channel width increased as a function of the *initial* rate of stream power expenditure per unit bed area in unstable channels. As larger falls in base level deliver larger increases in stream power, it may be hypothesised that the degree and upstream extent of widening will scale on the magnitude of the fall in baselevel. However, in situations where the fall in base level is both large and instantaneous, though ultimately the degree and extent of widening will both be large, the onset of widening may be delayed until the end of a phase of erosional narrowing.

3.3.1.3 Long profile adjustments

The longitudinal changes in the fluvial system that will occur within the reservoir area are inextricably linked to the adjustments of the cross-sectional channel geometry discussed above. This is the case because the timing and degree of channel change associated with cross-sectional adjustments are functions of location on the delta and, particularly, distance upstream from the AMD (Figure 3.3i, ii). Previous discussion of controls on the nature, rapidity and extent of cross-sectional adjustments has already touched on the importance of bed slope and changes therein and this section expands consideration of the significance of slope adjustments and the role that armouring may play in affecting changes in slope.

The slope and long profile concavity of a channel from source to mouth can be considered to be a semi-independent variable when considering the evolution of a channel towards steady-state equilibrium during a period of graded time (section 3.1). This is because it takes longer to adjust the long profile than it does other variables associated with the other degrees of freedom in the channel, allowing slope to exert a certain degree of control over their evolution (Figure 3.5) (Knighton, 1998). The slow response of the long profile occurs principally because any significant changes to



Figure 3.4. (Previous page). The Lake Mills delta during the April 1994 drawdown experiment.
a-c: Lower, middle and upper delta respectively on the 12th April, three days after the start of the drawdown experiment and after a drawdown of about 2.7 m (9 ft).
d-f: Lower, middle and upper delta respectively on the 16th April at the end of the period of drawdown and after a drawdown of about 5.5 m (18 ft).
g-i: Lower, middle and upper delta respectively on the 23rd April after one week of holding the water surface elevation at the level attained on the 16th April.

channel slope entails the mobilisation and transport of considerable quantities of bed material load over relatively long distances when compared to the transfers of sediment required to elicit marked changes through vertical or lateral adjustments.

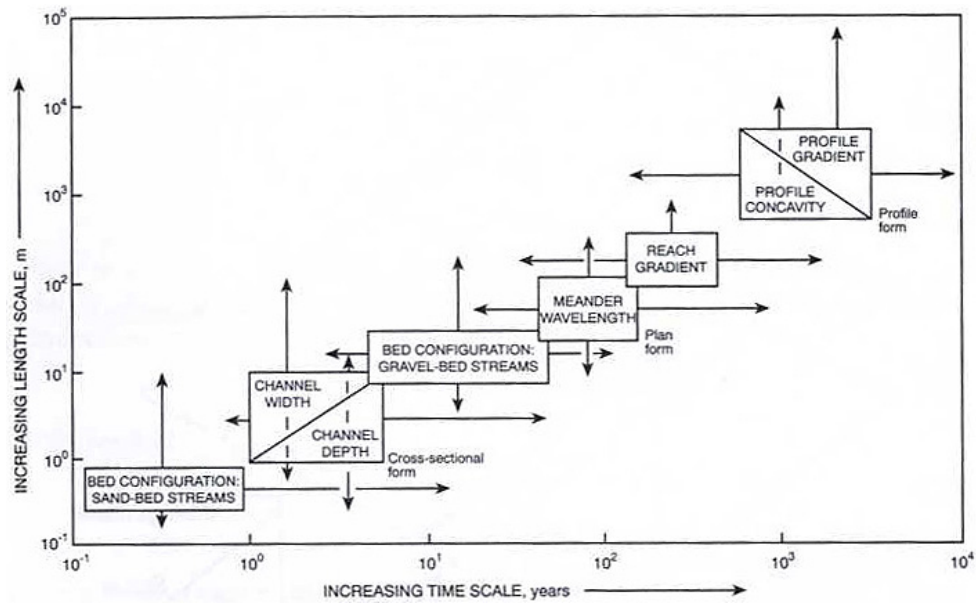


Figure 3.5. Schematic diagram of the timescales of adjustment of various channel form components with given length dimensions in a hypothetical basin of intermediate size (Knighton, 1998).

For instance, planform metamorphosis in channels with meandering and braided channels is, in terms of sediment transfer, a much more efficient way of dissipating excess stream power than is incision (Schumm, 1977). According to Figure 3.5, this reasoning may also be applied to the adjustments of channel slope at the reach scale, (that is over a length of channel ranging from several tens to a hundred or more times the width, which is the length scale relevant to the delta in Lake Mills). It follows that significant adjustments to the long profile may require decades to centuries to be completed. Adjustments of the long profile are likely to take even longer in coarse-bedded streams where sediment transfer takes place as bedload (*i.e.* episodic, occurring just a few days a year and with short transport distances) and bed scour is limited by the formation and persistence of an armour

layer at the bed surface. Not only does armouring protect the underlying, finer substrate from scour, it also adjusts rapidly to increases in stream power through coarsening by selective entrainment of the finer material. For example, Simon and Thorne (1996) showed that, in the North Fork Toutle River following the eruption of Mount St Helens, decreased bedload transport rates and increased energy losses due to bed coarsening were more important than bed slope adjustments in governing the nature and extent of adjustments to the fluvial system.

In the context of changes in the composition of the surface layer, Parker *et al.* (1982) distinguish between paved gravel-bed rivers, in which the coarse surface pavement is mobilised several days a year, and a gravel-bed river with static armour in which the surface layer is almost never mobilised. Flume experiments reported by Dietrich *et al.* (1989) show that static armour forms when the supply of bedload is less than the local transport capacity, *i.e.* where the sediment movement is supply limited. This observation has subsequently been verified using high quality field data (Reid *et al.*, 1999).

In Lake Mills, dam removal will occur under low flow conditions when the supply of coarse sediment from upstream to the delta will be negligible, and while the transport capacity within the delta reach will be very high due to the large increases in stream power caused by substantial falls in base level. It is therefore anticipated that a static armour layer will form in the upstream portion of the delta (where coarser sediment is concentrated) and this is likely to restrict the extent to which the channel in the proximal area of the delta incises and adjusts laterally, due to impacts of the type identified by Simon and Thorne (1996). If coarsening of the armour layer does limit bedload availability, inhibit bed scour and result in increased energy dissipation through bed roughening, the outcome will be a marked reduction in the volume of sediment eroded from the delta for a given fall in base level. There is evidence to support this inference. For example, a reduction in the degree of channel adjustment in the proximal area of the delta was clearly visible during the 1994 drawdown experiment (Figure 3.4). It follows that bed armouring must be mimicked in the physical model of Lake Mills if the behaviour of the incising channels is to be accurately simulated.

3.3.2 Planform adjustments

3.3.2.1 Planform definitions and controls

As mentioned in the last section, cross-sectional and long profile adjustments may be accompanied by planform changes as the channel responds to the additional stream power introduced by the reductions in base level associated with lowering of pool level during dam removal. Planform changes are especially likely when the fall in base level is large.

Leopold and Wolman (1957) distinguish between straight and meandering planforms on the basis of arbitrarily assigned values of sinuosity. According to their classification, in single-thread rivers, straight channels have a sinuosity between unity and 1.1, sinuous channels have sinuosities between 1.1 and 1.3 and meandering channels have sinuosities greater than 1.5. In Leopold and Wolman's (1957) paper, braided rivers are considered to be straight, having sinuosities close to unity.

Laboratory experiments were conducted by Schumm and Khan (1972) to explore geomorphic controls on planform and planform change. These experiments were performed with a constant discharge and only flume slope being changed, which is equivalent to changes in valley slope. Their results suggested that planform changes from straight, to meandering and then to braided (Figure 3.6a) were related to distinct threshold values of available stream power, expressed in terms of the product of discharge and valley slope. This finding is consistent with the opinions of both Leopold and Wolman (1957) and Antropovskiy (1972, cited in Richards, 1982), who found that braided channels are higher energy environments than meandering channels.

Richards (1982) argued against the existence of geomorphic thresholds between different planform types. He proposed that the distinction between planforms masks a continuous relationship between stream power and sinuosity. On this basis, he proposed that total sinuosity, P , be used to represent channel form. This is defined by the total active channel length divided by valley length. Richards plotted total sinuosity as a function of stream power (Figure 3.6b), claiming that the resulting graph supported his hypothesis. There is a significant degree of scatter in this plot that may be due to the difficulty of collecting discharge measurements of a similar magnitude and frequency from both lowland single-thread and upland multi-thread

channels (Richards, 1982). It may also reflect the widely differing resistances to entrainment that different channel boundary materials create (Richards, 1982). More importantly, closer inspection of the graph shows how the data points actually cluster by planform type to produce a clear distinction between single-thread and braided channels in terms of stream power and total sinuosity. This observation brings into question the proposal that total sinuosity is able to describe channel planform adequately.

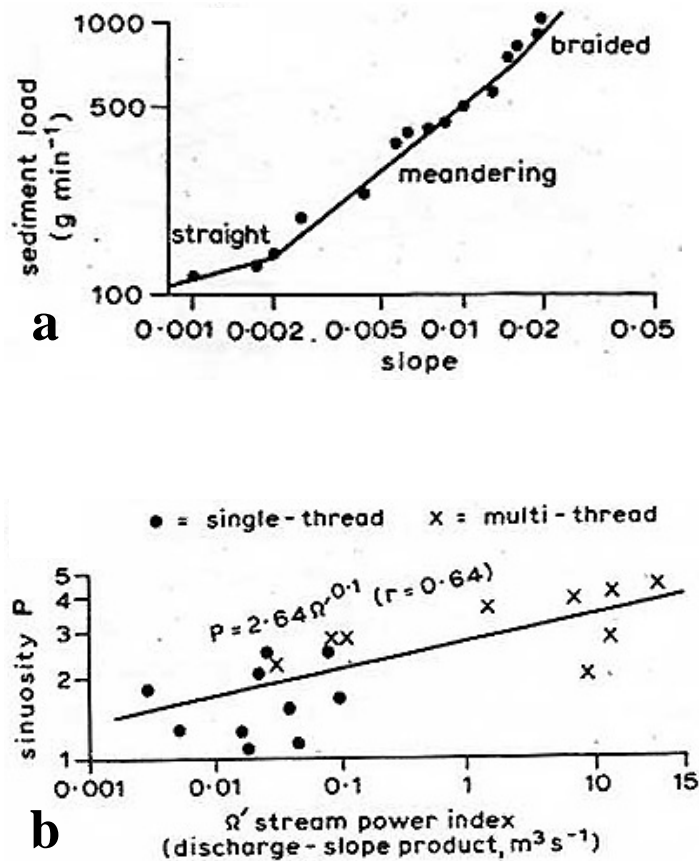


Figure 3.6. Channel planform and stream power. (a) Channel planform as a function of stream power, in which changing slope with constant discharge represents stream power in the experiments of Schumm and Khan (1972) (from Richards, 1982). (b) Increasing stream power moving from single-thread to multi-thread channels (Richards, 1982).

Furthermore, it may be questioned whether stream power is actually the best variable with which to predict planform characteristics. As long ago as 1933, Rubey pointed out that stream power does not represent solely the energy that may be used to transport sediment and so adjust the planform of the channel (Rubey, 1933). In this context, excess stream power (Bagnold, 1966) or the portion of the boundary shear

stress attributable to grain roughness might be a better metric. Finally, only 19 data points are used to fit the regression line in the plot, which is not a large number, and the points are not evenly distributed over the range of data, weakening the validity of regression analysis (Soar and Thorne, 2001).

Based on the available evidence, there do appear to be morphological distinctions between straight, meandering and braided channels in terms of stream power, with a modest increase in energy from a low base likely to produce an increase in the sinuosity in single-thread channels and larger increases in higher energy systems liable to trigger planform metamorphosis from single-thread to braiding. Such a relation need not be hypothesised purely on the form of statistical association but may also be explained through consideration of the process-response mechanisms that operate in alluvial channels. This may be illustrated by examination of fluvial processes and morphological changes involved in planform change from straight to meandering.

The initial classification of channel planform into straight, meandering and braided by Leopold and Wolman (1957) is now known to be inadequate to describe the full spectrum of planforms found in nature (Knighton, 1998), yet it remains useful as a framework on which to base discussions of the role and purpose of different general types of planform, particularly as they relate to the likely response of a channel on a prograding delta surface during dam removal.

3.3.2.2 Meandering channels

Pools and riffles are features common to both straight and meandering gravel-bed and mixed sand- and gravel-bed rivers (Clifford, 1993). Perhaps the most comprehensive mechanism to explain their formation is that provided by Yalin (1971b; 1992), who argued that macro-turbulent eddies formed at the boundary of a straight channel of uniform cross-section (Figure 3.7i) generate alternating zones of accelerating and decelerating flow spaced at mean intervals of $2\pi w$ (where w = mean channel width) (Figure 3.7ii). The product of 2π is 6.28, which is within the 5-7 channel widths that usually separate pools and riffles (Leopold *et al.*, 1964). At channel-forming discharges, the zones of accelerating flow generate shear stresses sufficient to scour the bed. In zones of decelerating flow, the shear stresses drop sufficiently to allow the

Figure 3.7. (Previous page). The role of hydraulics in meandering channel formation. **(i)** The growth of vertical macro-turbulent eddies (a, b) and the coherent structure formed by the fully-developed eddy and its surrounding flow complex (Yalin, 1992). **(ii)** Longitudinal flow accelerations and decelerations (Yalin, 1992). **(iii)** The formation of horizontal macro-turbulent eddies that scale to channel width (Yalin, 1992). **(iv)** Models of spiralling flow after (A) Einstein and Shen (1964) and (B) Thompson (1986) (from (Knighton, 1998)).

scoured material to deposit, thus forming the riffle. The channel banks are rough, as well as the channel bed, however, and this generates macro-turbulent eddies with vertical axes (Figure 3.7iii) that may interact with the spanwise eddies in straight channels to generate stress-induced secondary currents (Prandtl's flow of the second kind) (Bathurst *et al.*, 1979; Yalin, 1992). These are velocities that occur in the plane normal to the axis of primary flow. They form coherent flow structures that are often characterised as two cells of cross-channel circulation, rotating in opposite directions.

In pools, the secondary cells converge at the water surface and sink to diverge at the bed. The sinking flow carries high velocity, near surface water close to the bed, steepening the near-bed velocity gradient and so locally increasing boundary shear stress. At the same time, bedload diverges beneath the sinking flow due to diverging secondary currents. The outcome of this flow/sediment interaction is to promote bed scour. Conversely, at riffles, the cells converge at the bed, lifting slow, near-bed water higher into the flow. The effect is to reduce the velocity gradient and boundary shear stress while concentrating bedload to promote medial bar formation (Hey and Thorne, 1975; Keller and Melhorn, 1973). In three-dimensions, secondary circulations are superimposed on the downstream (primary) flow to produce the helicoidal flow characteristic of many fluid shear flows in nature (Figure 3.7iv).

Spiral flow is widely believed to be a pre-requisite for the development of meandering in straight rivers (Richards, 1982). It can explain the formation of pool-riffle morphology in a straight channel, which occurs when there is sufficient excess energy to entrain sediment and deform the channel bed. Because of stress-induced secondary circulation, the deformation of the bed is cross-sectionally asymmetrical, *i.e.* the pools and riffles are offset from the channel centre line. This morphological response allows form to begin to affect process, with topographic steering driving curvature effects that act to amplify the strength of secondary currents (Richards, 1976). These stronger secondary currents are skew-induced (Prandtl's flow of the first kind) (Bathurst *et al.*, 1979).

Skew-induced secondary currents are highly effective in convecting high velocity primary flow across the channel, and the spiral flow carries fast flow close to the channel bank at the outer margins of pools, promoting toe scour and fluvial bank erosion. The resulting bank retreat increases flow curvature, strengthening flow asymmetry and further increasing boundary shear stresses on outer banks by over 100% compared to straight channels (uniform flow) (Ippen and Drinker, 1962). Through time, bank retreat at the outer margins of pools (hence, located along alternate sides of the channel at intervals of about six times the width) creates a sinuous channel. Once bends become sufficiently pronounced that the channel is meandering, bend growth and migration will continue through a process of positive feedback (Hickin and Nanson, 1975).

As the amplitude of the meander bends increase, sinuosity increases and the energy slope and stream power per unit channel length both decrease. Furthermore, as pool curvature increases, through decreasing bend radius of curvature, r_c , there is an increase in macro-scale (related to large bars and planform) flow resistance (Richards, 1982) which reduces the amount of excess stream power available to entrain and transport sediment. Increased flow resistance at bends occurs because of intense turbulent eddying and strong secondary flows, which are collectively termed internal distortion resistance (Leopold *et al.*, 1960). Sinuosity continues to increase until the remaining excess energy is balanced by erosion and transport of sediment that translates bends downstream at a constant amplitude and, therefore, further bend growth is prevented (Richards, 1982)¹⁰.

Equilibration in meander bend development appears to occur at remarkably consistent values of the ratio of bend curvature to channel width, r_c/w , irrespective of channel size, location and whether the channel is in the field or laboratory. Bagnold (1960) suggested a range of 2-3 for r_c/w , based on theoretical considerations and experimental observations. Hickin (1974) cited a mean value of 2.11 for bends on the Beatton River, Canada. Leopold and Wolman (1960) noted that bends from field and laboratory channels have a mean r_c/w of 3.1, with two-thirds in the range 1.5-4.3 and one-quarter in the range 2.0-3.0. Davies and Sutherland (1980) suggested a value of

¹⁰ Yalin actually uses this mechanism to explain the onset of meandering, but Richards (1982) notes that all the empirical evidence indicates that this spacing is only half that of meander wavelengths and that the mechanism must instead explain the formation of the pool-riffle sequence, which is generally (but not always) a pre-cursor to meandering.

about 2.5. Apmann (1972) proposed a range from 2.0, based on field observations, to approximately 4.5 based on theoretical work and laboratory observations. Because laboratory channel widths tend to scale to about $Q^{0.4}$ compared to $Q^{0.5}$ in real rivers (Ackers, 1972), they are proportionately narrower than real channels and will therefore produce proportionately larger values for r_c/w . The upper limit to Apmann's and Leopold and Wolman's proposed ranges, when applied to real rivers, should therefore be somewhat less than 4.5 and 4.3, respectively.

Theory and observation suggest that river meanders grow until the ratio of radius of curvature to width has attained a critical value, which generally requires an increase in the amplitude of the meander bend. During the recovery of two Iowan rivers from artificial straightening, Noble and Palmquist (1968) found that meander amplitude increased at a greater rate than meander wavelength. In flume studies of meander development, both Friedkin (1945) and Tiffany and Nelson (1939) found that meander wavelength and amplitude increased with increasing discharge and flume (valley) slope, *i.e.* with an increase in stream power (equation 3.5). Using observations from aerial photographs of meandering channels in Russia, Kondratiev *et al.*, (1982, cited in Yalin, 1992) showed that when the angle of deviation of the flow from the down-valley direction, θ , is small (equivalent to a large r_c/w) the downstream migration of meander waves tended to dominate over meander amplitude growth, but that as θ exceeded 65° - 75° (decreasing r_c/w ; sinuosity 1.35-1.6), this tendency was reversed. Furthermore, the maximum meander amplitude growth rate occurred when $\theta = 70^\circ$, which corresponds to the tightest curvature ratio of the sine-generated curve. In a similar vein, Schumm (1977) used observations from the Mississippi and Jordan Rivers to show that channel sinuosity, and therefore the degree of meandering, was greater along steeper sections of valley floor. A steeper valley slope increases the available stream power for a given discharge. Its effect is, therefore, analogous to that of lowering the base level in a reservoir.

3.3.2.3 Braided channels

A meandering channel may be expected to respond to the excess stream power introduced by a drop in base level through increasing its sinuosity and meander amplitude. However, in a braided channel the morphological response will be different. According to Yalin (1992) braided channels respond to increased stream

power through an increase in the braiding intensity that reduces the hydraulic efficiency of the channel, decreasing excess energy available to transport sediment and increasing the equilibrium slope. Based on the evidence collected during the 1994 drawdown experiment (Figure 3.4), braiding should be expected to occur during the removal of the Glines Canyon Dam and it is also expected to occur in the physical model of Lake Mills.

Explanations for the onset of braiding fall into two main categories. The first explains its occurrence as a function of one or several of discharge, valley slope (which together determine stream power), sediment size and bank erodibility, while the second invokes instabilities of two-phase (water and sediment) flows at the channel bed (Ashmore, 1991a).

Yalin (1992) argued that the fundamental mechanism causing the onset of braiding is a continuation of that which explains meandering. As the energy slope increases, for example due to a drop in base level downstream or aggradation in the channel upstream, then the number of rows, N , of macro-turbulent cells increases from $N = 1$ to $N = 2$ (Figure 3.8). The first two horizontal bursts from the left and right banks accelerate the flow, and thus sediment in transport, through the channel centre. Because there are two rows of horizontal turbulence, this takes place over a distance of $6(B_o/2) = 3B_o$. Further downstream the flow decelerates and the sediment is deposited to form a central bar (central bar I). As the steepness of the still submerged bar increases, more flow is directed into the two flanking channels, causing them to deepen and widen, which causes central bar I to emerge as a medial island. This change to the flow's plan geometry alters the '*intended*' location of central bar II, which would have formed downstream from central bar I. Because the sum of the transport capacities of the two anabranch (second-order) channels flanking the central bar I is less than that of the original undivided flow (because sediment transport capacity is proportional to discharge to about the 1.5 power), it cannot transport the sediment supplied from upstream and locally eroded from the retreating banks. The excess sediment is, consequently, deposited in the zone of flow expansion where the channel bifurcates around bar I: that is closer to central bar I than central bar 2 *would* have been formed; to form two smaller bars - bars II' and II". These smaller bars then themselves act as central bars in the anabranches, dividing each of the second-order channels into two, third-order channels. Yalin (1992) argues that this

self-induced mechanism of braiding is the only one capable of initiating true braiding, since it is the only one that explains the self-generating nature of the individual braid bars. He suggests that the process continues until the width-depth ratio of the lowest order channel is such that it develops $N = 1$ rows of macro-turbulent cells and begins to meander rather than braid, at which point it minimizes any remaining excess energy by reducing its bed slope rather than by any further sub-division of the flow.

The sequence of morphological developments produced according to Yalin's braiding mechanism is essentially identical to the central bar deposition mechanism observed in flume experiments by Leopold and Wolman (1957) and its key features (reduced transport capacity due to flow division, positive feedback between bank erosion and bar growth, deposition of sediment in the zone of flow expansion). In contrast, in a flume study, Ashmore (1991a) identified that the central bar initiation mechanism is actually just one of four initiating processes, the others being the chute cutoff, transverse bar conversion and multiple bar braiding. He suggested that central bar initiation was associated with the lowest stream power per unit length and amongst the lowest braiding index values¹¹ found in any of his experiments. Ashmore (1991a) also noted however that, while there are four separate processes, they were all caused by one fundamental sedimentation mechanism; that of the stalling and vertical aggradation of bedload sheets in a zone of expanding flow, which does accord with Yalin's (1992) theory.

More recently, Thomas (2006) performed an extensive review of braided river literature and concluded that braiding is an emergent phenomenon that is simply a function of the width-depth ratio and fundamental flow instabilities at the channel bed that allows bed load to stall and form the nucleus of braid bars. Richardson and Thorne (2001) used detailed three-dimensional measurements of the flow field in an anabranch of the Brahmaputra-Jamuna River to show that the bed load stalls when flow with a single-thread of high velocity splits into two or more threads of high velocity within a single-thread channel. This occurs when the depth-width ratio drops below a threshold value for a given value of specific energy, thus providing a hydraulically-based explanation for the onset of braiding. Once the flow has split, the bed aggrades in the zones between the high velocity filaments and incises below them, thus forming a submerged bar. If these hydraulic conditions persist for a

¹¹ Defined as the mean number of active channels per cross-section (Ashmore, 1991a).

sufficient length of time, the local bed morphology begins to influence the flow hydraulics in a positive feedback, which can then lead to the emergence of a braided channel morphology (Richardson and Thorne, 2001).

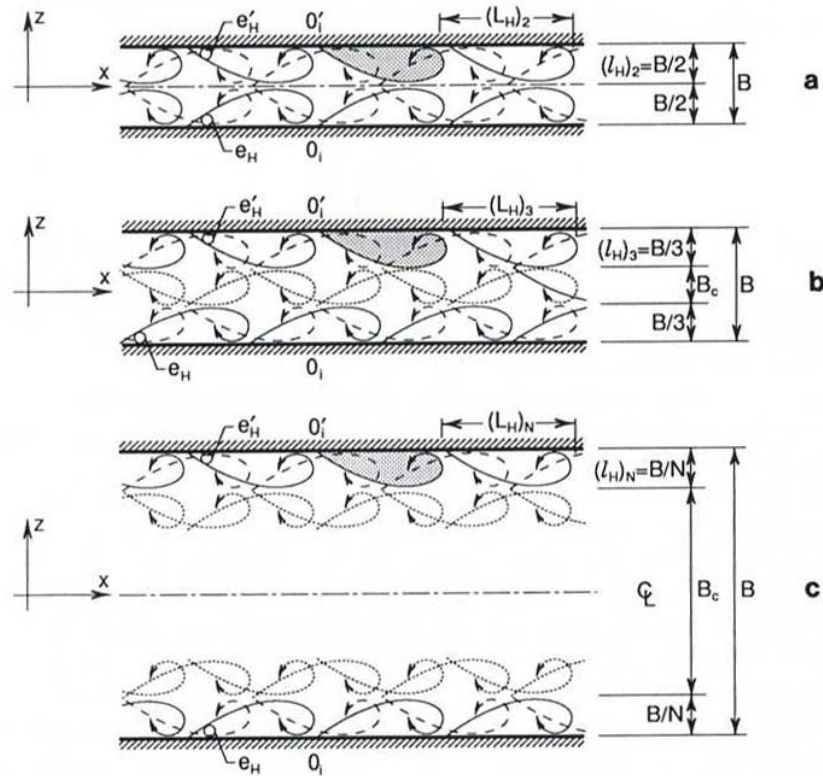


Figure 3.8. Increase in the N -row configurations as increasing bed friction effects (increasing width-depth ratios or relative roughness) reduces the maximum size of the horizontal macro-turbulent eddies.

Irrespective of the mechanism by which braiding is initiated, its occurrence is clearly associated with higher energy environments than meandering channels (Figure 3.6) and, just as meandering has been interpreted as a means of reducing excess stream power (Richards, 1982), so braiding can be similarly interpreted (Schumm & Khan, 1972; Antropovskiy, 1972 – cited in Richards, 1982; Leopold & Wolman, 1957), particularly in environments where non-cohesive channel boundary sediments may make it difficult for meanders to develop (Schumm and Khan, 1972). Increased braiding intensity, expressed by the number of braid bars and anabranch channels in a cross-section, in response to an increase in stream power has been observed in both the laboratory (Ashmore, 1991b) and the field (Howard *et al.*, 1970). It may be hypothesized, therefore, that the intensity of braiding, and thus total sinuosity, is likely to increase with the magnitude of the fall in base level. This morphological response will create a wider channel and therefore more delta erosion, since the

creation of successively lower-order bars and channels will continue to force the flow into the banks/terraces.

Based on this brief review, it may be hypothesized that a significant reduction in base level will tend to trigger meandering in an initially straight channel flowing across the sediment delta, an increase in sinuosity through bend growth in a mildly meandering channel, and metamorphosis of a strongly meandering channel into a braided pattern. These types of planform change usually entail the erosion of additional sediment from the banks, and so it may be expected that the volume of delta sediment eroded during base level lowering events that trigger planform adjustment will exceed those that do not affect the planform.

3.4 Working hypotheses

On the basis of the arguments presented in this chapter, the following working hypotheses have been formulated.

Hypothesis 1

The larger the **magnitude of each incremental reduction** in base level and the longer the time allowed for the channel(s) crossing the delta to adjust to the increased stream power:

- (a) the further the sediment will prograde longitudinally into the reservoir;
- (b) the more rapidly sediment will erode from the delta surface;
- (c) the greater the total volume of sediment that will be eroded for a given drop in base level.

Hypothesis 2

The shorter the relaxation time allowed for the delta channel(s) to adjust following an incremental reduction in baselevel:

- (a) the further the sediment will prograde longitudinally into the reservoir;
- (b) the more rapidly sediment will erode from the delta surface; and
- (c) the greater the total volume of sediment that will be eroded during the next incremental reduction in base level.

The rationale for Hypothesis 2 is that, by preventing the delta surface channel(s) from completely adjusting to the effects of an incremental reduction in baselevel before the base level is further reduced, the cumulative effects of two or

more smaller drops in base level will be similar to that of a single, larger drop, because the excess energies introduced by the sequential, small reductions in base level will act cumulatively rather than independently.

Chapter 4 Scaled Physical Model Design

A model is a simplification of a phenomenon that exists in the real world and is created conceptually, numerically or physically in order to study that phenomenon. The model provides the primary link between the aspects of the phenomenon that can be measured and observed in the real world and how scientists think about how and why the phenomenon occurs (Rhoads and Thorn, 1996). Once created, a numerical or theoretical model's components can be adjusted to see how they affect the phenomenon, thus furthering the scientists' understanding of that phenomenon.

Conceptual models are a crucial first step in the creation of numerical and physical models and are perhaps the most important stage of the entire modelling exercise, because they identify the processes and form-process-response interactions of importance to the phenomenon to be modelled. This is particularly true for numerical models because unless the relevant processes and form-process-response interactions have been correctly identified, they cannot be properly represented in the model. This is important for modelling dam removal, in that many of the relevant form-process-response interactions such as the transport of widely graded sediments over partially armoured beds, upstream migration of knickpoints/zones in layered sediments, sediment transport during overbank flows, channel evolution involving bank erosion/width adjustment, and vegetation effects on sediment transport and morphological adjustment are either incompletely represented numerically or, in some cases, are not represented at all (Pizzuto, 2002). It is, therefore, of the greatest importance to the nascent study of dam removal (and many other modelling applications too), that as many observations and as much data from the field and laboratory are collected to allow the development of conceptual models that are as sophisticated and insightful as possible and which, therefore, are able to support numerical models that are as inclusive and accurate as possible (Grant, 2001).

In this respect, physical models have a potential advantage over numerical models in that many processes and form-process-response interactions (including most of the poorly understood ones) can be recreated intrinsically. The extent to which this can occur, however, depends on how accurately the relevant geometrical, dynamic and kinematic criteria are recreated in the model (section 4.1). This capability can be used to identify previously unknown fluvial phenomena and to

examine the causal factors behind form-process-response interactions whose existence is already known, but which cannot be reduced to the form of a differential equation. They have a further advantage over numerical models in that they recreate highly complex fluvial phenomena in three-dimensions despite the lack of sufficient mathematical equations to represent them numerically.

Conversely, it is not possible to faithfully recreate *all* the fluvial phenomena operating in the prototype at any model scale less than 1:1. Consequently, processes and interactions that are fully documented can be fully represented in numerical models, which have an advantage in this respect. Also, some important parameters are difficult or impossible to scale. Good examples are the problems with representing the properties of cohesive bank sediments and the stability of banks with respect to mass failure in a physical model (ASCE, 2000). Additionally, once a good quality numerical model has been developed, it can easily be modified and used to examine a wide range of possible future scenarios more quickly and for much less cost than a physical model. Numerical models therefore become the more flexible and powerful tool in assisting with options appraisal when there are multiple possible solutions or futures to be investigated in design, planning and management.

There are, then, advantages and disadvantages to the use of physical and numerical models and the choice of model will depend on the nature of the problem being addressed, the scale of the reach to be modelled and the funding/expertise available. Currently, however, our understanding of the form-process-response interactions occurring in a reservoir during dam removal is not fully understood and cannot be fully expressed numerically. Also, the incision and lateral shifting of a stream channel crossing an alluvial delta involve strongly three-dimensional fluvial processes and morphological changes and there are only limited knowledge, few observations and a serious lack of field data with which to define and describe the relevant phenomena. These factors suggest that physical modelling is the preferred approach to investigate the fluvial processes and morphological changes and so add to our understanding of the sediment dynamics during dam removal.

4.1 Introduction to physical modelling

Several different classes of physical models may be used by river scientists to study fluvial phenomena depending on how accurately it is necessary to represent the

phenomena in question (Figure 4.1). Perfect replication, or complete similitude (section 4.2), can only be achieved with a model scale of 1:1, *i.e.* through recreation of the full size prototype in the laboratory, since this is the only way that the forces (including gravity), dynamics (fluid and mechanical) and geometrical relations present in the prototype can be recreated perfectly and simultaneously in the model. Hence, the ideal class of model employs full-scale replication of the prototype. Clearly, this is rarely feasible in fluvial investigations, although it is common in some highly sensitive modelling applications, performed by agencies such as NASA. The second most accurate class of models employ Froude-scaling, since the relationship between inertial and gravity forces is the most important force-balance governing fluvial processes in open channels, together with full geometric similitude in an undistorted model. The third class of models also employs Froude-scaling, but uses different vertical and horizontal scales in a distorted model. These distorted models are intended to meet the requirements for Froude similitude, while keeping the horizontal dimensions of the model manageable and adjusting the slope or the vertical scale from their geometrically correct values in order to allow the model to function practically (Peakall *et al.*, 1996). The fourth most accurate class of models are Generic Froude-scale models (FSMs) (not shown in Figure 4.1), which are designed according to the principles of Froude-scale modelling, so that the important flow and sedimentary parameters are within reasonable proportion, but which do not correspond exactly to any particular prototype location (Peakall *et al.*, 1996). Finally, a class of less formal models that do not obey the Froude similitude criterion even approximately, but seek to mimic fluvial processes and morphological changes at a small scale, are termed ‘analogue’ (Chorley, 1967) or ‘similarity-of-process’ (Hooke, 1968) models.

Moving further to the right along the abscissa in Figure 4.1 implies a reduction in the overall accuracy with which prototype phenomena are replicated in the model, although some specific phenomena, such as sediment transport, can be represented more accurately in a distorted model than an undistorted one. Further, a reduction in accuracy does not mean that model results are not still useful or informative. In this context, Paola (2000) argues that the physical nature of an analogue model makes it suited to the investigation of fundamental system behaviour, since it allows complex interactions to develop fully, which is not possible in existing numerical or theoretical

models. For example, qualitative similarity-of-process models have been used successfully to develop our understanding of knickpoint migration (*e.g.* Brush and Wolman, 1960; Holland and Pickup, 1976; Schumm *et al.*, 1987), while quantitative analogue models have been used to examine landscape evolution (Van Heijst *et al.*, 2001) and long profile adjustment to changes in sea-level (Van Heijst and Postma, 2001).

Similarly, the results of generic FSMs have been upscaled within the bounds imposed by the scale ratios for comparison to real world examples and found to recreate many of the intended fluvial forms with an acceptable degree of accuracy, (*e.g.* Ashworth *et al.*, 1994; Moreton *et al.*, 2002). It may also be possible to upscale the results of these models to prototype sites larger than those apparently permissible according to the scale ratios, although this would effectively transform the generic FSM into an analogue model.

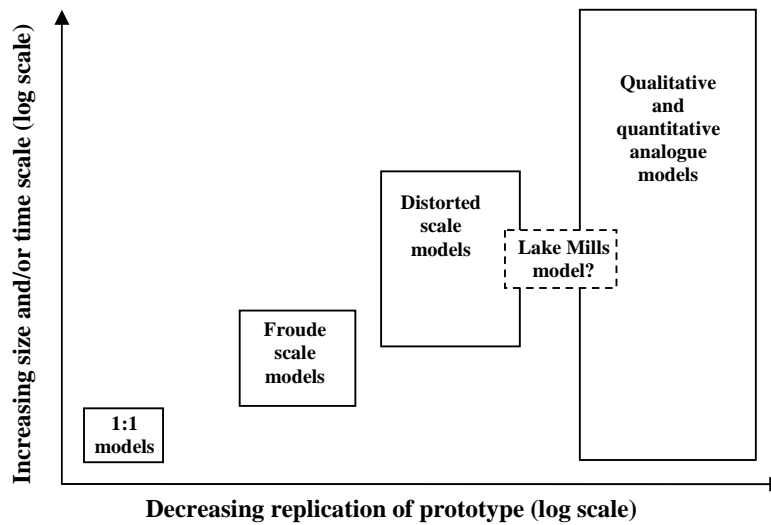


Figure 4.1. Different classes of physical model (modified from Peakall *et al.* (1996)). The relative positioning of the boxes is schematic but aims to make two important points. First, there is a significant decrease in overall model accuracy when moving from 1:1 to Froude-scale models and from Froude-scale to analogue models and that this is greater than the loss of accuracy incurred when moving from an undistorted Froude-scale model to a distorted model. Second, the positioning and size of the boxes illustrates the relative size of prototype that the particular model attempts to simulate (Peakall *et al.*, 1996). The position of the Lake Mills model suggests that, given the amount of space available in which to model such a large prototype, the model may be at, or even exceeding, the upper limit of what can be quantitatively achieved with a distorted Froude-scale model and that some or all elements of the model may be more appropriately considered to be a analogue model (for more on this, see sections 5.3.1 and 8.1.2).

4.2 Principles of scaled physical modelling

Scaling in physical modelling is based on the need to maintain dynamic, geometric and kinematic similitude (*i.e.* similarity of force, geometry and velocity respectively) between model and prototype. If perfect dynamic and geometric similitude are obtained then kinematic similitude automatically follows (ASCE, 2000). There are three ways of obtaining model similitude (ASCE, 2000):

- i) Through matching the ratios of the forces relevant to the particular study in the model to those in the prototype. This approach requires careful definition of the processes to be simulated and a deep understanding of how they operate, and is the approach outlined in section 4.2.1.
- ii) Through the use of dimensional analysis, in which all of the key variables affecting the physical processes of the system being studied are grouped together into a series of dimensionless parameters. This approach is briefly exemplified in section 4.2.2.
- iii) Through manipulation of the governing equations of fluid and sediment dynamics. This is the most rigorous approach, but it relies on all the governing equations being known, which is rarely the case.

4.2.1 Fixed-boundary models

A fixed- or rigid-boundary model is generally taken to mean one whose boundary does not have the capacity to change under any circumstances, although Yalin (1971a) describes two situations when this is not strictly true. When a channel has a bed of loose granular material, but the flow conditions are below those required for incipient motion, then the mobile bed is effectively rigid. Second, when a mobile bed is being transported as bed load but the flow conditions are not inducing any variation in the *geometry* of the bed, *i.e.* they are not creating a changing sequence of bedforms, the channel can similarly be considered to have a rigid bed (Yalin, 1971a).

In a fixed-boundary hydraulic model the fluid (usually water), will generally be moving as a single-phase flow, *i.e.* it will not be transporting any other material. Accurate simulation of single-phase flow is of paramount importance in

morphological modelling because it forms the basis of all subsequent two-phase¹² flow modelling (ASCE, 2000). In this context, of greatest importance is the need to achieve dynamic similitude, which requires achieving similitude in terms of flow inertia, gravity, pressure, the physical properties of the fluid (viscosity, density, surface tension and vapour pressure), and the drag forces (friction) imposed by the channel boundary or by objects immersed in the flow. If dynamic and geometric similitudes are achieved then kinematic similitude follows automatically (ASCE, 2000). However, as noted above, it is not possible to achieve perfect dynamic similitude unless a modelling scale of 1:1 is used and in practice a choice must be made concerning which forces are the most important for the problem at hand and which, therefore, should be matched to the prototype.

Fluid inertia is an important force in almost every problem involving fluid flow, while gravity is the driving force in all open channel flows (ASCE, 2000). The ratio of these two forces yields the Froude number, Fr , which is given by:

$$Fr = \frac{U}{\sqrt{gH}} \quad (4.1)$$

where U = mean flow velocity (m/s); g = gravitational acceleration (m/s^2); and H = flow depth (m). The Froude number is thus the most important parameter to be replicated between the prototype and models of open channel flows. The Froude number scale ratio to be achieved between prototype and model is therefore given by (ASCE, 2000)

$$Fr_r = \frac{Fr_p}{Fr_m} = \frac{U_r}{\sqrt{g_r H_r}} = 1 \quad (4.2)$$

where the subscripts r , p and m refer to scale ratio, prototype parameter and model parameter values, respectively.

Flow, fluid and sediment properties can all be expressed in terms of their fundamental dimensions of mass, M , length, L , and time, T (ASCE, 2000). This being so, equation 4.2 can be rewritten as:

$$U_r = \frac{L_r}{T_r} = \sqrt{g_r L_r} \quad (4.3)$$

¹² Two-phase flows are those involving liquid and gas, gas and solid, or liquid and solid, which in river models is usually water and sediment.

As gravity is the same in the prototype and model, $g_r = 1$ and equation 4.3 simplifies to:

$$U_r = L_r^{0.5} \quad (4.4)$$

Substituting equation 4.4 into 4.3 and solving for T_r then produces:

$$T_r = L_r^{0.5} \quad (4.5)$$

The velocity and time scales represented by equations 4.4 and 4.5 (also 4.7, 4.8 and 4.10, 4.11) are the two most important scaling relationships in hydraulic modelling because they establish the relationship between kinematic and geometric variables (ASCE, 2000). Which pair of the aforementioned equations is selected for use in scaling a model depends on the nature and objectives of the modelling exercise, since the nature of equations 4.4 and 4.5 changes depending on which force ratios are most important given the issue in question.

Another important force ratio is that of inertial to viscous forces, since this determines whether fluid shearing is dominated by laminar or turbulent processes, which controls how velocity varies as a function of distance from channel boundaries such as the bed. This ratio is called the Reynolds number, Re , and its open-channel form is given by:

$$Re = \frac{UR_h}{\nu} \quad (4.6)$$

where R_h = hydraulic radius (m) and ν = kinematic viscosity (m^2/s). The velocity and time scales required to match the Reynolds number in the model to that in the prototype are defined by:

$$U_r = \frac{\nu_r}{L_r} \quad (4.7)$$

and

$$T_r = \frac{L_r^2}{\nu_r} \quad (4.8)$$

where, ν_r is the scale ratio of prototype to model fluid kinematic viscosity (ASCE, 2000). Similitude of both the Reynolds and Froude numbers can only be achieved using a modelling fluid with a lower viscosity than that of the prototype. As water is

usually the only modelling fluid available, the only way to reduce the viscosity is by raising the water temperature – which is seldom feasible. However, most open channel flows of interest have very large Reynolds numbers, indicating that the flow is fully turbulent. Under these circumstances, it is only necessary to ensure that the Reynolds number in the model is also high enough to be fully turbulent (Peakall *et al.*, 1996), because this ensures that the effects of viscosity are not exaggerated relative to those of turbulence, which would lead to an overall increase in the friction coefficient. To ensure that the flow is sufficiently deep to produce a Reynolds number that is fully turbulent, either the model's overall size or the vertical scale can be increased (ASCE, 2000). Several values for the minimum model Reynolds number to ensure fully turbulent flow are quoted in the literature. For example, Peakall *et al.* (1996) suggest 500; Chadwick and Morfett (1998) suggest 1,000; Chanson (1999) suggests 2,000 to 3,000, while ASCE (2000) suggest 10,000. The roughness of the channel boundary can also be increased to induce a greater degree of turbulence where necessary (Chadwick and Morfett, 1998).

A third form of the relationship between kinematic and geometric variables is established if the ratio of inertial to surface tension forces is considered. This ratio is called the Weber number, We , and is given in general form by:

$$We = \frac{\rho U^2 L}{\sigma} \quad (4.9)$$

Where, ρ = density of water (kg/m^3) and σ = surface tension (kg/s^2). This produces the following scales for velocity and time, respectively:

$$U_r = \sqrt{\frac{\sigma_r}{\rho_r L_r}} \quad (4.10)$$

and

$$T_r = \sqrt{\frac{\rho_r L_r^3}{\sigma_r}} \quad (4.11)$$

The effects of surface tension in prototype surface flows are generally negligible, because they are much weaker than gravity, but they can become significant in the slower, shallower flows encountered in models. There is no consensus in the literature concerning the minimum flow depth or Weber number needed to avoid the

risk of surface tension effects becoming significant. Novak and Cábélka (1981) state that surface wave height should exceed 0.017 m, surface flow velocity should exceed 0.23 m/s and flow depth should exceed 0.015 m, while ASCE (2000) state that flow depth should exceed about 0.02 m. However, minimum Weber numbers of 11 (Novak and Cábélka, 1981) and >100 (Peakall and Warburton, 1996) have also been quoted. As with the Reynolds number, the dimensions of a model can be increased or its scale can be vertically distorted to ensure that surface tension effects are insignificant.

The final dimensionless number that should be considered is the ratio of pressure to inertial forces, which produces a pressure coefficient, C_p , also known as the Euler number, Eu . This is defined by:

$$C_p = \frac{\Delta p}{0.5\rho U^2} \quad (4.12)$$

where p = pressure (kg/m/s^2). The value of Eu will be determined by that for the Froude number (ASCE, 2000) and, since this is the most important force ratio for the physical modelling of open channel flows, the former is considered no further here.

4.2.2 Mobile-boundary models

A mobile-boundary river model is one in which both fluid (generally water) and sediment are in motion, which therefore constitutes a two-phase flow. Such models must not only conform to the similitude criteria discussed in the previous section, but must also satisfy similitude criteria relevant to the movement of sediment. The precise nature of these criteria may vary depending on the task at hand, which usually involves investigation of one, or several, of the following (ASCE, 2000):

- i) flow over a mobile, planar bed,
- ii) rates of sediment transport (bedload and/or suspended load),
- iii) flow interaction with mobile bedforms,
- iv) patterns of flow, sediment movement and morphological change around hydraulic structures.

In the current study, the aim is to simulate flow phenomena, sediment transport processes and morphological responses in the Elwha River to draw down in Lake Mills during the decommissioning of the Glines Canyon Dam. The reach of interest

not only includes the area currently occupied by Lake Mills but extends upstream into Rica Canyon – which constitutes the sediment supply reach for the reservoir reach. The rationale for the selection of the modelled reach and characterisation of the model parameters is fully explained at the start of section 4.3. What can be stated at this stage is that investigations (i) and (ii) will be of greatest significance in this study.

Dimensional analysis can be used to organise key variables into dimensionless groupings when the physical processes that comprise a phenomenon are not fully defined from theory. This is based on the Π theorem, the most comprehensive version of which is Buckingham's Π theorem (ASCE, 2000). This is explained in detail in the relevant text books (*e.g.* Novak and Cábélka, 1981; Yalin, 1971a). According to the Π theorem, a physical phenomenon with a specified geometry can be completely defined using a number, n , of independent¹³ quantities, $a_1, a_2, a_3, \dots, a_n$, which are called *characteristic parameters*. Any quantitative property or process, A , of the phenomenon must therefore be a function, f_A , of its characteristic parameters, a_i , (where $A \neq a_i$) (Yalin, 1992):

$$A = f_A(a_1, a_2, a_3, \dots, a_n) \quad (4.13)$$

The subscript A in f_A indicates that the form of this functional relationship depends on the nature of the quantitative property A . Each quantitative property, $A_1, A_2, A_3, A_4, \dots$, of a phenomenon will therefore be a specific function of the same n characteristic parameters (Yalin, 1971a).

Buckingham's Π theorem states that a quantitative process, A , influenced by n characteristic parameters¹⁴ with m fundamental dimensions, can be reduced to $n - m$ dimensionless parameters, or Π numbers¹⁵. For the case of steady, uniform water flow over a bed of cohesionless particles, one important physical process is the resistance to flow imposed by the channel boundary. If flow resistance is denoted by A , its functional dependence on its characteristic parameters is given by:

$$A = f_A(\rho, \nu, D, \rho_s, H, S, g) \quad (4.14)$$

¹³ The n quantities are independent when they cannot be defined as a function of any of the other quantities (Yalin, 1992).

¹⁴ Characteristic parameters can be dimensional, dimensionless, constants or variables (Yalin, 1992).

¹⁵ In mathematics Π is a term that means 'product of variables' (ASCE, 2000).

or

$$A = f_A(\rho, \nu, D, \rho_s, H, u_*, gR) \quad (4.15)$$

where, f = the mass rate of sediment transport per unit channel width (kg/m), ρ = fluid density (kg/m³); ν = kinematic viscosity (m²/s); D = particle diameter (m); ρ_s = sediment density (kg/m³); H = flow depth (m); S = channel slope; g = gravitational acceleration (m/s²); $u_* = (gHS)^{0.5}$ = shear velocity in uniform flow (m/s); and $gR = g((\rho_s/\rho) - 1) =$ submerged specific particle weight (m/s²). It should be noted that if a process is not fully understood, such that not all the necessary characteristic parameters can be identified, then dimensional analysis may not be useful because not all the Π numbers necessary to describe the phenomenon may be formulated. Furthermore, the fact that two functional relationships have been created to describe the same phenomenon points to the fact that dimensional analysis does not automatically produce the most physically meaningful set of Π numbers for that phenomenon (ASCE, 2000). The two equations are essentially the same, but in 4.15 the variables u_* and gR have replaced S and g because the Π numbers obtained using these parameters are more physically relevant to processes of incipient motion and sediment transport. As there are $n = 7$ characteristic parameters in equation 4.15 and $m = 3$ fundamental dimensions (MLT), it follows that there are $7 - 3 = 4$ dimensionless Π numbers, as follows (ASCE, 2000):

$$\Pi_A = \varphi_A \left(\frac{\rho u_*^2}{gRD}, \frac{u_* D}{\nu}, \frac{H}{D}, \frac{\rho_s}{\rho} \right) \quad (4.16)$$

The first term in the parentheses of equation 4.16 is the Shields number, τ^* , which represents dimensionless shear stress and expresses the relationship between the fluid drag force applied to a sediment particle (equation 4.19) of grain of size, D , and the force resisting sediment motion, gRD . The second term in the parentheses is the particle Reynolds number, Re_* , which expresses the relationship between the size (roughness) of bed sediment of size D and the thickness of the viscous sub-layer (Peakall *et al.*, 1996). The third term is a geometric scale defining the scale of flow patterns, turbulence and bedforms in wide channels, while the fourth term is the ratio of sediment to water density. Ideally, all four similitude criteria should be met if

processes of flow resistance and sediment transport are to be modelled accurately (ASCE, 2000). However, given that this study focuses on the entrainment, transport and deposition of sediment moving as bedload it is only essential that the first two criteria are satisfied.

The Shields and particle Reynolds numbers represent the ordinate and the abscissa of the Shields diagram (Figure 4.2), which illustrates how the critical dimensionless shear stress for sediment entrainment varies as a function of flow conditions (hydrodynamically smooth or rough) at the bed. The particle Reynolds number is a specific formulation of the Reynolds number (equation 4.6) relevant to flow adjacent to the bed. In the particle Reynolds number, the representative length is the diameter of sediment grains on the bed. As with the Reynolds number, it is not necessary to match the particle Reynolds number in the model with that in the prototype provided that the value of the modelled value is sufficiently high to ensure that flow adjacent to the bed is hydrodynamically rough. However, the minimum value at which this occurs is unclear. ASCE (2000) suggest that, strictly, a value of 400 should be sought (Figure 4.2a) but note that the effects of viscosity become progressively less important above a value of about 60. This note is consistent with the advice of Chanson (1999), who suggests a value in excess of 100, and Yalin (1971a), who states that a value of 70 is usually sufficient (Figure 4.2b). Values as low as 5 and 15 and as high as 350, 400 and 1,000 have also been suggested (see discussion in Peakall *et al.*, 1996). These differences are due, in part, to scatter in the data on the Shields diagram, which makes the placing and precise shape of the Rouse curve (for the threshold of sediment transport) a partially subjective exercise (*cf.* Figures 4.2a and b). The Rouse curve should, therefore, only be taken as an approximation of the point at which incipient motion occurs (ASCE, 2000).

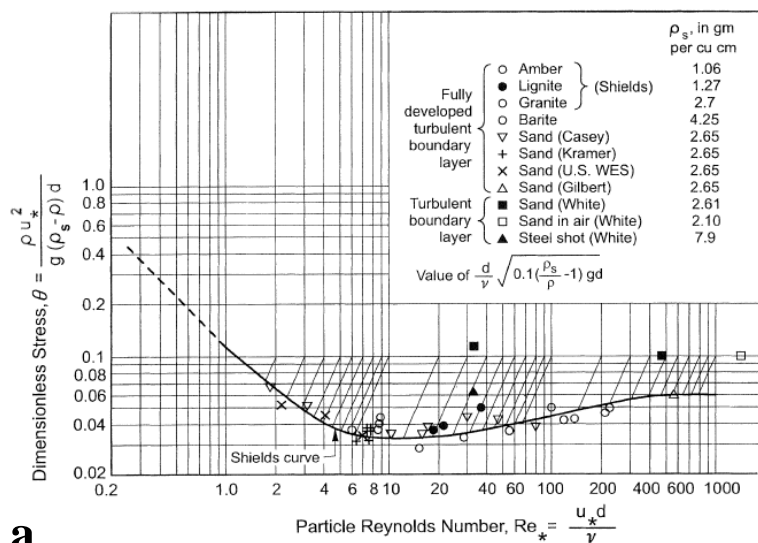
It follows that, as long as Re_* in the model is sufficiently high to ensure that flow at the model bed is hydrodynamically rough, the model will replicate the sediment transport phenomena in the prototype provided that the condition

$$\tau_r^* = \frac{\tau_p^*}{\tau_m^*} \frac{\rho_r U_{*r}^2}{g_r R_r D_r} = 1 \quad (4.17)$$

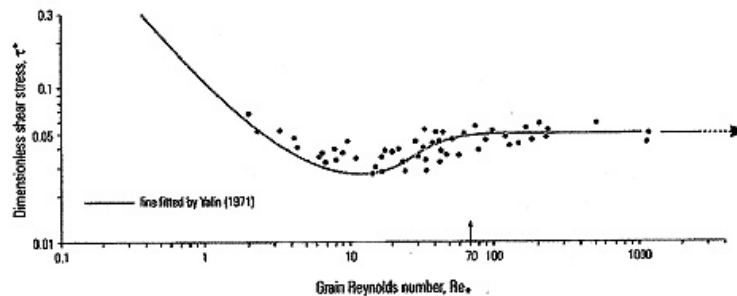
is met.

4.3 Design of the Lake Mills – Glines Canyon Dam model

The Lake Mills model was designed to achieve similitude of the Froude and Shields numbers, as described by equations 4.2 and 4.17, in the sediment delivery channel immediately upstream from the reservoir (that is the ‘Rica Canyon’ reach of the model). Consequently, no attempt was made to achieve dynamic similitude in the reservoir reach of the model. Two key factors dictated this approach. First, although some data were collected from delta surface channels in the reservoir area during the 1994 drawdown experiment (United States Geological Survey, 2000) the information available were insufficiently detailed to provide a basis from which to develop meaningful scaling relationships. Second, even if data from the reservoir area had been sufficiently detailed, it would have been very difficult to specify representative channel geometry and hydraulic data from which to develop scaling relationships.



a



b

Figure 4.2. The Shields diagram shows the approximate point of incipient motion for a range of grain sizes (a) from ASCE (2000); (b) from Yalin (1971) (after Peakall *et al.*, 1996).

This second problem was compounded because of uncertainty about the way hydraulics and channel geometries might be expected to change during the experimental runs. In light of experience gained during the 1994 prototype drawdown experiment (Figure 3.4) and given the magnitude of disturbance to be imposed on the delta system during the experimental runs, morphological response in the model would be highly dynamic and would involve large magnitude and high frequency fluctuations in both flow hydraulics and channel forms through time, with very different hydraulic conditions and channel geometries existing simultaneously in different anabranches and sub-reaches. In summary, the high potential for temporal and spatial variability in the channels in the delta area effectively rules out scaling the model channel based on conditions in the reservoir area. In contrast, the channel in the Rica Canyon reach immediately upstream from Lake Mills is formed in bedrock. Its hydraulics are known and its geometry is stable making it possible to estimate sediment transporting characteristics and relatively straightforward to scale them.

The rationale behind this approach is that by accurately scaling the flow and sediment transport characteristics of the Elwha River using the Rica Canyon reach, and correctly scaling the geometry of the reservoir basin (albeit with vertical distortion) to guide the erosion and redeposition of deltaic sediments, it should be possible to design a physical model capable of simulating the morphological behaviour of the prototype in a realistic and meaningful fashion using a series of experimental runs (Parker, Personal Communication, 2003).

4.3.1 Hydraulic equations and prototype calculations

This section sets out the computations performed to derive the relevant prototype and model parameters. Because the experiments are to be performed with a constant discharge, a condition of uniform, steady flow in the delivery channel can be assumed. Conservation of water mass indicates that discharge per unit channel width is therefore given by:

$$q_w = \frac{Q}{B} = \frac{UBH}{B} = UH \quad (4.18)$$

where, q_w = discharge per unit channel width (m^2/s); Q = discharge (m^3/s); B = mean channel width (m); U = mean flow velocity (m/s); and H = mean flow depth (m). For

steady, uniform flow, balancing forces acting on the fluid leads to the DuBoys equation:

$$\tau_b = \rho g H S \quad (4.19)$$

where, τ_b = cross-section averaged boundary shear stress (kg/m/s²); ρ = water density (kg/m³); g = gravitational acceleration = 9.81 m/s²; S = channel slope. Consideration of flow resistance yields,

$$\tau_b = \rho C_f U^2 \quad (4.20)$$

where C_f = dimensionless bed resistance coefficient (related to the dimensionless Chézy C , C_z , by $C_f^{-1/2} = U/u_* \equiv C_z$). Combining equations 4.19 and 4.20 produces:

$$C_f U^2 = g H S \quad (4.21)$$

Substituting equation 4.18 into 4.21 and rearranging to solve for flow depth yields:

$$H = \left(\frac{C_f q_w^2}{g S} \right)^{1/3} \quad (4.22)$$

The Froude number may be written as:

$$Fr = \left(\frac{q_w^2}{g H^3} \right)^{0.5} \quad (4.23)$$

(Note that this formulation gives exactly the same value for the Froude number as equation 4.1). The Shields number, which is the ratio of the fluid drag force (equation 4.19) to the particle's immersed weight is given by,

$$\tau^* = \frac{\tau_b}{\rho R g D_{50}} = \frac{\rho g H S}{\rho R g D_{50}} = \frac{H S}{R D_{50}} \quad (4.24)$$

where, $R = (\rho_s/\rho) - 1$ = submerged specific gravity of sediment (assumed to be 1.65 in these experiments since a silicate sediment was used); and D_{50} = median grain diameter of the gravel component of the modelling sediment (m). (Note that this formulation of the Shields number produces exactly the same value as that obtained using the first term in the parentheses of equation 4.16).

Using equations 4.18 to 4.24, the following prototype hydraulic conditions in Rica Canyon are calculated (Table 4.1)

From equation 4.18 $q_{w_p} = \frac{Q_p}{B_p} = \frac{59.4}{25.91} = 2.29 \text{ m}^2/\text{s}$

From equation 4.22 $H = \left(\frac{C_f q_w^2}{gS} \right)^{1/3} = \left(\frac{0.01 \times 2.29^2}{9.81 \times 0.017} \right)^{1/3} = 0.68 \text{ m}$

From equation 4.23 $Fr = \left(\frac{q_w^2}{gH^3} \right)^{0.5} = \left(\frac{2.29^2}{9.81 \times 0.68^3} \right)^{0.5} = 1.30$

From equation 4.24 $\tau^* = \frac{HS}{RD_{50}} = \frac{0.68 \times 0.017}{1.65 \times 0.012} = 0.584$

It follows that to achieve the desired similitude, the model must be scaled to generate a Froude number of 1.30 and a Shields number of 0.584 in the approach reach immediately upstream of the reservoir area.

4.3.2 Scaling calculations

The first step is to decide on the length scale, which is given by

$$L_r = \frac{L_p}{L_m} \quad (4.25)$$

and the value of which is limited by the space available in which to build the model. In this case, an area measuring 12 m long by 6 m wide was available on the model floor of the St. Anthony Falls Hydraulic Laboratory at the University of Minnesota (Figure 5.8a). To allow space for a headbox and tailbox, the maximum model length was set at 10.65 m. The length of the reservoir and approach channel is 3.3 km (Table 4.1), and so the model's horizontal length scale is defined as:

$$L_r = \frac{L_p}{L_m} = \frac{3,300}{10.65} = 310 \quad (4.26)$$

The prototype elevation range to be modelled is 48.8 m, which is the difference between the maximum elevation of the delta surface and the base of the pre-dam channel at the dam site. This may be termed the 'effective vertical geomorphological range', since all the geomorphological work of interest in this study will take place between these elevations. The undistorted height of the model would therefore be given by:

$$L_m = \frac{L_p}{L_r} = \frac{48.77}{310} = 0.155 \text{ m} \quad (4.27)$$

However, using an undistorted model would result in very shallow flows, making it impossible to generate values of Re and Re_* in the model that correspond to fully turbulent flow over a hydrodynamically rough boundary. The maximum available height in the modelling area, which was fixed by the base of the instrumentation carriage (Figure 5.8), was 0.597 m. This made it feasible to partially solve the scaling problem by vertically distorting the model (see section 8.1.2). This means using a different length scales for the vertical, Y_r , and horizontal, X_r , dimensions. The maximum horizontal and vertical length scales that may be used within the available space are given by equation 4.25:

$$X_r = \frac{X_p}{X_m} \quad (4.28)$$

and

$$Y_r = \frac{Y_p}{Y_m} \quad (4.29)$$

The horizontal scale, X_r , remains at 310, while the maximum vertical scale is given by

$$Y_r = \frac{Y_p}{Y_m} = \frac{48.77}{0.597} = 81.7 \quad (4.30)$$

This means that the model is vertically distorted by a factor of $310/81.7 = 3.79$, which is well within the maximum upper limits cited in the literature, *e.g.* ≤ 10 (Chanson, 1999) or ≤ 6 (ASCE, 2000). While vertical distortion in a model is not ideal because it reduces model accuracy and complicates the interpretation of the results, it is an accepted and sometimes necessary practice in physical modelling. In this study, given the very large size of the prototype relative to the available floor space, it was necessary to increase the vertical scale to bring flow depths over the delta surface up to the minimum necessary for flow to be fully turbulent so minimizing any of the viscous and surface tension effects described above.

Vertical distortion changes the fundamental scaling relationships established for velocity (equation 4.4) and time (equation 4.5). Simplified from equation 4.3 these now become:

$$U_r = Y_r^{0.5} \quad (4.31)$$

$$T_r = \frac{X_r}{U_r} = \frac{X_r}{Y_r^{0.5}} \quad \text{for horizontal motion} \quad (4.32)$$

$$T_r = \frac{Y_r}{U_r} = \frac{Y_r}{Y_r^{0.5}} = Y_r^{0.5} \quad \text{for vertical motion} \quad (4.33)$$

In addition, vertical distortion produces different scale ratios for key parameters. The ratio for discharge is given by:

$$Q_r = U_r B_r H_r = Y_r^{0.5} X_r Y_r = X_r Y_r^{1.5} \quad (4.34)$$

That for bed slope is given by:

$$S_r = \frac{Y_r}{X_r} \quad (4.35)$$

The ratio for the friction coefficient is given by:

$$C_{f_r} = \frac{Y_r}{X_r} \quad (4.36)$$

Discharge per unit channel width is given by:

$$q_{w_r} = U_r H_r = Y_r^{0.5} Y_r = Y_r^{1.5} \quad (4.37)$$

Flow depth is given by:

$$H_r = \left(\frac{C_{f_r} q_{w_r}^2}{g_r S_r} \right)^{1/3} = \left(\frac{Y_r Y_r^3 X_r}{1 X_r Y_r} \right)^{1/3} = Y_r \quad (4.38)$$

The time scales in equations 4.32 and 4.33 are relevant to similitude in fluid motion. In a distorted model, the fluid time scale differs from the sediment transport time scale, T_{s_r} , which must be obtained in a different fashion. The scale ratio for sediment transport per unit channel width, q_{s_r} , can be derived from any appropriate bed material load transport equation, as shown by Novak and Cábélka (1981) and takes the form:

$$q_{s_r} = H_r^{1.5} S_{e_r}^{1.5} \quad (4.39)$$

The sediment transport time scale ratio can now be calculated as the time taken for a given bed material load transport rate, $Q_s = q_s \times B$, to fill a specified volume, V , of the channel or reservoir (ASCE, 2000; Novak and Cábélka, 1981). This is given by:

$$T_{s_r} = \frac{V_r}{q_{s_r} B_r} = \frac{V_r}{H_r^{1.5} S_{e_r}^{1.5} B_r} = \frac{X_r X_r Y_r X_r^{1.5}}{Y_r^{1.5} Y_r^{1.5} X_r} = \frac{X_r^{2.5}}{Y_r^2} \quad (4.40)$$

Having established these scaling ratios, all the hydraulic parameters necessary to design the model can now be calculated.

Model discharge, Q_m , is given by:

$$Q_m = Q_p \times X_r^{-1} Y_r^{-1.5} = \frac{59.4}{310 \times 81.7^{1.5}} = 0.000259 \text{ m}^3/\text{s}$$

This equates to $Q_m \times 60,000$ litres/min. = 15.57 litres/min.

Model channel slope, S_m , is given by:

$$S_m = S_p \times X_r Y_r^{-1} = 0.017 \times \frac{310}{81.7} = 0.065$$

Model friction coefficient, C_{f_m} , is given by:

$$C_{f_m} = C_{f_p} \times X_r Y_r^{-1} = 0.01 \times \frac{310}{81.7} = 0.038$$

Model discharge per unit channel width, q_{w_m} , is given by:

$$q_{w_m} = q_{w_p} \times Y_r^{-1.5} = \frac{2.29}{81.7^{1.5}} = 0.0031 \text{ m}^2/\text{s}$$

Model flow depth, H_m , is given by:

$$H_m = H_p \times Y_r^{-1} = \frac{0.68}{81.7} = 0.0083 \text{ m}$$

The Froude number in the model is then found by substituting these values into equation 4.23:

$$Fr_m = \left(\frac{q_{w_m}^2}{g_m H_m^3} \right)^{0.5} = \left(\frac{0.0031^2}{9.81 \times 0.0083^3} \right)^{0.5} = 1.30$$

which indicates that the requirement for Froude similitude has been met. Similarly, the Shields number for the model is found using equation 4.24 and the relevant values for the model,

$$\tau_m^* = \frac{H_m S_m}{R_m D_{50m}} = \frac{0.0083 \times 0.065}{1.65 \times 0.000557} = 0.584$$

which indicates that the requirement for Shields similitude has also been met.

The time required for one week of prototype flow time (in seconds) to occur in the model is:

$$T_m = T_p \times \frac{Y_r^{0.5}}{X_r} = 604,800 \times \frac{81.7^{0.5}}{310} = 4.9 \text{ hours,}$$

while the time required for one week of prototype sediment transport to occur in the model is:

$$T_m = T_p \times \frac{Y_r^2}{X_r^{2.5}} = 604,800 \times \frac{81.7^2}{310^{2.5}} = 0.66 \text{ hours.}$$

4.3.3 Model sediment

The prototype delta in Lake Mills is composed of 23.7% clay and silt, 61.4% sand, 14.2% gravel and 0.7% cobble and boulder (United States Geological Survey, 2000). Because of the impossibility of scaling the clay and silt fraction using silicate sediment at this model scale, it was decided to ignore it when calculating the scaled model grain size distribution. This action was based on the fact that silts and clays constitute less than a quarter of the deltaic sediments and are likely to move as wash load once entrained - quickly being evacuated from the reservoir area by transport in suspension once they are disturbed by erosion of the original-delta. For these two reasons, it was concluded that the silt/clay fraction is likely to play a negligible role in the subsequent evolution of the prograding delta system.

The sediment scale for the model is obtained from equation 4.24 for the Shields number. Rearranging 4.24 to solve for D yields the sediment scale ratio from:

$$D_r = \frac{H_r S_r}{R_r \tau_r^*} = \frac{Y_r Y_r}{1 \times 1 X_r} = \frac{Y_r^2}{X_r} \quad (4.41)$$

Parameter	Prototype value	Prototype data source	Model value	Scale ratio/equation
Reservoir length (straight line from mouth of Rica Canyon to dam)	3.3 km	USGS (2000)	10.65 m	X_r
Maximum reservoir width	1.067 km	USGS (2000)	3.44 m	X_r
Effective vertical geomorphological range	48.8 m	(Bureau of Reclamation, 1995b)	0.597 m	Y_r
Delta length	1,000 m	USGS (2000)	3.23 m	X_r
Maximum delta width	400 m	USGS (2000)	1.29 m	X_r
Increments of baselevel drop	2.29 m	(Bureau of Reclamation, 1996a)	0.028 m	Y_r
Mean channel width	25.91 m	USGS (2000)	0.084 m	X_r
Bed slope (S)	0.017	(Bureau of Reclamation, 1996b)	0.065	Y_r / X_r
Channel friction coefficient (C_f)	0.01	Estimated (Parker, Written Communication, 2003)	0.038	$C_{f,r} = \frac{Y_r}{X_r}$
Discharge (Q)	$59.4 \text{ m}^3\text{s}^{-1}$	(Bureau of Reclamation, 1996b)	15.57 l/min	$Q_r = X_r Y_r^{1.5}$
Discharge per unit width (q_w)	$2.29 \text{ m}^2/\text{s}$	$q_w = Q / B$	$0.0031 \text{ m}^2/\text{s}$	$q_{w,r} = Y_r^{1.5}$
Flow depth (H)	0.68 m	$H = \left(\frac{C_f q_w^2}{gS} \right)^{1/2}$	0.0083 m	$H_r = Y_r$
Froude number (Fr)	1.3	$Fr = \left(\frac{q_w^2}{gH^3} \right)^{0.5}$	1.3	$Fr_m = \left(\frac{q_{w,m}^2}{g_m H_m^3} \right)^{0.5}$
Shields number (τ^*)	0.584	$\tau^* = \frac{HS}{RD_{50}}$	0.584	$\tau_m^* = \frac{H_m S_m}{R_m D_{50m}}$
Flow time (T_f)	1 week	-	4.9 hours	$T_r = \frac{X_r}{Y_r^{0.5}}$
Sediment transport time (T_s)	1 week	-	0.66 hours	$T_{s,r} = \frac{X_r^{2.5}}{Y_r^2}$

Table 4.1. Summary of prototype and model geometrical hydraulic variables.

Prototype size category	Prototype size (mm)	Calculated model size (mm)	Percentage finer than
Fine sand	0.075 - 0.425	0.02	33.9
Coarse sand	0.425 - 5.00	0.23	80.5
Fine gravel	5 - 19	0.88	93.8
Coarse gravel	19 - 75	3.48	99.1
Fine cobble	75 - 125	5.81	99.8
Coarse cobble	125 - 300	13.93	100

Table 4.2. Truncated prototype delta grain size distribution (data from United States Geological Survey, 2000) and model values calculated using equation 4.42. (Size classification based on United Classification System).

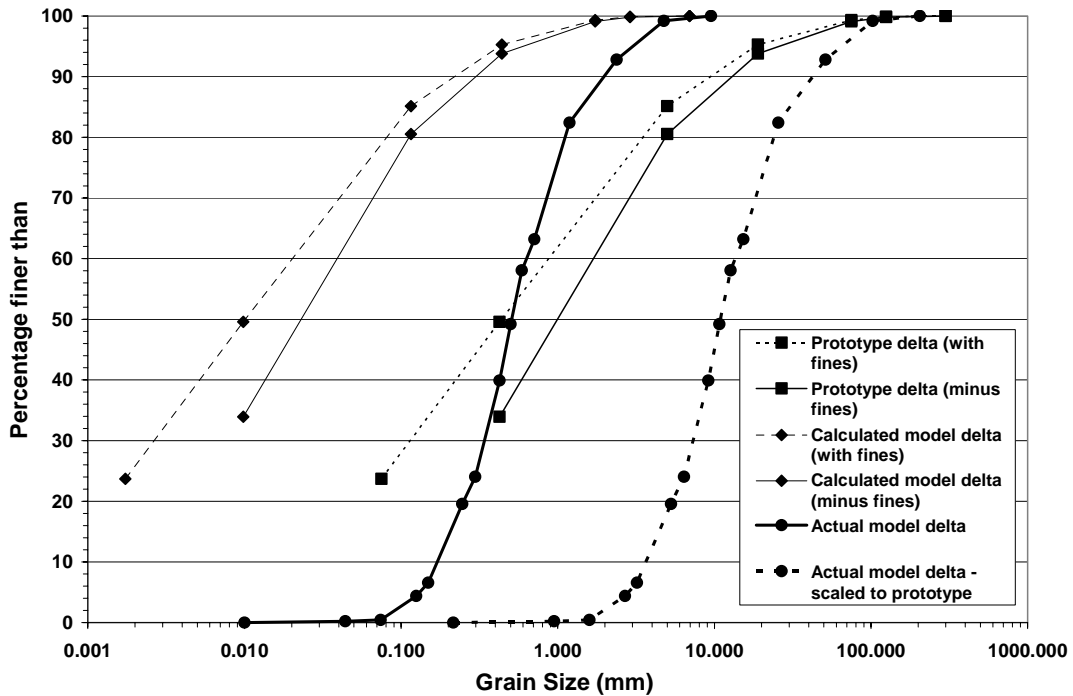


Figure 4.3. Prototype and model grain size distributions.

The model sediment size distribution is calculated using:

$$D_m = D_p \times X_r Y_r^{-2} \quad (4.42)$$

Prototype and model delta grain size distribution data are summarised in Table 4.2 and illustrated in Figure 4.3. Despite omission of the silt/clay fraction in the prototype sediment for the reasons given above, the D_{50} and D_{84} for the model are still very fine, being 0.022 mm and 0.15 mm, respectively. Consequently, a significant proportion of the model sediment would still be composed of grain sizes capable of acting as a cohesive unit (which begins to occur with grain sizes less than about 0.1 mm (ASCE, 2000) and of forming lower regime bedforms such as ripples and dunes. This poses a problem because ripple and dune bedforms were not observed to be present in the prototype during the 1994 drawdown experiment (United States Geological Survey, 2000; Tim Randle, Personal Communication, 2003) and because cohesion is not a significant factor in the morphological behaviour of the prototype delta. It follows that their presence would have been highly undesirable in the model delta.

The conventional approach to avoiding lower regime bedform and cohesion effects in a mobile boundary model with fine grain sizes is to match the mobility of

the sediments in the model to those in the prototype using characteristics other than particle size. This is usually achieved by using material with a specific gravity less than the 2.65 generally associated with quartz sand (ASCE, 2000) in the model or by manipulating other variables, as described in section 5.3.1. A list of lightweight materials, compiled from a survey of hydraulic laboratories around the world, together with their specific gravities and range of particle sizes used, is presented in Table 4.3. However, Whipple *et al.* (1998) have shown that mixed-density models are subject to scale effects that further complicate interpretation of the results in the context of the prototype.

Sediment	Specific gravity	Range of sizes used (mm)
Polystyrene	1.035 – 1.05	0.5 – 3.2
Sawdust treated with asphalt	1.05	0.6 – 1.0
Granulated obeche wood	1.10	0.8
PVC	1.14 – 1.25	1.5 – 4.0
Nylon	1.16	0.1 – 5.0
Perspex	1.18 – 1.19	0.3 – 1.0
Acrylonitrile Butadienne Styrene (ABS) (Ter Polymer)	1.22	2.3 – 3.0
Bakelite	1.3 – 1.45	0.3 – 4.0
Ground walnut shells	1.33	0.15 – 0.41
Coal	1.37 – 1.61	0.1 – 40.0
Sand of Loire	1.5	0.63 – 2.25
Lightweight aggregate	1.7	1.0 – 3.0

Table 4.3. List of lower density modelling material used in hydraulic modelling practice around the world. Data from Bettess (1990).

Given that the model being designed for use in this study is already subject to complexities due to vertical distortion it was thought prudent to avoid introducing another source of complexity that would further complicate the interpretation of the results at the prototype scale, at least for the first set of experimental runs. Had sufficient time been available, one or two runs utilising a lightweight sediment would have been performed. In any case, budgetary constraints precluded purchase of expensive modelling materials in the quantities that would have been required. For these reasons, a relatively coarse 100%-silicate, sediment mixture was selected for use in the model (Figure 4.3). Selection of the final size distribution was based on testing a variety of mixtures to find the finest overall distribution that would still allow the formation of an armour layer and antidunes in the incising delta surface channel, as both of these sediment features were observed during the 1994 drawdown experiment. The final size distribution (Figure 4.3) is fine enough to be entrained and transported

by the modelled flows while being sufficiently coarse to avoid cohesive effects and preclude the formation of lower regime bedforms. It should be noted, however, that all but the largest 2% of the size distribution is significantly coarser than would be required by the scaling calculations, representing a considerable departure from sediment similitude.

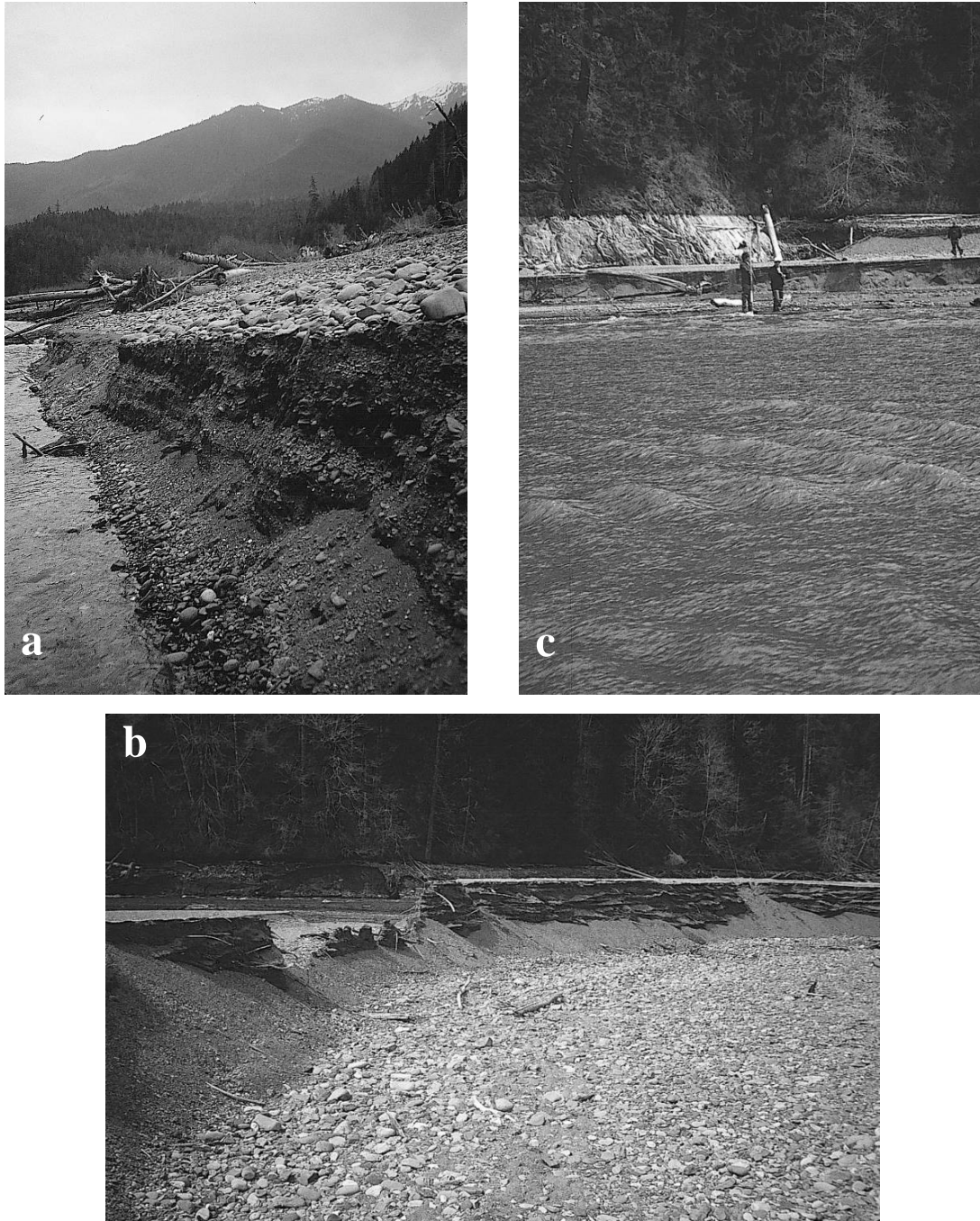


Figure 4.4. (a & b) Armour layer on abandoned channel bed surfaces. (c) Standing waves on the surface indicate the presence of upper regime bedforms (antidunes) on the incising channel bed.

Chapter 5 Model Construction, Operation and Data Collection

5.1 Model construction

The shape of the experimental basin was developed by extracting elevation data from the intersection of a series of cross-sections with every contour on a map of the 1926 (pre-dam) topography of the Elwha River valley in the area that is now Lake Mills (Figure 5.1). The cross-sections were placed by the author to capture major breaks of slope and valley line along the valley sides and bottom. The elevations and their spacing along each cross-section were scaled in Excel using the vertical and horizontal scales (section 4.3.2), plotted, and transferred to plywood sheets, which were then cut to create the valley topography at the actual model size (Figure 5.2a). The plywood cross-sections were placed inside a stud-wall frame and held in place with a breeze- (cinder-) block and sand filling (Figure 5.2b & c). The model was capped with concrete laying on a geotextile base, the joints were sealed and the entire basin painted to prevent seepage into the concrete and its fill (Figure 5.2d-f). At the downstream end of the model a tailbox was built (Figure 5.2g) and two pairs of angle irons formed the dam's 'abutments'. Each pair was fitted with four bolts that enabled the dam pieces to be squeezed in place, thus helping to reduce leakage (Figure 5.2h). Each individual dam piece was tightly wrapped in a rubber 'skirt' that overlapped onto the piece immediately below (Figure 5.2i), thus holding the pieces tightly together and further reducing leakage through the dam. The entire dam was pressed tightly onto a foam bed that was sealed to the laboratory floor with silicone sealant, thus minimising leakage underneath and round the base of the dam. These measures reduced leakage to the point that it was no longer an impediment to the accurate control of reservoir water surface elevation during the runs (section 5.4.1). At the upstream end of the model a headbox was built that contained two baffle boards to help still the water before it entered the delivery channel (Figure 5.2j).

5.2 Experimental runs

5.2.1 Introduction

Glines Canyon Dam is 64 m (210 feet) high and is to be removed by draining the first 15.24 m (50 feet) of the reservoir through the spillway gates, removing this height from the top of the structure and thereafter draining the reservoir and cutting the dam down in increments of 2.29-m (7.5 feet), as described in section 2.3.2. These

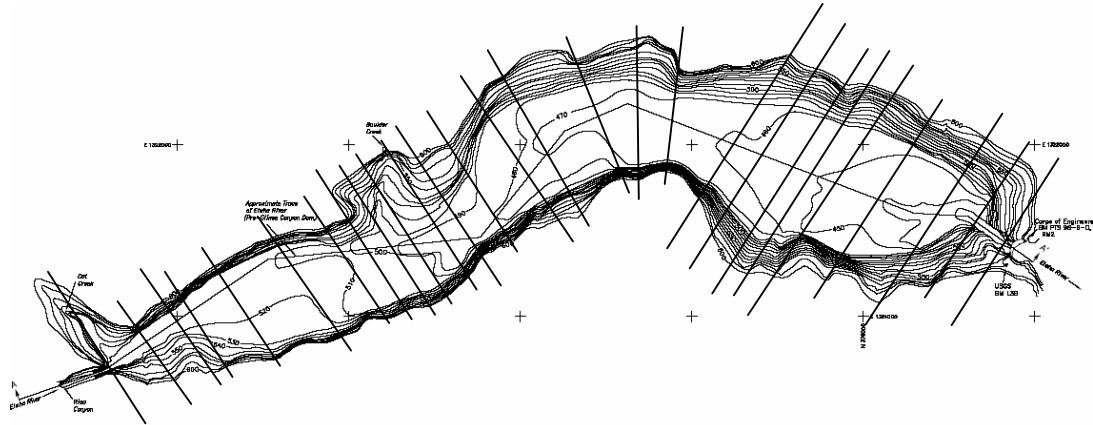
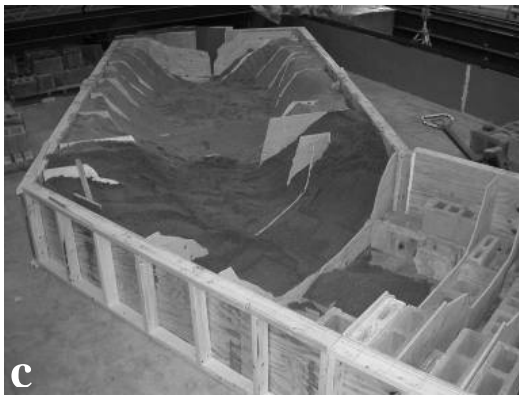
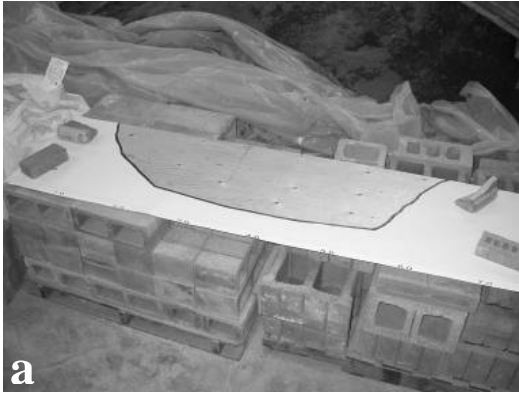


Figure 5.1. Contour map of pre-dam Elwha River valley showing location of model construction cross-sections. Adapted from Bureau of Reclamation (1995c).

2.29-m sections were used as the base unit for investigating the effects of varying the magnitude of baselevel drop during dam removal (Hypothesis 1, section 3.4). The effective vertical geomorphological range is 48.8 m (section 4.3.2) and the 2.29-m high increments divide into this height 21.3 times. The model dam was thus composed of 21 0.028-m high¹⁶ wooden blocks and each experiment examined the effects of removing the entire dam in increments of the same number of dam pieces, with the number of dam pieces per increment varying from run to run (Table 5.1).

The initial plan for the sequence of experimental runs had been to increase the number of dam pieces per increment of dam removed from run to run, starting with one dam piece, then two, then three, *etc.* In addition, the incising channel would be allowed to find its own course across the delta topset at the start of each experiment, just as it would do in the prototype. Following the first two runs, however, it became apparent that the highly asymmetrical nature of the reservoir basin in the delta area

¹⁶ 2.29 m divided by the vertical scale of 81.7 yields 0.028 m.



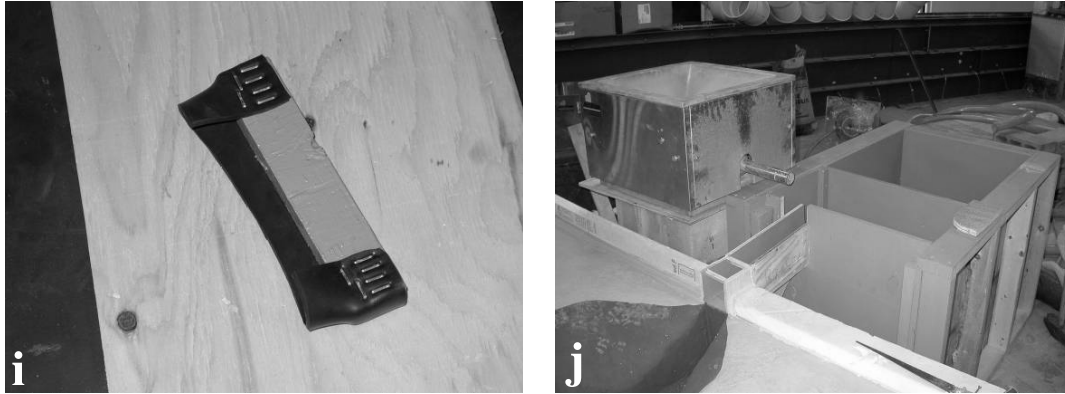


Figure 5.2. Stages of model construction. (a) Pre-dam valley topography transferred to plywood sheets that (b) provide the model's framework shape. (c) The framework is filled with breeze blocks and sand, (d) capped with a geotextile and concrete shell and made water-tight with (e) sealant and (f) paint. (g) Model tailbox and two pieces of angle iron to form the dam's 'abutments'. (h) View of the downstream face of the 21-piece model dam. (i) Individual dam piece with its tightly-fitted rubber 'skirt'. (j) Headbox with stilling baffles and 'Rica Canyon' delivery channel.

Run Number	Run Name	No. of dam pieces removed per increment of dam removal	Delta surface channel position at start of run*	Model sediment mixture $D_{16}, D_{50}, D_{84}, D_{90}$ (mm)	Standard deviation (mm) / geometric standard deviation	Discharge during dam removal (litres/min)	Recurrence interval of storm flows
1	2xR	2	Right	-	-	15.57	No flood flow
2	3xR	3	Right	0.15, 0.42, 1.30, 1.98	1.53, 2.89	15.57	2-yr; 2-yr; 5-yr
3	1xL	1	Left	0.19, 0.40, 1.38, 2.04	1.47, 2.78	15.57	2-yr; 2-yr; 5-yr
4	3xL	3	Left	-	-	15.57	2-yr
5	3xL(A)	3 (accelerated removal)	Left	0.16, 0.44, 1.36, 1.99	1.51, 2.85	15.57	2-yr
6	6xC [†]	6	Centre	0.16, 0.43, 1.33, 1.97	1.52, 2.86	15.57	No flood flow
7	12xC [†]	12	Centre	0.14, 0.43, 1.33, 1.96	1.54, 2.90	15.57	No flood flow
8	3xC [§]	3	Centre	-	-	15.57	2-yr
9	21xC ^{††§}	21	Centre	0.16, 0.50, 1.51, 2.05	1.51, 2.85	15.57	No flood flow
10	2x split-flow ^{†§}	2	Two channels either side of topset centre line	-	-	15.57	No flood flow

Table 5.1. Experimental parameters. *The channel position is assigned looking downstream from the upstream end of the delta. [†] Partial runs – only a total of 12 dam pieces removed. ^{††} Run terminated once the entire dam had been removed but before the system had reached a static equilibrium. [§] Runs performed for the author by staff at the St. Anthony Falls Laboratory.

was having a profound influence on how the runs were evolving, a factor which had not been considered up to that point. Mindful of the need to produce information that would be of practical use to the project sponsors (U.S. National Park Service and Bureau of Reclamation), as well as pursuing the more purely research-oriented hypotheses, it was decided to introduce an additional variable to the experiments by exerting a degree of control on the position of the incising channel. In the first two experimental runs (Table 5.1), the channel had naturally begun to incise along the streamwise right half of the delta. In runs 3-5 the channel was therefore forced to incise along the left side of the delta. This was done by scraping a small amount of the delta surface material at the upstream end of the delta into a small levee that directed the flow towards the left at the very start of the dam removal process. In runs 6-9 the initial channel was kept as far away as possible from the basin boundary by digging a shallow pilot channel with the same width as the delivery channel along the centre of the topset surface.

5.2.2 Experimental overview

Each experiment was started by hydraulically growing the model delta to the same extent as the 2002 prototype delta (section 5.3.2), although no attempt was made to try and recreate the bottomset deposits (see section 8.1.1). In order to isolate the effects of the magnitude of baselevel drop, the dam removal phase of each experiment was performed using a constant discharge of 15.57 litres per minutes, which scales to a prototype discharge of $59.4 \text{ m}^3/\text{s}$ (2,098 cfs) and is close to the values under which the prototype will be removed (Bureau of Reclamation, 1996a). The removal of each dam increment was also performed so that the reservoir water surface elevation fell at the same rate of 2.8 cm per 15 minutes (section 5.4.1).

Following the removal of each dam increment, the delta surface channel system was allowed to adjust until virtually all sediment transport had ceased, *i.e.* until a static equilibrium condition was attained, which was defined as the slow movement of only a few sand grains along the channel bed, at which point the next dam increment was removed. It was possible to reach a static equilibrium since each run was performed without a sediment feed. While this is not completely representative of real prototype conditions – there will be some, albeit small, volumes of sediment transported into the reservoir by the discharges experienced during

prototype removal - it was done to again isolate as far as possible the morphological response to the drop in baselevel. A continuous sediment input, while small, would have been sufficient to maintain delta progradation and lateral channel movement and thus obscure the endpoint of this response.

In most runs in which the dam was completely removed, one or several flood flows were run through the model once the delta surface channel system had reached a static equilibrium condition following the removal of the last dam increment (Table 5.1). Scaled two- and five-year return interval flows were used, since these have a statistically very good chance of occurring during or shortly after the dam removal period, which is scheduled to last about two years (Bureau of Reclamation, 1996b). Each flood flow cycle was performed by ramping the discharge up to the peak flood value, then back down to the baseflow value of 15.57 litres per minute, over a period of time equivalent to two prototype weeks. The system was then allowed to fully adjust at the baseflow until a static equilibrium was reached (section 5.4.3). While not directly addressing the research hypotheses, these flows nevertheless provided information that helped to further understand the morphodynamic response to dam removal and that will be of use during prototype removal (see sections 7.2.2, 8.2.3 and 8.3).

During the periods of system relaxation during the dam removal phase of each run, the model's discharge was switched off and the reservoir drained at intervals of 1.5, 3.5, 5.5 and 9.5 hours of run time, and sometimes at additional intervals in between, in order to scan the entire delta surface (section 5.5.1). These scans provided the raw data used to perform the volumetric analyses necessary to address the two research hypotheses. The delta surface was scanned at the start of each run following hydraulic delta growth, but prior to the onset of dam removal; at the aforementioned intervals; and at each static equilibrium interval, including those after each flood flow. A range of other data were collected during and after each run and these are described in sections 5.5.2 to 5.5.4.

All runs were performed by the author except runs 8 to 10 (Table 5.1), which were performed after the author's visa had expired and he had returned to the U.K. Runs 8 (3xC) and 9 (21xC) were performed by Corey Markfort, a graduate student working at SAFL. Corey received two full days of training from the author, which covered all aspects of experimental preparation, procedure and data collection. In

addition, he was working under the direct supervision of Dr. Alessandro Cantelli, who has also performed experimental dam removal research and who was fully conversant with the aims and objectives of the author's research programme. It is very clear from the time lapse movie that the unusual nature of system response during run 8 resulted from the reduced relaxation intervals used - the delta surface channel system was still clearly adjusting each time the next dam increment was removed - and did not occur due to the change in model operator. Run 10 was performed by a laboratory technician, again under the supervision of Dr. Cantelli, but mostly to address a request from the research sponsor (Bureau of Reclamation) and the results from this run are only referred to briefly in Chapter 7.

5.3 Experimental preparation

5.3.1 Model calibration

Before performing any experimental work it was necessary to verify that the calculated values for the Froude and Shields number were being generated in the delivery channel and that the flow was sufficiently turbulent to avoid problems with viscous drag forces.

A short section of measuring tape was stuck to the inside wall of the delivery channel to allow flow depth to be measured. From this measurement and the relevant values presented in Table 5.3 a Froude number of 1.43 was calculated, which is 9.7% higher than the required value of 1.30. This probably occurred because the delivery channel had been painted and its surface was very smooth, thus making flow velocity too high and flow depth too low. The channel was therefore roughened by applying a further coat of paint and embedding several gravel grains that had been sieved from the modelling sediment mixture into the wet paint. A Froude number of 1.36 was calculated for the roughened channel, which is 4.7% greater than the required value but which was deemed acceptable.

Values for the Shields parameter, grain Reynolds number and Reynolds number were then calculated for the original and roughened delivery channel as shown in Table 5.2 and using the necessary parameters from Table 5.3. Values of the Shields and grain Reynolds numbers are calculated for both the entire sediment mixture and only the gravel and coarser component. The Reynolds number of 8,183 is

Parameter	Actual model value	Difference from target value (%)	Comment
Froude number (target value = 1.30)			
Before roughening	1.43	9.7	Calculated using equation 4.23.
After roughening	1.36	4.7	Calculated using equation 4.23.
Reynolds number (target value > approximately 1,000 – 10,000)			
Before roughening	8,183	-	H used in place of R_H in equation 4.6 because delivery channel B:H is low (Table 5.3) and H is more accurate indicator of flow depth.
After roughening	8,183	-	“ “
Shields number (for entire mixture D_{50} - target value = 0.757)			
Sediment mixture before roughening	0.714	-5.7	Calculated using equation 4.24.
Sediment mixture after roughening	0.736	-2.7	“ “
Shields number (for gravel D_{50} - target value = 0.584)			
Gravel component before roughening	0.096	-83.6	Calculated using equation 4.24.
Gravel component after roughening	0.099	-83.1	“ “
Grain Reynolds number (for D_{50} – minimum value > ~15 - 100)			
Sediment mixture before roughening	20.0	-	Calculated using $Re_* = (u_* D_{50})/\nu$.
Sediment mixture after roughening	20.3	-	“ “ “
Gravel component before roughening	148.5	-	“ “ “
Gravel component after roughening	150.8	-	“ “ “

Table 5.2. Hydraulic parameters in model delivery channel before and after channel roughening. The sediment mixture refers to that used to grow hydraulically the model delta (section 5.3.2).

Parameter	Symbol	Value	Units	Value obtained from
Discharge	Q_m	0.00026	m ³ /s	$Q_p / X_r Y_r^{1.5}$
Delivery channel width	B_m	0.0834	m	B_p / X_r
Specific discharge	q_{wm}	0.0031	m ² /s	Q_m / B_m
Kinematic viscosity at 5°C	ν	1.52×10^{-6}	m ² /s	(Yang, 1996)
Sediment specific gravity	R	1.65	-	$(\rho_s / \rho) - 1$
Modelling mixture D_{50}	-	0.43	mm	Sieve data
Gravel D_{50}	-	3.2	mm	Sieve data
Channel slope	S_m	0.0645	-	$S_p \times X_r Y_r^{-1}$
Gravitational acceleration	g	9.81	m/s ²	-
Flow depth before channel roughening	H_{bm}	0.00789	m	Measured
Flow depth after channel roughening	H_{am}	0.0081	m	Measured
Flow velocity before channel roughening	U_{bm}	0.3958	m/s	$Q_m / (B_m \times H_{bm})$
Flow velocity after channel roughening	U_{am}	0.3836	m/s	$Q_m / (B_m \times H_{am})$
Width-depth ratio before channel roughening	-	10.6	-	B_m / H_{bm}
Width-depth ratio before channel roughening	-	10.3	-	B_m / H_{am}

Table 5.3. Model hydraulic and sedimentary variables used to calculate values in Table 5.2.

towards the upper limit of the range indicated and exceeds the values of 1,000 and 2,000 – 3,000 need for fully turbulent flow proposed by Chadwick and Morfett (1998) and Chanson (1999) respectively. The effects of skin drag relative to form drag should therefore not be an issue in the delivery channel (Peakall *et al.*, 1996). The significance of the values of the grain Reynolds number is somewhat less clear cut. The values of around 150 for the gravel and coarser component of the sediment mixture comfortably exceeds the minimum values cited by most workers (section 4.2.2), but the values of around 20 for the entire sediment mixture are much closer towards the lower limit of the range of values presented in section 4.2.2. It is therefore uncertain whether or not viscous drag forces will be operating.

Parameter	Sediment	Required value
Flow depth, H (silicate sediment)	Mixture D_{50}	0.0064 m
	Gravel D_{50}	0.0478 m
Slope, S (silicate sediment)	Mixture D_{50}	0.051
	Gravel D_{50}	0.381
Sediment D_{50} (silicate sediment)	-	1 mm
Sediment specific gravity	Mixture D_{50}	2.605
	Gravel D_{50}	1.28

Table 5.4. Parameter values required to obtain the calculated value of the Shields number in a roughened delivery channel.

The values of the Shields parameter for the entire sediment mixture before and after channel roughening are only 5.7% (0.714) and 2.7% (0.736) respectively less than the target value of 0.757. The values for the gravel component of the mixture, however, fall short of the target value of 0.584 by 83.6% (0.096) and 83.1% (0.099). The two sets of values indicate that, while the value for incipient motion, which is usually in the range 0.052 - 0.086 or 0.030 – 0.073 (Buffington and Montgomery, 1997) is comfortably exceeded in all model cases, there may be a lower rate of transport of the gravel fraction in the model delivery channel than in the prototype. This occurs simply because the gravel is coarser than required by the scaling calculation and the denominator of equation 4.24 is too large.

All four variables in equation 4.24 could theoretically be manipulated to obtain the target Shields number. The values that each of the four variables would have to assume, with all others being held constant at their current values and using a silicate sediment (except when ρ_s was varied), are presented in Table 5.4. Increasing the size of the numerator would require very large increases in flow depth or slope,

which could be achieved respectively by greatly increasing the roughness of the channel bed or by ‘tilting’ the delivery channel. An increase in depth of this magnitude, if it could actually be achieved by bed roughening alone, would result in a Froude number of 0.09, however, while the large increase in slope would increase flow velocity and decrease flow depth which would both act to increase the Froude number. Both numerator changes would therefore upset the near perfect Froude similitude. The denominator of equation 4.24 could be decreased by decreasing the gravel D_{50} to 1 mm, which would be much closer to the 0.56 mm required by the sediment scaling calculation. The sediment testing runs (section 4.3.3) showed that sediment of this calibre, present in the small proportions required to simulate the prototype gravel fraction, would be insufficient to prevent the formation of bed forms such as dunes and ripples, which tends to occur with sediments less than about 0.6 mm in diameter, as used in this study (Table 5.1). The only remaining alternative would therefore be to use a lower density modelling material. Given that the Shields number for the entire sediment mixture is so close to the calculated value, it would probably not make much difference to use a silicate sediment. In any case, Table 4.3 shows that no materials with a specific gravity of about 2.6 are currently in use in hydraulic modelling practice. Bakelite, with a lower limit to its range of specific gravities of 1.3 and a range of grain sizes in use in laboratories of 0.3 – 4.0 mm, would appear to be the most appropriate material to use to simulate the gravel fraction of the sediment mixture, but it is far from certain that this would be able to adequately simulate channel armouring and, as noted in section 4.3.3, it might introduce additional scaling effects that would further complicate the interpretation of model results.

These problems exemplify the difficulty of trying to scale such a large prototype into such a relatively small laboratory space and help to explain the suggested position of the Lake Mills model in the schematic of model types (Figure 4.1). The preceding discussion has been restricted to the model delivery channel only, but the issues raised here will be equally applicable when examining the implications of model channel behaviour in the reservoir area. These will be considered in section 8.1.2.

5.3.2 Growing the model delta

As described below, the model delta was grown using an accelerated sediment feed and a continuously high discharge. The rationale for this is three-fold. First, it was necessary to grow the delta in a timely fashion so as to maximize the amount of experimental run time. Scaling the prototype delta growth time (75 years from 1926-2002) would have completely precluded this. Second, it was deemed necessary for the model delta to be hydraulically sorted, since the prototype is similarly sorted (Figure 7.1) and this may have a significant effect on the way in which the delta incises, in particular, because of the large proportion of armour-forming sediment grains in the proximal original delta (Figure 7.16). Such sorting could not be achieved by placing the delta by hand, which would have been much quicker. Third, the model discharge used scales to a prototype flow with a recurrence interval of about 3.3 years (see below). It is reasonable to expect that such flows will have occurred frequently (about 22 times) since the dam was closed and, since they will have transported significant volumes of sediment, that they are likely to have been responsible for building a significant proportion of the prototype delta.

Each run was started by installing 16 of the 21 dam pieces and filling the reservoir with water to this level. An accelerated sediment feed was then used to grow the model delta to the longitudinal extent of the 2002 prototype delta (Stage 1 growth) (Figure 5.4). The model sediment mixture was shaken from a trowel into the delivery channel and a discharge, Q_m , of 109 l/min., which scales to a prototype discharge, Q_p , of 1,795.25 m³/s – a recurrence interval of about 3.3 years. Once the delta had grown to the required longitudinal extent two more dam pieces were installed to raise the reservoir water surface to enable the delta to grow vertically to the correct elevation under a less rapid growth regime (Stage 2 growth). In theory, this would result in a more natural slope to the delta surface (Parker, Personal Communication, 2003), since the high feed rate of the accelerated growth phase created very steep topset surfaces. In practice, stage 2 did not work well because the lower discharge was insufficient to grow the upper layer of the delta in a downstream direction. Instead, the sediment deposited around the mouth of the delivery channel and gradually spread out onto the flat model top (Figure 5.3a). It was therefore necessary to use the stage 1 growth discharge along with a lower sediment feed rate, in order to obtain longitudinal

growth. The two-stage growth process is shown in the Run6xCCam1-DeltaGrowth time lapse movie (DVD 6).

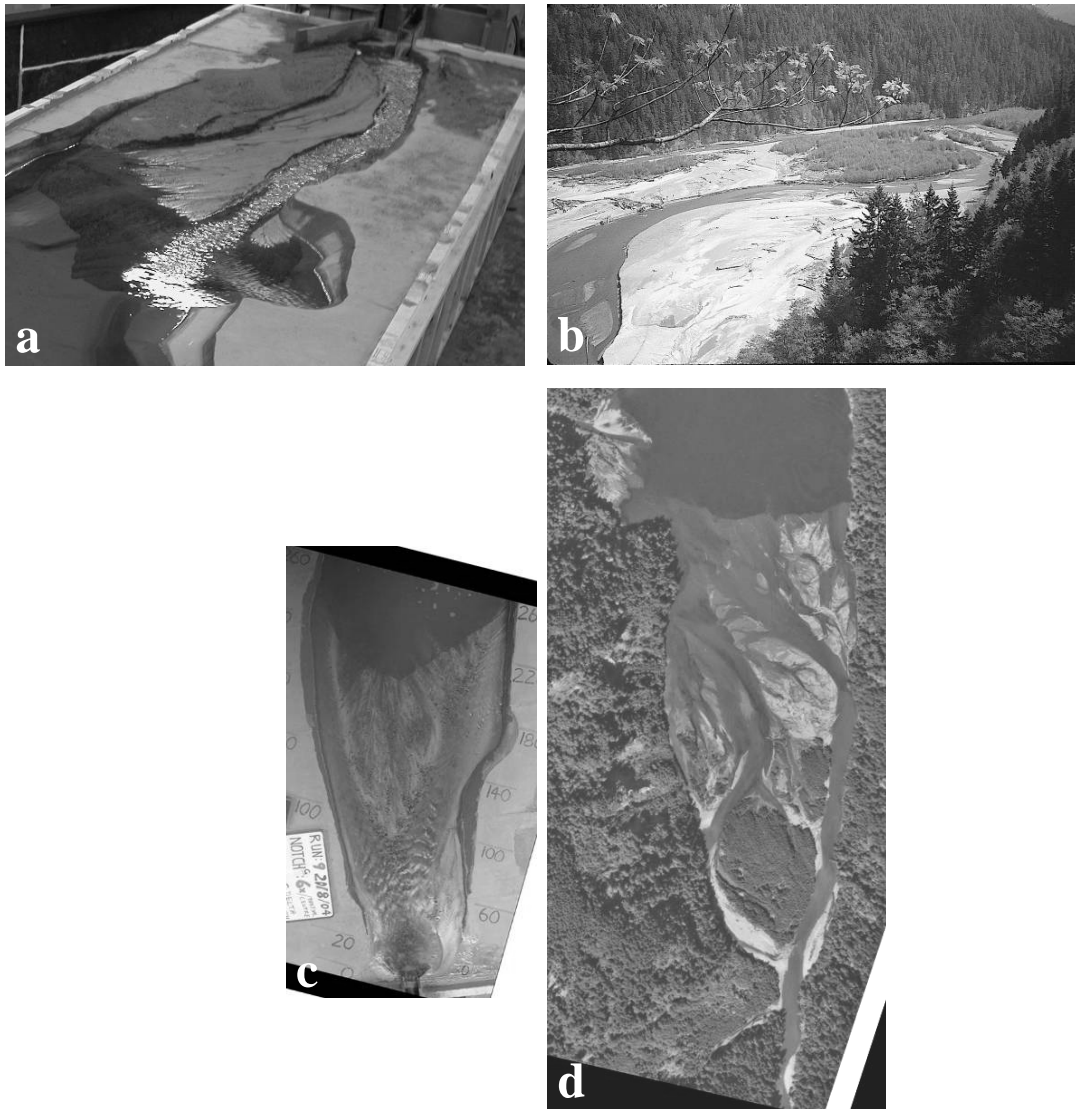


Figure 5.3. Comparisons of the model delta with the prototype during the 1994 drawdown experiment. (a) Sediment spilled onto flat model top on either side of the delivery channel during delta growth phase. (b) Steep valley sides prevent this from occurring in the prototype. (Photograph courtesy of the U.S. Bureau of Reclamation). (c) Model delta with preferential growth along the left and right sides of the basin. This would persist indefinitely unless the flow was encouraged to flow towards the central portion of the prograding delta front. (d) Prototype delta with evenly distributed delta front. (Photograph courtesy of the U.S. Bureau of Reclamation).

During both stages of growth, there was a natural tendency for the delta front to preferentially prograde along the left and right sides of the basin boundary as it approached the extent of the 2002 prototype delta, at the expense of filling the central portion of the prograding delta front (Figure 5.3c). This created a horn-shaped profile

that was unrepresentative of the prototype. It was therefore necessary to occasionally scratch a shallow channel into the topset in order to guide sediment towards the centre of the basin to create a front more representative of the prototype (Figure 5.3d). This tendency for flow to split over the delta topset was observed during the 1994 drawdown experiment, however, and so is not totally unrepresentative of prototype behaviour (Figure 5.3b). As the prototype Elwha River emerges from the narrow, bedrock-dominated, Rica Canyon it expands into the much wider reservoir, thus causing the deposition that lead to the formation of the vegetated island (Figure 5.3b&d). A similar expansion and deposition effect occurred during the model delta growth, thus splitting the flow in the proximal delta (Figure 5.3c). The prototype delta front does not have a horned appearance, however, so this suggests that there is nevertheless some scale-effect or geometrical inconsistency between model and prototype that affects sediment progradation and deposition in the more distal regions of the model delta, hence the need to periodically guide the sediment flow.

Two factors may explain the lack of success with the planned stage 2 growth strategy. First, the flat model top is not representative of the steep valley topography of the prototype Elwha River at the upstream end of Lake Mills, so part of the lateral spreading is due to the lack of model valley confinement (Figure 5.3a&b). Second, because the modelling sediment mixture was much coarser than that required by the scaling calculations, a lower discharge was incompetent to transport it longitudinally over the delta surface. This meant that more sediment was deposited immediately upon entering the model reservoir basin than would have occurred in the prototype, thus hastening the arrival of the point at which sediment began to spread laterally onto the flat model top. Once this occurred a positive feedback developed in which further sediment deposition directed increasing amounts of discharge over the model top, thus further reducing the transport competence of flow moving longitudinally into the model basin.

Another problem with the two stage growth is that when the sediment feed rate was suddenly dropped off at the start of stage 2, the finest sediments in the mixture were still entering into suspension and moving through the reservoir at the same rate as during the stage 1 growth, while the coarser fraction, due to the reduced stage 1 growth topset slope, was prograding much more slowly than during stage 1 growth. This allowed significant proportions of fines to deposit on the stage 1 growth

topset, before eventually being buried by the prograding coarser fraction of the stage 2 growth. This resulted in an inter-stage topset surface being deposited between the stage 1 growth and stage 2 growth portions of the delta (Figure 5.4), which is not present in the prototype delta.

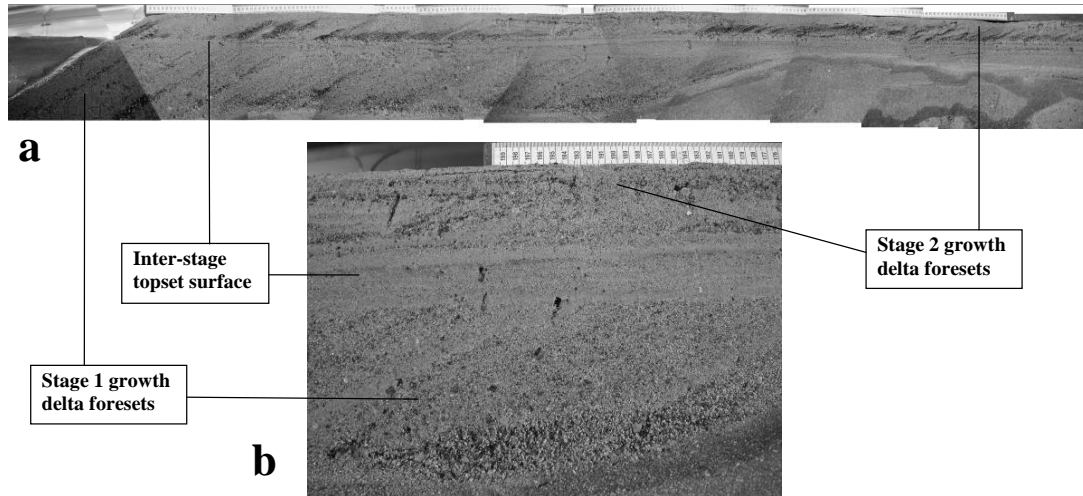


Figure 5.4. (a) Long profile of the dissected delta showing the essentially horizontal contact plane of fine sediment between the Stage 1 and 2 growth surfaces. (b) Close up of the contact plane.

5.4 Experimental procedure

5.4.1 Baselevel control

Once the model delta was fully grown, the remaining dam pieces were installed and the reservoir filled with water until it was overflowing the dam. Discharge was reduced to 15.57 l/min (prototype value = 59.4 m³/s; 2,098 cfs) and the first increment of the dam was removed. The wooden blocks were gradually lifted from the top of the dam, such that the reservoir drained through the gap between the top and second-top dam pieces, in order to achieve a water surface (baselevel) fall rate of 2.8 cm per 15 minutes, which scales, using equation 4.32 and $Y_r = 81.7$, to a prototype rate of baselevel fall of 2.29 m (7.5 ft) in just over 8.5 hours, which is easily achievable in the prototype. The fall rate was controlled by monitoring the water surface elevation against a length of measuring tape stuck to the model dam's left abutment, which was tied into the coordinate system used by the laser, and a stop watch, and by adjusting the position of the top-most dam piece to regulate the outflow. Once the baselevel had dropped the required distance the top-most dam piece

was adjusted until outflow through the dam matched inflow at the upstream end of the delta. This was controlled by repeatedly checking the baselevel to ensure that it was constant - initially every five minutes but then at progressively longer intervals as it stabilised - and by adjusting the position of the top-most dam piece as necessary. Despite the simplicity of this method it was possible to control the periods of both falling and constant baselevel with a good degree of accuracy. The notable exception occurred towards the end of the period of falling baselevel, when the dam had been almost completely removed. At this stage of the run the reservoir was almost non-existent and even very small changes in the outflow had sudden and large effects on baselevel, which was almost impossible to control. This is shown clearly by the tail end of the plots for runs 3xR, 3xC and 3xL (Figure 5.5).

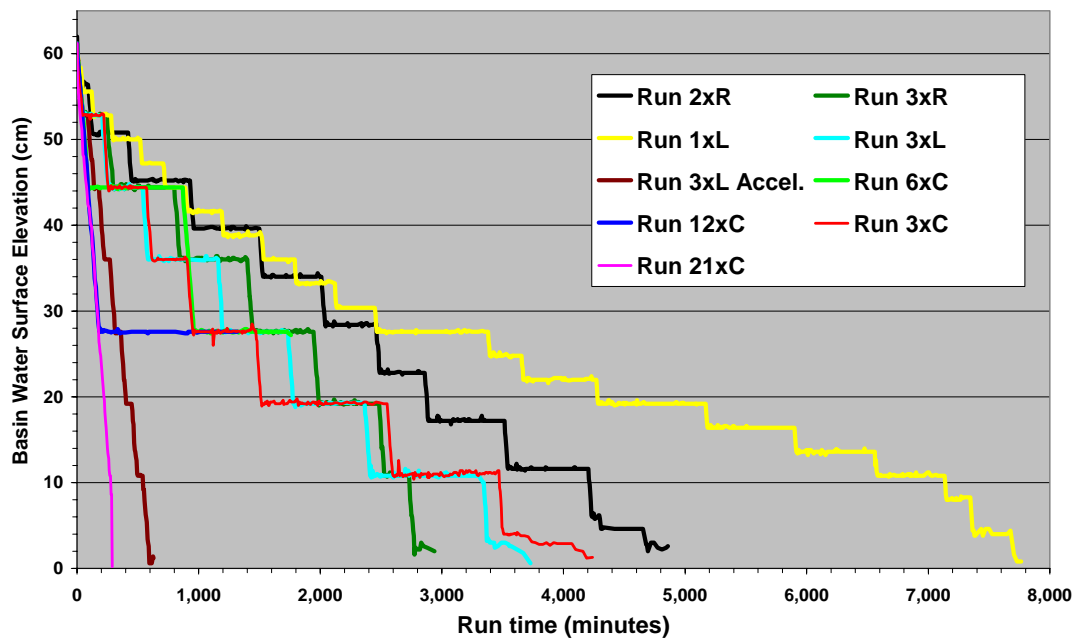


Figure 5.5. Pattern of baselevel fall for each experimental run.

5.4.2 Discharge control

Discharge to the model was controlled using a manometer attached to two orifice plates (Figure 5.6a). The orifice plates have one hole each drilled through their middles, which are both smaller than the diameter of the white pipe feeding into them. The diameter of the left orifice plate is 3.8 cm (1.497 inches) and was used to measure the larger discharges used for delta growth and flood flows. The diameter of the right orifice plate is 1.91 cm (0.75 inches) and was used to measure the smaller discharge that provides the model's base flow during dam removal. Both plates were attached

via flexible plastic tubing to the valves at the top of the manometer's U-tube (Figure 5.6b). The system works by the water-filled plastic tubing transmitting the pressure differences, which develop as water squeezes through the hole in the orifice plate, to the U-tube. The pressure causes a displacement of the organic dye in the U-tube which can be read off the scale (Figure 5.6c).

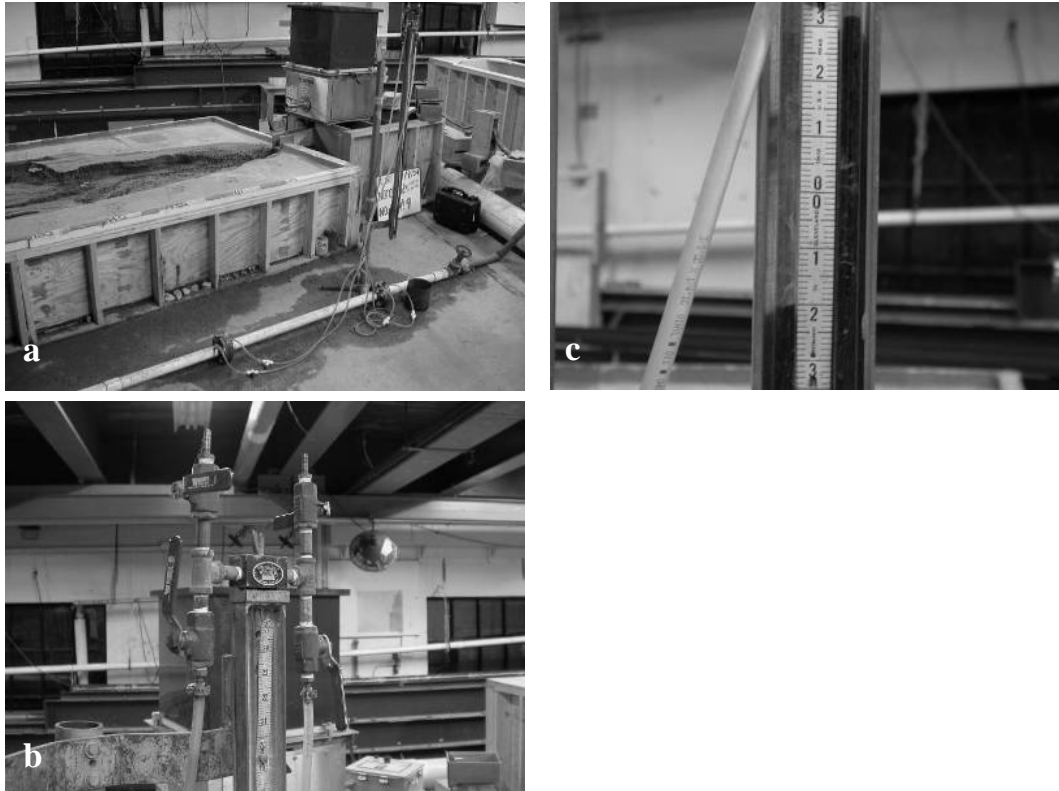


Figure 5.6. Model discharge control. **(a)** Manometer and headbox supply valve. **(b)** Control valves at the top of the manometer. **(c)** Displacement of organic dye in the manometer's U-tube, here measuring about 5.26 inches (15.57 l/min.), the model's base discharge.

5.4.3 Flood flows

The cycle described in section 5.4.1 was repeated until the entire dam had been removed, using the same constant discharge of 15.57 l/min. This flow represents the prototype discharge ($59.4 \text{ m}^3/\text{s}$) that would be required to transport the mean daily total load of sediment required to fill the reservoir to its current extent over the 79 years of its existence (Bureau of Reclamation, 1996b). For all runs where the entire dam was removed, except Run 2xR, a sequence of one or several two- and five-year recurrence-interval flood hydrographs were run through the reservoir area (Table 5.1). The base flow of 15.57 l/min. at the end of each hydrograph was run until the system

again reached a static equilibrium, with the sediment surface being scanned one final time at this point (section 5.5.1).

The model flood hydrographs were developed based on the balanced-hydrographs created by the Bureau of Reclamation (1995a) for the McDonald Bridge gauging station (ELWP)¹⁷ just upstream from Lake Aldwell (Figure 2.1). The balanced-hydrographs were created by using the log-Pearson Type III analysis to obtain the peak flow values for recurrence interval flows of 2, 5, 10, 25, 50, 100, 200 and 500 years, based on the entire period of record for the ELWP station (1898-1902; 1920-1992) (Bureau of Reclamation, 1995a). The mean flow values for 1-, 3-, 5-, 7- and 15-day periods following the peak flow for each of these events was then calculated. The hydrographs for each recurrence interval event were then balanced by calculating the mean daily flows for days 2-3, 4-5, 5-7 and 8-15 of the 15-day flood hydrograph. The 15-day hydrograph was identified as the typical event length from the full ELWP record (Bureau of Reclamation, 1995a). The balanced hydrographs for the 2-year and 5-year recurrence interval floods were transposed to the temporary Elwha River gauging station (ELWW)¹⁸ immediately upstream from Lake Mills (Figure 2.1) using the area-ratio method. The process of transposition transfers a flow record from a gauged site to an ungauged one by adjusting the flow values based on the ratio, Q_R , of the square root of the ungauged to gauged drainage basin area (McCuen and Levy, 2000), as follows:

$$Q_R = A_u^{0.5} / A_g^{0.5} \quad (5.1)$$

and

$$Q_u = Q_g \times Q_R \quad (5.2)$$

where A_u = the drainage basin area at the ungauged site (L^2); A_g = the drainage basin area at the gauged site (L^2); Q_u = the discharge at the ungauged site (L^3/T); and Q_g = the discharge at the gauged site (L^3/T). The area-ratio method was appropriate to use since the two sites fulfil all the necessary criteria outlined by McCuen and Levy (2000) for the accurate application of this method:

¹⁷ USGS 12045500 Elwha River at McDonald Bridge Near Port Angeles, WA

¹⁸ USGS 12044900 Elwha River Above Lake Mills Near Port Angeles, WA

- i) that the gauged record should be sufficiently long to include periods of high flow. [Since there is a 76-year record, there will have been a number of 2- and 5-year return interval floods in that time];
- ii) that both sites should have similar channel and watershed characteristics. [The two sites are relatively close together on the same river and they are both located in narrower, canyon-like channel reaches immediately upstream from the wider reservoir areas]; and
- iii) the two sites should be on the same river.

The drainage basin areas at the ELWP and ELWW gauges are 696.7 km² (269 miles²) and 512.8 km² (198 miles²) respectively. This produces a scaling factor, Q_R , of

$$512.8^2/696.7^2 = 0.86.$$

The data for the balanced hydrographs at ELWP, ELWW and in the model, whose values were obtained using the scale ratio given by equation 4.34, are presented in Table 5.5, while the 2-year and 5-year model flood hydrographs are shown in Figure 5.7.

Recurrence interval (years)	Peak discharge (m ³ /s)	Average flows (m ³ /s)														
		Day of hydrograph														
		1	2	3	4	5	6	7	8	9	10	11	12	13	14	15
McDonald Bridge gauging station (ELWP)																
2	382	241	160	160	109	109	96	96	80	80	80	80	80	80	80	80
5	583	374	225	225	147	147	125	125	100	100	100	100	100	100	100	100
Temporary gauge (ELWW)																
2	328	207	137	137	94	94	83	83	69	69	69	69	69	69	69	69
5	501	321	193	193	126	126	107	107	86	86	86	86	86	86	86	86
Lake Mills model																
Recurrence interval (years)	Peak discharge (l/min.)	Average flows (l/min.)														
		Day of hydrograph														
		1	2	3	4	5	6	7	8	9	10	11	12	13	14	15
2	86	54	36	36	25	25	22	22	18	18	18	18	18	18	18	18
5	131	84	51	51	33	33	28	28	22	22	22	22	22	22	22	22

Table 5.5. Balanced flood hydrograph data.

5.5 Data acquisition

5.5.1 Laser profiling and sediment collection at the model's outlet

The model was run for a length of time before the inflow was shut off and the reservoir drained until all of the foreset and part of the bottomset beds were exposed. The entire delta surface (topset and foreset beds) and the limited bottomsets that

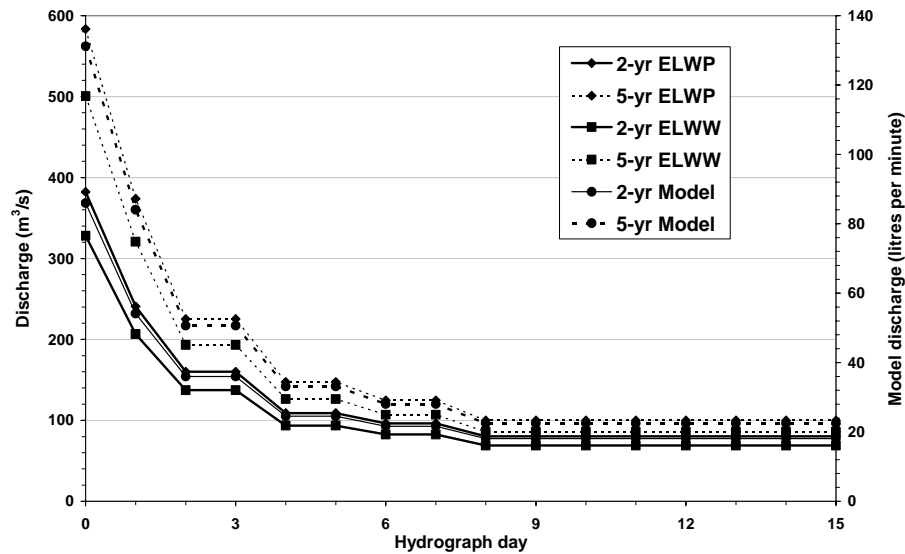


Figure 5.7. Balanced hydrographs for the McDonald Bridge gauge (ELWP), the temporary gauge (ELWW) and the Lake Mills model.

developed during delta growth and subsequent incision were then scanned using a Keyence LK-503 laser mounted on a hand-movable instrument carriage (Figure 5.8). The surface was scanned along a series of cross-sections spaced longitudinally (y) at 5-cm intervals. Delta surface elevation (z) was measured across each section (x) at 0.5-cm intervals and with a sub-millimetre vertical accuracy. Additional cross-sections were scanned to capture details of breaks in slope and bank line where these fell in between the 5-cm cross-sections in order to accurately record the deposit topography. The basin was then refilled to its previous elevation and the incoming flow switched back on. The system was scanned in this way after 1.5, 3.5, 5.5, and 9.5 hours of run time and sometimes at additional intervals in between, or until it reached a static equilibrium in between one of these intervals, at which point it was scanned one final time. This final scan also provided the baseline condition for the next set of scans. Once the entire surface had been scanned, the data were saved to a text file (*.txt) as columns of x , y , z , coordinates.

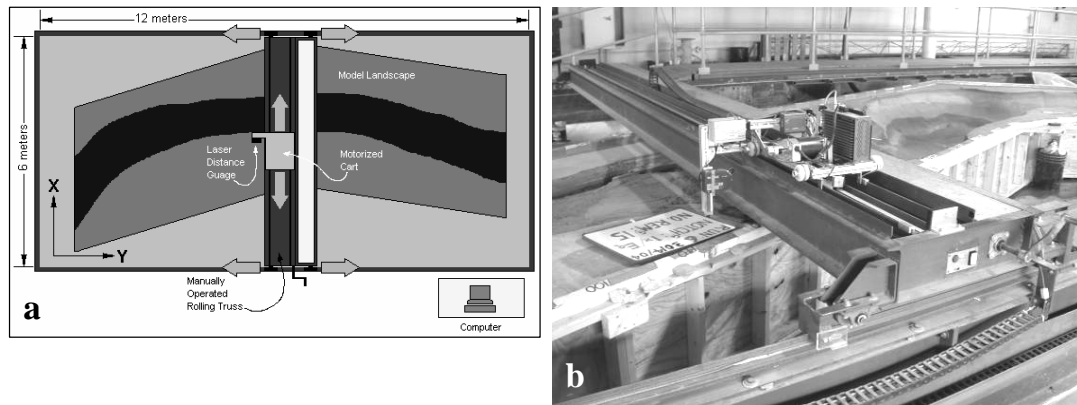


Figure 5.8. (a) Schematic and (b) photograph of the Keyence LK-503 laser and instrument carriage. Note the directions of the x and y coordinates. Schematic courtesy of Brett Otteson, St. Anthony Falls Laboratory, University of Minnesota.

Because the laser was not capable of measuring sediment once it began to pass through the dam site, this material was collected in buckets and its volume measured in order to close the sediment budget for each time step. Most of the material passed through a pipe from the laboratory floor on which the model was located (model floor) to the floor below (shop floor), where it was collected. In addition, a small amount of sediment was deposited in the model's tailbox (Figure 5.2g) and this was also collected into a bucket to allow its volume to be measured.

5.5.2 Time lapse photography

The evolution of each experimental delta was recorded, essentially continuously, using four Olympus C-4000 digital cameras mounted directly above the model basin and connected to a desktop computer. The cameras were controlled using the shareware version of Pine Tree Computing's Camera Controller, which was downloaded for free from <http://www.pinetreecomputing.com/camctl.asp>, and were set to take photographs simultaneously at 30-second intervals for the duration of each run. During the period of delta growth they were set to take one photograph per minute. Once taken, the photographs were automatically downloaded to the computer for storage.

In addition to the overhead photographs, which present a two-dimensional record of experimental progress, oblique-angled photographs were taken from nine photopoints around the basin to provide a three-dimensional record of delta surface

evolution. These photographs were taken every time the delta surface was scanned from Run 3 onwards.

5.5.3 Sediment sampling

5.5.3.1 Delta growth mixture and sediment coring

Three samples were collected from the sediment mixture prior to delta growth. Once the delta had been grown, but prior to the onset of dam removal, a total of nine sediment cores were removed along three transects at $Y = 0.5$ m, 1.5 m and 2.5 m along the delta surface (Figure 5.9a). Each core was broken down into 5-cm sections, as measured from the base of the core upwards (Figure 5.9b), oven dried and sieved in order to quantify the original delta's grain size distribution.

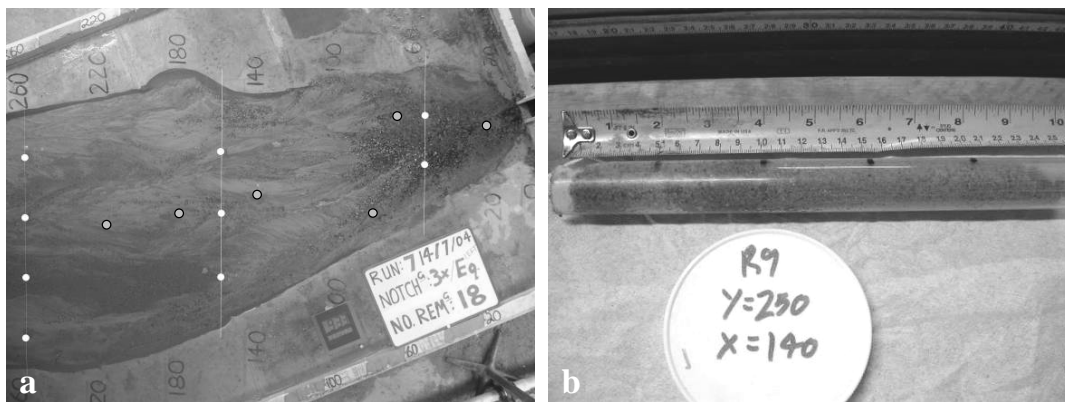


Figure 5.9. (a) Model delta coring (white circles) and approximate prototype delta borehole locations (grey circles). (b) Example of one of the delta sediment cores.

5.5.3.2 Armour and sub-armour sampling

Once the delta system had reached a static equilibrium following the removal of the last section of the dam and again following the flood flows, samples of the armour and sub-armour were collected at one-meter intervals along the full channel length (Figure 5.10a). The laser was used to locate the middle of the channel and a 10 cm x 10 cm cardboard square was placed on the bed, centred on the laser point, such that the top and bottom edges of the square were parallel with the channel banks (Figure 5.10b). Once the pieces of surface gravel were removed and retained, the largest piece of gravel embedded in the channel bed was gently removed. The base of the indentation left by this piece of gravel defined the lowest elevation of the armour layer (Bunte and Abt, 2001), which was removed from within the square and retained

in the same container as the surface gravels. A sub-armour layer of similar thickness was then removed and stored in a separate container. Downstream of about five or six meters, once the system had quasi-equilibrated following the removal of the dam and the 2-year flood flow, the channel had in places cut through to the hard basin boundary. Where this occurred it was not always possible to sample the sediment at whole-meter intervals, *i.e.* at 7 m, 8 m, 9 m and 10 m, and so samples were collected from the patches of sediment where they occurred. Most of these patches had no armour layer and a bulk sample of sediment was instead collected by excavating the sample square to a depth of 1 – 2 cm. All samples were oven dried and sieved.

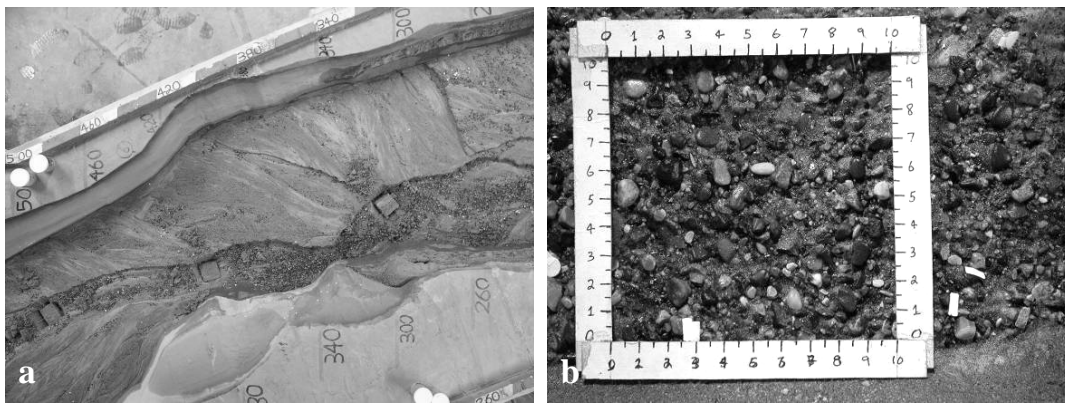


Figure 5.10. (a) Armour and sub-armour sampling. (b) Cardboard sampling square for delineating armour and sub-armour sample area.

5.5.4 Particle Tracking Velocimetry

Three video cameras were mounted above the model looking vertically down onto sections of the delta surface. At regular intervals over the duration of each run, a number of small white paper floats¹⁹ was introduced at the upstream end of the model and filmed as they moved downstream over the delta surface, their colour making them easily identifiable against the generally darker sediment. Mean flow velocities can be estimated by averaging the product of distance travelled per unit time, multiplied by 0.8 (Leopold, 1994), of several floats. This method was chosen because it was low cost and, more importantly, was non-invasive and would not deflect the flow and potentially trigger morphological adjustments unrelated to the changing baselevel. On a number of occasions in all runs, when the delta surface system was very close to a threshold of instability, barely perceptible changes in streamline

¹⁹ The floats were fabricated using a hole-punch.

direction triggered sometimes extensive periods of morphological adjustment (section 7.2), so this was a real possibility. In addition, given the sometimes very shallow channel flows, it would have been impossible to obtain measurements using a current meter.

Chapter 6 Data Reduction

This chapter describes how the model measurements were processed to produce the base data on which subsequent analyses and results are based. It focuses on the volumetric sediment data developed from laser measurements and on the time lapse photographs of the delta surface and channel morphology. It also includes a detailed account of the steps taken to identify, quantify and correct for errors in the measurements as the treatment of errors is fundamental to understanding and minimising uncertainty in the results of subsequent analyses.

6.1 Volumetric analysis

6.1.1 Overview of volumetric analysis

The data collected with the laser (section 5.5.1) were used to perform three different sets of volume calculations. For every scan performed in every run, the volumes of sediment eroded (cut) and deposited (fill) were calculated for:

- (i) the original delta area;
- (ii) the entire sediment surface; and
- (iii) discrete, 50 cm-long sections of the entire delta.

For each run, the volume of sediment in the original delta area is defined as that within the area delineated by the delta topset and foreset surfaces and the reservoir basin boundary prior to the onset of dam removal (Figure 3.1; Figure 7.16). It does not include the bottomset deposits produced during the period of accelerated delta growth. Hence, this model area corresponds to the area of the prototype delta in 2002. The entire sediment surface is defined as the entire original delta area plus the bottomset deposit. While no deliberate attempt was made to recreate the prototype bottomset deposits, a small but measurable bottomset surface was the inevitable by-product of building the model delta hydraulically, because the finest grains were bound to settle out of suspension downstream of the original delta area.

Calculations were performed in ArcGIS 9.0 using the cut-fill tool in the 3-D Analyst extension. The process of inputting the data files, creating the necessary digital elevation models (DEMs), performing the cut-fill analysis, and generating the

output files was automated using an Arc Macro Language (AML) script. This script, along with a detailed explanation of all the commands used and of their significance to ensuring calculation accuracy, is presented in Appendix B. The cut-fill tool calculates the volume of sediment that has been eroded, V_c , and deposited, V_f , during a period of time by subtracting the DEM for a surface from that of the preceding surface, a process known as *differencing*. For a closed system in which no sediment enters or leaves the study area, cut and fill volumes should be equal and are given by,

$$V_c = V_f = DEM_{t+1} - DEM_t \quad (6.1)$$

Where, t = time.

Prior to running the AML for each surface, a Triangulated Irregular Network (TIN) was generated in ArcMap and exported into ArcScene for visual examination. Any troughs and stripes created in the surfaces by the surface fitting process were identified and manually removed and an ArcGIS shapefile (*.shp) was then generated using a Python script to create the input files used by the AML.

6.1.2 Assessment of DEM quality and reduction of DEM errors

Lane (1998) used the term *quality* in reference to a DEM to describe the amount of error that occurs when it is used to represent a terrain surface. DEM quality is affected by the method by which data are collected and the way these data are processed (Ackermann, 1978, cited in Lane, 1998). (Lane *et al.*, 1994) showed how DEM quality in turn affects the quality of the information obtained from DEM differencing through four main categories of error. These are associated with:

1. the individual data points that represent the surface;
2. the surface fitted to the data points;
3. the degree to which the DEM represents the real topography of the surface and its changes through time;
4. the algorithm used to perform the cut-fill analysis.

Errors associated with each of these categories are examined in the following subsections.

6.1.2.1 The quality of individual data points

The quality of individual data points is affected by random, systematic and gross errors (also known as blunders). Random errors control the level of precision in coordinate data and represent the variation that occurs when a value, *e.g.* surface elevation, is measured several times under the same conditions. Systematic errors control the accuracy of individual coordinates (Lane *et al.*, 1994; Lane *et al.*, 2000) and determine whether a DEM systematically under or over-estimates real elevations (Wise, 1998b). Gross errors are those made by observers, such as an accidental shift in a datum (Brasington and Smart, 2003), or caused by an equipment malfunction. If the surface being analysed is not being compared to any other surface, either real or modelled, the presence of these errors is unimportant provided that they are evenly distributed over the surface, because all measurements taken from the surface will be accurate relative to each other. However, if one surface is to be compared to another, as in this study, then these errors must be accounted for as their magnitude may vary from surface to surface (Brasington and Smart, 2003).

In this analysis, the effect of systematic errors on data accuracy was represented using the mean error (ME) (equation 6.2),

$$ME = \frac{\sum_{i=1}^n (z_{i\ est} - z_{i\ obs})}{n} \quad (6.2)$$

while the effect of random errors on data precision can be quantified using the root mean square error (RMSE) (equation 6.3), or the standard deviation of error (SDE) (equation 6.4) (Lane *et al.*, 2000).

$$RMSE = \sqrt{\frac{\sum_{i=1}^n (z_{i\ est} - z_{i\ obs})^2}{n}} \quad (6.3)$$

$$SDE = \sqrt{\frac{\sum_{i=1}^n ((z_{i\ est} - z_{i\ obs}) - \overline{(z_{i\ est} - z_{i\ obs})})^2}{n}} \quad (6.4)$$

Where, $z_{i \text{ est}}$ = linearly-interpolated elevation of the i th point; $z_{i \text{ obs}}$ = measured elevation of the i th point; and n = total number of data points per surface.

The recorded elevation of each point scanned by the Keyence laser is an average value based on 10 individual elevation measurements, which were not recorded by the laser-controlling software (Otteson, 2004). It was therefore impossible to determine the magnitude of any random errors that may occur, although the laser's sub-millimetre accuracy, the number of measurements used to obtain the average, and the fact that both control points and none-control points were collected at the same time using the same equipment (see below) suggest that random errors should be small. In light of this, only systematic errors were evaluated numerically. To calculate the mean error statistic, it was necessary to obtain measurements of surface elevation that are independent of the point data used to create the DEM (Lane *et al.*, 2000; Wise, 1998a; 1998b). Ideally, these measurements should be distributed randomly across the surface but, because the laser was constrained to move along a fixed cross-section, they were selected at random from the population of points created by the cross-sectional scans for each experimental surface. Numbers of control points reported in the literature range from 40 (Brasington and Smart, 2003) to 867 (Lane *et al.*, 2000) and, based on this range, 500 points per surface were used in this study. Linear interpolation was used to generate elevation values for all non-measured delta surface points during lattice resampling in the cut-fill analysis (section B.3.3) and so the elevation of each randomly-selected control point was linearly interpolated using the elevations of the adjacent points along the cross-section (ESRI, Written Communication, 2007).

An unavoidable problem with the use of control points as independent arbiters of DEM surface point accuracy is that they must themselves be measured and, as such, they are as much subject to error as the measured points used to construct the DEMs (Lane *et al.*, 2000). In this study, control points and all the other surface coordinates were measured at the same time and using the same equipment, so random errors in the two sets of measurements should cancel out. Consequently, the DEMs are subject mostly to systematic errors and the mean error will provide a very accurate indicator of how well the DEM surface represents real elevations, *i.e.* how realistically the algorithm triangulates between measured data points. This is in contrast to studies where surface coordinates and control points are collected using

different techniques at different times, for example using photogrammetry and surveying (*e.g.* Brasington and Smart, 2003; Lane *et al.*, 1994; Lane *et al.*, 2000). In those cases, the DEMs will be subject to both systematic errors and higher magnitude random errors.

Mean and maximum errors for each run are summarised in Table 6.1. The mean, minimum and maximum mean surface errors are very small and correspond well to the sub-millimetre accuracy of the Keyence laser, indicating that DEM triangulation between the measured points is generally very realistic (section 6.1.2.2). Maximum point errors are large relative to the surface means and are associated with areas where elevation changed by a large amount within a very small cross-sectional distance, *i.e.* near the faces of steep banks and terraces. A similar finding has been reported by Carlisle (2005).

The mean error associated with each surface was used to estimate systematic errors in the volume of sediment eroded from the original delta and erosion volumes were corrected accordingly, as described in section 6.1.3.

Run	Mean error of all run surfaces (cm)	Minimum surface mean error (cm)	Maximum surface mean error (cm)	Maximum point negative error (cm)	Maximum point positive error (cm)
2xR	0.004	-0.02	0.04	-5.18	15.42
3xR	0.002	-0.02	0.04	-6.02	8.05
1xL	0.0006	-0.03	0.03	-4.9	5.66
3xL	0.002	-0.02	0.03	-7.43	0.36
3xL(A)	0.003	-0.02	0.04	-3.13	4.6
3xC	0.0004	-0.02	0.01	-5.0	4.43
6xC	0.004	-0.01	0.02	-3.8	9.0
12xC	0.002	-0.01	0.01	-4.41	2.38
21xC	0.0001	-0.004	0.005	-2.32	1.74
2xSplit	0.003	-0.005	0.01	-2.16	2.1

Table 6.1. Summary of mean error statistics used to assess the magnitude of systematic errors.

6.1.2.2 The quality of the surface fitted to the data points

The quality of the surface that is fitted to a set of point data, *i.e.* the degree to which it represents the real surface, is a function of the effectiveness with which the data points are used to construct the surface (Lane, 1998). Surfaces can be fitted to a set of points either by interpolation or triangulation to form a TIN. In interpolation, individual data points may or may not be present in the surface, but in a TIN all points are included as the vertices of each triangular face of the surface (Milne and Sear,

1997; Wise, 1998a). Several authors have shown that triangulation recreates the real surface more accurately than interpolation (Siska and Hung, 2001; Wise, 1998b) due to this explicit use of the data points (McCullagh, 1998). The Delaunay method of triangulation provides the most accurate representation of a surface, provided that break lines have been used (see below) and that data points accurately represent the topography of the real surface (McCullagh, 1998).

Lane *et al.* (1994) showed that two further aspects of surface fitting can have significant effects on the representativeness and accuracy of a DEM. The first and most important of these is the use of break lines to delineate linear features such as the bank top, the bank toe and terrace edges. Break lines prevent triangulation across these features and thus the creation of topographical features that do not exist. Because the laser was constrained to move along a cross-section, however, it was not possible to scan such features, resulting in an artificially stepped appearance to bank and terrace edges (Figure 6.1b). While the points necessary to create break lines could have been selected from the DEM files manually, the number of points required to delineate all the necessary break lines for one DEM, multiplied by the hundreds of DEMs used in this study, would have made this a colossally time-consuming task and so it was not attempted. The problem was partially circumvented by the close spacing of survey points (0.5 cm intervals) along each cross-section and by inserting additional cross-sections wherever there was a change in direction of a break line feature (section 5.5.1). This resulted in model topographies in the vicinity of break line features that are reasonable at the meso- to macro-scale, although accuracy is lower at the micro- to meso-scale (Figure 6.1).

Break lines are also useful in maintaining surface representativeness where the density of points in one area of the surface is much higher than that in an adjacent area. This often occurs when a higher density of points has been used to represent an area of particular interest or with more complex topography (*e.g.* Lane *et al.*, 1994). Where this occurs there is a risk that multiple points from the densely populated area will interact with individual points in the sparsely populated area, distorting the topography of the fitted surface. Appropriately placed break lines avoid this problem by preventing triangulation across the boundaries between areas with the different point densities (Lane *et al.*, 1994), although this situation did not arise in this study

because of the regular spacing of points both longitudinally and laterally across the delta surface.

The second aspect of triangulation identified by Lane *et al.* (1994) as affecting DEM quality are edge effects at the boundary of the study area, which occur due to triangulation between points at the boundary of a surveyed area. Edge effects can create surface features that do not really exist and must be eliminated. In the physical model each scanned cross-section extended into the flat surface at the top of the model (Figure 6.1a) so that this feature was represented in the DEM. However, as the flat surface was of no interest to the study, it was a simple matter to avoid edge effects by using a clip polygon to exclude the flat area from the differencing calculations (section B.3.5).

6.1.2.3 The overall quality of the topographic representation

It is important to assess the overall quality of the topographical representation to establish the degree to which the methods of data collection that were employed are capable of accurately representing the actual shape of the model delta surface. This is the case because there are several areas of concern regarding the representativeness of the surface. Issues concern:

- (i) the size of the various components that make up a topographical surface (Lane *et al.*, 1994);
- (ii) estimation of the initial volume of sediment in the original delta and the reservoir basin as a whole at the beginning of each run;
- (iii) the presence of overhanging channel banks and terraces;
- (iv) the vertical range over which the laser is able to collect data.

i) The size of topographical components

To generate a DEM that perfectly recreates the delta surface at each time step it is necessary to use a technique that can measure surface topography at the scale of the individual grains forming the surface (Lane *et al.*, 1994). This was theoretically possible in the model basin as the laser used to scan the surface had a sub-millimetre vertical accuracy and it could comfortably have measured surface elevation at millimetre intervals both cross-sectionally and longitudinally. However, such detailed measurements were impractical due to the excessive length of time that would be

required to complete each scan. In practice, and given the study objectives, it was necessary to select a spatial resolution that balanced the degree to which the DEM represents the true surface against the time required to perform a scan. The spatial resolution of sampling was selected based on a visual inspection during test runs of the size of topographical features typically formed in the delta (Milne, 1982, cited in Milne and Sear, 1997). The selected cross-sectional spacing of sample points (0.5 cm) was capable of distinguishing details of the armour layer, while longitudinal spacing of cross-sections (5 cm) but with additional cross-sections inserted where necessary, was designed to capture breaks in slope, changes of bank line direction and the edges of depositional lobes (Figure 6.1).

The sensitivity of the accuracy of the selected sampling resolution to change in the spacing of sample points was investigated by progressively removing points used to create the surface of Run 8 (3xC) after 1,800 minutes of run time. Progressively sparse DEMs were, in turn, subtracted from the DEM for the surface of Run 8 after 1,680 minutes (equation 6.1) with the results used to assess the how much information was lost for each degree of thinning in the density of the points used to fit the surface (Lane *et al.*, 1994). First, the DEM for 1,800 minutes was thinned laterally by removing every second, every second and third, up to every second to eleventh point from each cross-section to create 10 increasingly sparse DEMs. Second, the original DEM was thinned longitudinally by removing every other, every second and third, and every second to fourth cross-section. Only the cross-sections routinely spaced at 5 cm intervals were removed in this way, since removal of any of the cross-sections that were added to tie down key topographical features might have disproportionately affected the results. This created a further three data sparse surfaces. Finally, the original DEM was thinned by combining the outcomes of both cross-sectional and longitudinal thinning criteria to create a further 30 thinned DEMs. In total there were, therefore, 43 increasingly sparse surfaces and one dense surface.

The results of this exercise are presented in Figure 6.2 for fill volumes, which are used instead of cut volumes to represent the volume of sediment eroded for the reasons explained in section (iii) below. The results indicate that the fill volume is progressively over-predicted by a greater amount as point density is reduced. In Figure 6.2, results for increasing point spacing along cross-sections suggest that errors are small and insensitive to point spacing for densities greater than about 0.2 points

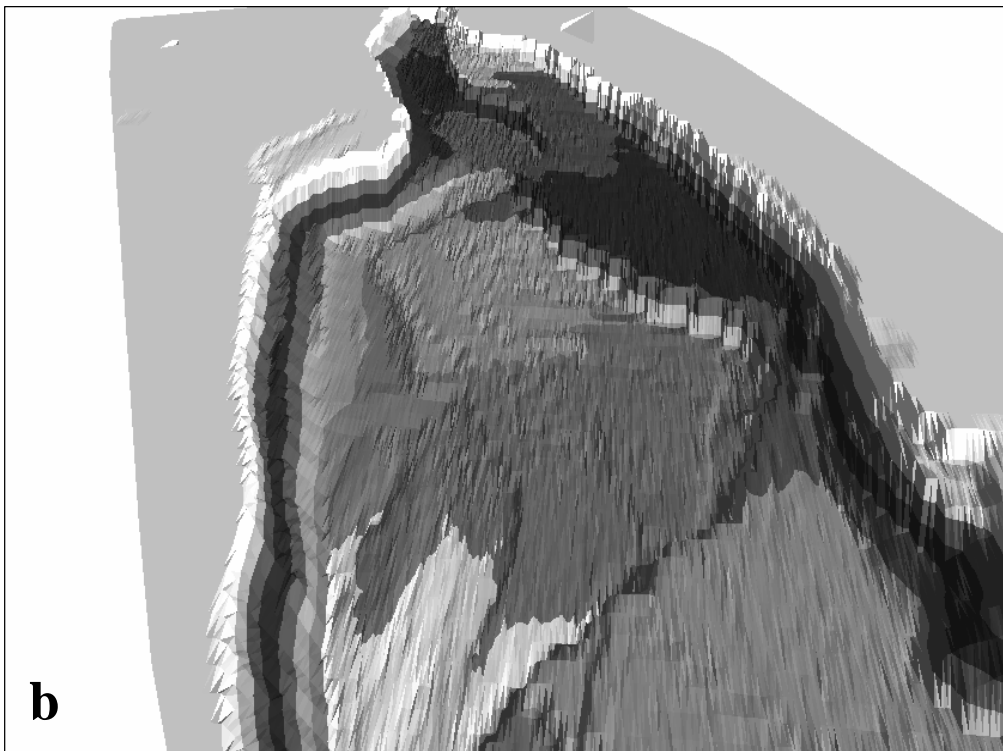


Figure 6.1. (a) Photograph and (b) DEM of the original delta area in run 3xC after 2,550 minutes. Note how the level of detail visible in the photograph is also identifiable in the DEM, with features such as the armour layer, terraces attached to the basin walls and lenses of sediment on the flat basin boundary present in the DEM. However, note also the artificially stepped appearance of linear features such as bank and terrace edges, in the DEM, which is due to the longitudinal spacing of the cross-sectional laser scans.

per cm². Consequently, a surface density of 0.445 points per cm² (as used in the study) results in the loss of only 1.3% of the information gained at the highest density. The effects of progressively removing cross-sections while maintaining full point density along each cross-section produce a similar trend, though the cross-sectional spacing actually used in the study is associated with greater uncertainty. This suggests that the 5-cm cross-section spacing used in the study was the factor limiting the accurate quantification of morphological adjustments, although the inclusion of additional cross-sections at key breaks of slope and bank line should have offset this problem. The plotting positions of the points for increased cross-sectional spacing relative to those showing the effects of combining cross-sectional point removal with the removal of 0 – 3 cross-sections further illustrates that it was the spacing of cross-sections that ultimately determined the accuracy of the cut-fill analysis in this study. This is the case because in each of the four plots representing the combined effects of increased cross-sectional and along-cross-section spacing, the magnitude of the minimum loss of volume information is controlled by the loss of information associated with cross-sectional spacing rather than increased along-cross-section spacing.

The absolute volume of sediment mixture used to build each model delta was not measured precisely, but was observed to range from 40 to 45 buckets-full²⁰, which corresponds to 0.56 m³ to 0.85 m³ of sediment. The results of the point thinning analysis indicate that all the volumetric changes reported herein overestimate the true volumes of erosion and deposition. Hence, a more appropriate upper bound estimate of the initial sediment volume is provided by the corrected laser-based estimates listed in Table 6.2.

Errors in the cut-fill volumes may be estimated by fitting regression curves through the points in Figure 6.2 but there is no rational way to select the best type of curve fit *a priori*. Also, there is the option to fit a curve by eye (Figure 6.3). In Figure 6.3, the polynomial curve fit is clearly inappropriate as it indicates an increase in information loss with increasing point density. The logarithmic curve is also inappropriate as it indicates that a 0% loss in volume information would require less than 0 cm³ of sediment in the model. Similarly, the exponential progression would require about 0 cm³ for a 0% loss. The power curve is also inappropriate as it

²⁰ Each bucket contained about 14,000 cm³, up to an absolute maximum of 18,927 cm³ of sediment.

approaches an asymptotic value with about 60% less sediment in the model than was estimated from the laser data for all runs. This is unrealistic as it would require that there was far less sediment in the model than was known to be there, based on the minimum bucket-based estimate (Table 6.2). In contrast, the curve fitted by eye seems to be the most appropriate for use in estimating errors. The curve fitted by eye suggests that the laser data overestimate actual sediment volumes by about 18%, which would require a point density of about 1.2 points/cm² (Figure 6.3) in order to be accurately measured by the laser. Reducing the corrected laser data by 18% produces estimated absolute sediment volumes close to the minimum bucket-based estimate of 0.56 m³ (Table 6.2), which suggests that these values and those indicated by the curve fitted by eye are reasonable. The shape of this curve also captures the asymptotic decline in error associated with increasing the number of points along each cross-section (Figure 6.2), which further supports its validity.

The point densities used to produce Figure 6.2 are based on a total delta surface area of 113,764 cm². Approximately $1.2 \times 113,764 = 136,517$ laser-measured points would, therefore, be required to provide laser-based volume estimates with minimal absolute error. However, this would have necessitated the cross-sections being spaced only about 0.8 cm apart (Figure 6.4), which would have required prohibitively long scan times.

While the laser-based sediment volume measurements used in the study tend to overestimate the absolute volumes of sediment involved, they do not preclude comparison between runs because the cross-sectional spacing and point densities were unchanged between runs and errors should cancel out. All the subsequent volumetric analysis will therefore be based on the corrected laser data.

ii) Estimation of original delta and total reservoir sediment volumes at time zero

The volumes of sediment contained in the delta at the beginning of each run, $ODV_{t=0}$, and in the entire delta, $FSV_{t=0}$, were calculated by subtracting the original delta surface, $OD_{t=0}$, and the full delta surface, $FS_{t=0}$, at 0 minutes from the empty basin scan, EB , using clip polygons in ArcGIS to constrain the areas being compared. The relevant functions are:

$$ODV_{t=0} = EB - OD_{t=0} \quad (6.5)$$

$$FSV_{t=0} = EB - FS_{t=0} \quad (6.6)$$

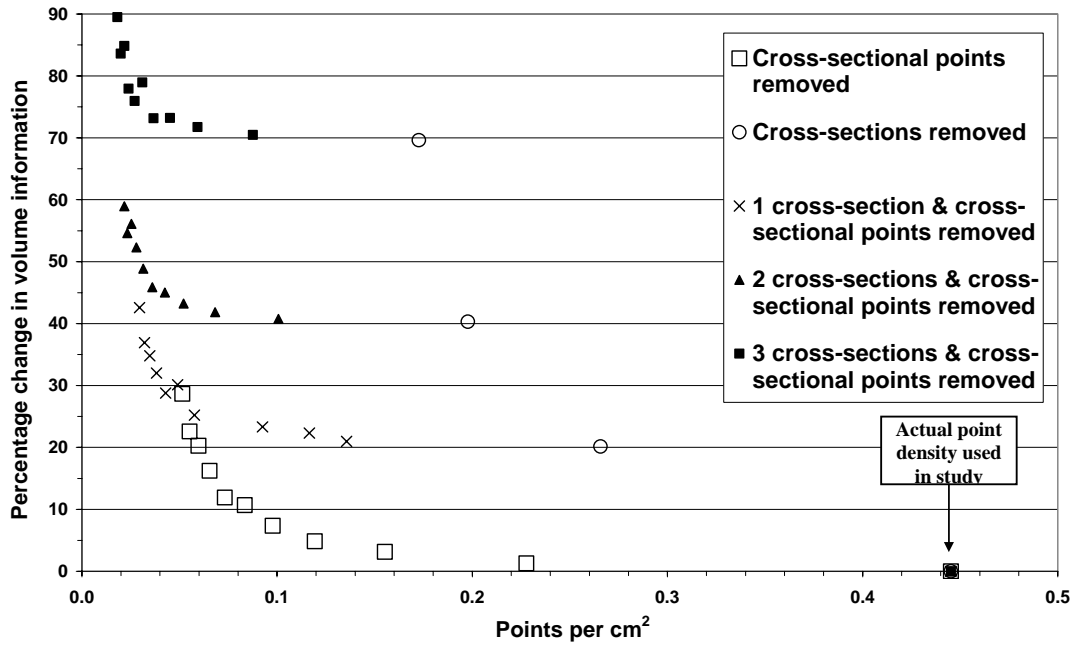


Figure 6.2. The gain in fill volume information as point density is progressively increased.

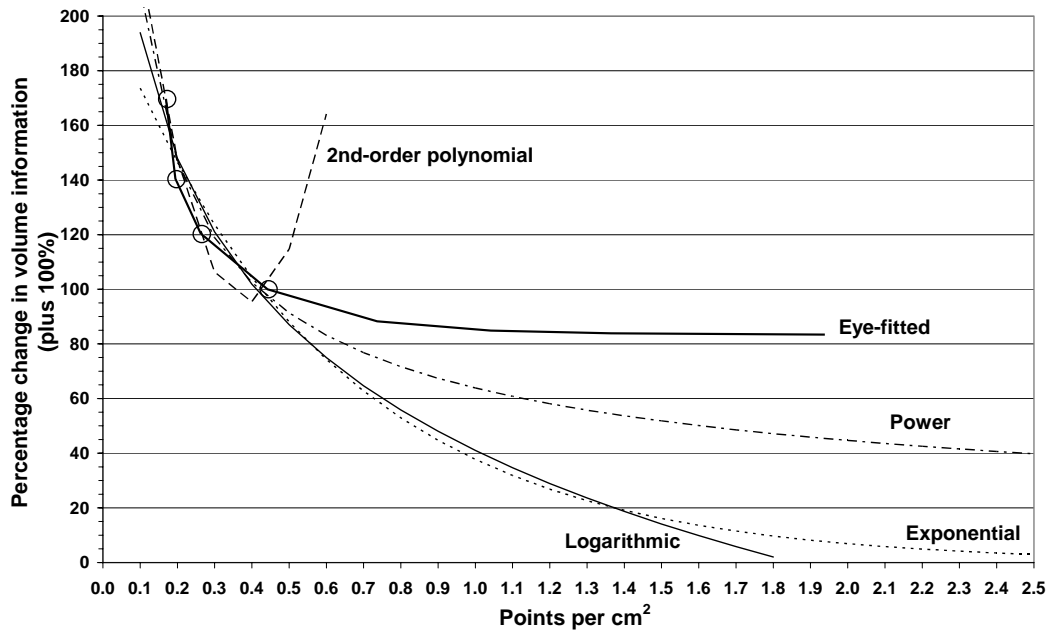


Figure 6.3. Regression curves for volume information lost as a function of cross-sectional point spacing. Note that 100% has been added to each value of the ordinate to allow the power and exponential curves to be plotted, since these cannot be applied to negative values. 100% in the graph thus represents the actual volume information provided by the laser data.

As expected, these calculations show large amounts of fill but, unexpectedly, they also show very small amounts of cut (Table 6.3). This must be an error since the empty basin was exactly the same shape at all times, so there should be no cut volume

Run	Total reservoir sediment volume based on corrected* laser data (cm ³)	Absolute sediment volume based on power equation (60% < laser-measured volume) (cm ³)	Absolute sediment volume based on power equation (18% < laser-measured volume) (cm ³)
2xR	674,397	269,759	553,006
3xR	639,920	255,968	524,734
1xL	681,614	272,646	558,923
3xL	649,128	259,651	532,285
3xL(A)	701,747	280,699	575,432
3xC	695,675	278,270	570,454
6xC	681,179	272,472	558,567
12xC	698,188	279,275	572,514
21xC	714,429	285,772	585,832
2x Split	702,560	281,024	576,099

Table 6.2. Progression of laser-based volume data to estimate absolute sediment volumes.
* These corrections are detailed in sub-sections (ii) and (iv) below.

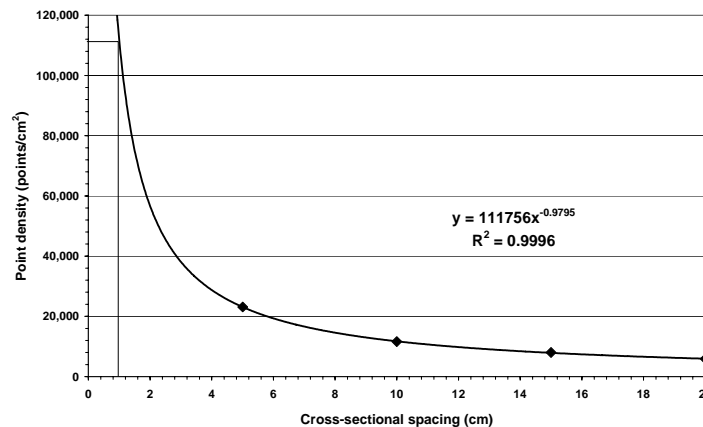


Figure 6.4. Cross-sectional spacing required to produce absolutely accurate sediment volume measurements.

whatsoever. This error occurs because it was impossible to scan the same cross-sections in *exactly* the same place each time and also because the positions of cross-sections added to account for edge features in the model varied from scan to scan. As a result, the shape of the solid basin boundary in the DEMs of the two surfaces being compared varied slightly, producing small amounts of apparent cut and fill that did not actually exist. All of the cut volumes but only a small fraction of the value of the fill volumes in Table 6.3 are due to this basin shape error, *BSE*. It is impossible to isolate the errors in the fill volumes that occurred due to the *BSE*, but their likely

magnitudes are indicated by the erroneous cut volumes, which are likely to be of similar magnitude. Apparent cut volumes were therefore subtracted from the fill volumes to obtain adjusted starting volumes for both the volumes of sediment in the original delta and the reservoir as a whole (Table 6.3).

In all cases apparent cut volumes constituted only a tiny percentage of the fill volumes, although they were larger relative to the total reservoir sediment volumes than the original delta volumes (Table 6.3). In the full reservoir cut-fill analysis, the basin surface area was a larger proportion of the total surface area (basin surface + sediment surface) than in the original delta cut-fill analysis, despite the clip polygons excluding as much of the basin boundary as possible from the cut-fill calculations.

Run	Original delta volume				Total reservoir sediment volume			
	Cut (cm ³)	Fill (cm ³)	Adjusted fill (fill – cut) (cm ³)	Cut as % of fill	Cut (cm ³)	Fill (cm ³)	Adjusted fill (fill – cut) (cm ³)	Cut as % of fill
2xR	47	596,808	596,761	0.008	349	622,281	621,933	0.06
3xR	17	593,401	593,384	0.003	384	611,130	610,746	0.06
1xL	131	620,612	620,481	0.02	2,526	635,604	633,078	0.4
3xL	81	619,276	619,194	0.01	2,165	631,553	629,388	0.3
3xL(A)	52	653,218	653,165	0.008	2,070	667,777	665,707	0.3
3xC	41	636,827	636,786	0.006	1,807	653,965	652,158	0.3
6xC	97	641,036	640,939	0.02	1,818	658,022	656,204	0.3
12xC	136	639,845	639,709	0.02	1,453	656,766	655,314	0.2
21xC	251	657,682	657,432	0.04	1,112	680,293	679,181	0.2
2x Split	167	639,891	639,723	0.03	2,203	650,290	648,087	0.3

Table 6.3. Correction of starting sediment (fill) volumes due to basin shape errors.

iii) The effect of overhanging channel banks

Despite the absence of cohesive sediments, the heterogeneity of the model sediment mixture (Table 5.1) promoted mechanical interlocking of the grains, allowing very steep banks and terraces to develop during the course of each experiment (Figure 6.1a) and, in some cases, led to the generation of cantilever features (Thorne and Tovey, 1981).

To the best of the author's knowledge, the problem of how to deal with such overhangs has not previously been addressed in any of the literature relating to DEM differencing. Lane (1998) referred to the presence of riparian vegetation hanging over and thus obscuring part of the channel, but he dealt with this problem by simply eliminating the affected area prior to differencing. In this study, overhanging banks

were integral to system behaviour and their effects clearly cannot be ignored. The problem arose because surface elevation data were collected using a laser looking vertically down on to the delta surface. As it moved along each cross-section, the laser could not ‘see’ the volume of the bank or terrace that had been eroded beneath overhanging (cantilevered) banks (Figure 6.5). This volume was, therefore, unaccounted for in the DEM generated from these data, thus *underestimating* the cut volume when the DEM was differenced. Only when a cantilever eventually collapsed could the laser detect that sediment had been eroded (Figure 6.5), thus *overestimating* the cut volume when the DEM was differenced for that time period. Errors associated with overhanging banks cancel out as runs progress and have little effect on the overall volume eroded, although they may slightly alter the time distribution of erosion. The impact of these errors is potentially significant with respect to erosion volumes calculated for individual time steps, however, and so they should be corrected for as much as possible.

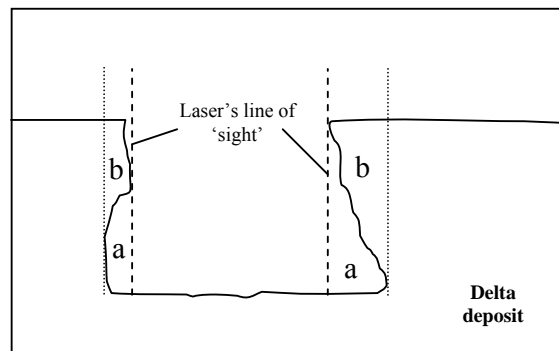


Figure 6.5. The effect of overhanging banks and terraces on laser data collection. Overhanging banks/terraces ‘b’ prevent the laser ‘seeing’ areas ‘a’, leading to an underestimate of the volume of sediment eroded in the first time step. In a subsequent time step, when the cantilevers have collapsed to the dotted lines, the laser can now ‘see’ areas ‘a’, leading to an overestimate of the volume eroded in the second time step.

A correction for errors associated with overhanging banks is possible because the model was a closed sediment system: that is, there was no sediment input from upstream once dam removal had started, while all the sediment that was eroded could be accounted for, either through being measured by the laser within the reservoir basin or being collected and measured as it left the basin. The correction is most simply applied to the cut-fill data for the total reservoir sediment. In this case, cut data are subject to overhang errors, while fill data provide an accurate representation of all the sediment deposited within the basin (subject to the errors discussed in the

preceding sections). Since all deposited sediment must have been eroded from somewhere within the delta, the cut data can be ignored and the changes in cumulative fill from one time step to the next can be taken to represent the volume of erosion.

iv) Delta surface sections out of the laser's vertical measuring range

The vertical range over which the Keyence laser could measure elevation was 55.9 cm, while the model's calculated effective vertical geomorphological range (see section 4.3.2) was 59.7 cm. While every effort was made to keep the highest delta surface elevations within this range, it was impossible to control the delta building process in the model delta precisely to ensure that it matched the prototype delta exactly (see section 5.3.2). Consequently, in each run, some small areas of the proximal end of the original delta topset were out of range. These out of range areas can be identified by comparing the DEM to the photograph in Figure 6.1. Out of range areas could have been removed manually, but it was identified at the outset of the experiment that this would disturb the delta's natural surface topography, preventing the incising channel from finding its natural course across the topset and potentially jeopardising the process-basis for the experimental runs. In the event, the incising channel was artificially directed along the left, centre or right sides of the delta topset after the first two runs, for the reasons stated earlier and, in retrospect, it would probably have been acceptable to remove out of range areas of the topset.

With the benefit of hindsight, a better approach would have been to build the bulk of the delta hydraulically (so ensuring that the vast majority of the sediment was hydraulically sorted) before sculpting the topset and foreset surfaces manually using some of the wetted sediment mixture. This would have eliminated the variability between model deltas in different runs that occurred due to lack of control over the delta building process (section 5.3.2).

As the exact volume of sediment used to build each experimental delta was not recorded, a correction to the laser-measured volumes was developed to estimate the volume of out of range sediment. The correction again makes use of the fact that the reservoir basin is a closed sediment system. At the start of each run the laser measured an initial original delta volume, $ODV_{t=0}$, and a volume of total reservoir sediment, $FSV_{t=0}$, of which a proportion, $V_{t=0}$, was the total out of range sediment,

occupying an out of range area, $A_{t=0}$, of the original delta topset. By the time that sediment began passing downstream, a proportion of the out of range sediment, V_E , occupying an area A_E , had been eroded and deposited at a lower elevation - where it could be 'seen' by the laser, resulting in an increase in the total measured reservoir sediment volume, FSV_{last} . The entire original delta topset was not eroded in any of the runs, so a remnant of out-of-range sediment, V_R , occupying an area, A_R , was in each case left behind. Because the experiments were run without a sediment feed:

$$V_E = FSV_{last} - FSV_{t=0} \quad (6.7)$$

$A_{t=0}$ and A_E were accurately measured from the relevant DEMs in ArcMap and:

$$A_R = A_{t=0} - A_E \quad (6.8)$$

Because the area A_E is associated with the volume V_E , the volume V_R was estimated from:

$$V_R = \frac{A_R}{A_E} \times V_E \quad (6.9)$$

The total estimated volume of out of range sediment, $V_{t=0}$, was then found from:

$$V_{t=0} = V_E + V_R \quad (6.10)$$

$V_{t=0}$ was then used to update the estimates of the total original delta volume, the total reservoir sediment volume and the volume of the bottomset deposit. This correction assumes that the mean volume of sediment per unit area of eroded out-of-range sediment is the same as that of the remaining out-of-range sediment, which is reasonable. The corrected original delta and total reservoir sediment volumes were used to normalise the erosion volumes for the cut-fill analysis of the whole delta and thus to allow direct comparison between runs. However, no similar correction could be made for the cut-fill analysis of the 50-cm sections of delta surface, as explained at the start of section 7.3.

6.1.2.4 The quality of the algorithm used to perform the cut-fill calculations

Historically, surface comparisons have conventionally been undertaken using data collected from cross-sections, with volumetric changes calculated using either the trapezoidal (mean end area) or prismatic methods. Both methods are subject to errors since they cannot account for the spatial variability of erosion and deposition that occurs between cross-sections (Lane, 1998). In contrast, a much more accurate estimate of cut and fill volumes can be obtained by comparing DEMs whose origins

and grid spacings are identical and whose grid nodes are perfectly aligned in the vertical (Lane, 1998). On this basis, the cut-fill AML (Appendix B) used herein adopted this approach. In the AML, the TIN of each surface was converted to a lattice (grid), which was then resampled to ensure that the origin and grid nodes were aligned and that there were an equal number of nodes in the two surfaces being compared (sections B.3.3 and B.3.6). Hence, the small remaining errors in the volume data obtained using this method are a function only of inaccuracies in the way the DEMs represent the delta surface and no additional error was introduced by the calculations themselves (Lane, 1998).

6.1.3 Calculating original delta and full reservoir erosion volumes

As discussed in sections 6.1.2.3iii and 6.1.2.3iv, the full surface fill volumes, FSV_f , provide the most accurate measure of the sediment eroded from the delta, as they account for the removal of sediment from both overhanging banks/terraces and out-of-range areas. Because the full surface cut-fill analysis was performed between each time step and the delta surface at zero minutes (when virtually all the sediment in the entire reservoir was within the original delta area), the full surface fill volumes also provide the most accurate measure of delta erosion, although this only remains true up to the point when sediment began to pass downstream of the dam. The cumulative volume of original delta erosion for each time step up to this point, $ODV_{e_{t=n+1}}$, was thus found from:

$$ODV_{e_{t=n+1}} = FSV_{f_{t=n+1}} = (FS_{t=0} - FS_{t=n+1}) - (FS_{t=0} - FS_{t=n}) \quad (6.11)$$

Equation 6.11 includes corrections for sediment lost from overhanging banks and out-of-range areas, but not for the basin shape errors (section 6.1.2.3ii). The total basin shape error, BSE_T , for any time step is composed of the error in the original delta area, BSE_{OD} , and the error in the prograding delta area, BSE_{PD} , such that:

$$BSE_T = BSE_{OD} + BSE_{PD} \quad (6.12)$$

The value of the $BSE_{OD_{t=n}}$ is the cut volume obtained by subtracting the original delta surface for each time step from the empty basin surface:

$$BSE_{OD_{t=n}} = EB - OD_{t=n} \quad (6.13)$$

As described in section 6.1.2.3ii, equation 6.13 assumes that the cut volume provides a reasonable indicator of the fill volume. The partially-corrected cumulative original delta erosion volume, $ODV_{pce\ t=n}$, was therefore obtained from:

$$ODV_{pce\ t=n} = FSV_{f\ t=n} - BSE_{OD\ t=n} \quad (6.14)$$

ODV_c is composed of the sediment that the laser could ‘see’ had been eroded plus the cut volume associated with BSE_{OD} . These quantities are also included in the FSV_c because the original delta and full surface cut-fill analyses compare the delta surface at each time interval to the delta surface at zero minutes. However, FSV_c also includes the cut volume associated with BSE_{PD} , as the full surface cut-fill analysis incorporates that part of the basin surface downstream from the original delta area (equation 6.15). Once the bottomset sediments begin to be eroded, the FSV_c also includes this eroded volume, BV_e , (equation 6.16). Hence:

$$FSV_{c\ t=n} - ODV_{c\ t=n} = BSE_{PD\ t=n} \quad (6.15)$$

$$FSV_{c\ t=n} - ODV_{c\ t=n} = BSE_{PD\ t=n} + BV_{e\ t=n} \quad (6.16)$$

It follows that, as FSV_f was used to determine ODV_e , the volumes associated with BSE_{PD} and BV_e had also to be subtracted from FSV_f (equation 6.18).

The correction required in generating volumetric data for the cut-fill analysis relates to the systematic error associated with each surface and the effect that this will have had on mean surface elevation, and thus erosion volumes (section 6.1.2.1). The mean error, ME , calculated for each surface was used to estimate the volume of sediment related to errors in surface elevations for both surfaces in each cut-fill calculation (equation 6.17). The full surface fill area, FSA_f , was taken as the area over which the systematic error was effective because FSV_f was used to determine the original delta erosion volume. The systematic error volume, SEV , for a cut-fill calculation was thus found from:

$$SEV_{t=n} = (FSA_{f\ t=n} \times ME_{t=n}) - (FSA_{f\ t=n} \times ME_{t=0}) \quad (6.17)$$

The final, corrected, original delta erosion volume for each time step, $ODV_{ce\ t=n}$, up to the point at which sediment began to pass downstream of the dam was thus obtained from:

$$ODV_{ce\ t=n} = FSV_{f\ t=n} - BSE_{OD\ t=n} - (FSV_{c\ t=n} - ODV_{c\ t=n}) - SEV_{t=n} \quad (6.18)$$

This approach ignores overhang errors associated with the channel incising into the bottomset deposits, which is acceptable as banks and terraces in the prograding delta area were much lower than those in the original delta area. Combining equations 6.14 and 6.18 produced:

$$ODV_{ce\ t=n} = ODV_{pce\ t=n} - (FSV_{c\ t=n} - ODV_{c\ t=n}) - SEV_{t=n} \quad (6.19)$$

The corrected original delta erosion volume per time step, $ODV_{ce\ ts}$, was then found from

$$ODV_{ce\ ts} = ODV_{ce\ t=n+1} - ODV_{ce\ t=n} \quad (6.20)$$

For time steps in which sediment was passing through the dam site a slightly different approach was required, since FSV_f decreased, reflecting the net loss of sediment from the reservoir, and was no longer an accurate guide to ODV_e . At this stage in each run, there was no alternative to using the relevant ODV_c values, even though these were known to be potentially inaccurate due to uncorrected overhang and out-of-range errors. In practice, it was found that in all but two of the non-flood flow time steps in which sediment was passing downstream, ODV_c values were smaller than BSE_{OD} values, indicating that any original delta erosion that might have occurred could not be distinguished from overhang and out-of-range errors. Examination of the time lapse movies, however, indicated that there was no original delta erosion in these late time periods, so that ODV_c values were not actually subject to any overhang or out-of-range errors. It follows that, for all but two of the non-flood time steps in which sediment was passing downstream of the dam, the corrected volume of original delta erosion was given by:

$$ODV_{ce\ t=n} = 0 \quad (6.21)$$

The two exceptions were Runs 3xL(A) after 630 minutes and 3xC after 4,240 minutes. In both cases, the ODV_c comfortably exceeded the BSE_{OD} and examination of the CAM1 time lapse movies indicated that erosion did occur in the original delta area. In Run 3xC this was only a very small amount of erosion near the base of the distal original delta and the cut volume was not subject to overhang or out-of-range errors. The corrected volume of original delta erosion for this time step was therefore calculated using equation 6.22.

In Run 3xL(A), examination of the CAM1 time lapse movie and the relevant DEMs showed that there are no out-of-range errors but that there appeared to be some sediment erosion from underneath an overhanging bank that may have caused the measured cut volume to underestimate the true cut volume. Unfortunately, there was no way to correct for this potential error, since the FSV_f was no longer an accurate represent of original delta erosion. The original delta erosion for this time step was thus estimated from equation 6.22, although the accuracy may be lower than that for the Run 3xC time step. These two erosion volumes are also subject to systematic errors, whose effects were evaluated as described above. Because ODV_c was used instead of FSV_f , however, the original delta cut area, ODA_c , was used in equation 6.17 to calculate SEV instead of FSA_f . ODV_{ce} was thus found from:

$$ODV_{ce\ t=n} = ODV_{c\ t=n} - BSE_{OD\ t=n} - SEV_{t=n} \quad (6.22)$$

In these runs, SEV for the original delta surfaces during flood flows was similarly evaluated using ODA_c .

6.2 Analysis of channel form adjustments

6.2.1 Measurement of channel form from the time lapse photographs

In the model basin, the laser moved along a series of fixed trajectories. As the orientation of the channel crossing the delta changed during each experimental run, laser-measured widths were not always perpendicular to the channel. In light of this, channel top and wetted widths were measured from photographs instead of being derived from the laser data.

6.2.1.1 Developing algorithms for correcting photographic errors

Before taking measurements from the photographs, it was necessary to correct them for distortion introduced by the curvature of the cameras' lens' and perspective errors due to some parts of the image being further away from the centre of the lens than others. Images were corrected by setting up a photographic target over the model surface (Figure 6.6), directly beneath each of the four overhead cameras. After ensuring that the target was perfectly level in all directions it was photographed. The correction algorithms were then developed in Adobe Photoshop, using the

Andromeda Software Lensdoc filter (Version 1.3). The algorithms so created were then applied to all the photographs taken from the camera using the batch processing functionality of Photoshop. It was necessary to create a new set of correction algorithms every time the overhead cameras were moved, as was the case, for example, between runs 3 (1xL) and 4 (3xL).

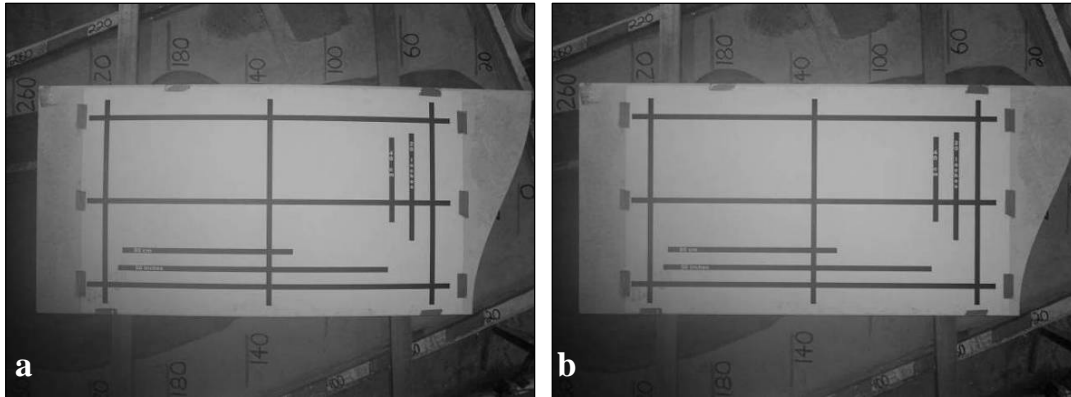


Figure 6.6. Example of photo target used to develop algorithms to correct for lens distortion and perspective errors. **(a)** Before correction – notice the curvature in all the target lines, which are straight and at perfect right angles to each other on the target itself; **(b)** after correction – note how all target lines are now perfectly straight and parallel.

6.2.1.2 Calibrating the photographic measurements

When applied to the model run photographs the distortion and perspective-correction algorithms provide accurate corrections for all features that lie *in the same plane as the correction targets* and allow an accurate scale to be developed for these features. Unfortunately, erosion of the delta surface meant that its elevation relative to the datum plane changed during the course of each run. Consequently, corrections produced by the algorithm were imperfect and variable errors occur in the measurement scale depending on location and time step.

In theory, as the photographs from which measurements were taken are effectively aerial photographs, the principles of aerial photogrammetry could have been used to remove distortion, *i.e.* the photos could have been orthorectified to allow accurate measurements at all delta surface elevations. However, orthorectification would have required that x , y and z coordinates be known for several control points in each image. This would have required targets to be placed, surveyed and removed from the delta surface every time it was photographed, which would have added very

significantly to experimental run times. In practice, therefore, such an approach was infeasible.

To assess the errors associated with the simpler method reported in section 6.2.1.1, channel centreline length was measured for each 50 cm section of the delta in one photograph, per camera per run. These lengths were compared to the equivalent channel lengths measured from the DEM and the results used to develop a calibration factor for each 50 cm section in each run (Table 6.5). These factors reveal that errors in sector length measurements taken from the photographs range from -15% to +8%, with the mean error being +6%. In considering these apparent errors, it should be borne in mind that the channel sector lengths obtained from the DEMs are imperfect representations of the true lengths. While the laser data on which the DEMs are based are highly accurate, the resolution at which they were collected introduced some uncertainty in the identification of precise channel paths, especially when the channel was within an area of low relief such as the braided, prograding delta surface. On this basis, it was concluded that sectoral channel lengths measured from the photographs were good approximations of their true values.

As a final check on the reasonableness of the corrections based on the photographic calibration factors, overall channel lengths was measured from the DEMs for several time steps in three runs and compared to total channel lengths obtained by summing the equivalent calibrated and uncalibrated 50-cm-section channel lengths (Table 6.6). In all cases, the calibrated lengths were substantially more accurate than the uncalibrated lengths. Calibration generally reduced errors to 1-2%, with the largest error being 6%, which is acceptable.

The spacing of triangulation points in the DEM was also an issue with respect to measuring the cross-sectional dimensions of the channels. DEM resolution was only sufficient to locate the breaks of slope delineating bank and terrace edge features to within a few centimetres, introducing errors that could easily equal or exceed those associated with measurements based on photographs. In light of this, and to ensure consistency between longitudinal and cross-sectional representations, all lateral measurements were based on the photographs rather than taken from the DEMs.

The limited resolution of the DEMs precluded the development of calibration factors for photogrammetrically-derived measurements of the channel width, terrace edges and other delta surface features using the approach developed for channel

length. Instead, the calibration factor for each cross-section was approximated by the average factor for the 50-cm sections of delta surface immediately up and downstream. For example, in Run 1xL, the factors for the 350-400 cm and 400-450 cm sections are 1.07 and 1.03 respectively (Table 6.4), and so a factor of 1.05 was applied for the lateral measurements made at the cross-section at 400 cm (Table 6.5). Where no calibration factors were available for the sections immediately adjacent to a cross-section, those for the nearest sections up or downstream were used.

6.2.1.3 Measurements from Run 1-3 photographs versus measurements from Run 4-9 photographs

The overhead cameras as they were positioned for runs 1-3 did not cover the entire delta surface. Following run 3 they were re-positioned to provide full coverage. This changed the perspective from which the same parts of the delta surface were being viewed in runs 4-9 compared to runs 1-3. In order to take the same measurements from the same places in each photograph and thus to enable direct

Delta surface section (cm)	Percentage increase in channel length measurements from photos to DEMs								
	2xR	3xR	1xL	3xL	3xL(A)	3xC	6xC	12x	21xC
0 - 50	d	d	d	1.08	1.10	1.12	1.14	1.10	1.11
50 - 100	d	d	d	1.03	1.03	1.02	1.01	1.03	1.02
100 - 150	1.06	1.07	1.02	1.04	1.05	1.07	1.06	1.05	1.06
150 - 200	1.05	1.04	1.08	1.08	1.07	1.06	1.07	1.07	1.05
200 - 250	1.05	1.05	1.06	1.09	1.09	1.09	1.09	1.09	1.09
250 - 300	d	d	d	1.09	1.09	1.10	1.10	1.10	1.11
300 - 350	1.13	1.15	1.09	1.09	1.09	1.10	1.09	1.10	1.09
350 - 400	0.97	1.00	1.07	1.08	1.08	1.08	1.09	1.09	1.08
400 - 450	1.03	0.99	1.03	1.11	1.10	1.09	1.09	1.06	1.07
450 - 500	d	d	d	d	d	d	d	d	d
500 - 550	d	d	d	1.01	1.03	1.05	1.05	1.09	1.06
550 - 600	1.06	1.03	1.04	1.07	1.07	1.06	1.06	1.06	1.09
600 - 650	1.05	1.08	1.05	1.06	1.06	1.07	1.07	1.06	1.06
650 - 700	1.08	1.06	1.08	0.92	0.99	1.06	-	-	1.02
700 - 750	d	d	d	d	d	d	-	-	d
750 - 800	d	d	d	1.06	1.05	1.05	-	-	1.01
800 - 850	1.04	1.03	1.04	1.03	1.04	1.05	-	-	1.03
850 - 900	1.02	1.06	1.06	1.01	1.03	1.05	-	-	1.01
900 - 950	1.09	0.93	0.98	0.97	1.01	1.05	-	-	1.00
950 - 1050	d	d	d	d	d	d	-	-	d

Table 6.4. Calibration factors for the channel lengths measured from the photographs. ‘d’ indicates a section where measurement was taken directly from the DEM. ‘-’ indicates that the delta front did not extend into that 50 cm section of reservoir basin.

Cross-sectional measuring location (cm)	Percentage increase in feature measurements from photos to DEMs for runs								
	2xR	3xR	1xL	3xL	3xL(A)	3xC	6xC	12x	21xC
50	-	-	-	1.054	1.063	1.072	1.077	1.067	1.064
100	1.064	1.068	1.021	1.034	1.039	1.045	1.036	1.043	1.039
150	1.057	1.056	1.049	1.057	1.061	1.065	1.062	1.061	1.057
200	1.051	1.044	1.069	1.084	1.081	1.078	1.077	1.080	1.069
250	1.052	1.046	1.059	1.088	1.092	1.097	1.095	1.096	1.096
300	1.127	1.153	1.088	1.086	1.093	1.100	1.097	1.098	1.098
400	1.002	0.996	1.050	1.097	1.091	1.084	1.088	1.076	1.079
500	1.047	1.010	1.036	1.012	1.030	1.049	1.052	1.091	1.060
600	1.055	1.058	1.045	1.066	1.065	1.064	1.066	1.060	1.075
700	1.083	1.060	1.085	0.917	0.987	1.057	-	-	1.017
800	1.038	1.034	1.045	1.046	1.048	1.050	-	-	1.021
900	1.059	0.997	1.022	0.993	1.019	1.046	-	-	1.009

Table 6.5. Calibration factors for cross-sectional feature measurements (channel, top terrace and delta surface widths). Calculation as described in text. ‘-’ indicates that no measurements were taken from these cross-sectional locations.

Run	Time step (mins)	Uncalibrated total channel length (cm)	Calibrated total channel length (cm)	Total channel length measured from DEM (cm)	% difference between uncalibrated length & DEM-measured length	% difference between calibrated length & DEM-measured length
6	2,450	589	605	605	-2.7	0.1
	2,480	610	627	621	-1.7	0.9
	2,540	616	632	633	-2.7	-0.1
	2,660	628	647	642	-2.1	0.8
	2,780	599	617	641	-6.4	-3.7
	3,020	647	668	675	-4.1	-1.1
10	0	274	304	300	-8.8	1.4
	90	325	360	368	-11.6	-2.2
	210	538	579	598	-10.0	-3.2
	330	629	672	666	-5.5	1.0
	570	645	690	697	-7.5	-1.0
	1,320	669	715	727	-8.1	-1.7
11	0	277	298	299	-7.2	-0.1
	90	301	324	322	-6.6	0.7
	220	327	352	346	-5.6	1.9
	300	393	426	426	-7.6	-0.1
	420	435	471	492	-11.6	-4.3
	570	377	407	417	-9.5	-2.3
	660	438	473	503	-12.9	-6.0
	780	473	511	539	-12.3	-5.3
	900	506	542	563	-10.1	-3.7

Table 6.6. Comparison of total channel lengths from calibrated and uncalibrated photo measurements with those from DEMs. Negative percentages denote shorter lengths than measured from the DEM, while positive percentages denote longer lengths.

comparisons of channel properties to be made between all runs, ‘measuring lines’ from which measurements were collected were placed on each photograph.

i) Placement of measuring lines

Vertical lines (from top to bottom on the photographs) were placed at 50-cm intervals from 50 cm to 300 cm (the original delta topset surface) and thereafter at 100 cm intervals (400 cm, 500 cm *etc.*) on the photographs from which measurements were taken for runs 4-9. These lines are termed *measuring verticals* and are the lines between which channel planform was assessed for each 50 cm section (section 6.2.2.4). The centre point between the left and right delta surface edges along each of these verticals was identified and a straight line running perpendicular to the delta surface at that location was drawn through it. This line, termed the *measuring guide*, was used to collect the cross-sectional measurements (section 6.2.3). Collectively, these lines are termed *measuring lines* (Figure 6.7).

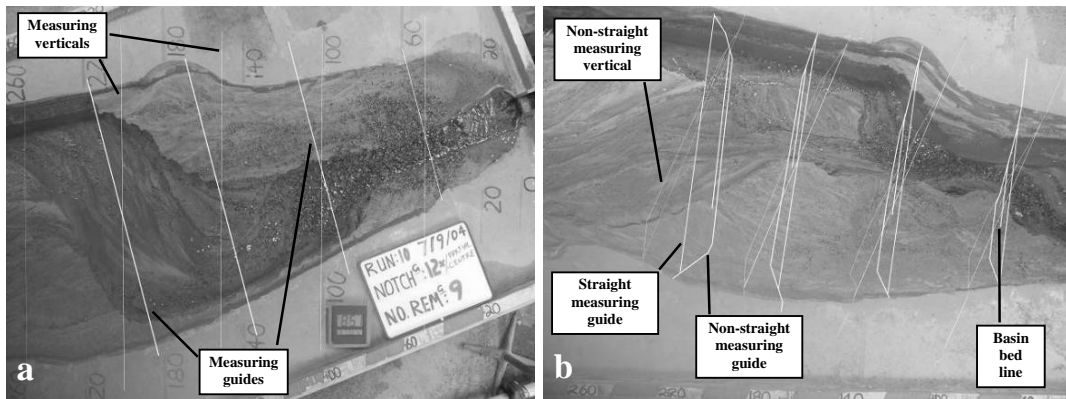


Figure 6.7. Measuring lines for the cameras in their two different positions.

(a) Runs 4-9: the thinner lines running vertically from top to bottom of the photograph are the *measuring verticals*. The thicker lines running at a slight angle to these are the *measuring guides*. Collectively, these are called ‘measuring lines’. (b) Runs 1-3: the straight-line measuring lines of (a) are transposed so that they occupy exactly the same parts of the *flat model top* as in (a). Their non-straight equivalents are also shown, which cover exactly the same parts of the *empty basin surface* as they would cover in (a) if no sediment was present. The partial measuring verticals and measuring guides, termed *basin bed lines*, represent the correction to the non-straight measuring lines to account for the presence of sediment (at a higher elevation than the empty basin bed) in the basin.

ii) Transferring measurement guides from run 4-9 photos to run 1-3 photos

Because the straight measuring lines shown in Figure 6.7a would no longer cover the same parts of the delta surface in the photographs of runs 1-3, it was necessary to use *non-straight* measuring lines (Figure 6.7b). These were developed using two sets of photographs of the empty reservoir basin: one set taken from the

camera position of runs 4-9 and the other from the camera position of runs 1-3. The portions of the empty basin boundary that were covered by the single *straight* measuring lines from the former camera position (Figure 6.7a) were covered by a series of shorter lines from the latter camera position (Figure 6.7b). The place where the channel bed or incised delta surface intersected the non-straight measuring guide along the basin wall marked the elevation of a *basin bed* line (Figure 6.7b). These lines were drawn parallel to the *straight* measuring guides, which ran between the points where the *non-straight* measuring guides intersected the pre-disturbance delta surface (Figure 6.7b). Along cross-sections where some of the pre-disturbance surface still existed, the basin bed lines were drawn from their origin to the point that they intersected this surface. At this point, the *straight* measuring guides denoted the track along which measurements should be taken.

6.2.2 Planform and longitudinal adjustments

6.2.2.1 Thalweg extraction macro

To analyse bed elevation changes, it was necessary to determine either mean bed or thalweg elevation at each cross-section. Thalweg elevations were selected as these were easier to obtain accurately and values were extracted from the laser data for each time step of every run using an Excel macro (Appendix C). The macro began by searching for the lowest point of the cross-section located at 0 cm, which corresponded to the scour pool at the mouth of the delivery channel. The macro recorded the coordinates of this point and then searched for the lowest point in the next cross-section downstream, but only within a pre-defined distance to the left and right of the upstream thalweg point's x (cross-sectional) coordinate. This distance was set to 8.4 cm, corresponding to the width of the upstream delivery channel, since this provided a reasonable indicator of single-thread channel widths over the delta surface and limited the search to roughly the channel area.

Thalweg elevations generated using this macro included some points that were clearly incorrect, in that they did not fit in with the thalweg long profile when considered within the context of the delta surface. Each thalweg elevation was therefore examined by superimposing it on the DEM for that time step in ArcMap (Figure 6.8a). Erroneous points were then identified and removed to produce a geomorphologically meaningful thalweg long profile (Figure 6.8b).

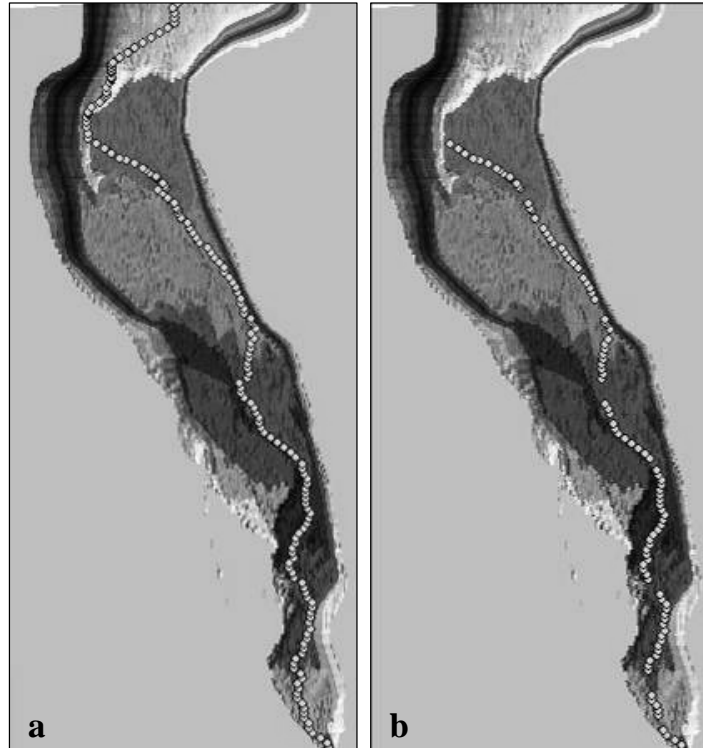


Figure 6.8. Thalweg extraction. (a) Run 2xR thalweg after 2,550 minutes as extracted by the thalweg-seeking algorithm. In sections its points change direction more suddenly than those of a real thalweg. (b) The same thalweg after these points have been manually removed.

6.2.2.2 Choice of photographs

Measurements were generally taken in Adobe Photoshop, using the penultimate photograph from each interval of run time (except for the first photo after the end of delta growth). The last photograph was not used as by that time flow in the model was beginning to recede, having being turned off at the mains.

6.2.2.3 Downstream extent of the armour layer

The maximum downstream extent (y coordinate) of the *continuous* armour layer (*i.e.* as opposed to isolated armoured patches) in each run was measured on the photographs. Measurements were taken from the centre of the channel at the downstream end of the armour layer and were referenced to the distance markers on the flat model top (Figure 6.7).

6.2.2.4 Channel planform

Channel planform was recorded as single-thread or braided for every 50 cm-section of the entire delta surface (as measured between the measuring verticals). If

both planforms were present within the same section their proportionate lengths were recorded.

6.2.3 Lateral adjustments

6.2.3.1 Active channel width

Most parts of the delta surface channel were active for significant proportions of each experimental run, and the active channel width was defined as the maximum width of channel containing water (the wetted width). Because the evolving system was generally highly dynamic, small side channels, such as those found in a braided channel, rarely contained standing or slowly moving water for more than the length of time required to take several overhead time lapse photographs (taken at 30-second intervals). Furthermore, it was frequently easier to locate the position of the water's edge than the channel bank top, which was frequently indistinguishable from a low terrace top.

Channel width was measured in pixels, perpendicular to the flow direction at the point where the measuring guide in the photograph was in the middle of the channel. This point was chosen to ensure that all width measurements were taken at the same cross-section and at a cross-section that was physically meaningful, *i.e.* perpendicular to the down valley direction of the delta surface, since the delta front essentially prograded in perpendicular increments. In contrast to the measuring guides, the measuring verticals were at an angle to the down valley delta surface direction. This angle was a function of the shape of the reservoir basin and the fixed trajectory of the laser and was unrelated to the way in which the delta surface prograded.

6.2.3.2 Top terrace width

Top terrace width was measured in the original delta area only and is defined as the terrace formed by the original delta topset or foreset surfaces. It was measured in pixels along the precise path of the measuring guides. When the original delta surface had been completely eroded at a point, this width was taken to be the reservoir width at the elevation of the original delta topset or foreset surface although, in effect, the terrace no longer existed.

6.2.3.3 Delta surface width

The width of the delta surface was also measured along the precise path of the measuring guides across both the original delta and prograding delta surfaces and was measured between the points where the surface intersected the hard basin boundary. Delta surface width varied, sometimes quite considerably, along the measuring guide as the experiments proceeded, so it was important to measure it at every time step. These variations had two principal causes: first, as a result of the incising channel cutting through the base of a terrace to the basin boundary, the terrace was left perched on the basin side no longer in contact with the main body of the delta. This can be thought of as a ‘terrace cut-off’ and it usually resulted in a sudden decrease in delta surface width. Second, and especially in the runs that eroded significant volumes of sediment from the original delta area (runs 6-9), lobes of sediment were deposited on the prograded delta surface and these caused delta surface width to increase.

Chapter 7 Analysis and Results

This chapter presents the qualitative and quantitative model results. For ease of comparison, the results for each run are plotted in the same colour, irrespective of the type of graph. In addition, continuous reference will be made to ‘marginal’, ‘central’ and ‘accelerated removal’ runs. Central runs are those that started with a central pilot channel along the middle of the original delta topset, *i.e.* runs 3xC, 6xC, 12xC and 21xC, while marginal runs are those in which incision started along either the left or right sides of the delta topset. The terms ‘left marginal’ and ‘right marginal’ are used to further distinguish between runs 1xL, 3xL and 3xL(A), and runs 2xR and 3xR respectively. The ‘accelerated removal’ runs are runs 3xC and 3xL(A), in which the delta system was not allowed to equilibrate before the next incremental drop in base level. Reference will also be made to the condition of static equilibrium attained at the end of the relaxation time following the removal of a dam increment, for which a shorthand expression will generally be used. Thus the phrase ‘12-piece equilibrium’ refers to the static equilibrium reached following the removal of the 12th dam piece. Throughout this chapter reference will be made to the time lapse movies and it is imperative that the reader reads this chapter while referring to the movies in order to fully understand the presentation of the results. The reader will need Quicktime to be installed on their PC in order to view the movies, which should be downloaded from the DVD in order to provide the smoothest playback. To move rapidly to the section of movie being referred to, the reader can drag the scroll bar at the bottom of the viewing screen.

7.1 Grain size analysis

Natural sediments that have been hydraulically-deposited into standing water generally exhibit a downstream fining and an upwards coarsening of the grain sizes (Knighton, 1998). This occurs because the coarsest grains are deposited as soon as the sediment being transported enters the body of standing water, while the finer grains travel progressively further before being deposited. As the sediment accumulates, coarse sediment is transported over the topset surfaces to be deposited on the previously deposited, finer material.

Figure 7.1 shows the grain size distribution of the prototype Lake Mills delta, as determined using the data from six boreholes (Figure 5.9a), together with the shape of the model basin along the cross-section on which each borehole was drilled. The delta generally conforms to the expected patterns, with a particularly noticeable reduction in D_{50} downstream of cross-section $Y = 60$ cm (Figure 7.1e) and a general downstream fining in the lower half of the downstream-most four boreholes (Figure 7.1a-d). Upwards coarsening is well developed in boreholes B-4 and B-5 (Figure 7.1a&b). Boreholes B-3 and B-2 also show upwards coarsening, although this pattern could also be interpreted as upwards coarsening over the first three-quarters of the borehole followed by upwards fining to the surface (Figure 7.1e&f). Boreholes B-1 and B-6 show upwards fining from the bottom to around the mid-point and then upwards coarsening to the top of the borehole (Figure 7.1c&d).

None of the model deltas that were cored (Figures 7.2 to 7.9) show any continuous trend of downstream fining in their D_{50} . Indeed they all show continuous downstream coarsening from the 50 cm to 250 cm cross-sections except runs 3xL(A), 3xR, 6xC and 12xC, which exhibit downstream fining from the 150 cm to 250 cm cross-sections (Figure 7.10a). Only 21 out of 70 cores exhibit upwards coarsening over at least three-quarters of their length and only run 3xR at $Y = 150$ cm and 50 cm (Figure 7.2b&c); run 1xL at $Y = 150$ cm (Figure 7.3b); and run 3xL at $Y = 50$ cm (Figure 7.4c) show upwards coarsening across the whole cross-section. Six cores show upwards fining to their mid-points and then upwards coarsening to the surface, a pattern also observed in boreholes B-1 and B-6 (Figure 7.1c&d), while three cores show upwards coarsening to their mid-points followed by upwards fining to the surface, a pattern which could be argued to be present in boreholes B-3 and B-2 (Figure 7.1e&f). The remaining 40 of 70 cores exhibit patterns not observed in the prototype delta: 30 show upwards fining over at least three-quarters of their length; three show upwards fining to their mid-points, a sudden coarsening and then a continuation of the fining to the surface, while seven show no distinct pattern at all.

Examination of D_{84} values (plots not shown) shows a change towards the expected grain size distributions. 26 of 70 cores show upwards coarsening, while nine show upwards fining to the core mid-point followed by coarsening to the surface. In contrast, only 24 cores show upwards fining. Longitudinally, one run shows continuous downstream fining from the 50-cm to 250-cm cross-sections, while only

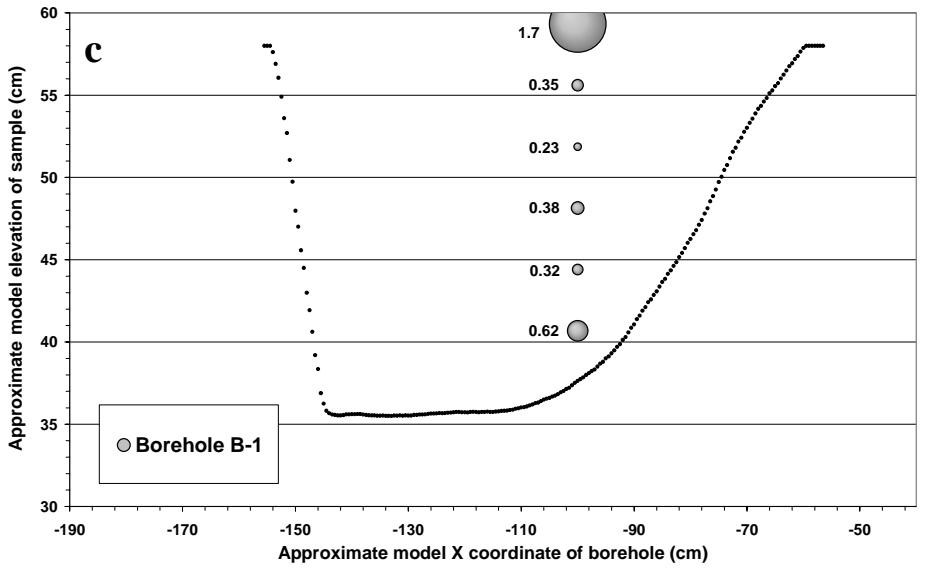
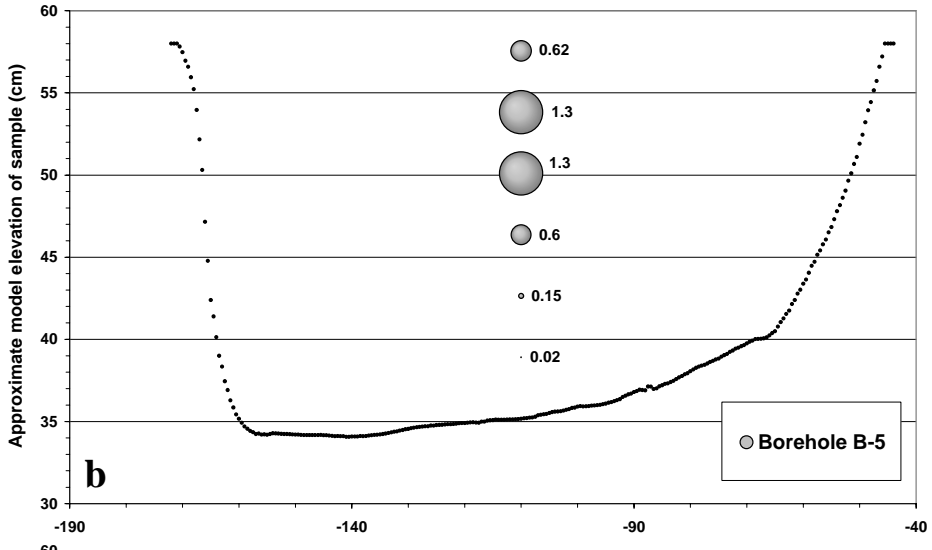
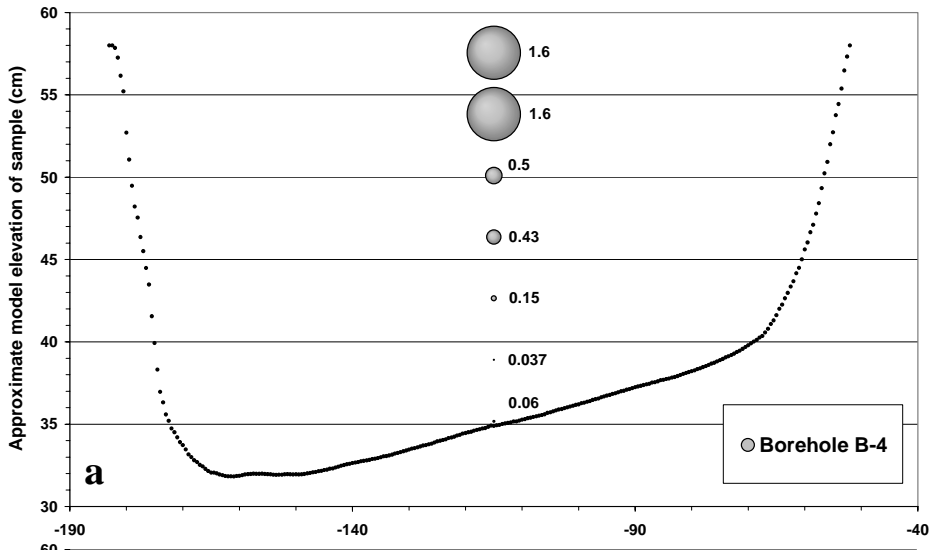
one run shows continuous downstream coarsening (Figure 7.10b). Two runs show downstream fining from 50 cm to 150 cm followed by coarsening or no change downstream to 250 cm, while three runs show downstream coarsening to 150 cm followed by downstream fining to 250 cm (Figure 7.10b). The expected pattern of downstream fining is even better developed for the D_{90} values: four runs show continuous downstream fining from 50 cm to 250 cm; one shows downstream fining to 150 cm followed by downstream coarsening to 250 cm; two runs show downstream coarsening to 150 cm and downstream fining to 250 cm; and one run shows continuous downstream coarsening from 50 cm to 250 cm (Figure 7.10c).

This change from a predominantly downstream coarsening in the composited core cross-sectional D_{50} s to a predominantly downstream fining in the D_{90} s (Figure 7.10) is important because of the effect that it has on the subsequent evolution of the armour layer during dam removal (section 7.3). Figure 7.11 shows the extent of armour layer development at various points along the original and prograding delta surfaces following complete dam removal and the occurrence of flood flows. This shows that the armour layer is generally well developed in the original delta area (1-3 m) and just downstream (4 m), and is certainly sufficiently well developed to protect against channel incision for long periods during most runs (sections 7.2 & 7.3). Table 7.1 shows the mean D_{50} of the armour layer in the original delta area each time it was sampled and expresses this value as the *percentage finer than* for each of the three coring cross-sections. That is, the table gives an indication of the distribution of the armour forming grains in the delta prior to dam removal. It clearly shows that the greatest proportion of armour-forming grains is found towards the upstream end of the model delta in the vicinity of the 50-cm coring cross-section. Because the armour layer D_{50} is close to or exceeds the mean cross-sectional D_{90} in almost all cases, Figure 7.10c provides a good indication of the relative distribution of armour-forming grains for each run at the onset of dam removal.

7.2 Volumetric analysis

7.2.1 Erosion of the original delta during dam removal

Eroded volumes and rates of sediment removal from the original delta for the central runs were significantly greater than those for the marginal runs (Figure 7.12). For example, the smallest erosion volume at the 12-piece equilibrium of a central run



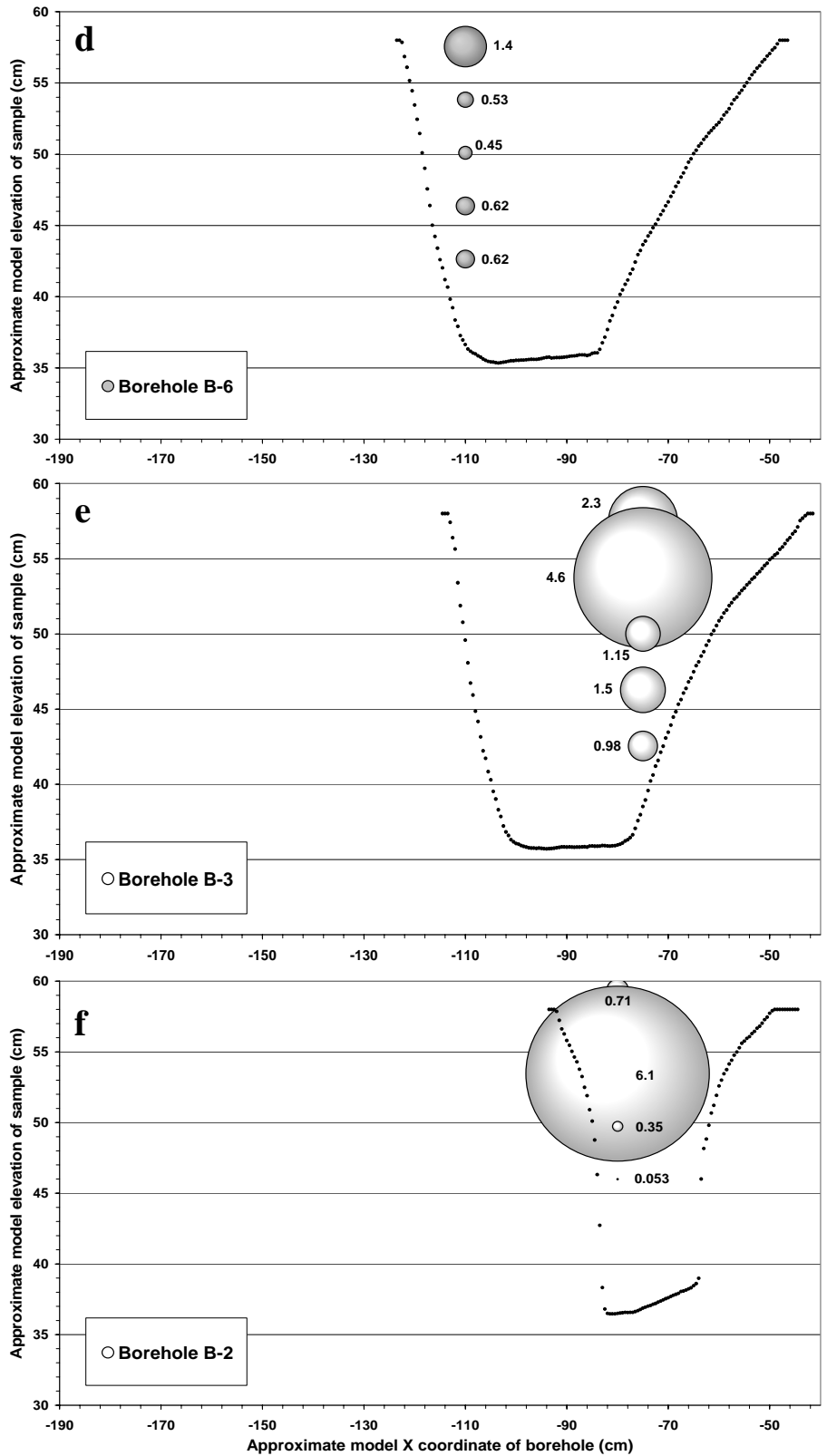


Figure 7.1. D_{50} (mm) of prototype delta borehole sediment samples, ranging from (a) downstream – most borehole to (f) upstream-most borehole. Approximate borehole locations are shown in Figure 5.10: (a) $Y \approx 210$ cm; (b) $Y \approx 175$ cm; (c) $Y \approx 135$ cm; (d) $Y \approx 75$ cm; (e) $Y \approx 60$ cm; (f) $Y \approx 25$ cm. The plots are to a different scale than those in Figures 7.2 to 7.9.

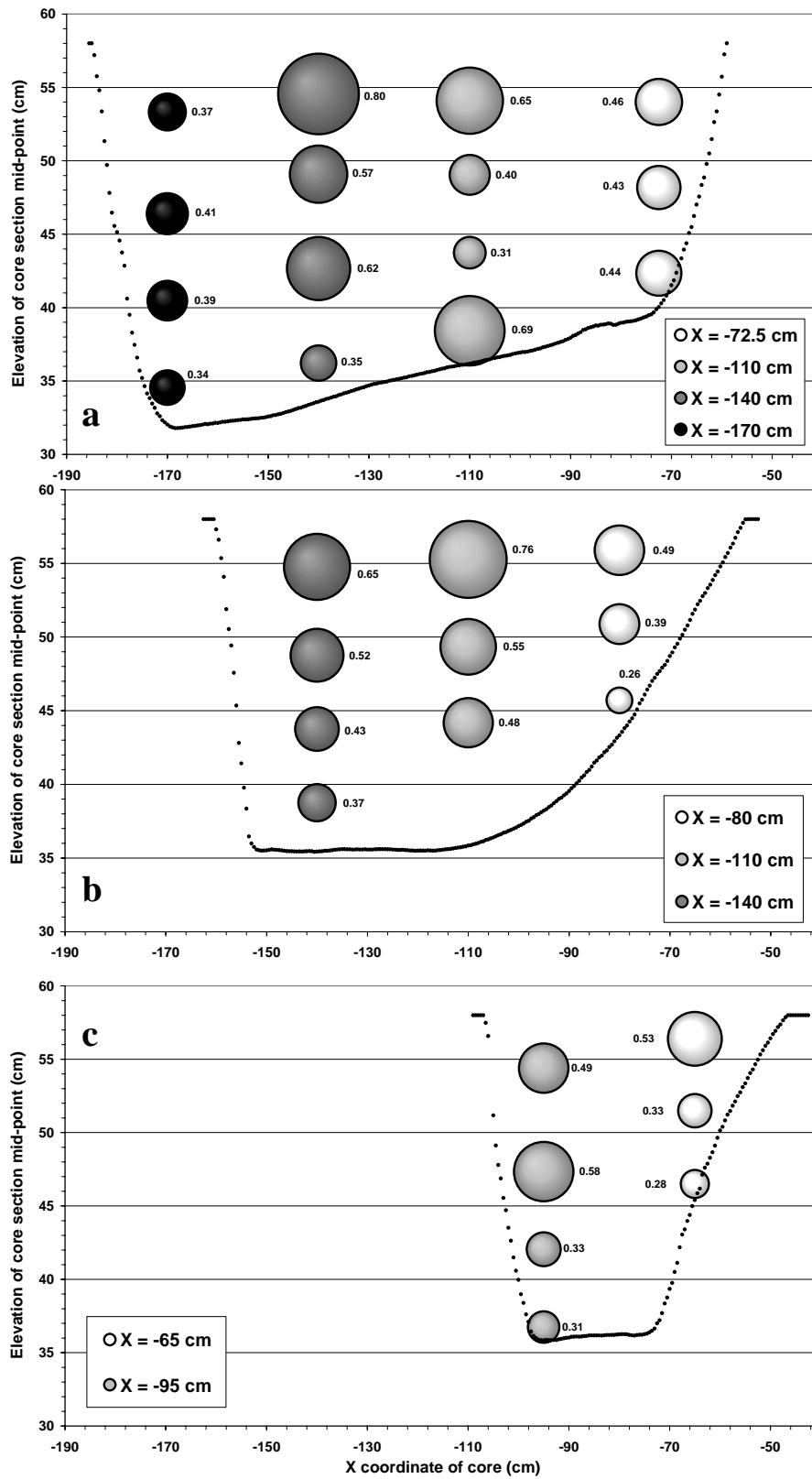


Figure 7.2. D_{50} (mm) of delta cores for Run 2 (3xR) at (a) $Y = 250$ cm, (b) $Y = 150$ cm and (c) $Y = 50$ cm. The model basin's form along the coring cross-sections and looking downstream is also shown.

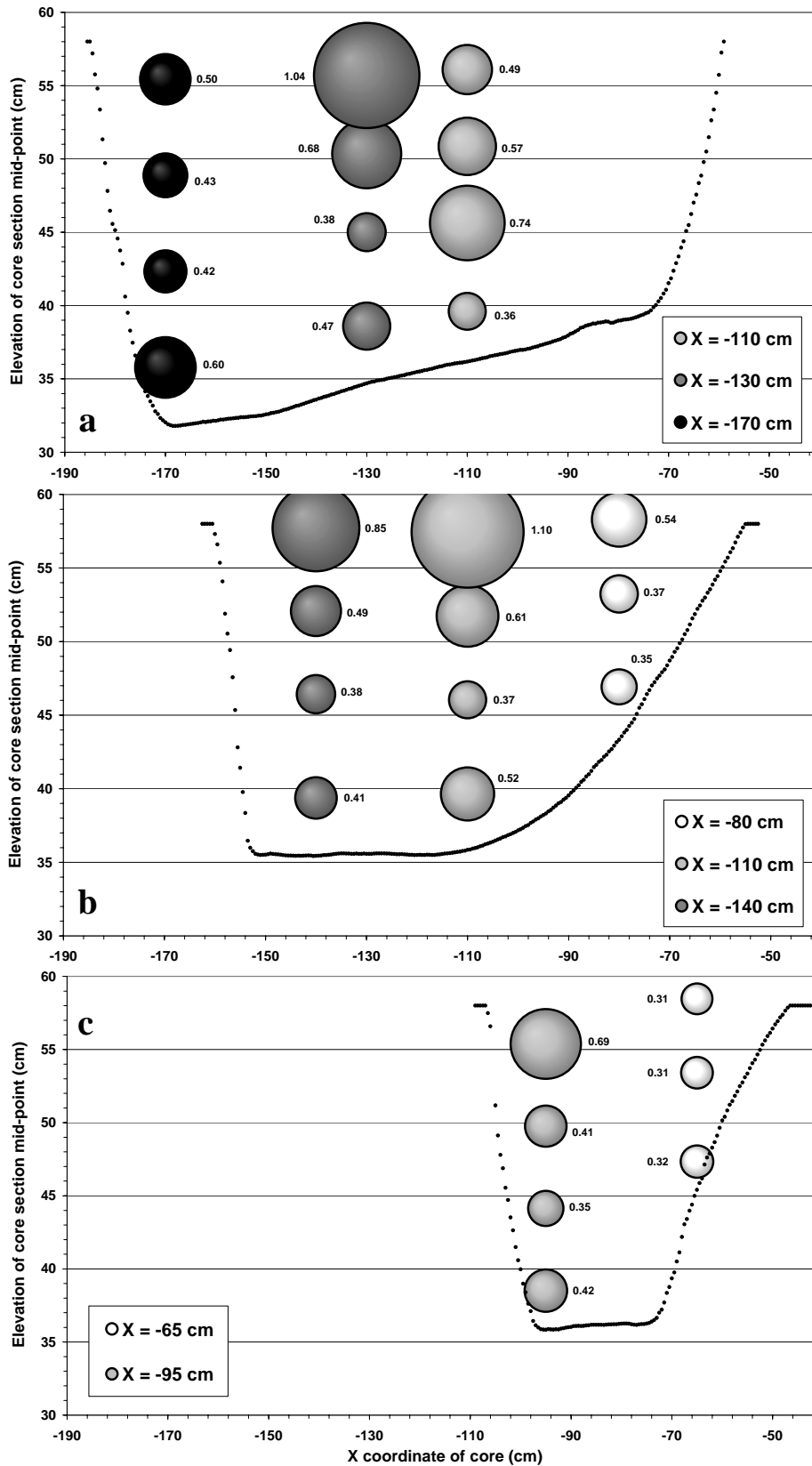


Figure 7.3. D_{50} (mm) of delta cores for Run 3 (1xL) at (a) $Y = 250$ cm, (b) $Y = 150$ cm and (c) $Y = 50$ cm.

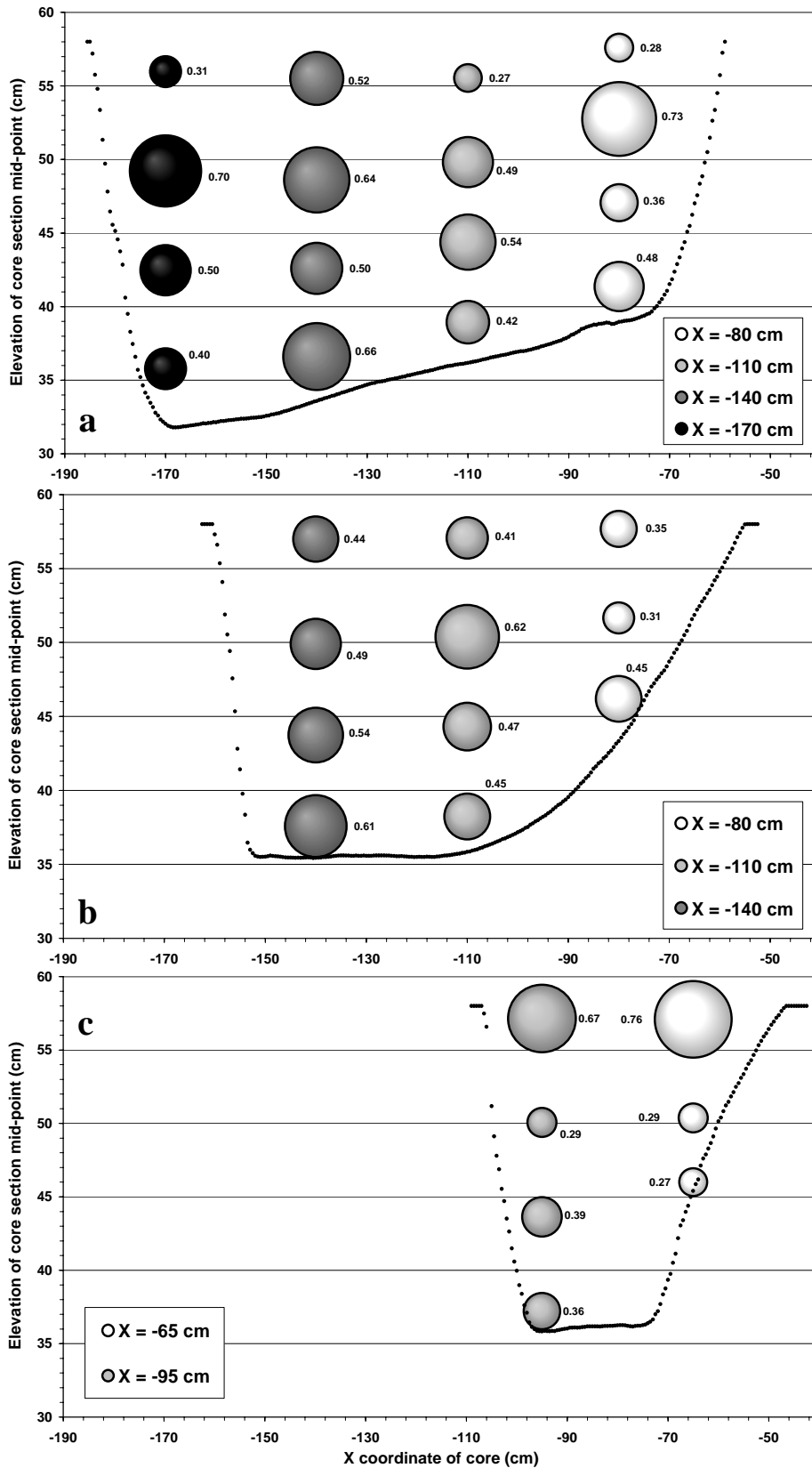


Figure 7.4. D_{50} (mm) of delta cores for Run 4 (3xL) at (a) $Y = 250$ cm, (b) $Y = 150$ cm and (c) $Y = 50$ cm.

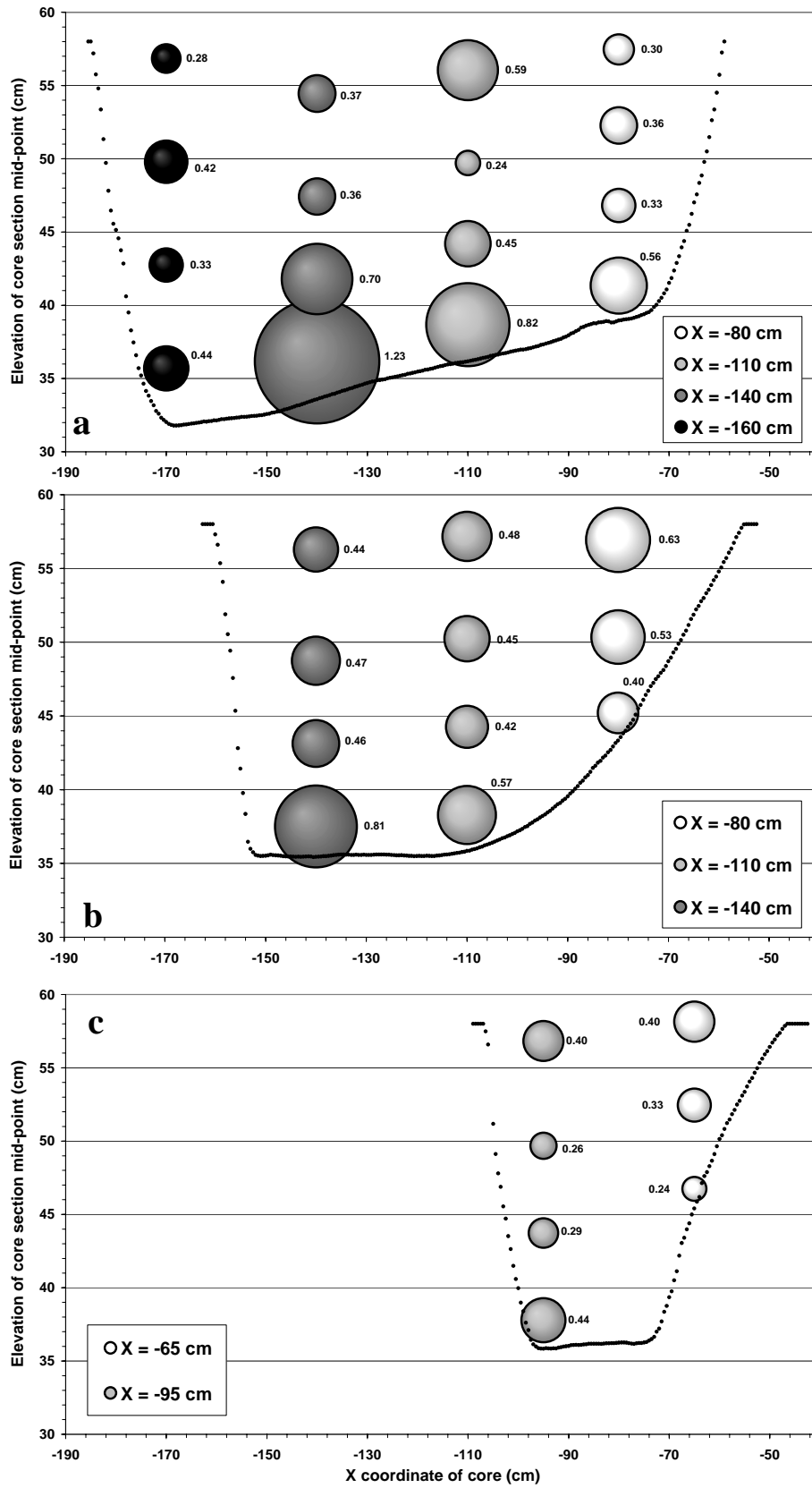


Figure 7.5. D_{50} (mm) of delta cores for Run 5 (3xL A) at (a) $Y = 250$ cm, (b) $Y = 150$ cm and (c) $Y = 50$ cm.

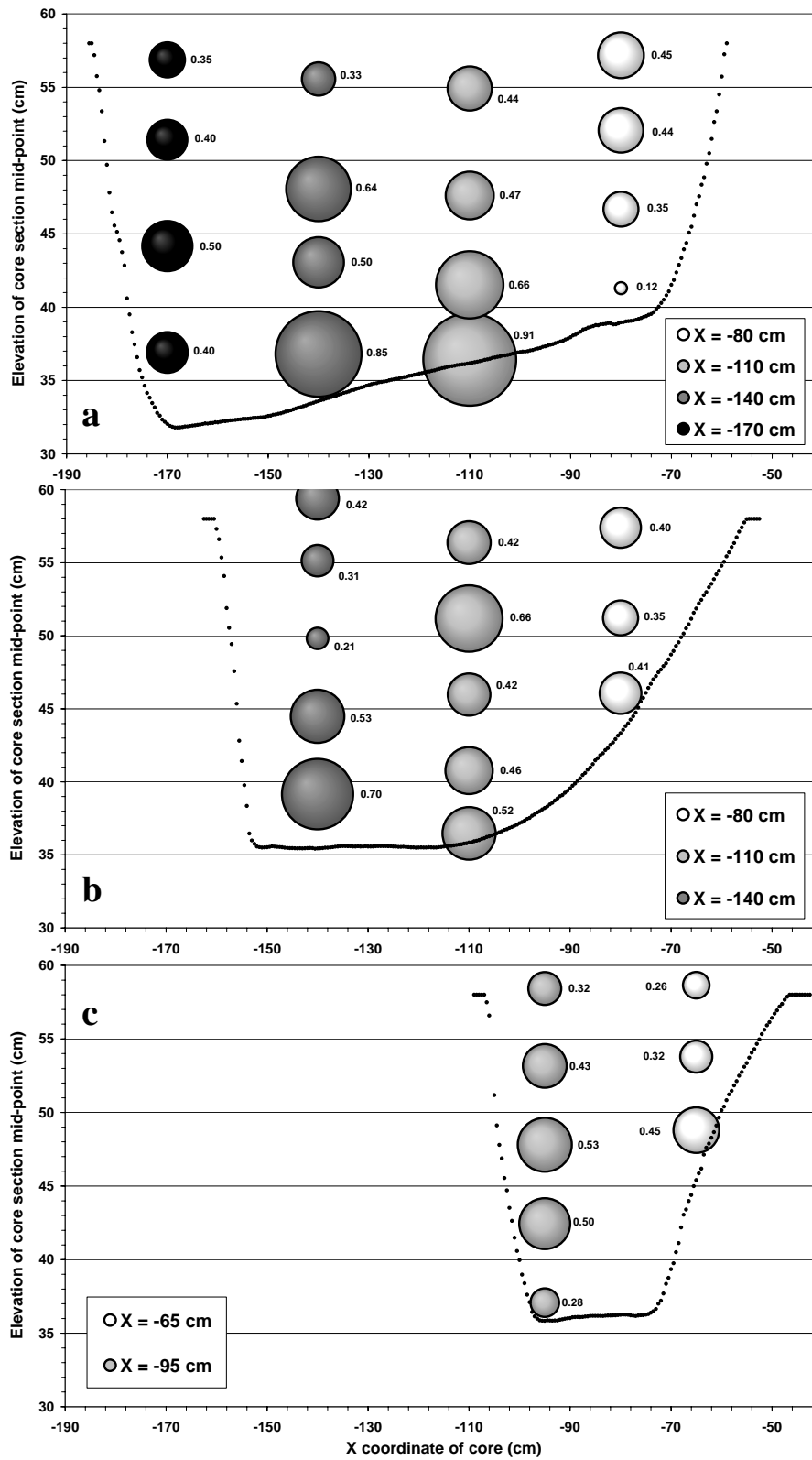


Figure 7.6. D_{50} (mm) of delta cores for Run 8 (3xC) at (a) $Y = 250$ cm, (b) $Y = 150$ cm and (c) $Y = 50$ cm.

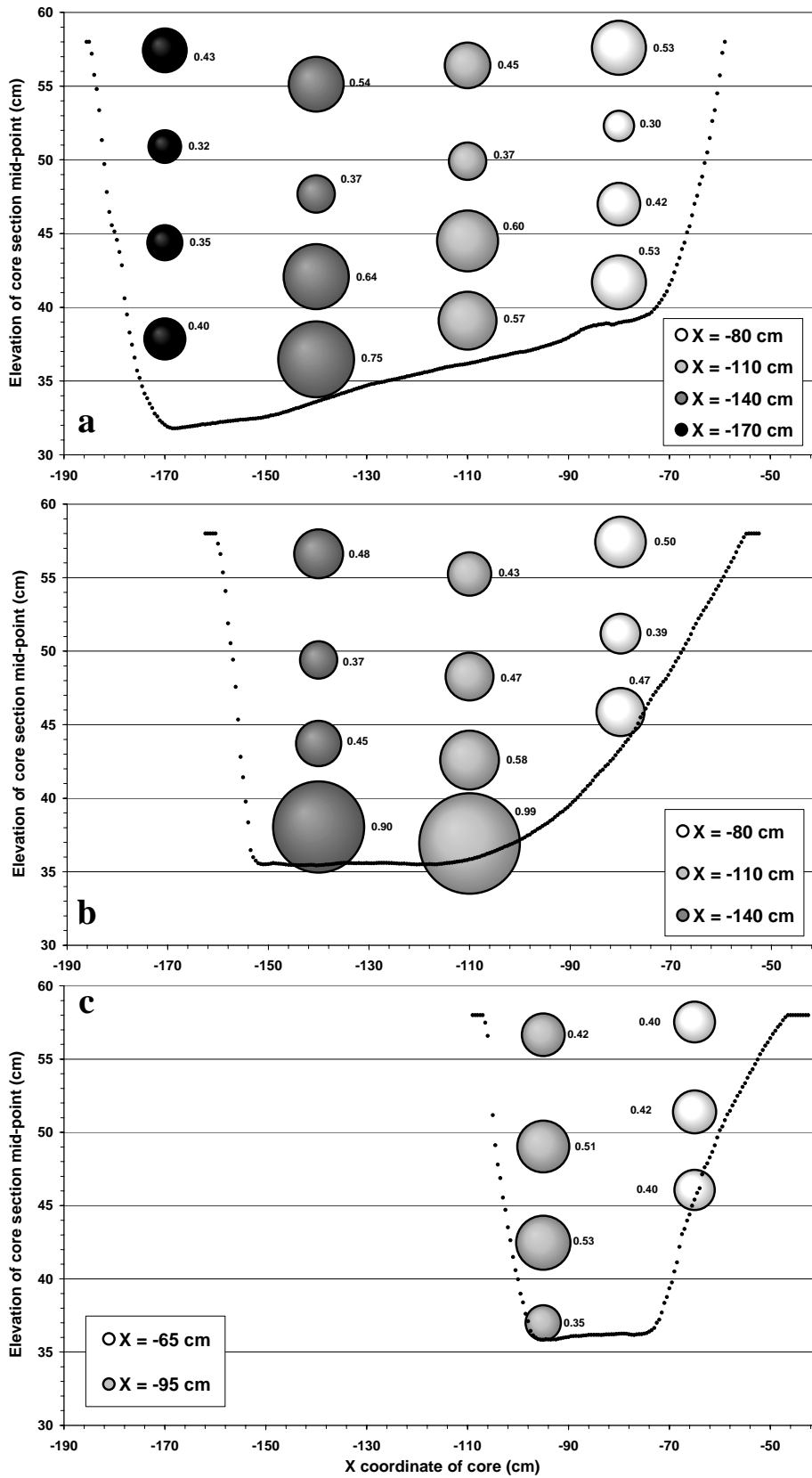


Figure 7.7. D_{50} (mm) of delta cores for Run 6 (6xC) at (a) $Y = 250$ cm, (b) $Y = 150$ cm and (c) $Y = 50$ cm.

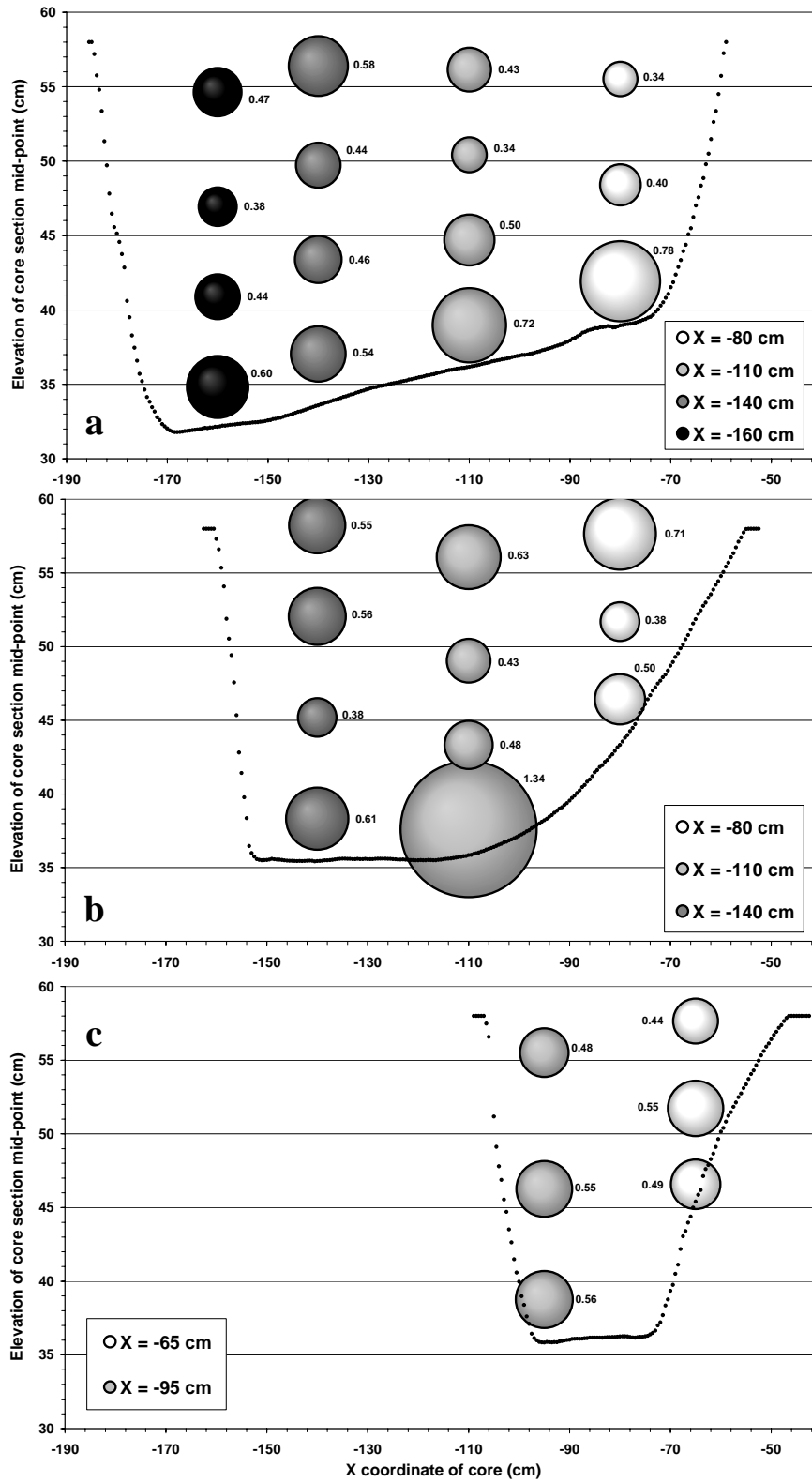


Figure 7.8. D_{50} (mm) of delta cores for Run 6 (6xC) at (a) $Y = 250$ cm, (b) $Y = 150$ cm and (c) $Y = 50$ cm.

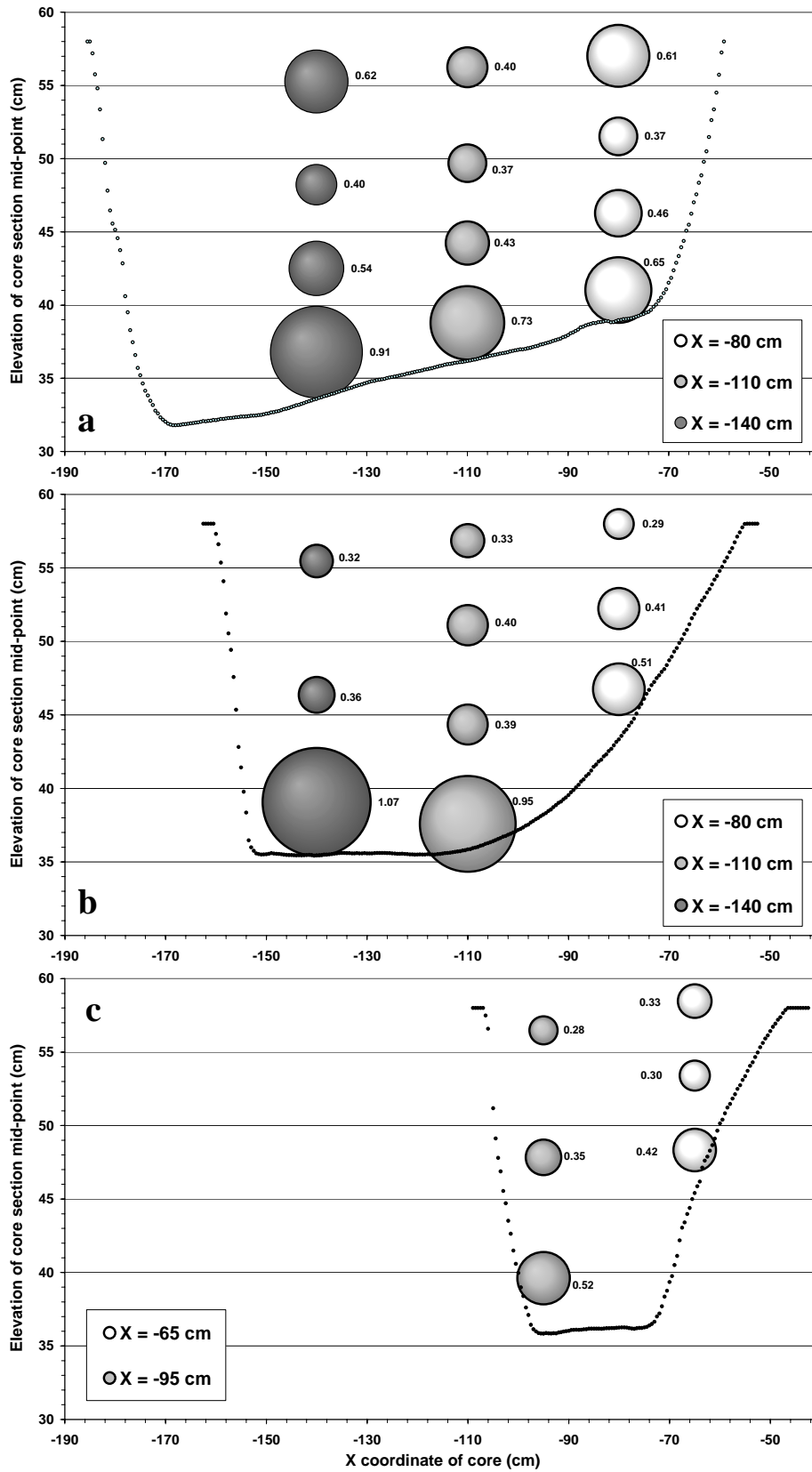


Figure 7.9. D_{50} (mm) of delta cores for Run 9 (21x C) at (a) $Y = 250$ cm, (b) $Y = 150$ cm and (c) $Y = 50$ cm.

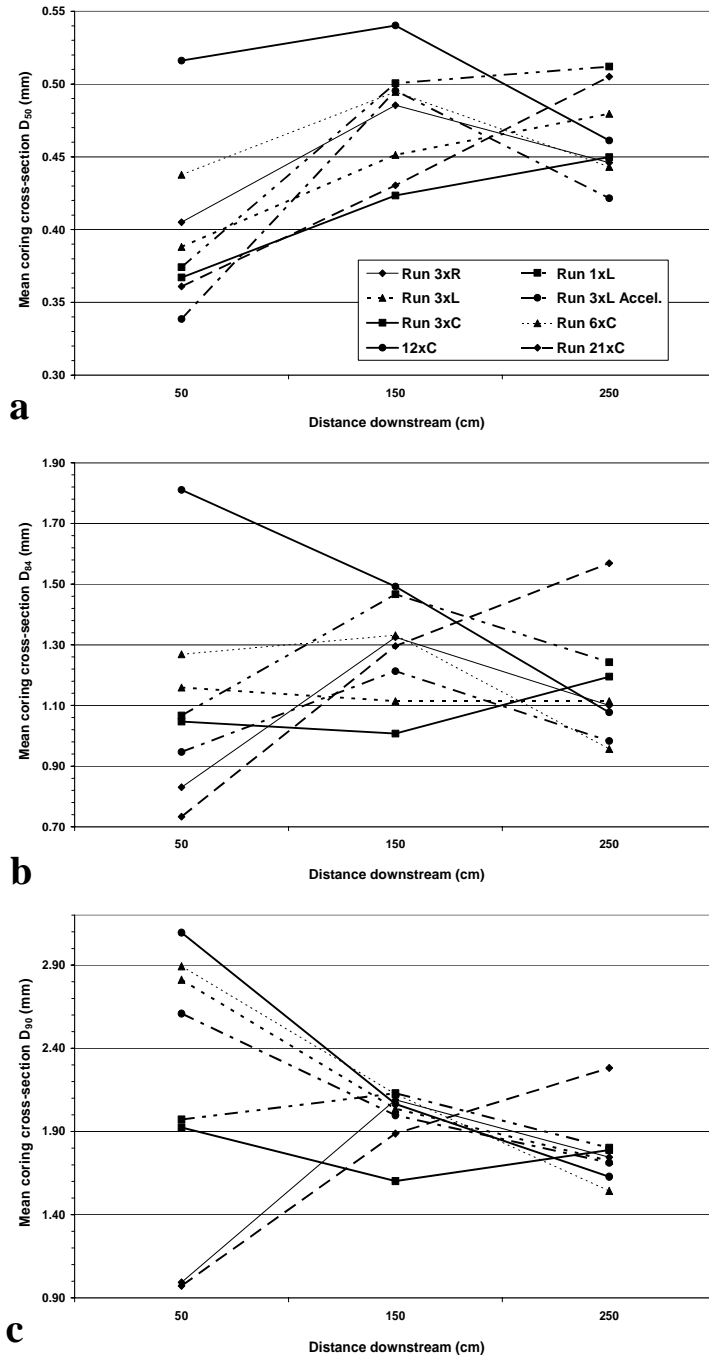


Figure 7.10. Mean values of (a) D_{50} , (b) D_{84} and (c) D_{90} for each coring cross-section.

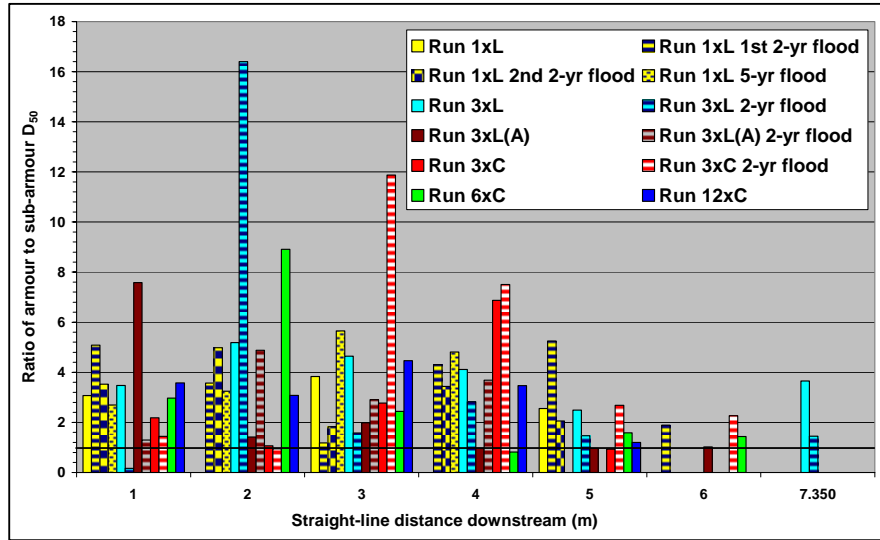


Figure 7.11. Extent of armour layer formation following complete dam removal and flood flows.

Run	Mean armour layer D_{50} in original delta area (mm)	Equal to D_x of composited 50-cm cross-section cores (%)	Equal to D_x of composited 150-cm cross-section cores (%)	Equal to D_x of composited 250-cm cross-section cores (%)
1xL	3.2	94	94.8	96
1xL – post 1 st 2-yr flood	2.02	90	89.2	92
1xL – post 2 nd 2-yr flood	2.17	91	90.8	93
1xL – post 5-yr flood	2.59	92.5	93.2	94.9
3xL	2.39	89.5	92	93.9
3xL – post 2-yr flood	1.48	86.6	87.9	89.2
3xL(A)	1.93	89.1	89.9	91.2
3xL(A) – post 2-yr flood	2.21	89.8	91.1	92.6
3xC	2.24	91.7	94.1	93.1
3xC – post 2-yr flood	2.26	91.7	94.1	93.2
6xC	2.16	88.6	90.8	93.2
12xC	2.95	89.3	94.8	96

Table 7.1. Relative abundance of the armour layer D_{50} at each coring cross-section.

(run 6xC) was still larger than the greatest erosion volume at the 21-piece equilibrium in a marginal run (run 2xR).

A consistent pattern of response is evident in the marginal runs. Excluding run 3xL(A), by the 12-piece equilibrium condition the four runs had, to within 2.3% of each other, eroded the same proportion of the original delta (Figure 7.12; Table 7.2). However, differences between the runs are apparent in the erosion rates. Run 1xL was the slowest, followed by 2xR, 3xR and 3xL. Beyond the 12-piece equilibrium, whereas runs 2xR and 3xL continued to erode a significant further proportion of the

original delta, runs 1xL and 3xR eroded a much smaller amount (Table 7.2). Original delta sediment was eroded at a similar rate to the central runs in run 3xL(A), but a smaller volume of sediment was eroded than in any other run, including the split-flow run by the 12-piece equilibrium. While accelerated scour increased channel slope and increased stream power in the delta topset, the shape of the basin focused much of this power on the left basin boundary, preventing the incising channel from migrating into the right half of the delta (section 7.3.2). The split-flow run had eroded the second smallest original delta volume by the 12-piece equilibrium and did so at the lowest rate, which clearly suggests that, in these experiments, concentration of flow of a given magnitude in a single channel has a much greater capacity to erode and transport sediment than the sum of the same flow divided between two channels.

A similar, albeit slightly less clear-cut, relationship is evident amongst the central runs. While there was a clear increase in the rate of original delta erosion moving from run 3xC through to run 21xC in the early stages of dam removal, by the 12-piece equilibrium (the point at which runs 6xC and 12xC ended) the rate and volume of original delta erosion of run 6xC had dropped below that of run 3xC, which in turn was less than that of run 12xC. As with the marginal runs, by the 12-piece equilibrium there was little difference (only 4.4%), in the total original delta volume eroded for runs 3xC, 6xC and 12xC (Figure 7.12; Table 7.2). Run 3xC eroded 3.4% more of the original delta than run 6xC by the 12-piece equilibrium, perhaps because the system was not allowed to stabilise before each dam increment was removed²¹.

Qualitative observations during the runs clearly showed that the armour layer was exerting a significant degree of control on rates of erosion and volumes of sediment removed from the original delta, particularly during the marginal runs. This observation is quantitatively confirmed in Figure 7.13, which shows the original delta erosion volumes during each time step plotted against time series data for the downstream extent of the armour layer and the downstream extent of the original delta measured along the channel thalweg. Once the channel bed armoured throughout the entire original delta area, the volume of sediment eroded dropped to zero or to very close to zero for most intervals of run time. This is shown clearly for run 2xR after 1,950 minutes, for run 3xR after 1,850 minutes, for run 1xL after 3,020 minutes, for run 3xL after 1,490 minutes and for run 3xC after 2,550 minutes. Also, the further

²¹ Due to laboratory time constraints.

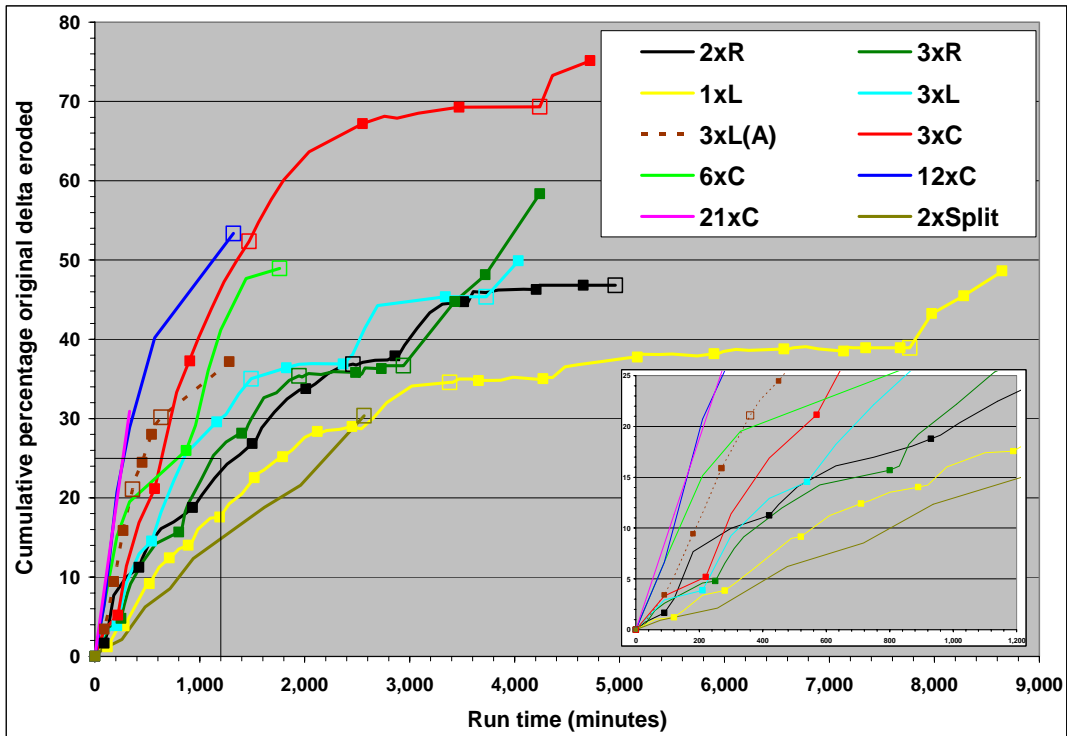


Figure 7.12. Proportion of the original delta eroded under different dam removal scenarios. The solid data markers denote the static equilibrium condition following the removal of one increment of dam, while the first and second empty data markers denote the 12 and 21-piece equilibrium conditions, respectively. The solid markers following the second empty marker denote the static equilibrium following the first two-year, the second two-year and the five-year flood flows respectively. The insert graph provides an expanded view of the area of the main graph enclosed between the black lines and the axes.

Run	Volume eroded from the original delta		0-12 as % of total (%)	12-21 as % of total (%)
	12-piece equilibrium (%)	21-piece equilibrium (%)		
2xR	36.9	46.8	78.7	21.3
3xR	35.4	36.7	96.5	3.5
1xL	34.6	38.9	88.2	11.2
3xL*	35.0	45.4	77.2	22.8
3xL(A)	21.0	30.2	69.8	30.2
3xC	52.4	69.3	75.5	24.5
6xC	49.0	-	-	-
12xC	53.3	-	-	-
21xC	-	-	-	-
2x split	30.4	-	-	-

Table 7.2. Summary of original delta erosion volumes during dam removal.

* The 12-piece equilibrium actually occurred after 1,735 minutes of run time but, for some unknown reason, the cut-fill calculation for this time step failed. The cumulative volume eroded for the previous time step, 1,490 minutes, was thus used as an approximation of the true 12-piece equilibrium erosion volume.

the downstream limit of the armour layer *within* the original delta area, the smaller the volume of sediment eroded, but only if the limit was close to or exceeded about 200 cm: *e.g.* the peaks in downstream armour layer extent centred on the 6- and 8-piece equilibriums in run 2xR, on the 6- and 9-piece equilibriums in run 3xR, on the 3-piece equilibrium in run 3xL and on the 12-piece equilibrium in run 6xC. When the downstream extent of the armour layer was less than about 200 cm, there did not appear to be any relationship between its downstream extent and erosion volume. This is probably because the bulk of the original delta sediment volume was located in the downstream half of the original delta area. Finally, irrespective of whether the armour layer's downstream extent lay within or out with the original delta area, a break up of the armour layer that extended far into the original delta would invariably result in a significant increase in erosion volume: *e.g.* run 2xR after 1,260, 1,830 and 2,950 minutes; run 3xR after 1,010 and 1,490 minutes; run 1xL after 610, 980, 1,280, 1,730, 2,000 and 2,780 minutes; and run 3xL after 1,370 and 2,575 minutes.

It is noteworthy that the strong, inverse relationship between armour layer extent and erosion volume is limited almost exclusively to the four marginal runs in which the system was allowed to adjust to a static equilibrium before the next baselevel drop. The accelerated rate of baselevel drop in run 3xL(A) meant that the armour layer never extended downstream of 200 cm during dam removal. A large total erosion volume was precluded by the channel's position against the left basin boundary, but erosion rates were consistently higher throughout the entire dam removal process than during the other marginal runs (Figure 7.14). Similarly, in run 3xC, the armour layer's downstream extent did not exceed 200 cm until just before the 15-piece equilibrium, which allowed both the erosion rates and volumes to remain consistently higher than in runs 2xR, 3xR, 1xL and 3xL up to the same time. The periods of greatest erosive activity in these four runs were all generally over by the 12-piece equilibrium, which corresponded closely to the time when the channel through the original delta area was almost permanently armoured, while a greater proportion of the total erosion volumes occurred during the removal of the 13th to 21st dam pieces in runs 3xL(A) and 3xC (Table 7.2).

Run 3xL(A) was performed with a deliberately accelerated rate of dam removal of 90 minutes per increment, while run 3xC was inadvertently performed with a slow mean removal rate of 606 minutes per increment (range 220 to 1,080

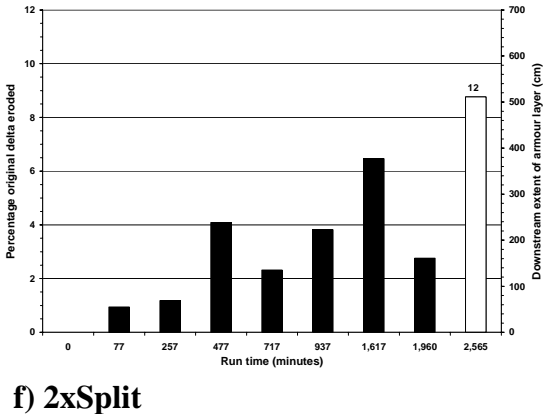
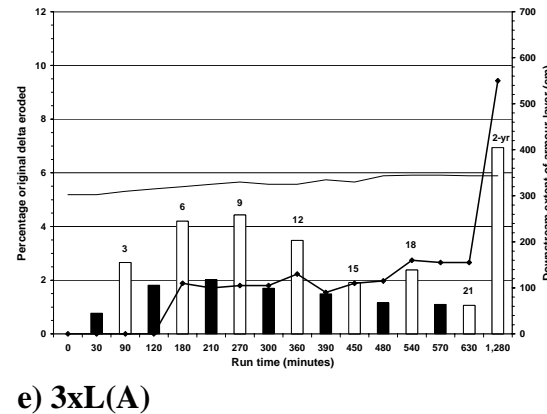
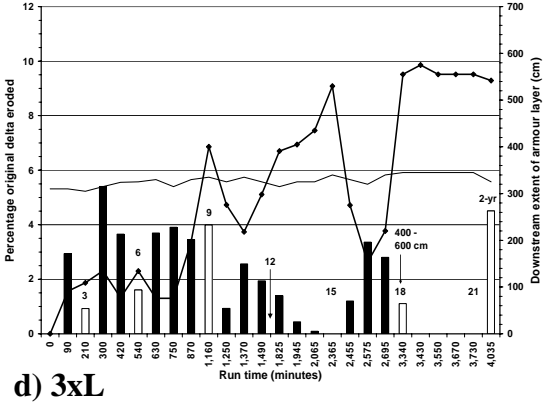
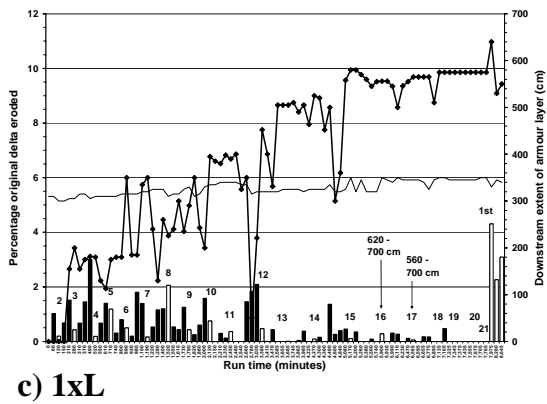
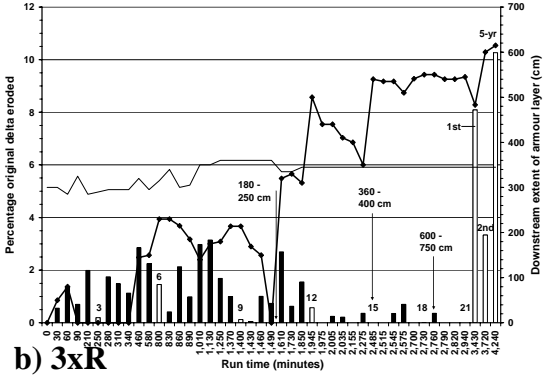
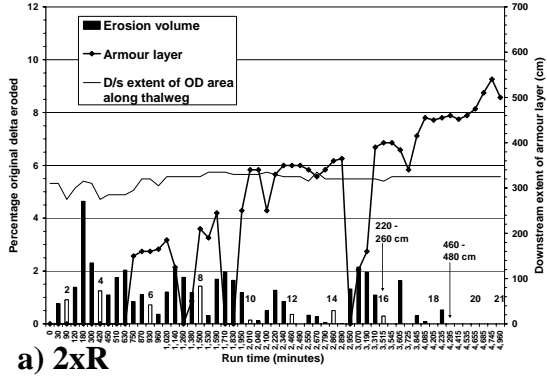
minutes). Although run 3xL(A) eroded over 50% less of the original delta than run 3xC (Table 7.2), given the influence of the left basin boundary and that the incremental rate of dam removal was about five times more rapid than in run 3xC, this is still impressive. It is possible that if a run 3xC(A) had been performed, with the same incremental rate of dam removal as in run 3xL(A), more of the original delta would have been eroded than was actually eroded by run 3xC, because energy would have been introduced much more rapidly to the incising channel. In effect, the hypothetical run 3xC(A) would have become more like runs 6xC, 12xC and 21xC, a supposition that is supported by the evidence from these three runs.

Runs 6xC and 12xC were similar to runs 3xL(A) and 3xC in that they did not allow the armour layer to extend beyond 200 cm until near the 12-piece equilibrium, while the short duration and massive base level drop of run 21xC allowed virtually no armour layer formation whatsoever (Figure 7.13). The net effect of this lack of armouring was that the three central runs generally eroded much more sediment and at a substantially greater rate than in any of the marginal runs and run 3xC (Figures 7.12 to 7.14).

7.2.2 Original delta volumes eroded by flood flows

The volumes of original delta eroded by the flood hydrographs are shown in Figure 7.12 and Table 7.3a. The flood flows in run 3xR eroded larger proportions of the original delta than other equivalent floods because a substantially smaller proportion of the original delta was eroded during the removal of the 13th to 21st dam pieces than in any other run (Table 7.2). This occurred because a large expanse of the hard basin boundary was exposed at an earlier stage of dam removal in run 3xR than in any other run, thus preventing almost any further original delta erosion during the dam removal phase (Figure 7.13b; Run3xRCam1 time lapse movie). Similarly, the two-year flood in run 3xL(A) eroded a relatively large amount of the original delta because of the smaller volumes of sediment eroded during the dam removal phase, although the flood's erosive capability was reduced by its interaction with the curvature of the left basin boundary. The two-year flood in run 3xC eroded relatively less of the original delta than runs 3xR and 3xL(A), probably because more of the original delta had been eroded during the dam removal phase, but more than in runs 1xL and 3xL, because the channel was more central through the original delta area at

the onset of the flood and was, therefore, unaffected by the curvature of the left basin boundary.



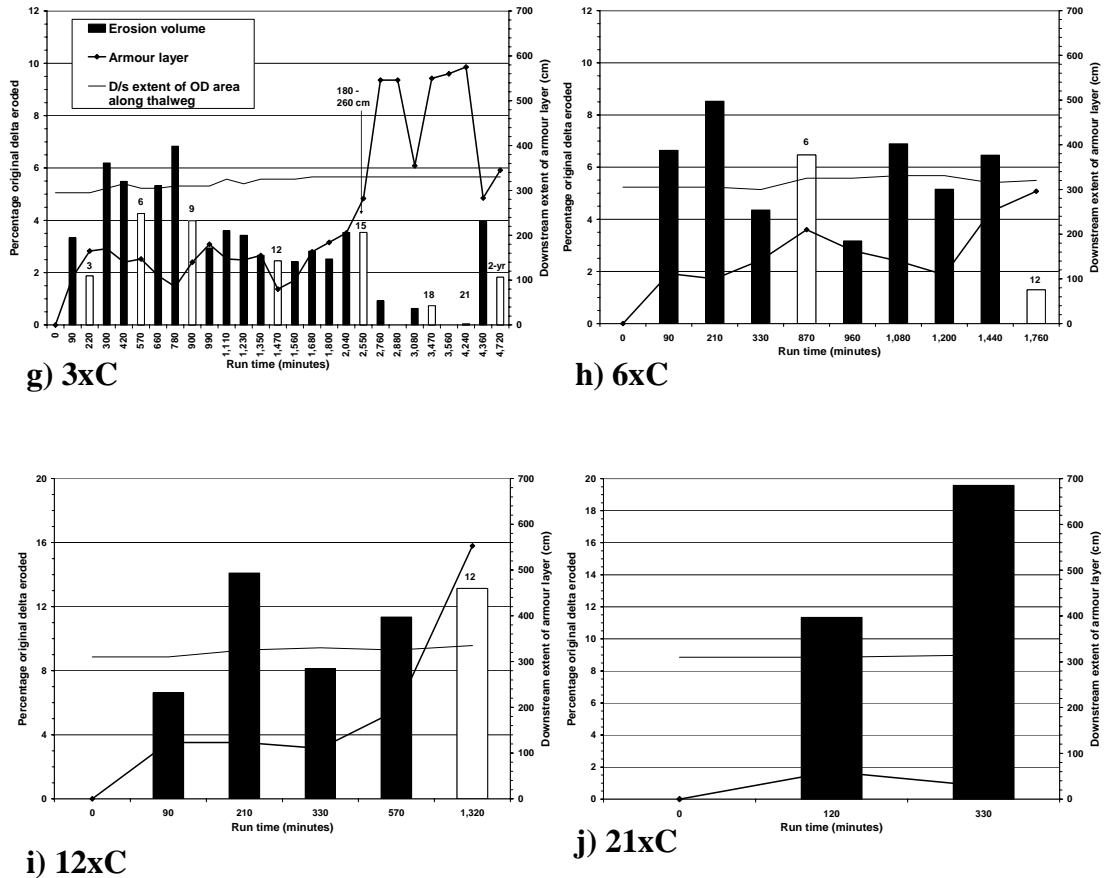
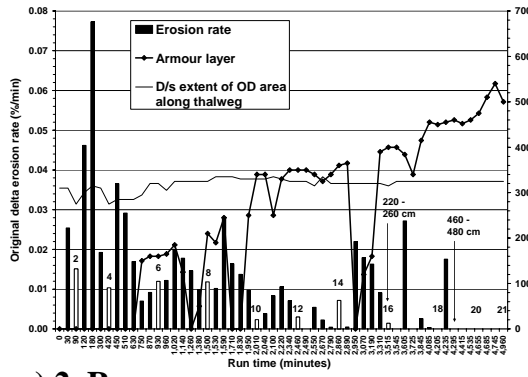


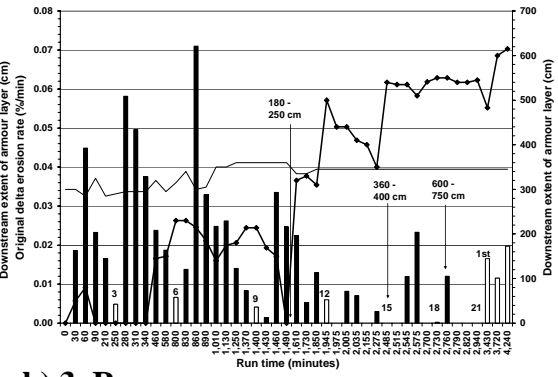
Figure 7.13. Original delta erosion volumes per time step and armour layer evolution. Volumes were normalised by the volume of sediment in the original delta at the start of the run. The white columns with a number above them denote an equilibrium interval after the removal of the number of dam pieces indicated. The thin black-lined plots denote the downstream-most point of the channel that is still within the initial original delta area. The figures in centimetres above the arrows indicate the time and longitudinal extent of basin bed exposures that subsequently exerted a significant grade-controlling effect on system evolution.

7.2.3 Sediment transport through the dam site

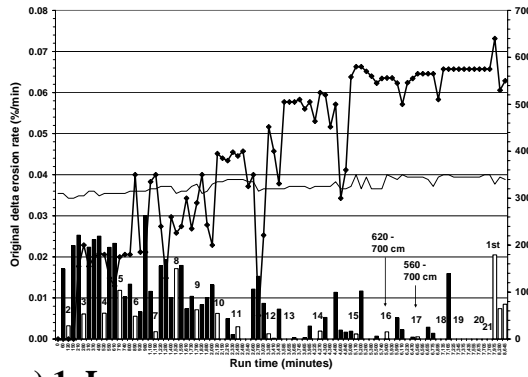
The total reservoir sediment volume transported past the dam site is shown in Figure 7.15 and Table 7.3b. By the end of the dam removal phase of run 3xC, more sediment was transported through the dam site (25.0%) than at any stage of any other run except run 1xL, in which 25.3% was transported by the end of the five-year flood. Following the two-year flood in run 3xC, a further 10% of the total reservoir sediment volume had been transported through the dam site. The ranking of the runs in order of



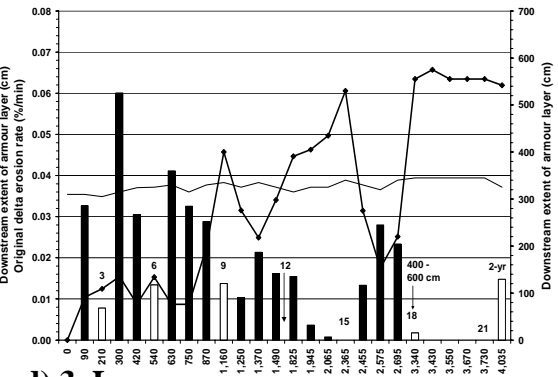
a) 2xR



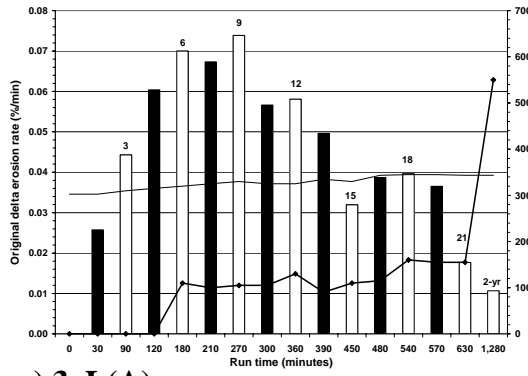
b) 3xR



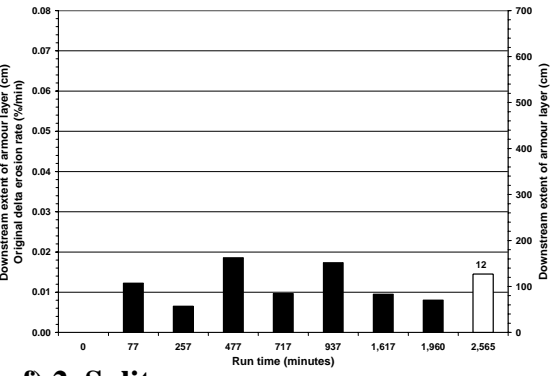
c) 1xL



d) 3xL



e) 3xL(A)



f) 2xSplit

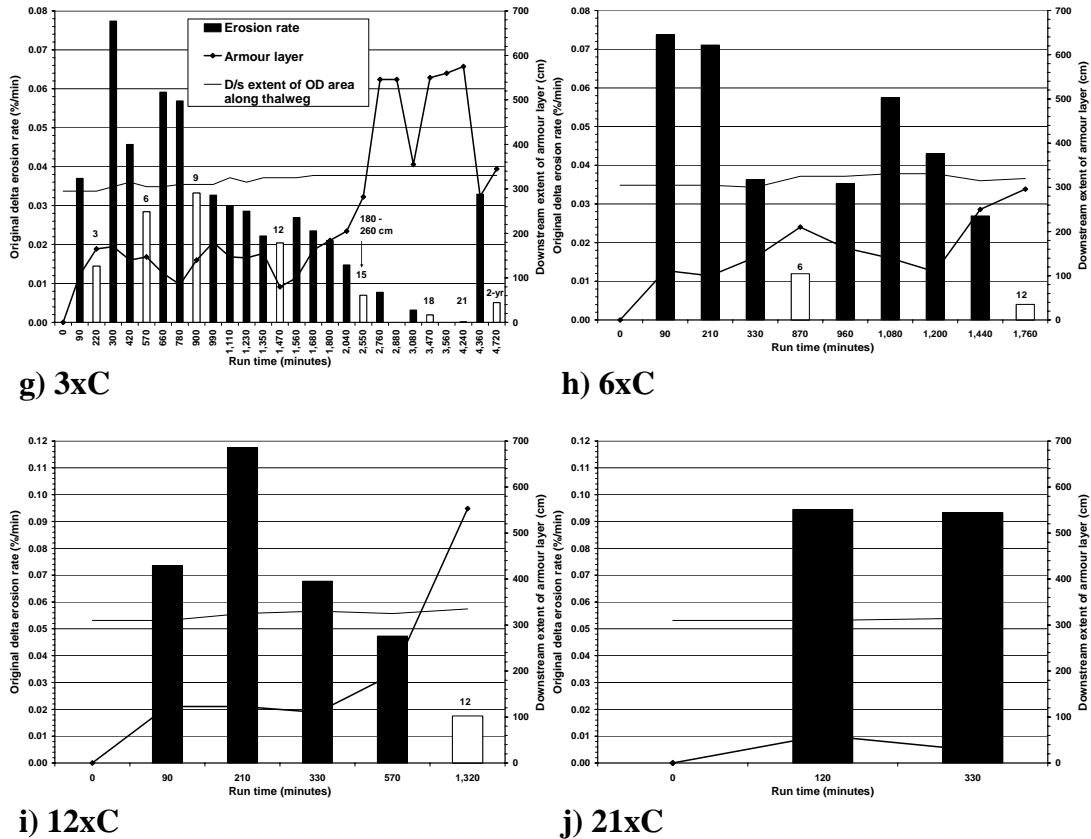


Figure 7.14. Original delta erosion rates per time step and armour layer evolution. Plots as described in Figure 7.13.

decreasing total sediment volume transported through the dam site corresponds almost perfectly with their ranking in order of decreasing original delta erosion volume (Table 7.3a), which suggests that as more sediment is eroded from the original delta more of it will pass downstream in the short-term following complete dam removal.

7.2.4 Summary of volumetric analysis

The results of the volumetric analysis show that the central runs eroded more original delta sediment than the marginal runs at comparable stages in the dam removal process. This occurred because the channels in the central runs were laterally unconstrained at the onset of dam removal and were able to develop fully-formed meander bends along almost the full length of the original delta (see the time lapse movies and description in section 7.3.3. In addition, the larger magnitudes of base level drop in the central runs (in run 3xC the greater rate of drop), restricted the

Run	Original delta volume eroded during.... (as % of total reservoir sediment volume)				Total volume passing downstream (rank)
	Dam removal (rank)	1 st 2-yr	2 nd 2-yr	5-yr	
2xR	45 (2)	-	-	-	45 (5)
3xR	35.7 (5)	7.9	3.2	10	56.8 (2)
1xL	38.2 (4)	4.2	2.2	3	47.7 (4)
3xL	44.6 (3)	4.4	-	-	49.1 (3)
3xL(A)	29.6 (6)	6.8	-	-	36.5 (6)
3xC	67.8 (1)	5.7	-	-	73.4 (1)

Run	Volume passing downstream during.... (as % of total reservoir sediment volume)				Total volume passing downstream (rank)
	Dam removal (rank)	1 st 2-yr	2 nd 2-yr	5-yr	
2xR	13.8 (3)	-	-	-	13.8 (5)
3xR	2.4 (5)	7.6	5.1	9.7	24.8 (3)
1xL	7.8 (4)	4.3	8.1	5.3	25.3 (2)
3xL	13.9 (2)	10.8	-	-	24.7 (4)
3xL(A)	0.3 (6)	11	-	-	11.4 (6)
3xC	25.1 (1)	9.8	-	-	35 (1)

Table 7.3. (a) Original delta erosion during flood flows. (b) Sediment volumes passing through the dam site.

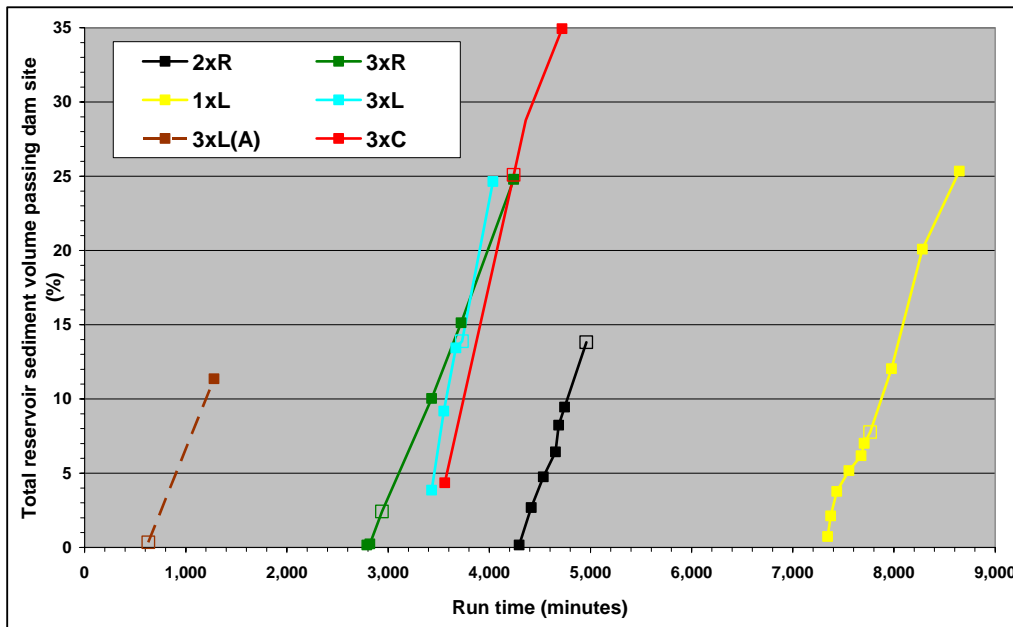


Figure 7.15. Total reservoir sediment passing downstream. The empty marker denotes the cumulative reservoir sediment volume transported during the dam removal phase. The solid markers following this denote the equilibrium following the first two-year, second two-year and five-year flood flows, respectively.

downstream extent to which the armour layer could form within the original delta, allowing the effects of the base level drop to migrate further upstream into the original delta. A more detailed examination of delta morphodynamics will now be undertaken to explain the reasons behind this behaviour.

7.3 Delta morphodynamics

In the following descriptions, reference is made to intervals of run time in order to describe when certain events occurred. These intervals are defined using numbers such as 2/21 (19/21), 4/21 (17/21), 6/21(15/21), *etc.*, which simply indicate that the system is adjusting to the removal of the first 2, 4 and 6 dam pieces, respectively. The numbers in parentheses denote the number of dam pieces (out of 21) remaining and correspond to the text in the time lapse movies, so the reader can refer to the relevant section of movie in order to view the processes being described.

Reference is also made to the original delta and prograding delta areas. The original delta is the deposit built hydraulically at the start of each experiment and whose topset surface extends from 0 cm to about 300 cm, while the prograding delta refers to the sediment deposition area downstream of the topset. Both the original and prograding delta are further defined in terms of proximal, medial and distal areas. The proximal, medial and distal original delta areas are from 0 to 100 cm, 100 to 200 cm and 200 to about 300 cm respectively. The proximal, medial and distal prograding delta areas are the bodies of sediment from ~300 to 550 cm, 550 to 800 cm and 800 to 1,050 cm respectively (Figure 7.16). If, for example, the prograding delta front is at 400 cm, it will be described as the proximal prograding delta because it is within the proximal zone of the reservoir basin, even though, strictly speaking, it is actually the distal delta since it is the downstream-most point on the prograding delta. The different areas of the delta and prograding delta are further defined as being to the left or right of the channel when viewed in the downstream direction.

Figures 7.18 to 7.23 are summary plots that show interactions between dimensionless bed elevations, dimensionless top terrace widths, dimensionless active channel widths and dimensionless original delta cut volumes in discrete, 50-cm reaches of the original delta. Because the cut volumes represent subsections of the original delta, the corresponding fill volumes cannot be used to correct them, as was

done for the whole original delta surface (section 6.1.2.3iii). Comparing the uncorrected cut

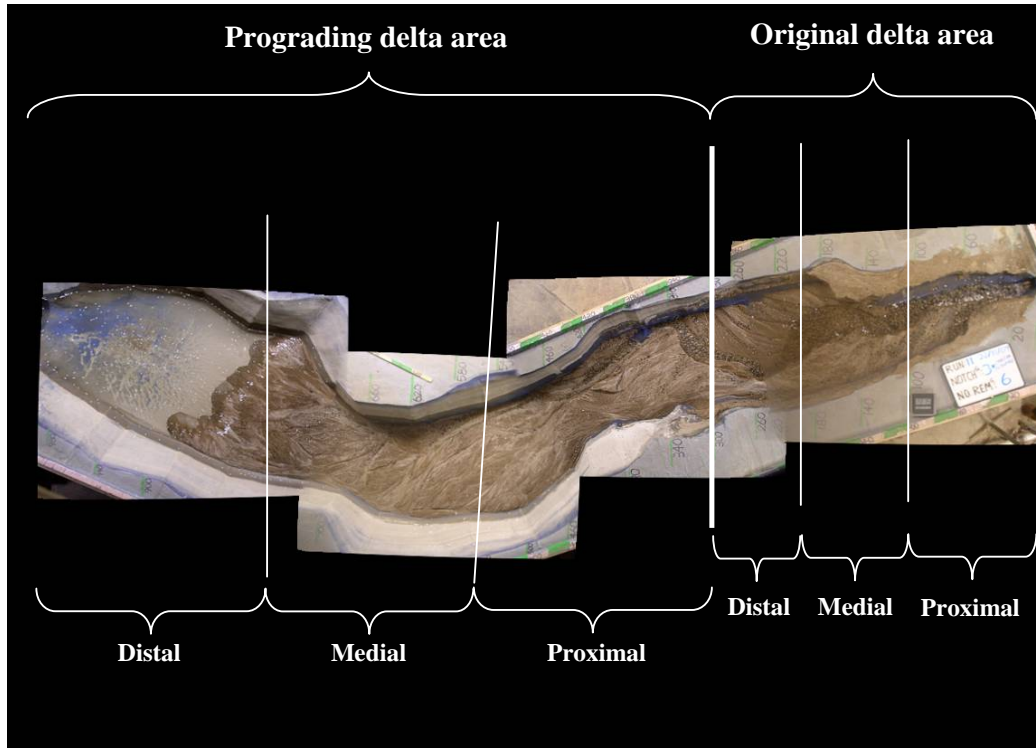


Figure 7.16. Delta surface zones.

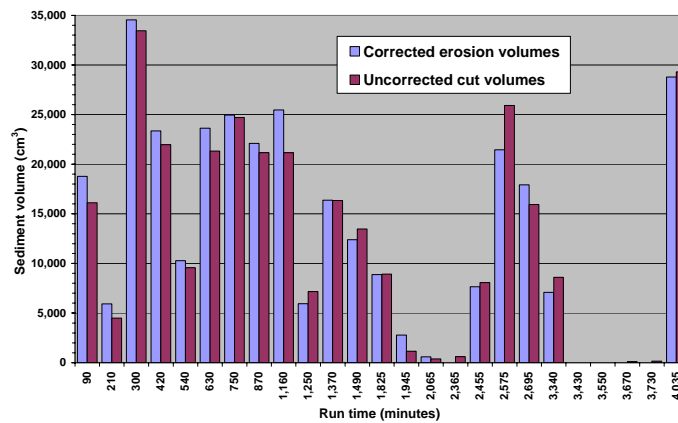


Figure 7.17. Erosive activity in the original delta represented by corrected and uncorrected erosion data. These data are from run 3xL, but all other runs showed the same level of comparability between datasets.

volumes summed for the whole original delta to the corrected original delta erosion volumes, however, it is clear that they closely follow the pattern of erosive activity described by the corrected data (Figure 7.17). It is therefore assumed that the relative differences in cut volumes shown in Figures 7.18 to 7.23 provide a reasonable

estimate of the true temporal distribution of erosive activity within each 50 cm reach during each run, even though the absolute cut values are incorrect²².

The cumulative change in dimensionless bed elevation, *i.e.* cumulative dimensionless incision, was calculated by dividing the cumulative change in thalweg elevation by the maximum sediment depth²³ at the cross-section. Maximum sediment depth was chosen as the denominator in the normalization calculation because it provided a direct measure of the extent of incision of the original delta under the different dam removal scenarios.

Top terrace width at a cross-section was normalized by the maximum delta surface width at the cross-section. This metric was developed to show the extent to which lateral channel adjustments were able to erode the delta deposit and thus to provide a method for ascertaining the relative contribution of lateral channel adjustments to the overall volume of original delta eroded. It is not a perfect metric in this respect, because a large amount of lateral channel movement at the start of a run could cause a great deal of terrace widening, which would mask subsequent erosion of lower elevation terraces as the channel incised. For example, the first bar for runs 2xR and 3xR at 250 cm (Figure 7.26e) shows very large and rapid widening of the top terrace, but the Run2xRCam1 and Run3xRCam1 time lapse movies show that these lateral adjustments were restricted to a relatively thin surface layer of the original delta. Examination of the time lapse movies for all runs shows that these are the only significant occurrences of this type, however. Hence, in the vast majority of cases top terrace width does provide a reasonable indication of the capability of an incising channel to erode terraces over their full height.

Active channel widths for each time step at every measuring cross-section were normalized using the delta surface width for that cross-section and time step. Using this parameter instead of maximum delta surface width shows the extent to which the active channel was able to occupy the delta surface at every time step during the run.

²² The cut volumes in Figures 7.18 to 7.23 were also increased by a factor of four to make them more legible on the plots.

²³ The maximum sediment depth at a given longitudinal position along the delta topset was calculated as the elevation difference between the thalweg of the channel at time zero and the thalweg of the empty basin, which lay along the left basin boundary.

7.3.1 Right marginal runs

Both right marginal runs were strongly influenced by the right basin wall in the proximal region of the original delta. As the channel heads cut back into the proximal original delta during the early stages of these runs, they attached themselves to the right basin boundary, which sloped towards the basin centre at an angle of roughly 45° (Figure 8.5a, arrow C). This initially straightened the channel through the whole delta area and directed it towards the centre of the prograding delta front, while also causing the channel bed to armour along the upstream half of the original delta. As flow exited the end of the sloping basin boundary, at a distance of around 100 cm downstream, it appeared to be directed into the right original delta terrace, becoming fixed along that trajectory during the 6/21(15/21) intervals of both runs by the armour layer that had developed downstream as far as 140 cm. The terrace was completely eroded by the 8/21(13/21) and 9/21(12/21) intervals in runs 2xR and 3xR respectively (Figure 7.19a&b). Despite these similarities in the right margin runs, there were also significant differences.

The first major difference was associated with migration of incision to the very upstream limit of the original delta. In run 2xR, this led to the erosion of a large portion of the proximal original delta during the intervals 8/21(13/21) and 10/21(11/21) by a section of the channel that was oriented obliquely across the delta topset and which migrated downstream from the upstream end of this zone (Figures 7.18a, 7.19a). In run 3xR, however, a much smaller portion of the downstream end of the proximal left terrace was eroded (Figures 7.18b, 7.19b). Beyond the 10/21(11/21) interval in run 2xR, the downstream-migrating section of channel eroded most of the remaining proximal delta during the interval 16/21(5/21) (Figures 7.18a, 7.19a), while small amounts of incision and lateral channel adjustment eroded small amounts of the left medial and distal original delta terrace (Figures 7.21a - 7.23a). Virtually no incision and only small lateral channel movements occurred in the original delta during the dam removal phase after the 9/21(12/21) interval during run 3xR and this eroded negligible volumes of sediment (Figures 7.21a - 7.23a).

A phenomenon of potentially substantial significance was first observed at the start of the 6/21(15/21) interval of run 2xR. Increased boundary shear stresses generated by the base level drop soon migrated into the medial portion of the original delta, but were insufficient to break up the armour layer that extended downstream as

far as 160 cm. They were, nevertheless, sufficient to cause a small amount of Bed Elevation Lowering Without Armour Layer Break-up – BELWALB, which migrated upstream from 160 cm to about 100 cm (Figure 7.20a) (section 8.2.2.1). This lowering is visible in the Run2xRCam1 movie from 04:28 to 04:30 minutes, although you must look carefully to see it, and took place over about 7 model minutes²⁴, yielding a migration rate of about 8.6 cm per model minute. This bed lowering may have altered the orientation of flowlines upstream from 160 cm sufficiently to cause the flow to erode the left terrace, which would have further changed the orientation of the flowlines. In turn, the influx of sediment from terrace erosion partially buried the armour layer and seemed to increase the rate of terrace erosion, perhaps because of increased flow velocities and shear stresses caused by hydraulic smoothing of the bed; an example of positive feedback. As the flow entrained the failure blocks it incised into the bed and both these actions delivered elevated gravel loads further downstream, which allowed the bed to armour as far as 200 cm (Figures 7.18a - 7.23a).

In both runs erosive activity was confined almost exclusively to the right half of the original delta. Initially, erosion was confined by the sloping basin boundary in the proximal original delta area. Later it was constrained by armouring and exposure of the basin bed, which stabilised the channel and greatly reduced the extent to which it could erode the large, left terrace deposit. This meant that the channel stabilised and, following the next drop in baselevel, incised mostly along the right half of the proximal prograding delta topset during intervals 9/21(21/21) to 21/21(0/21) in run 3xR, and along the right half of the proximal and medial prograding delta topset during intervals 6/21(15/21) to 16/21(5/21) in run 2xR. Terraces that decreased in size and volume with increasing distance downstream were thus formed along the left side of the proximal prograding delta zone in run 3xR and along the left side of the proximal and medial prograding delta area in run 2xR. Increasingly large volumes of sediment were eroded from these terraces, with erosion starting at their downstream ends and migrating towards the upstream, particularly in unarmoured channel reaches. The increasing ease with which the left terraces could be eroded with increasing distance downstream and the subsequent reduction in channel constriction between

²⁴ Each second of movie time is composed of 7.5 photographic stills, with each photograph taken at 30-second intervals during the model run.

the terraces and the right basin boundary, allowed a substantial increase in channel widths and in the frequency with which braiding occurred (Figure 7.28a&b) in the prograding delta area compared to the original delta upstream.

The greatest effect of the first two-year flood at the end of run 3xR was to rapidly reduce the very steep bed slope through the original delta and to move the channel into a more central basin position along a line extending from the sloping right basin boundary in the proximal original delta (Figure 7.25h-i; Figures 7.18b to 7.23b). As it centred itself, the channel rapidly eroded substantial portions of the lower elevation terraces in the distal original delta and in the proximal prograding delta (Figures 7.22b; 7.23b). The second two-year flood further straightened the channel in a more central position through the medial and distal original delta area, but it eroded a smaller volume of sediment from here and from the proximal prograding delta. Because of the channel's central position within the delta area at the start of the five-year flood and this flow's larger magnitude, a substantial portion of the left terrace through the entire original delta area was eroded (Figures 7.18b to 7.23b). A smaller volume of the left proximal prograding terrace deposit was eroded since this portion of the basin was more sheltered from the channel, which occupied a position along the right half of the proximal prograding delta surface as it flowed out of the right half of the original delta area.

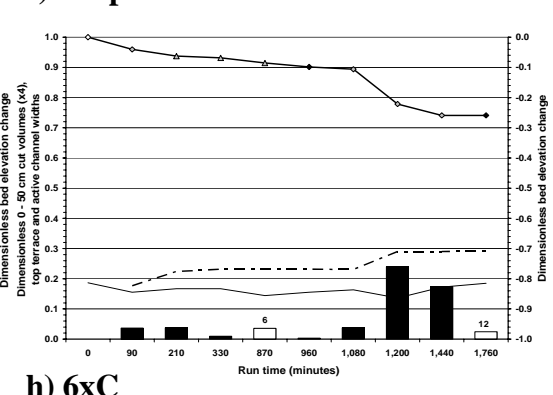
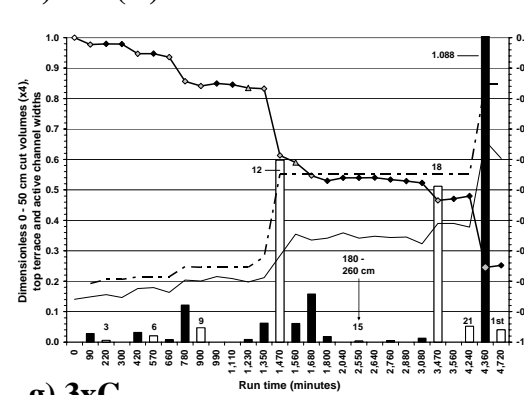
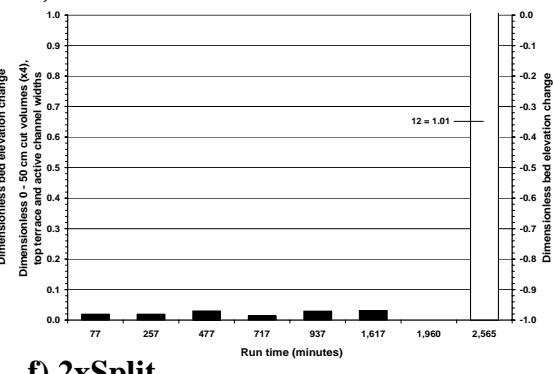
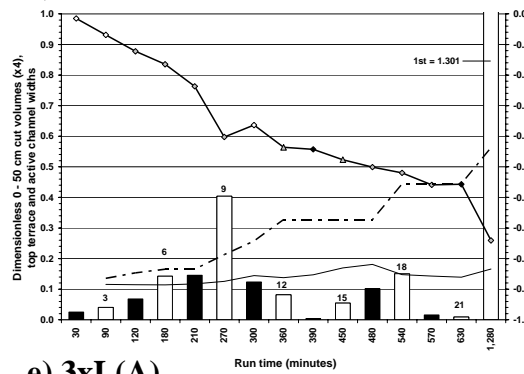
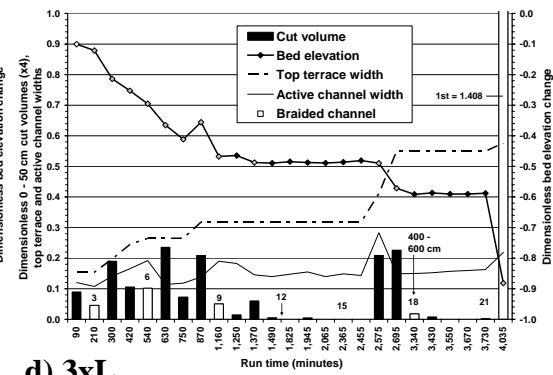
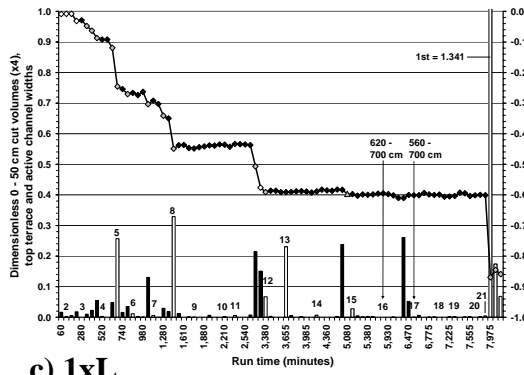
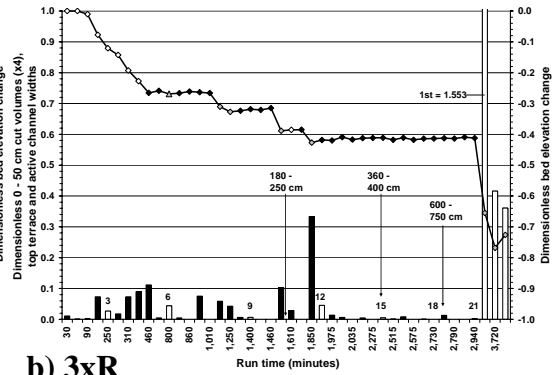
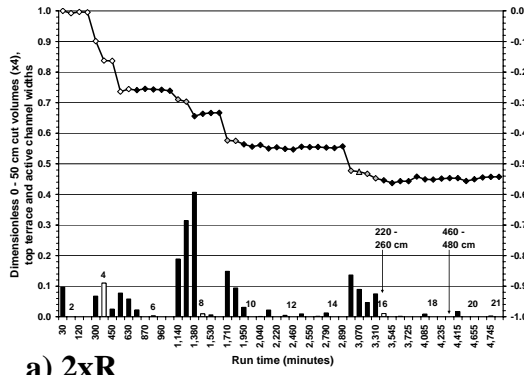
7.3.2 Left marginal runs

The evolution of the delta surface in all three left marginal runs was strongly affected by the interaction of the incising channel with the concave curvature of the left basin boundary in the original delta area, with the effect being most notable during run 3xL(A). Runs 1xL and 3xL exhibited a very similar response for almost their entire duration. In both cases, waves of BELWALB, partial armour break up and almost complete armour layer break up migrated far into the proximal original delta prior to and during the 12/21(9/21) interval. This resulted in a narrow, entrenched channel in the upstream half of the original delta that never moved away from the left basin boundary for long (Figures 7.18c-e - 7.19c-e). When the channel did erode the right terrace in this area, either upstream-migrating incision would re-straighten the channel against the boundary, or a mass wasted block of sediment would deflect the flow back towards the boundary. This meant that the incising channels could not

create enough space laterally in the upstream half of the original delta to move sufficiently far away from the boundary to enable them to take a more central route through the entire original delta topset, which would have allowed them to erode more of the right side of the deposit. This tendency for lateral stability was further enhanced in runs 1xL and 3xL by the large volumes of gravel stored in the upstream part of the proximal original delta (Figure 7.10c), which were recruited to the channel bed as soon as any mass wasting or incision occurred and which rapidly re-armoured and stabilised the bed following any partial or complete armour layer break up.

The run 1xL and 3xL channels were able to erode much more of the right terrace in the downstream half of the original delta prior to and during the 12/21(9/21) interval, possibly because there was a smaller supply of gravel and the armour layer took longer to reform following partial or complete break up (Figures 7.21c&d to 7.23c&d). In run 3xL(A), however, there was less lateral channel adjustment in the downstream half of the original delta than in the upstream half (Figures 7.18e to 7.23e), probably because the relaxation periods between intervals of base level drop were too short to allow the channel to incise to anything approaching an equilibrium slope. As a result, stream powers through this portion of the delta were permanently high, which acted to straighten the channel, thus effectively precluding any significant lateral channel movement.

The erosion mechanism in all three runs was very similar. A proto-bend would develop in the flow and begin to erode the right terrace. This led to the formation of a lateral bar or terrace against the left basin boundary that amplified the angle of deflection of the flow entering the bend, thus causing the bend to grow. In some cases, bend growth was rapid and extensive and the lateral bar would turn into a point bar. Two similar mechanisms were responsible for the formation of these lateral bars. In the first, which was most common in run 1xL, the coarse lateral bar head was formed from a small patch of armoured channel bed that *emerged* as the adjacent channel incised. The downstream, and generally finer, body of the bar then developed primarily as a result of continued channel incision but also partially due to the deposition of finer sediments in the lee of the coarse bar head. In the second mechanism, which occurred mostly in runs 3xL and 3xL(A), the gravels that formed the coarse bar head were generally *deposited* after having been entrained a short distance upstream. The finer body of the bar/terrace was primarily deposited due to



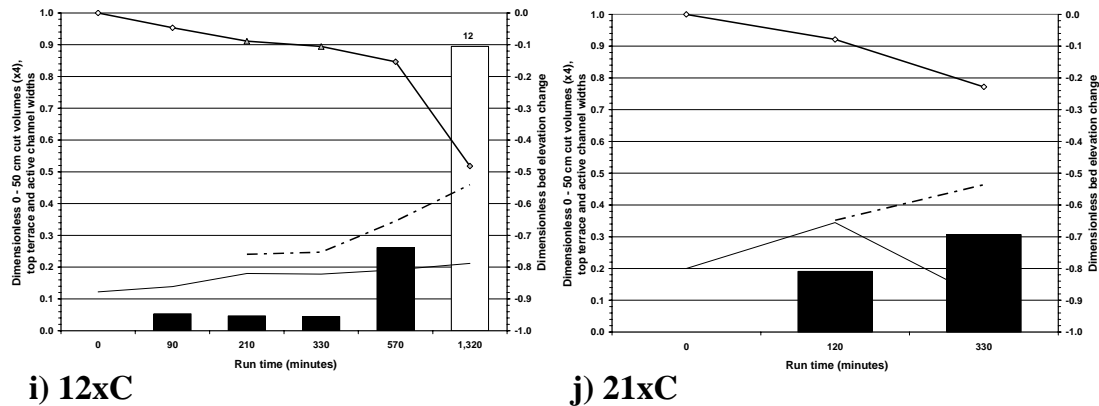
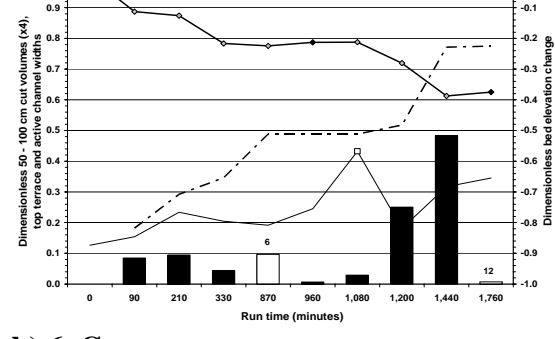
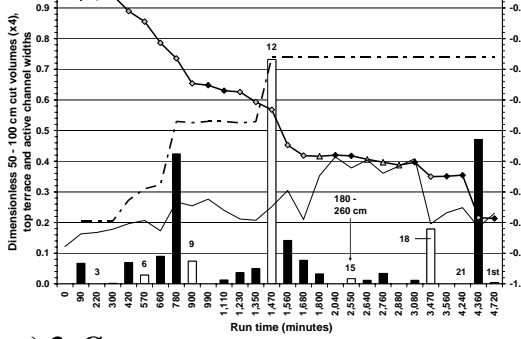
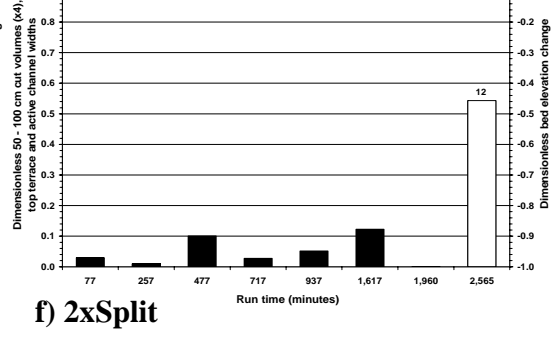
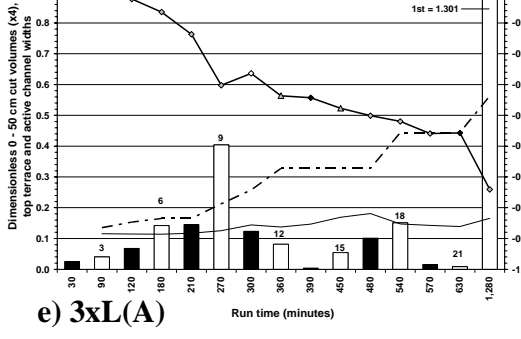
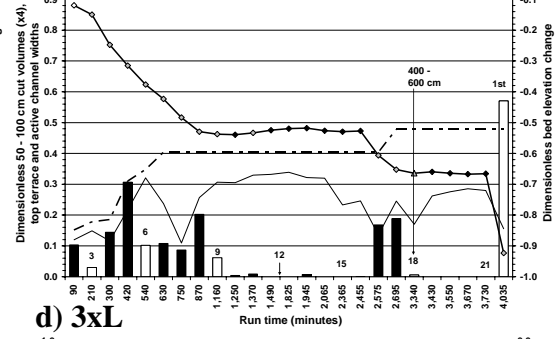
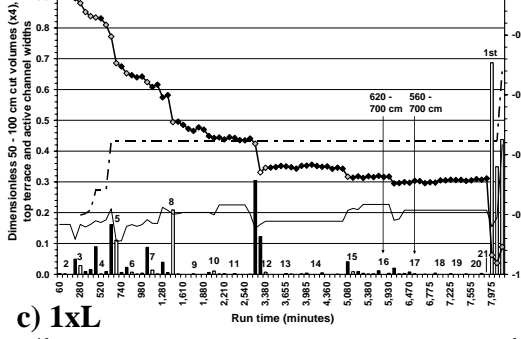
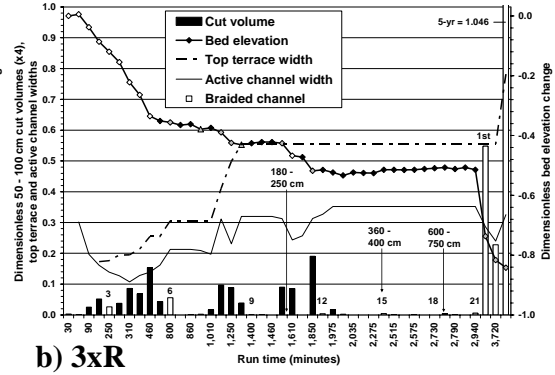
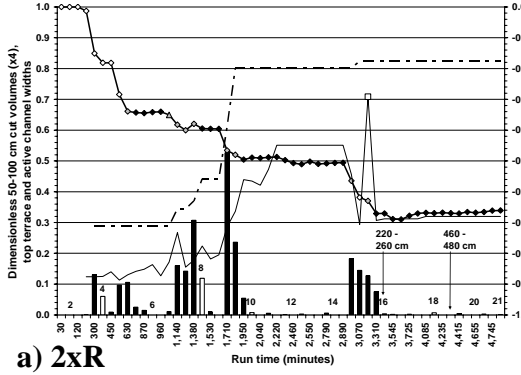


Figure 7.18. Dimensionless cut volumes, active channel widths, cumulative top terrace widths and cumulative thalweg elevation change from 0 – 50 cm in the original delta area. The following notes refer to Figures 7.18 – 7.23. In each graph, all plots except that for cut volume represent the downstream cross-sectional boundary of the 50 cm subsection. The different data markers in the bed elevation plots indicate the following: a solid black diamond indicates that the armour layer extended over at least 50% of the channel bed within that section and that it remained completely undisturbed for the entire interval of run time. A white diamond with black outline indicates that at least 50% of the channel bed within the section was completely unarmoured for the entire interval. A grey diamond with black outline indicates that the armour layer was partially or completely broken up one or more times within the section. A grey triangle with black outline indicates that Bed Elevation Lowering Without Armour Layer Break-up (BELWALB) occurred (see text for explanation). The numbers in the plots are as described in the caption of Figure 7.13.

the lower flow velocities in the lee of the head. In addition, the bars formed by this mechanism had a tendency to migrate downstream as the bend grew, which might reflect the higher energy environment associated with the removal of a three-piece dam increment. The bars formed by both mechanisms were eventually destroyed by upstream-migrating incision, which caused the channel to re-attach itself to the left basin boundary. This occurred particularly rapidly in run 3xL(A) due to the high energy slope that existed throughout the original delta and this explains why lateral erosion was so limited in that run.

Following the 12/21(9/21) interval, no further significant erosion took place in the original delta area during the dam removal phase of run 1xL (Figures 7.18c to 7.23c), but run 3xL experienced significant erosion throughout this entire area during the 18/21(3/21) interval (Figures 7.18d to 7.23d). This erosion started shortly after the 18th dam piece was removed but was not caused by its removal, since the delta front was at that time in the distal prograding zone far downstream and there was insufficient time for the effects of the base level drop to migrate so far upstream. The Run3xLCam2 movie clearly shows that there is no upstream-migrating disturbance to



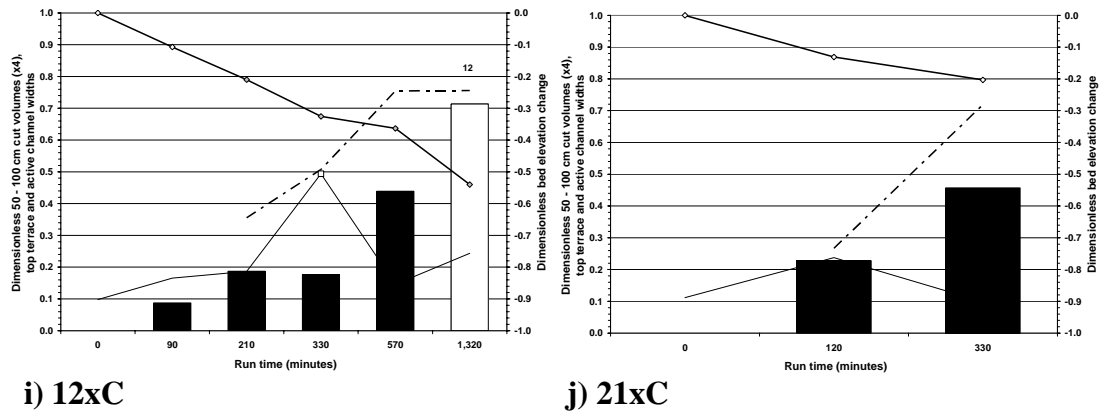
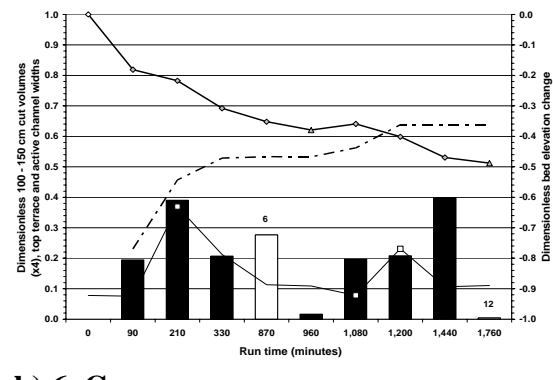
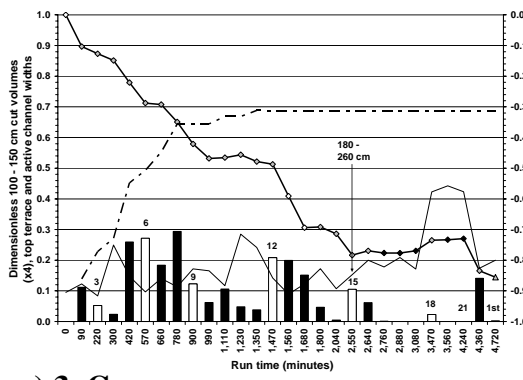
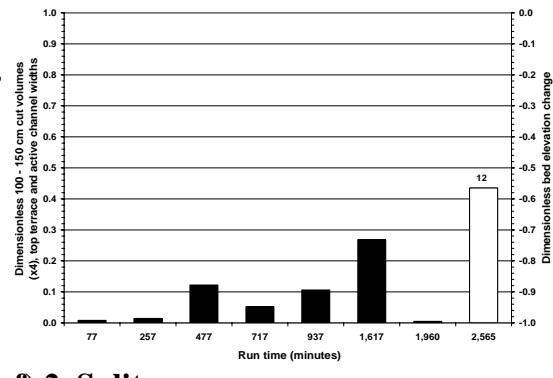
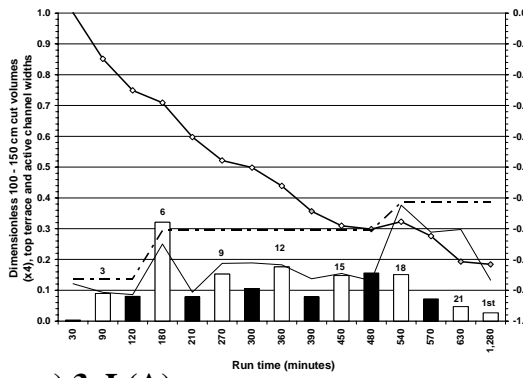
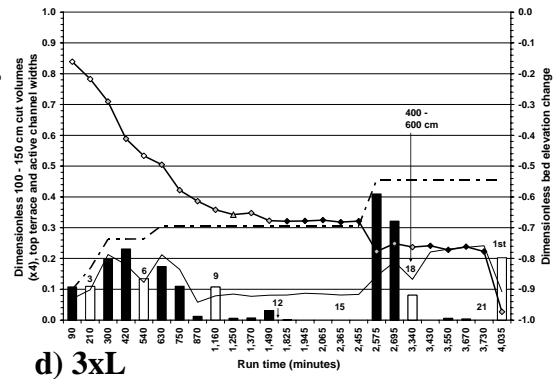
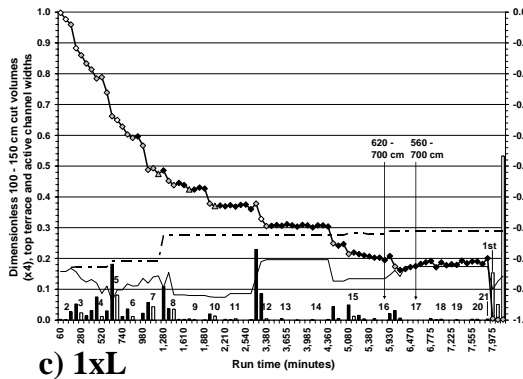
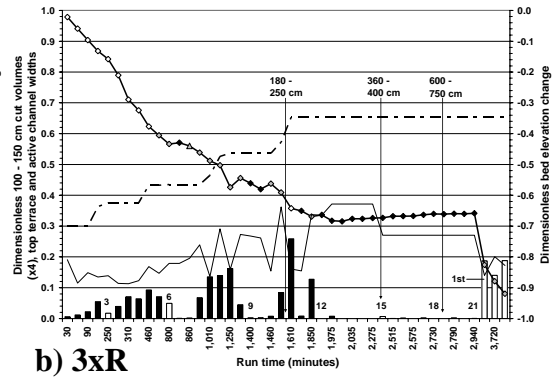
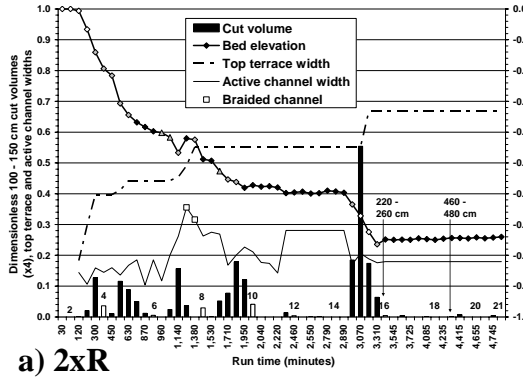


Figure 7.19. Dimensionless cut volumes, active channel widths, cumulative top terrace widths and cumulative thalweg elevation change from 50 – 100 cm in the original delta area.

the well-developed armour layer downstream from the origin of the erosion at 280 cm. The erosion was actually triggered by the movement of a few gravel grains at 280 cm at the base of the high terrace in the distal area of the original delta, which rapidly snowballed into very rapid erosion of this terrace. The resulting change in flow direction caused several waves of partial and complete armour layer break up to migrate into the medial and proximal areas of the original delta, where they triggered extensive mass wasting of the right terrace in the medial and proximal areas of the original delta. A substantial volume of gravel and finer sediment was delivered to the prograding delta, which caused most of the prograding delta surface to braid intensively and to gradually erode the remaining portion of right terrace deposit in the proximal to medial areas of the prograding delta. This deposition and braiding at the downstream end of the original delta caused a temporary increase in bed elevation (Figure 7.23d). The period of erosion may have been caused by a minor fluctuation in the flow hydraulics, perhaps a turbulent sweep, or a small alteration in the direction of flowlines at the base of the terrace that was sufficient to destabilise and entrain a few gravel grains. Whatever the cause, it suggests that this portion of the channel bed at least was very close to a threshold of instability that required very little further disturbance to be crossed. This behaviour also highlights the highly episodic, and possibly chaotic, nature of some of the system response to dam removal.

The flood flows in all three runs followed the curvature of the left basin boundary and eroded only small amounts of the original delta. In runs 1xL and 3xL erosion occurred mostly through extensive incision that triggered mass wasting in



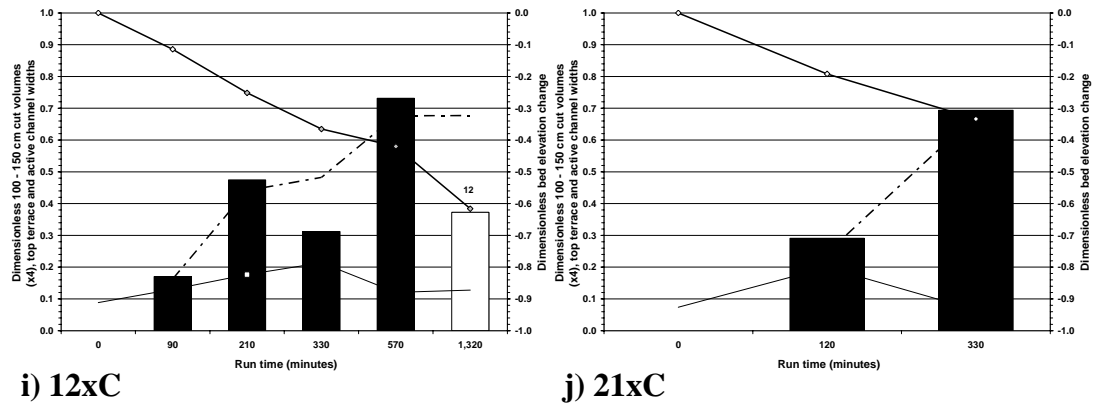
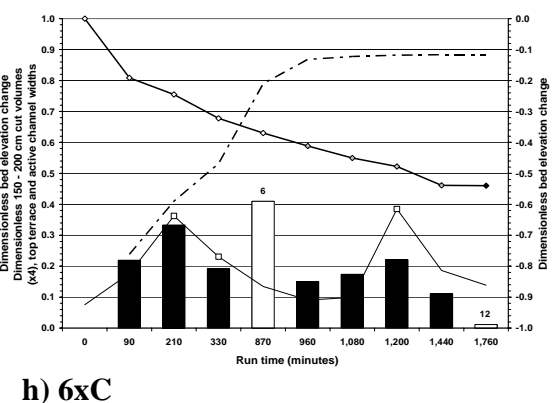
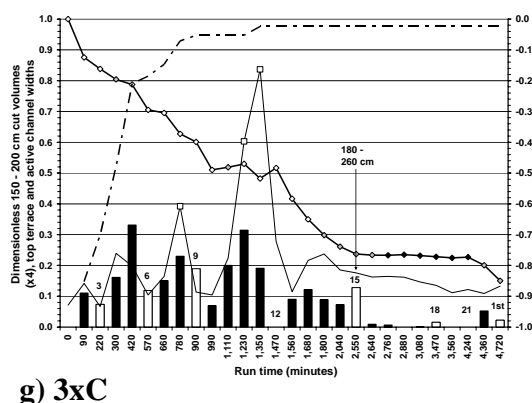
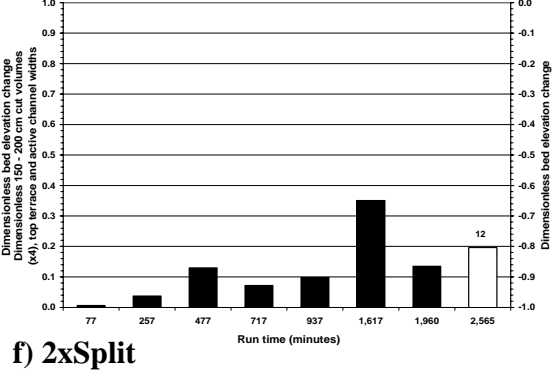
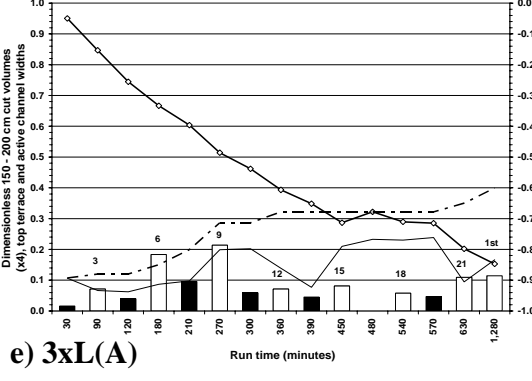
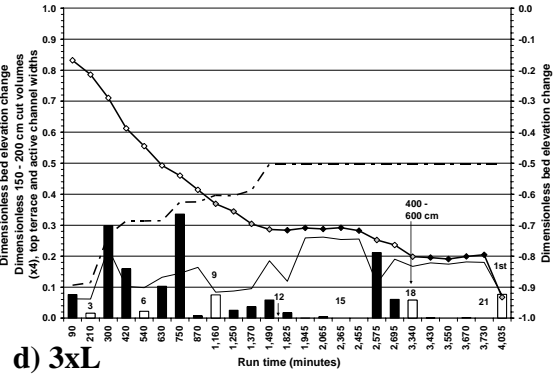
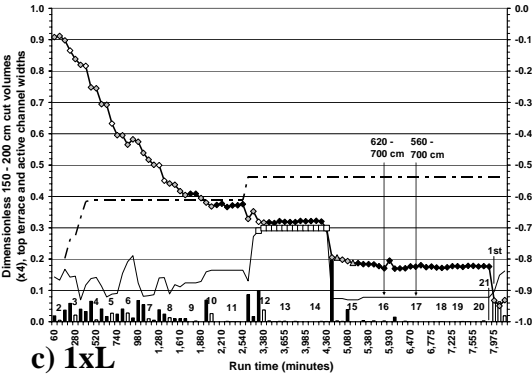
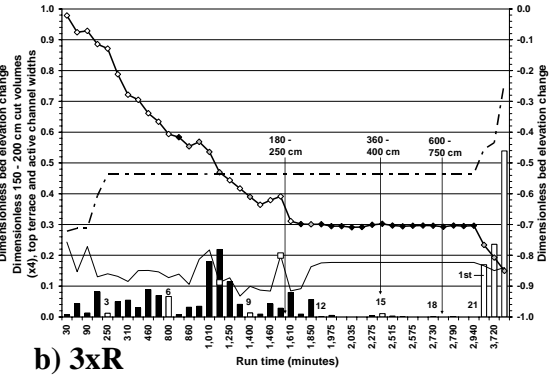
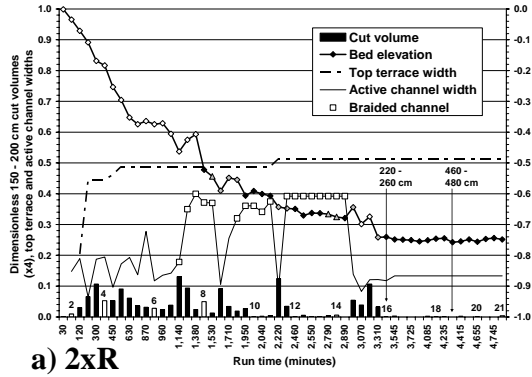


Figure 7.20. Dimensionless cut volumes, active channel widths, cumulative top terrace widths and cumulative thalweg elevation change from 100 – 150 cm in the original delta area.

parts of the proximal original delta (Figures 7.18c&d to 7.19c&d), which was quite extensive over the course of the three floods in run 1xL. During the two-year flood in run 3xL(A) there was less incision than during the same flood in the other two runs (Figures 7.18e to 7.19e) but a larger portion of the original delta was eroded (Figure 7.12).

7.3.3 Central runs

Runs 3xC, 6xC and 12xC followed a very similar pattern of response, despite the large differences in magnitude of baselevel drop and, in the case of run 3xC, not allowing a static equilibrium condition to develop between drops. Initially, the incising channels formed a right hand bend that quite rapidly cut through the right terrace in the distal area of the original delta to reach the basin boundary. The entire terrace was soon eroded away as the bend apex migrated downstream along the basin boundary. The increasingly strong right hand curvature of flow through these growing bends introduced increasingly strong left hand curvature in the flow immediately upstream, which caused a left hand bend to erode through the left terrace in the medial area of the original delta until it reached the basin boundary (Figures 7.22g-i - 7.23g-i). The left hand bend did not develop significantly in run 3xC until the right hand bend had completely eroded the right distal terrace and found a shorter path into the reservoir along the right basin boundary, since this introduced the necessary flow energy to erode the left medial terrace. In runs 6xC and 12xC, however, the two bends developed more or less in tandem. As the left hand bends developed they increased



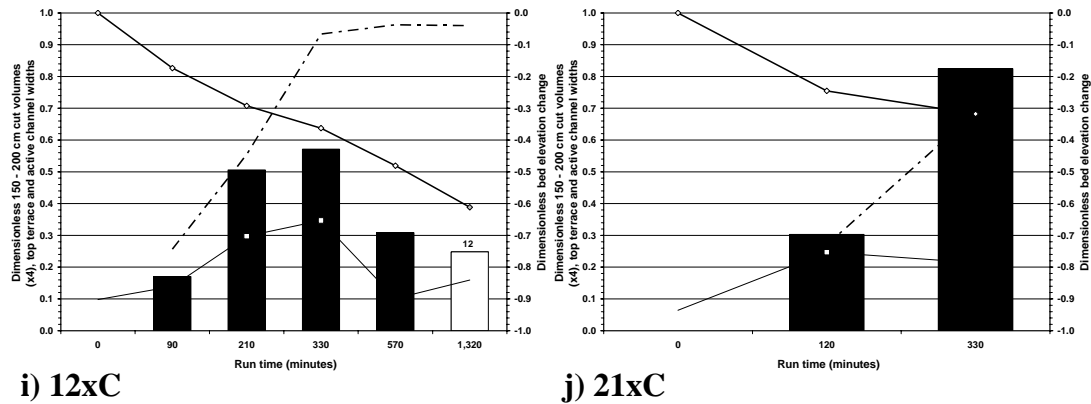
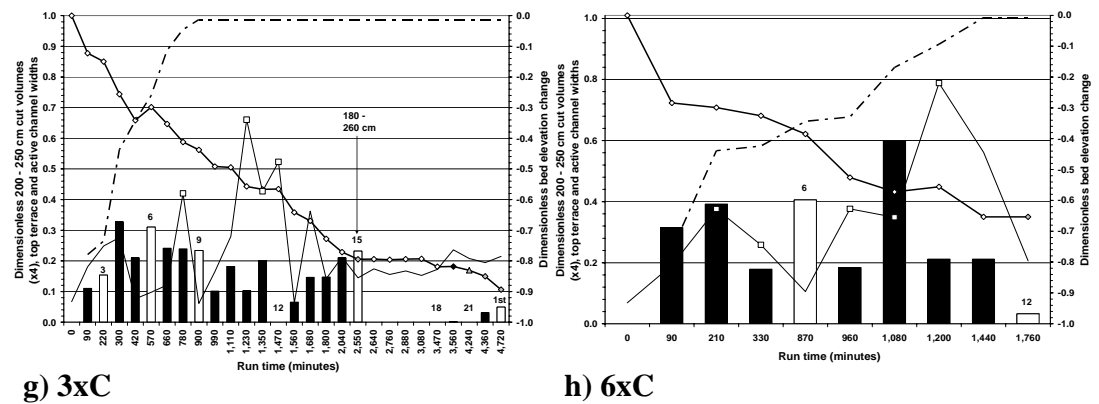
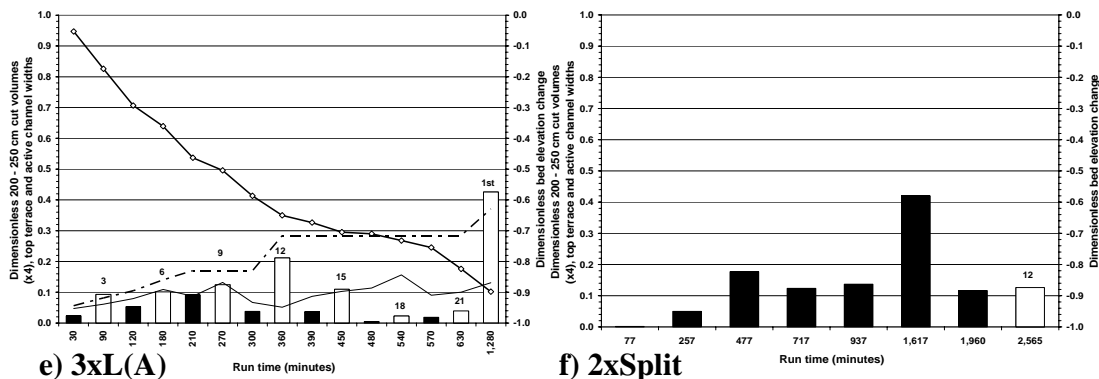
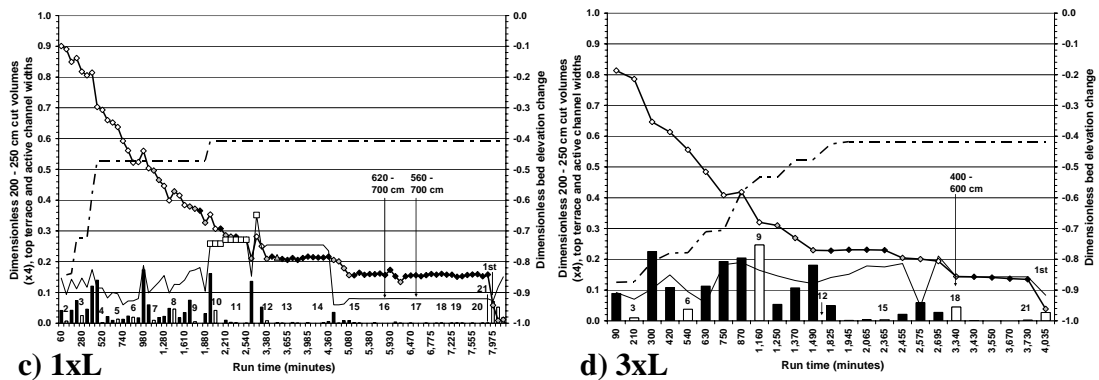
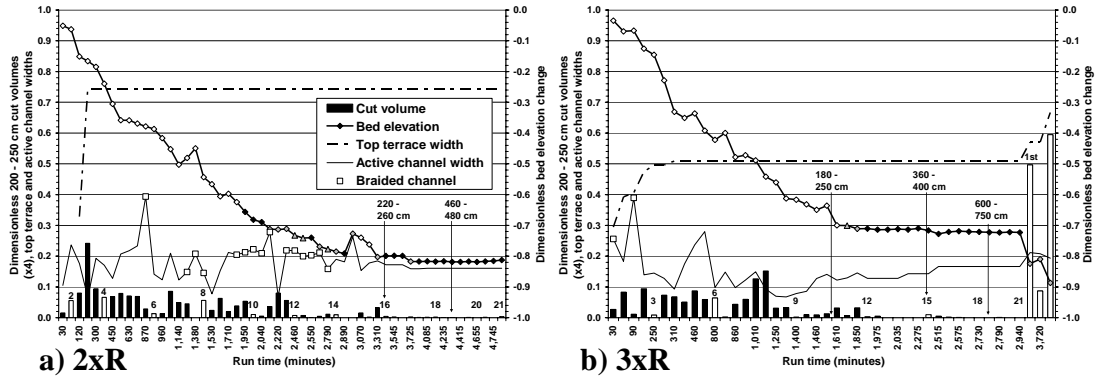


Figure 7.21. Dimensionless cut volumes, active channel widths, cumulative top terrace widths and cumulative thalweg elevation change from 150 – 200 cm in the original delta area.

the curvature of the left terrace edge, which increased the angle at which flow was deflected towards the right basin boundary until this was at, or very close to, 90° . In turn, this increased the angle of flow curvature through the left hand bends via positive feedback.

The bends in the distal area of the original delta consistently developed right hand bends probably because of the change in direction of the pilot channel at $Y = 84.5$ cm, which effectively acted as a shallow bend that deflected streamlines towards the left bank downstream from its apex. In turn, this deflected them towards the right bank in the downstream half of the original delta. This deflection can be seen by following the surface waves that are visible in the first few seconds of the Run12xCcam1 movie and by the sinuous thalweg in the first few seconds of the Run21xCcam1 movie. In all three runs, growth of the right hand bends was then amplified by essentially the same mechanism of positive feedback described above. In run 3xC, slight erosion of the left channel bank in the medial delta area increased the angle at which flow was deflected into the right bank. This angle of attack was subsequently locked in place by the exposure of an armour layer strip on the left half of the channel bed, thus allowing the right hand bend to cut through to the basin boundary through extension that was not accompanied by further translation or rotation. In run 6xC, an armour patch developed in the left half of the channel at about 140 cm that caused water to preferentially flow down the right half of the channel and into the right bank. As the channel incised, the armour patch emerged as an armoured point bar head, which increased the angle of flow attack on the right bank. Similarly, in run 12xC upstream-migrating incision caused the sinuous thalweg to incise, which

caused the slower-velocity portions of the channel bed to emerge as point bars that amplified the angle of right bank attack.



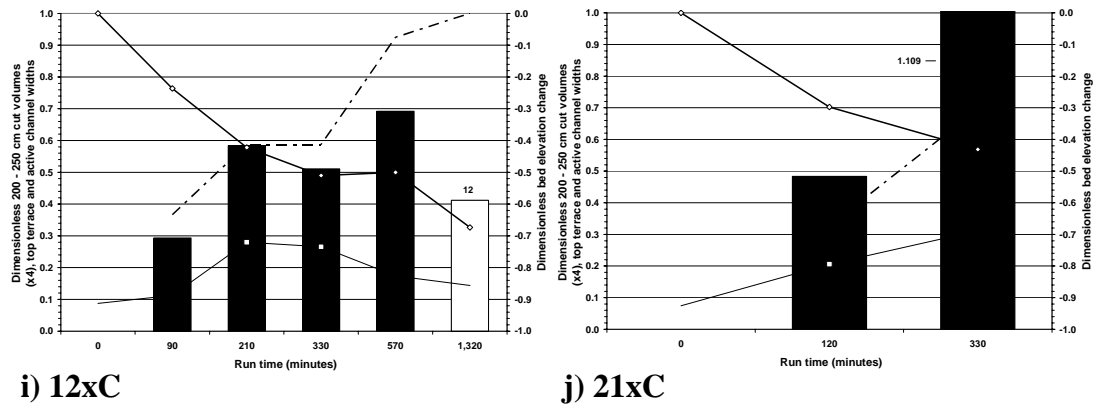
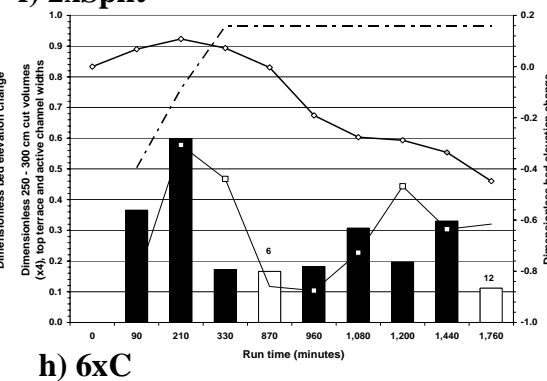
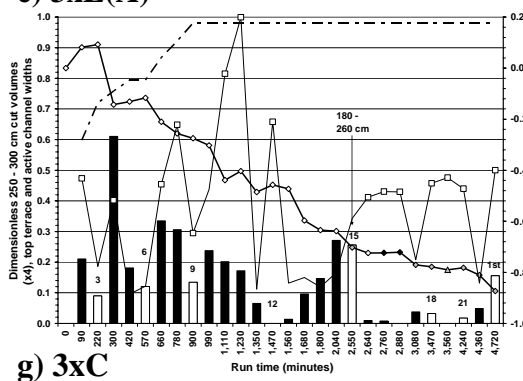
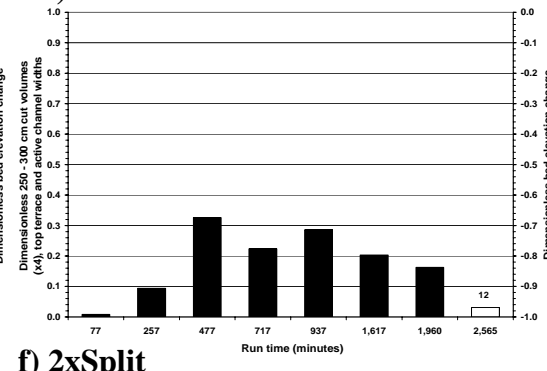
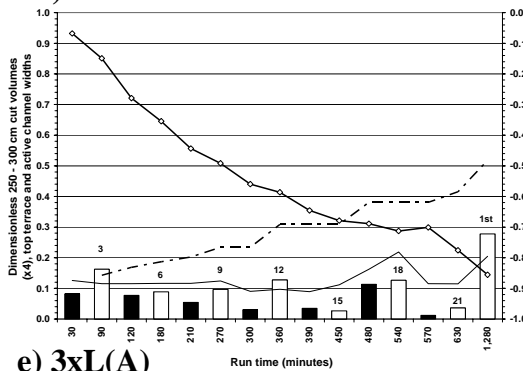
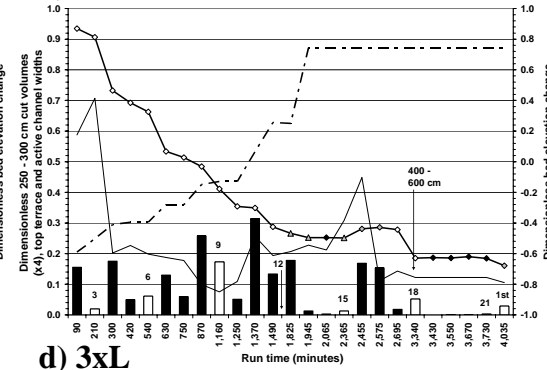
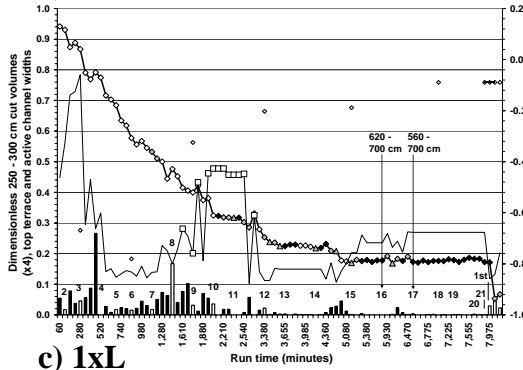
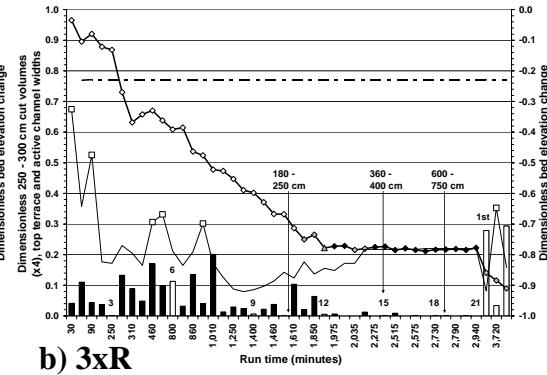
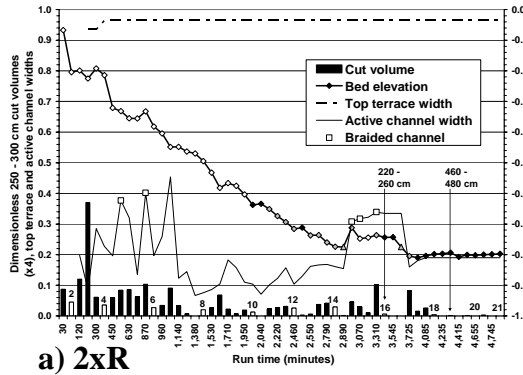


Figure 7.22. Dimensionless cut volumes, active channel widths, cumulative top terrace widths and cumulative thalweg elevation change from 200 – 250 cm in the original delta area.

There followed a period of left hand bend development, in which the bend apices and the channel segments exiting the bends migrated downstream at angles ranging from about 45° to 90° (cross-delta), eroding very substantial portions of the left medial and distal original delta terrace as they did so. This occurred up to 6/21(15/21) in runs 3xC and 6xC and in the early stages of 12/21(9/21) in run 12xC (Figures 7.20g-i – 7.23g-i). Multiple waves of BELWALB, partial and complete armour layer break up migrated into the proximal area of the original delta while this was occurring, which caused some erosion of the right terrace in the proximal and medial areas of the original delta (Figures 7.18g-i – 7.20g-i) and led to the formation of a complete meander loop. In run 3xC, the erosion of the right terrace was extremely limited and the resulting bend was really no more than a proto-bend whose development into a more fully developed bend was probably prevented by the well developed armour layer and the relatively low energy slope. In runs 6xC and 12xC, however, erosion of the right terrace was more extensive and the bend and meander loop was much more clearly defined.

Following periods of meander-loop growth (which were very short in the case of run 3xC), the flow avulsed out of its meandering channel. In all three runs this took place just downstream from the apex of the upstream bend of the meander loop, at the base of the right terrace in the medial area of the original delta, between about 120 and 140 cm. In runs 3xC and 6xC avulsions occurred towards the end of the 6/21(15/21) interval and in run 12xC shortly after 330 minutes run time (Figure 7.20g-i). There then followed periods of dynamic channel movement (although this period was very brief in the case of run 6xC), during which time quite large



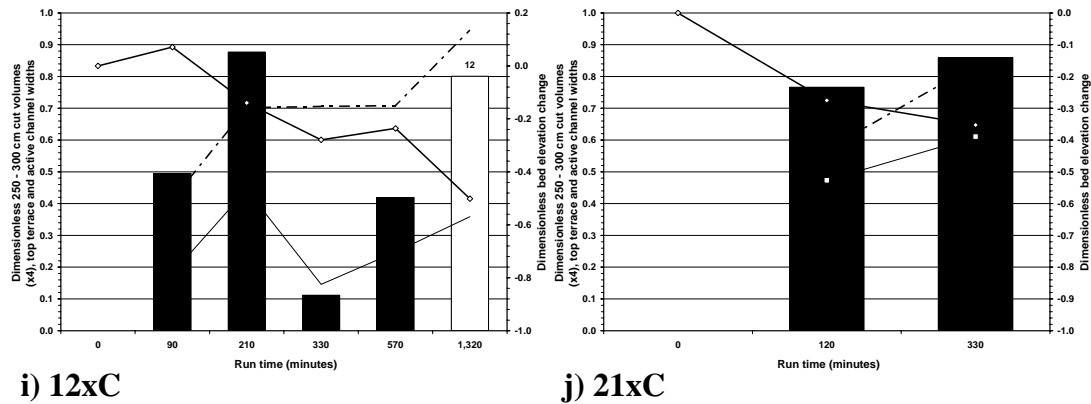


Figure 7.23. Dimensionless cut volumes, active channel widths, cumulative top terrace widths and cumulative thalweg elevation change from 250 – 300 cm in the original delta area.

proportions of the left and right original delta terraces were eroded and during which multiple waves of BELWALB, partial and almost complete armour layer break up migrated various distances into the proximal area of the original delta (Figures 7.18g-i – 7.19g-i), delivering gravel further downstream. This period of adjustment was particularly vigorous in run 12xC. The meander loops then reformed in all three runs in almost exactly the same position as the previous loops, but with a slightly better developed meander geometry, possibly because the upstream bend in particular was armoured, which partially locked in the meander loop.

A second period of avulsion then took place in all three runs. In run 3xC this occurred during the 12/21(9/21) interval, just downstream from the apex of the upstream bend of the loop between about 80 and 100 cm. It caused complete break up of the armour layer and the channel very rapidly eroded a large portion of the remaining right terrace in the proximal and medial areas of the original delta (Figures 7.18g – 7.19g), attaching itself to and straightening against the sloping proximal delta area boundary before rapidly incising by a large amount (Figure 7.18g). In run 6xC the channel also avulsed downstream from the apex of the upstream bend, but between about 140 and 180 cm (Figures 7.20h – 7.21h). This caused multiple waves of partial and complete armour layer break up to migrate to the upstream end of the proximal original delta, which allowed the channel to move across a substantial portion of the delta surface and to transport gravel further downstream. The channel eventually stabilised in the right half of the original delta and armoured throughout this entire area (Figures 7.18h – 7.19h). In run 12xC the channel avulsed out of the upstream end of the upstream bend of the meander loop at about 80 cm, but rapidly

stabilised in a mostly single-thread planform that was heavily armoured along the entire left half of the original delta topset. This armour layer was then completely broken up as the channel re-incised and stabilised in a narrow and heavily armoured single-thread channel against the left basin boundary through the entire delta area (Figures 7.18i – 7.23i).

It is noteworthy that all three runs experienced essentially the same sequence of channel adjustments, and that the second avulsion and major period of channel adjustment in run 3xC only took place once the 12th dam piece had been removed and thus after the same amount of base level drop as in runs 6xC and 12xC. This suggests that, when the incising channel was mostly free of interference from the basin boundary or was subjected to approximately the same type and amount of interaction with the boundary, it responded in a very similar way following the same amount of total base level drop, irrespective of the size of the individual increments of drop.

Prior to all the avulsions, the channel downstream from the armour layer had assumed a fairly narrow, single-thread configuration. This concentrated boundary shear stresses on the channel bed, allowing sediment to be transported more effectively and incision to propagate upstream. This incision then generated either BELWALB or a partial armour layer break up, one or the other of which triggered all the aforementioned avulsions. More generally, in all the runs, a single-thread channel was a necessary pre-requisite for incision to migrate upstream. As soon as the incision generated a sufficiently large volume of bedload transport that the channel braided, incision would cease until one of the braids was able to capture all the flow and reform a single-thread channel.

The channel in run 21xC evolved somewhat differently to the three other central runs. A very sinuous thalweg developed rapidly along the entire length of the original delta topset. Because incision was able to migrate rapidly downstream, however, it eroded both left and right banks/terraces evenly along their entire length, thus creating a very symmetrical trench within which the channel lay. It was only once this widening had migrated to the very upstream limit of the original delta and become attached to the left basin boundary that asymmetry was introduced to the trench. As occurred with the initial left hand bends in the medial area of the original delta during the other three central runs, the channel migrated downstream along the left basin boundary, eroding the left terrace from the upstream to downstream. This

deflected the flow at an increasingly large angle across the delta surface and into the right proximal and medial delta terrace. The channel rapidly cut through to the medial right basin boundary, by which point a bend had formed and flow exiting the bend had eroded the entire downstream half of the left distal terrace. The bend apex migrated along the right basin boundary, eroding most of the right medial terrace and a large part of the right distal terrace. At this point the bend's amplitude was the full width of the reservoir basin and would almost certainly have been larger had the delta been wider. The run was terminated due to time constraints, but there seems little doubt that, had the run continued, the channel would have rapidly eroded the remaining right distal terrace. In addition, the bend's upstream arm would have eroded a substantial portion and possibly the entire left delta terrace as it moved along the left basin boundary. Another point to note is that the steep energy slope through the original delta area allowed the flow to entrain and remove all the gravel from the eroded banks/terraces and transport it far downstream, thus preventing the formation of a static armour layer anywhere in the original delta (Figures 7.18j – 7.23j).

While the bend became very well developed it did not lead to a meandering pattern over the rest of the prograding delta surface. While the upstream half of the bend remained single-thread, the downstream half repeatedly switched between being single-thread, which directed flow more strongly towards the left terrace, and braided, during which the flow was oriented in a more downstream direction (Figures 7.21j – 7.23j). Braiding in the flow over the prograding delta surface, which was intensively developed and persisted for the entire run, was caused by the steep surface slope and by the large bedloads being generated in the original delta area. Unfortunately, the run was terminated before the delta surface slope and the rate of bedload generation could be reduced, so it is not known whether a meandering pattern would subsequently have been established over the entire length of the delta. It is therefore not clear whether the meander bend is an isolated feature that is forced or induced (by the upstream end of the left terrace), as occurred in the experiments of Quraishy (1944), Friedkin (1945) and Schumm and Khan (1972), or whether it would be capable of spawning a fully-developed and self-sustaining meandering planform, as observed by Clifford (1993).

Runs 3xC and 12xC both eroded almost the entire left and right original delta terraces by the 12/21(9/21) interval, which meant that the channels could move over the full width of the entire prograding delta surface, thus preventing the development

of any high, prograding delta terraces. Runs 6xC and 21xC were also well on the way to achieving this when they were stopped. The only significant terraces present at the end of dam removal in run 3xC were formed during and after the 15/21(6/21) interval, through the left half of the original delta and the proximal and medial prograding delta areas. At this point flow was exiting the right half of the original delta area, so the channel and terrace configuration was very similar to that of the right marginal runs, except that the terraces were much lower. This indicates that the central runs were much more effective at distributing the sediment evenly throughout the entire reservoir basin, a key sediment management objective for the removal of the prototype (section 2.3.4).

To further investigate morphodynamics within the reservoir, direct comparisons between the right marginal, left marginal and central runs will now be made for bed elevations, longitudinal profiles, terrace widths, channel widths and planforms.

7.4 Adjustments to channel bed elevations and the longitudinal profile

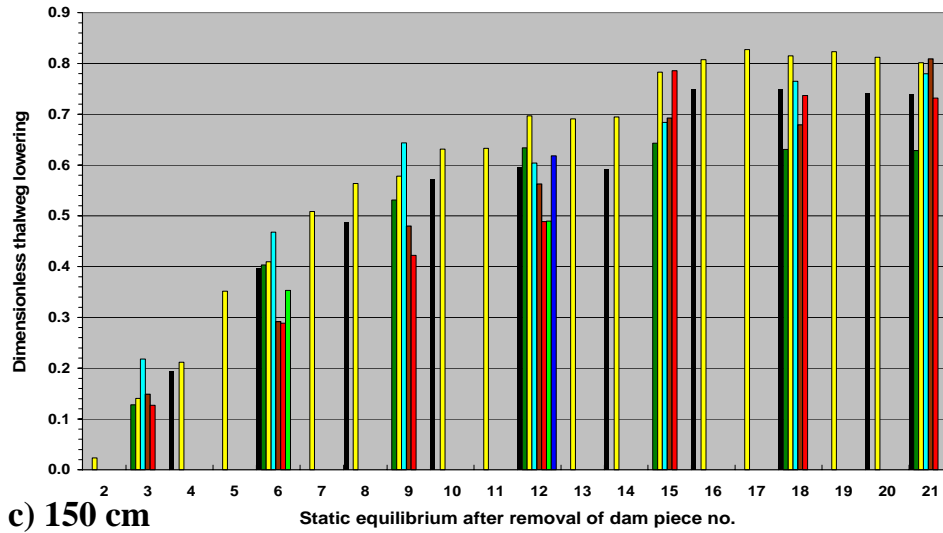
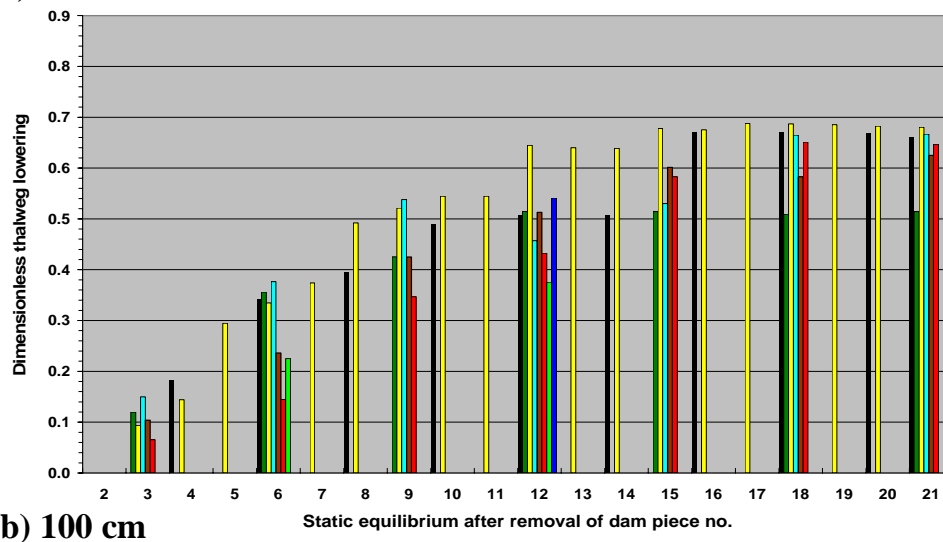
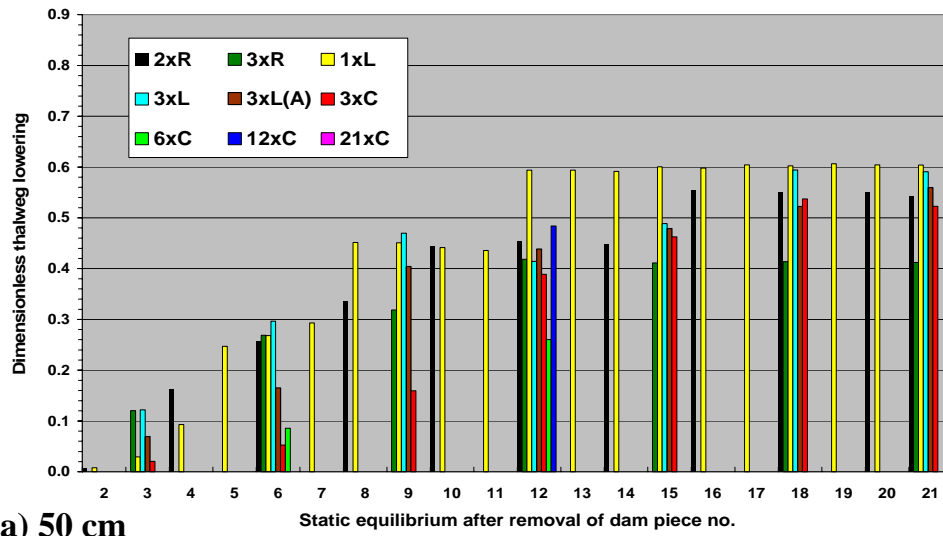
Across the delta surface, most of the changes in channel bed elevations were complete by the time that the 12-piece equilibrium condition had been attained. There were, however, clear differences in the distributions of change between the marginal and central runs. Along the full length of the original delta, channels generally incised more in the marginal runs than in the central and accelerated removal runs during the dam removal phase, with the left marginal runs generally incising more than the right ones, especially downstream of 150 cm. There were, however, three exceptions to this general finding. First, run 12xC incised the proximal original delta more than all marginal runs except run 1xL (Figure 7.24a-b). Second, run 3xR incised less than run 3xC after the 12-piece equilibrium due to the grade-controlling effect of the hard basin boundary. Third, run 3xL(A) generally incised more than the right marginal runs from the 18 to the 21-piece equilibrium along the entire original delta surface.

Before considering the evolution of the longitudinal profile (Figure 7.25), it should be noted that the current thalweg-seeking algorithm is imperfect in that it does not always find the path of the downstream-most lobe of the prograding delta front in the reach where it crosses the topset. Consequently, the thalweg plots sometimes fail

to reflect the true position of the downstream-most foreset surfaces. This leads to the plots sometimes under-representing differences between central and marginal runs. Another artefact of the thalweg-seeking algorithm is the artificial ridges in the plots for runs 3xR (Figure 7.25g-i) and 2xR (Figure 7.25h) between about 500 cm and 700 cm. These occur because the algorithm finds a ‘thalweg’ that deviates sharply from the centre towards the edge of the delta surface, taking it rapidly into an area of higher elevation. This could be resolved by adjusting the algorithm to consider only points with lower elevations than the preceding point(s) upstream, or those whose elevation falls within a pre-defined range of those upstream. However, despite these shortcomings, the plots are fit for purpose in that they do capture and display the most important facets of system behaviour.

Perhaps most significantly, the channels in all runs adjusted their long profiles to essentially the same slope by the end of dam removal (Figure 7.25h). Downstream of about 440 cm, and ignoring the artificial ridges, this slope was essentially the same as that of the empty basin thalweg, although upstream it was slightly steeper due to the armour layer stabilizing the bed at a slightly steeper slope. The steeper slopes upstream were, however, mostly eliminated by the two-year flood flows (Figure 7.25i), although the thalweg elevations and slope of runs 3xR, 3xC and 3xL(A) upstream of 280 cm remained slightly greater than those of runs 1xL and 3xL (Figure 7.25i). In the case of runs 3xR and 3xC, this was because the final channels were located to the right of the original delta area - where the empty basin elevation was slightly higher and steeper (Figure 8.5b). In the case of run 3xL(A), this may be the result of large amounts of energy being dissipated through intense turbulence against the hard basin boundary, which reduced the capability of the flood flows to drive incision. Throughout the entire reservoir area, and irrespective of the magnitude of drop in baselevel, the channel was therefore generally able to return to its pre-dam slope shortly after the end of dam removal. This occurred despite possible scale effects related to the size of the armour-forming sediment grains and model entrance effects that reduced flow velocities and shear stresses in the upstream reaches of the original delta (section 8.1).

Results for run 3xC are particularly interesting (Figure 7.25c-e) because the convex upwards section of the profile extended progressively further upstream from the topset-foreset interface, until it occupied almost the full length of the profile



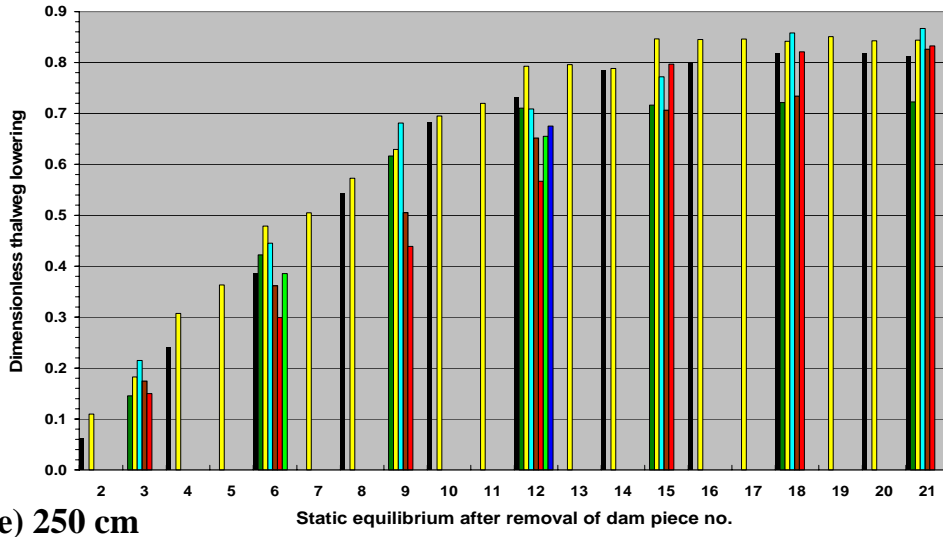
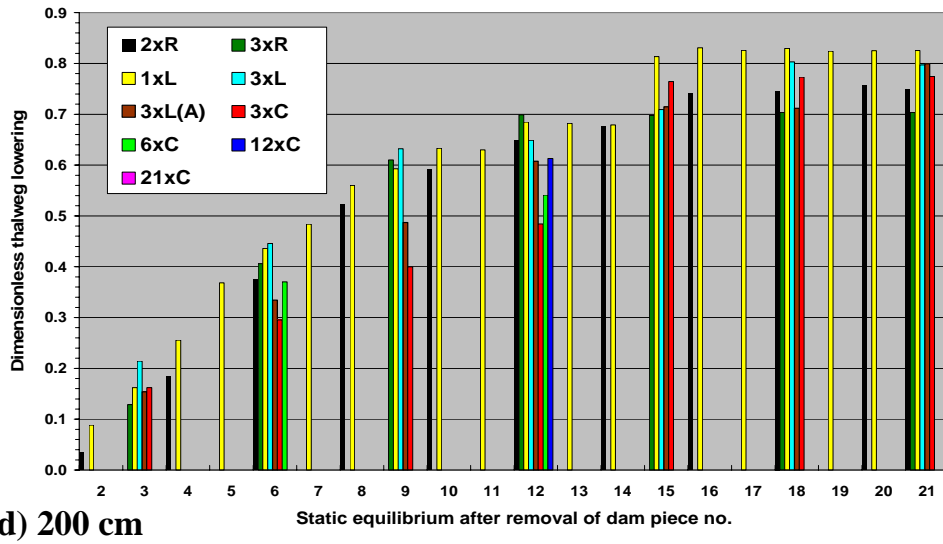
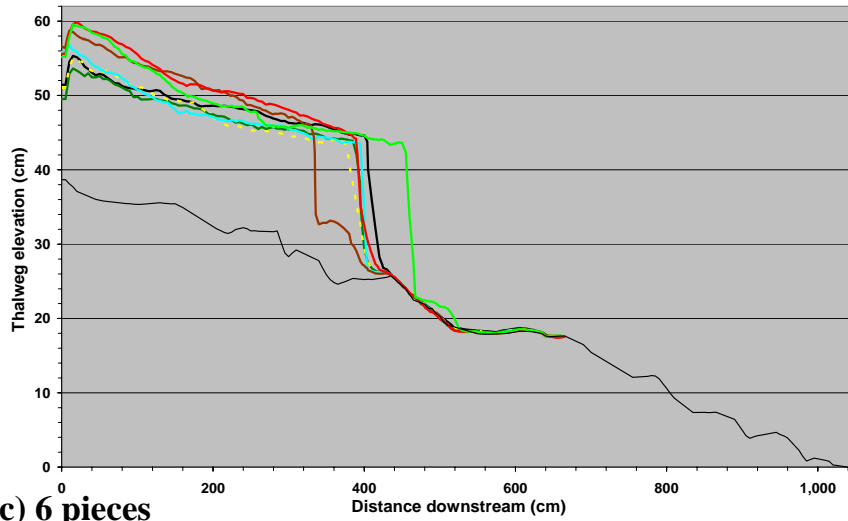
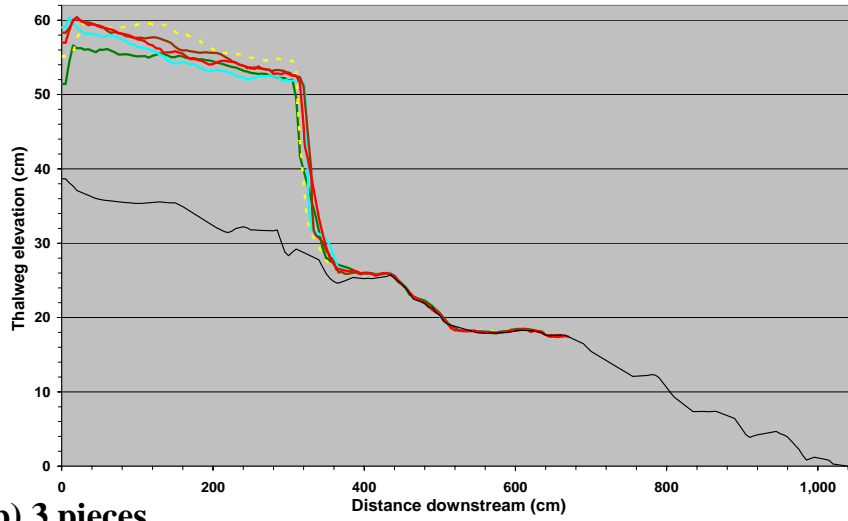
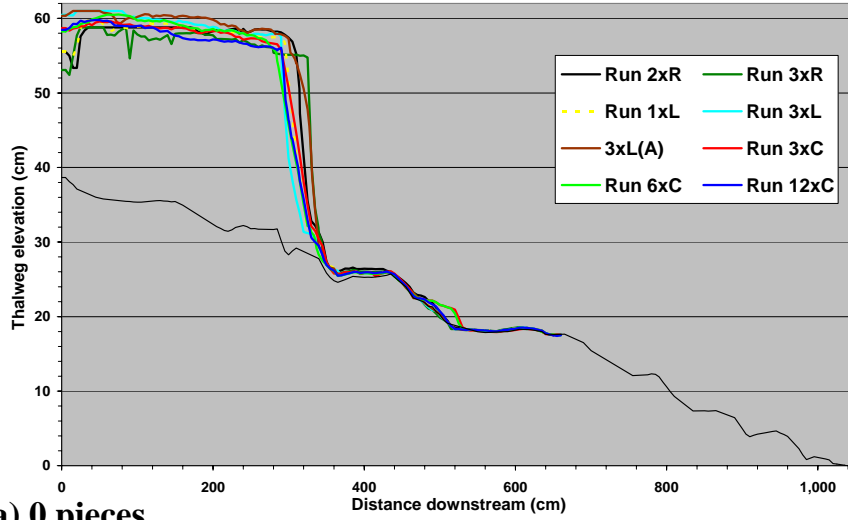
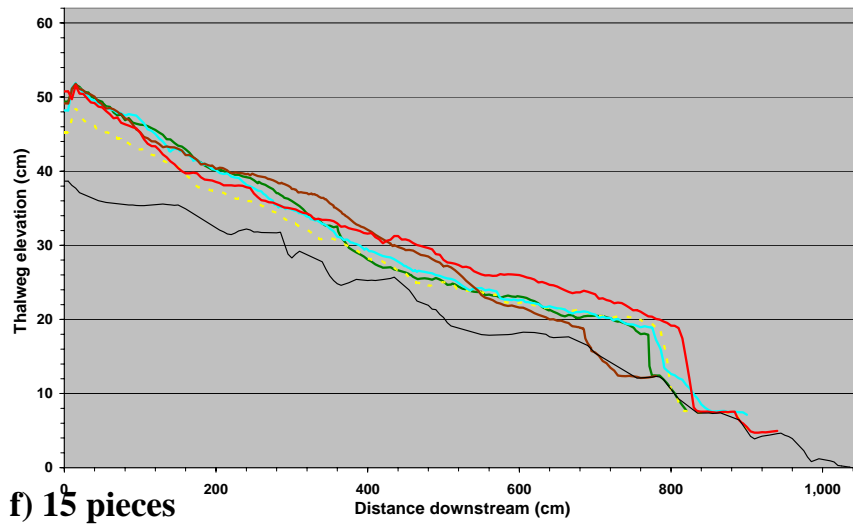
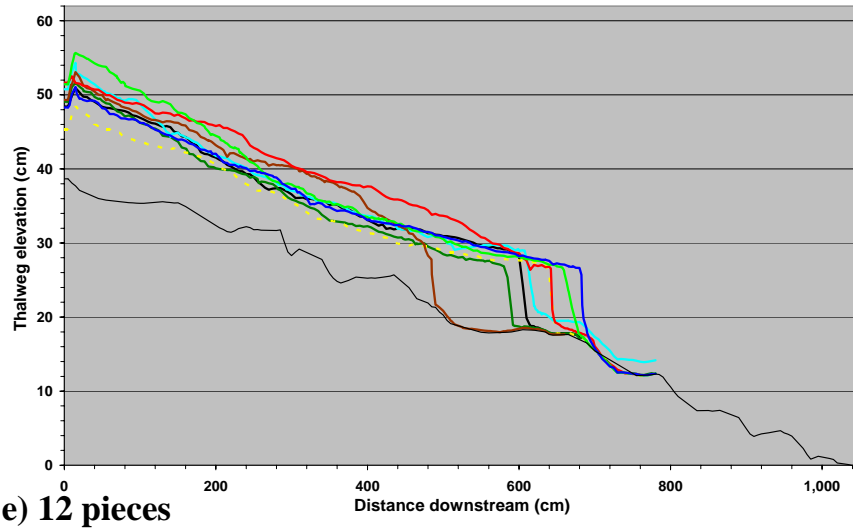
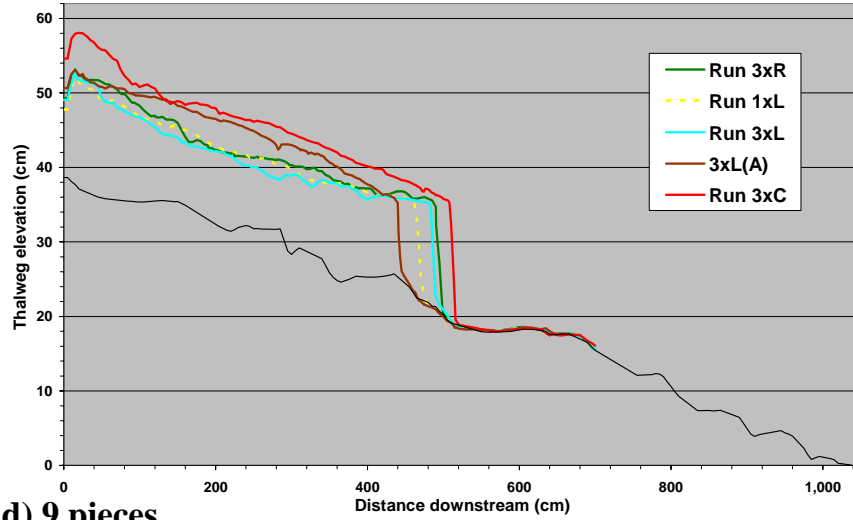


Figure 7.24. Cumulative change in dimensionless thalweg lowering in the original delta area.

(Figure 7.25e). In contrast, most of the profiles for the other runs were either concave upwards or more or less flat. This upwards convexity was probably caused by the fact that large volumes of sediment were being eroded but not completely transported out of the original delta area prior to the next incremental drop in base level. The scans at the 6, 9 and 12-piece equilibrium conditions thus recorded a delta surface channel that was frequently wide and braided, particularly downstream of 200 cm (Figures 7.21g – 7.23g).





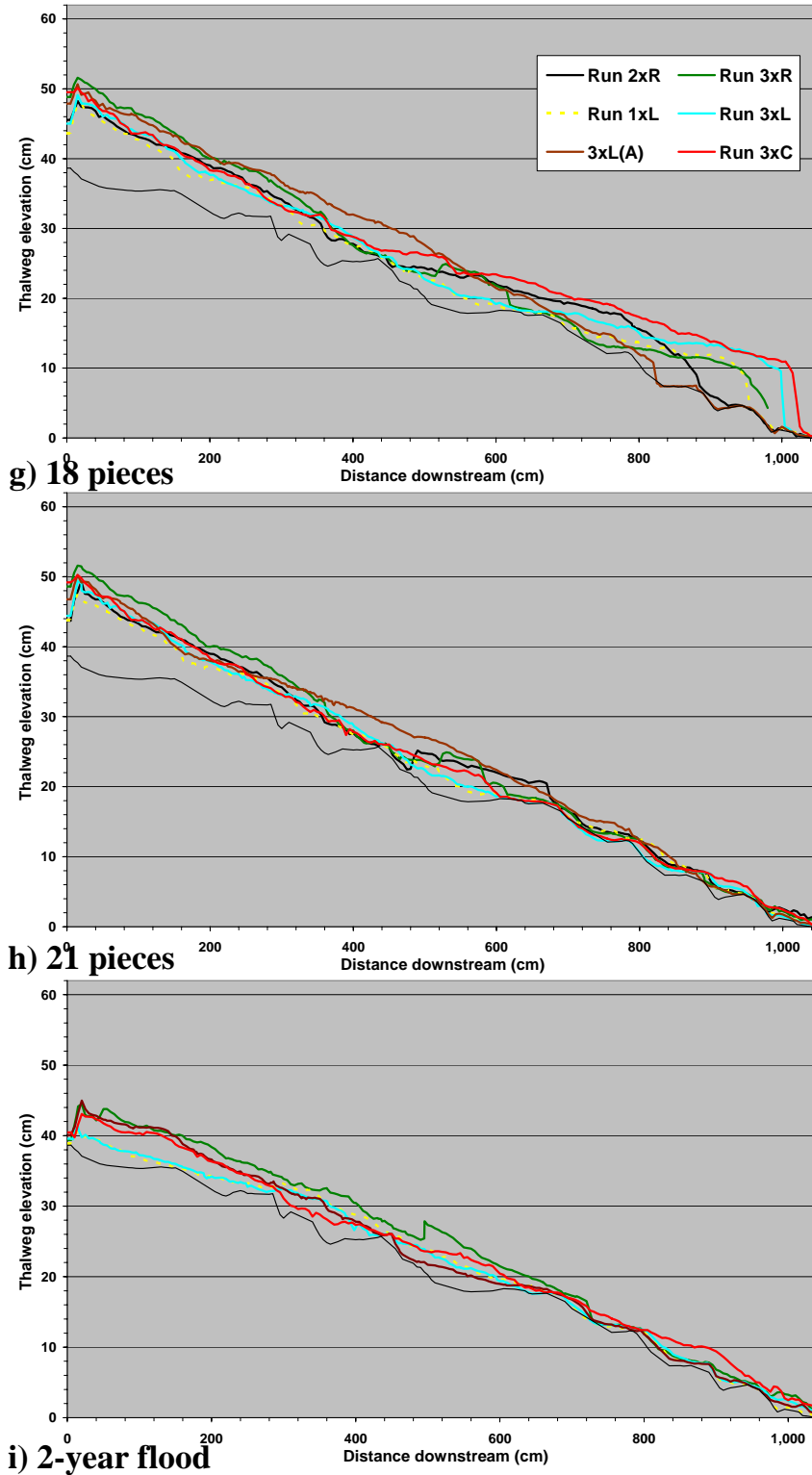


Figure 7.25. Longitudinal profiles at equivalent static equilibrium positions during dam removal.

7.5 Cross-sectional adjustments

7.5.1 Top terrace widths

Following the 6-piece equilibrium condition, erosion was greater at all cross-sections and a larger proportion of the delta width was eroded in the central runs than in all but one other run. The only consistent exception to this general finding occurred during run 2xR, in which an almost equal proportion of the delta width was eroded at the 300 cm cross-section from the 6-piece equilibrium onwards, and at the 100 cm cross-section, in which the width exceeded that of the central runs from the 12-piece equilibrium onwards (Figure 7.26). Also, run 3xL(A) eroded a smaller proportion of its terrace in the distal original delta area than any other run (Figure 7.26d-e). However, this was probably a local effect that occurred because the leftwards curvature of the basin boundary was particularly well developed in this area and this directed the flow away from the left terrace more strongly than at any other point along the boundary.

7.5.2 Active channel widths

Over the first 150 cm of the delta, channel widths rarely occupied more than about 40% of delta surface width, with the maximum occupancy being a short-lived peak of 71% during run 2xR (Figure 7.27a-c). This partly reflects the stabilizing effect of armour layers that were almost always present and strongly developed between 0 and 150 cm (Figures 7.18 – 7.23). Furthermore, for significant channel widening to develop, it was necessary for a sufficient quantity of the terraces to have been eroded to provide the lateral space required for a braided planform. Nevertheless, it is important to note that marginal runs 1xL and 3xL generally had the narrowest channels and the lowest frequency of changes in width. Runs 2xR and 3xR and the four central runs generally had larger average widths, bigger peak widths and higher frequencies of width change.

The results reveal a significant change in behaviour at the 200 cm cross-section. While the majority of channel widths downstream of 200 cm still occupied less than 40% of the delta surface, there were increases in the frequency and amplitude of channel switching for certain runs, including runs 2xR, 3xC and 6xC at 200 cm (Figure 7.27d); runs 3xC and 6xC at 250 cm (Figure 7.27e); and all runs at

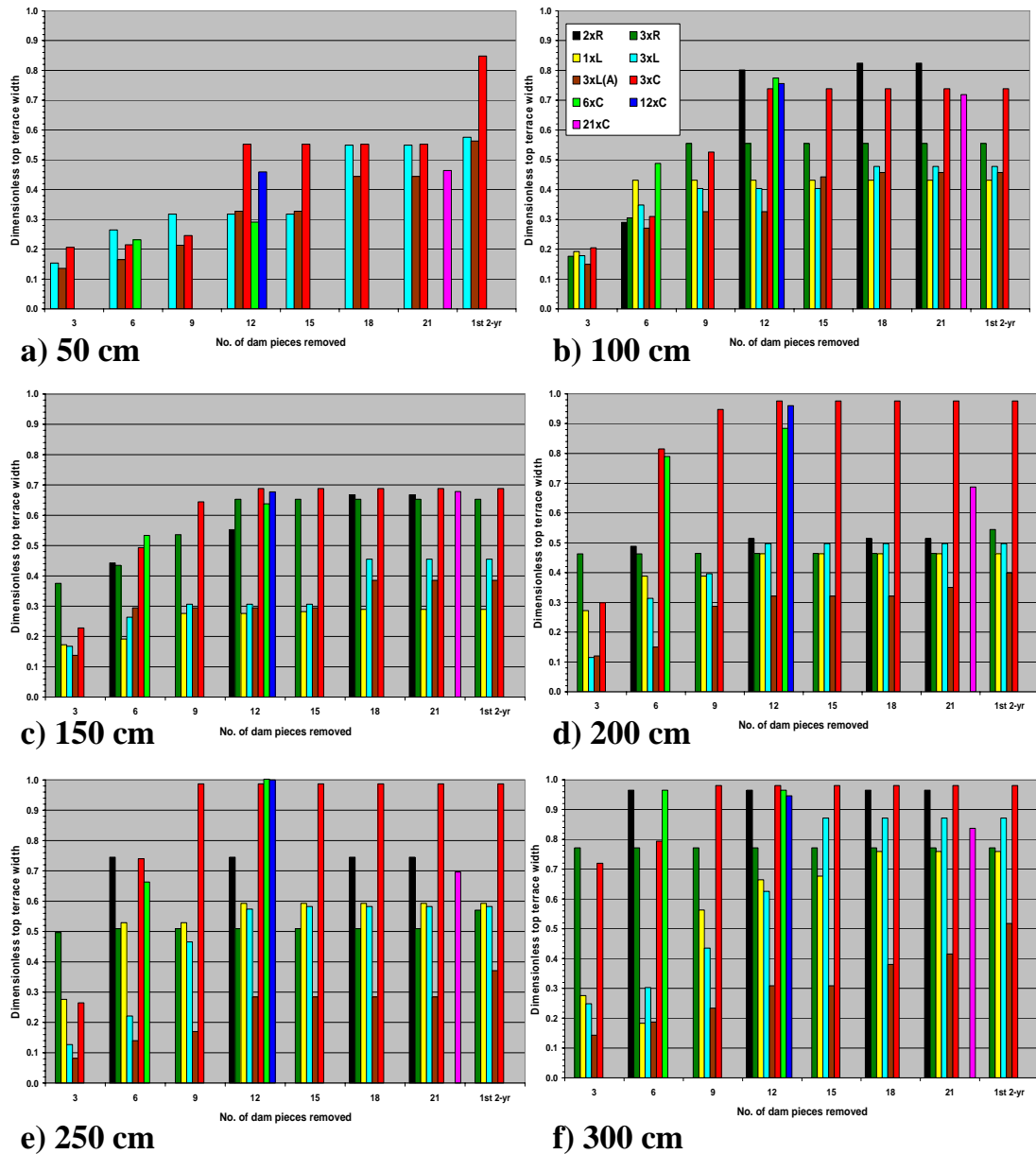
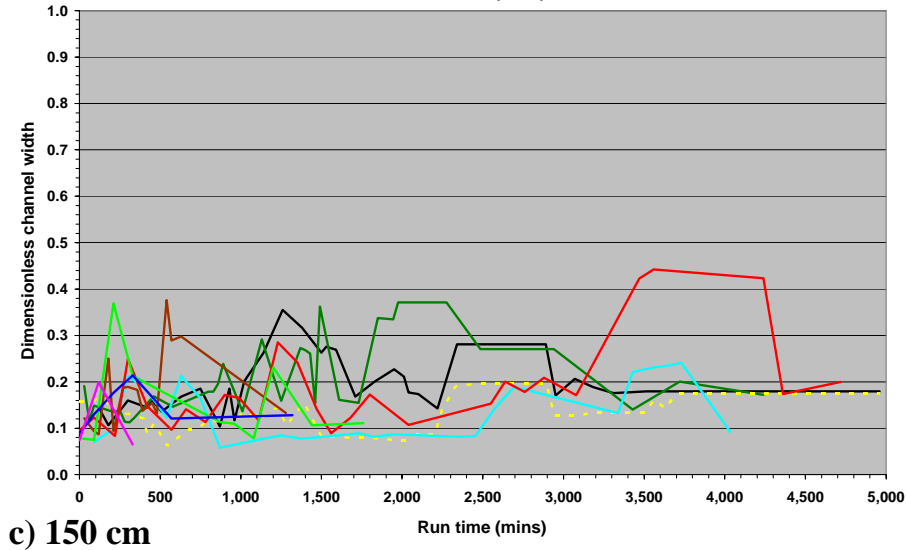
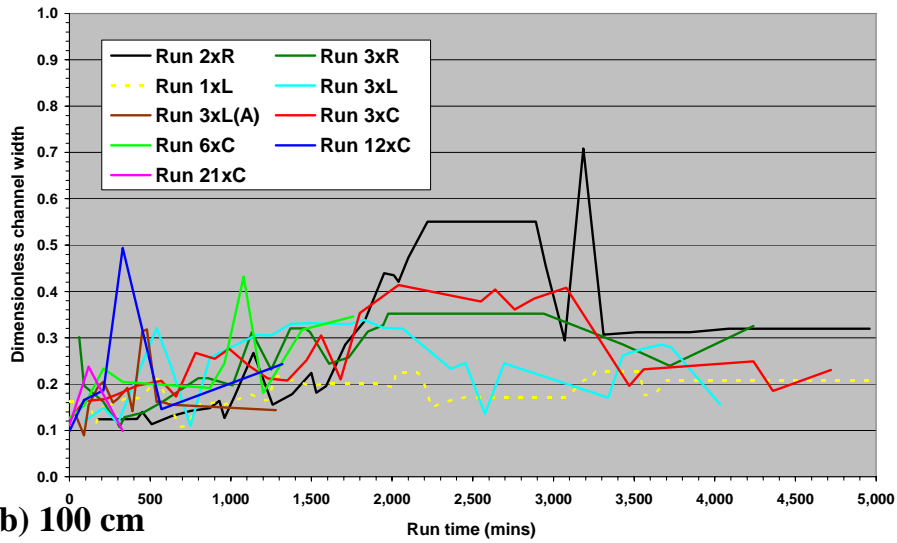
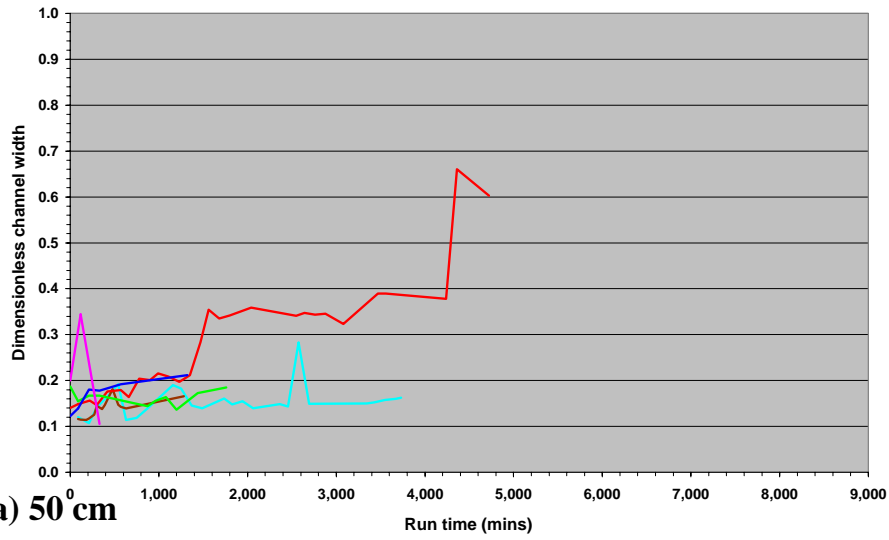


Figure 7.26. Dimensionless top terrace widths after equal amounts of baselevel drop.

300 cm (Figure 7.27f). At 300 cm, all runs demonstrated particularly dynamic adjustments during the first 2,000 minutes of run time because of all cross-sections in the original delta, this one was closest to the area of maximum disturbance. It was also close to the widest point of the delta surface at the start of each run and was thus located in the part of the original delta where lateral channel movements were least restricted by the presence of the basin boundary and large terraces. Maximum widths for all runs except 2xR and 12xC exceeded 50% at one time or another, mostly during



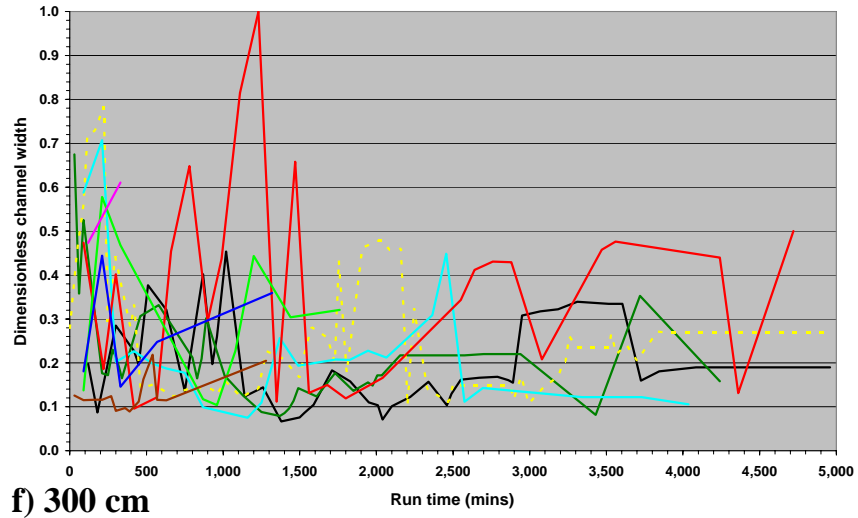
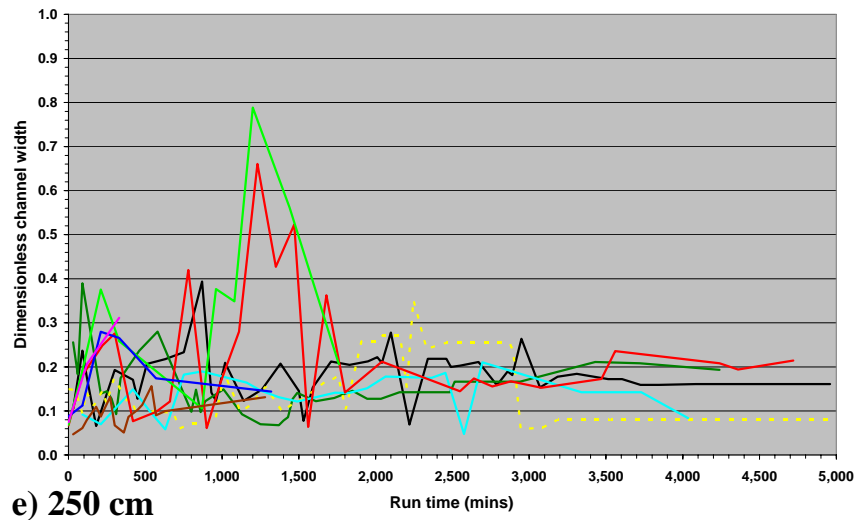
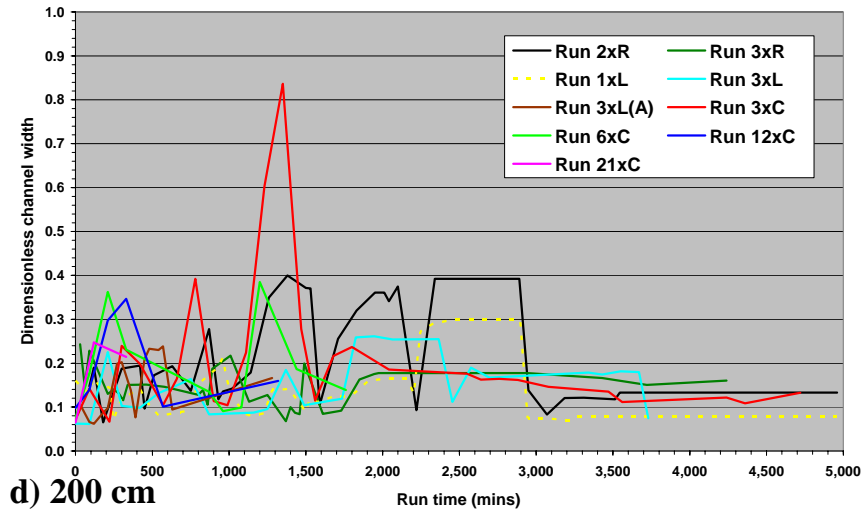


Figure 7.27. Dimensionless active channel widths. The duration of the run 1xL plots has been scaled to that of run 2xR in order to make the graphs more legible.

the very early stages of the run, with run 3xC doing so on three separate occasions, including one event when the channel width reached 100% of delta surface width.

7.6 Adjustments of channel planform

The channel planform in every 50-cm reach of the delta surface at every time step for each run was classified into one of nine categories. The broad classes were: braided, single-thread, and transitional. Each of these three main classes was subdivided according to whether the channel bed was fully armoured, unarmoured, or partially armoured, with the latter being defined as a fully developed armour layer that only extended partway along a 50-cm section of the delta surface. This yielded a total of nine planform categories. In the event, the transitional planform class and the partially armoured braided and single-thread categories were excluded from further analysis because together they accounted for only about 10% of the 50-cm reaches (see 'Other' plot in Figure 7.29). The mean thalweg slope for each 50-cm reach was then plotted against downstream distance (Figure 7.28) with the points coded by planform category.

Perhaps the most clear cut pattern in the results is in the spatial distribution of armouring. While unarmoured, single-thread reaches occurred along the full length of the delta surface in all runs and unarmoured, braided reaches occurred in almost all sections downstream from the 100-150 cm cross section inclusive (Figure 7.28). Fully armoured reaches of either kind were not found downstream of 550-600 cm. Furthermore, there were clear differences in the downstream extent of the fully armoured reaches between the marginal, central and accelerated removal runs (Table 7.4). The maximum downstream extent of armouring in the marginal runs ranged from 450-600 cm, with armoured reaches rarely²⁵ extending beyond 350-550 cm. The maximum downstream extent of armouring in runs 3xL(A) and 3xC was 500-550 cm, with armoured reaches rarely extending downstream of 200-250 cm. In contrast, the maximum downstream extent of armoured reaches ranged from 200-400 cm in runs 6xC and 12xC, with few reaches extending further downstream than 100-150 cm. In summary, there appeared to be a significant decrease in the downstream extent of armoured reaches moving from the marginal to the accelerated to the central runs.

²⁵ The term 'rarely' is somewhat subjective, but the transition from one 50-cm section to the next where the number of armoured points drops substantially is nevertheless clearly defined in the plots of Figure 7.28.

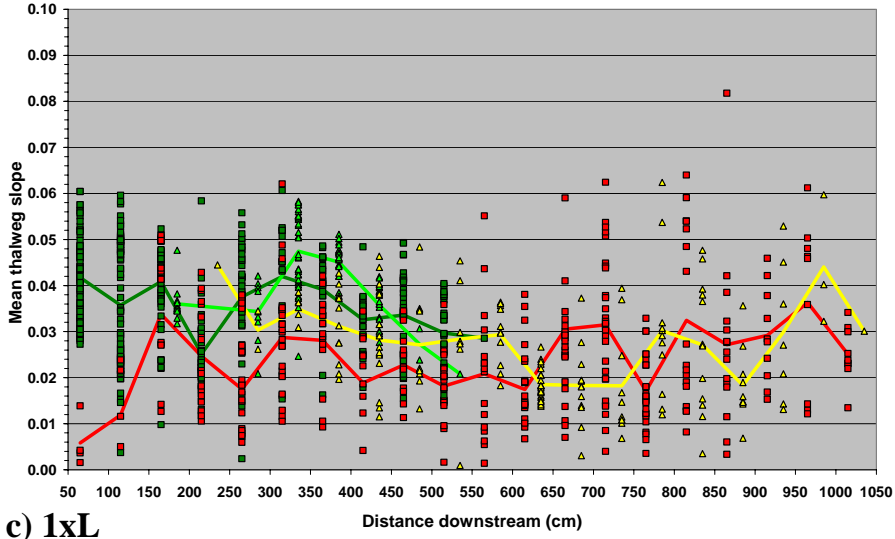
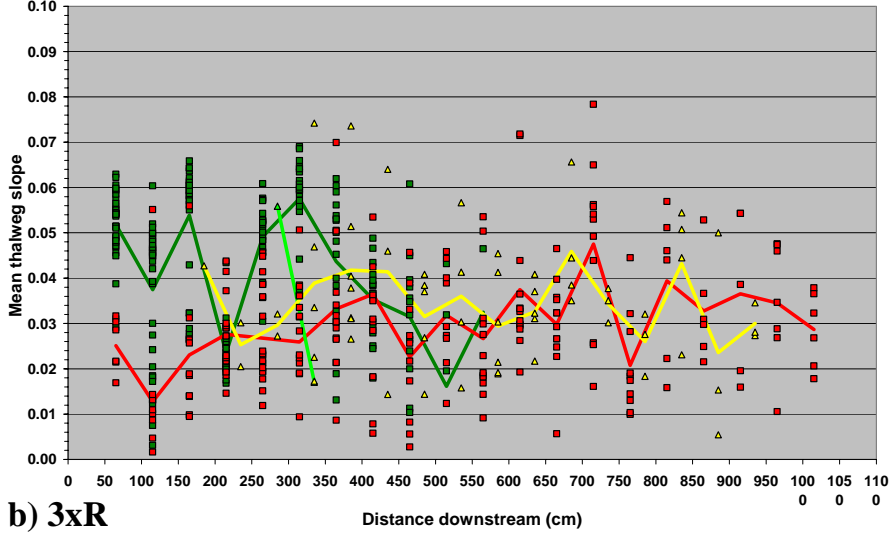
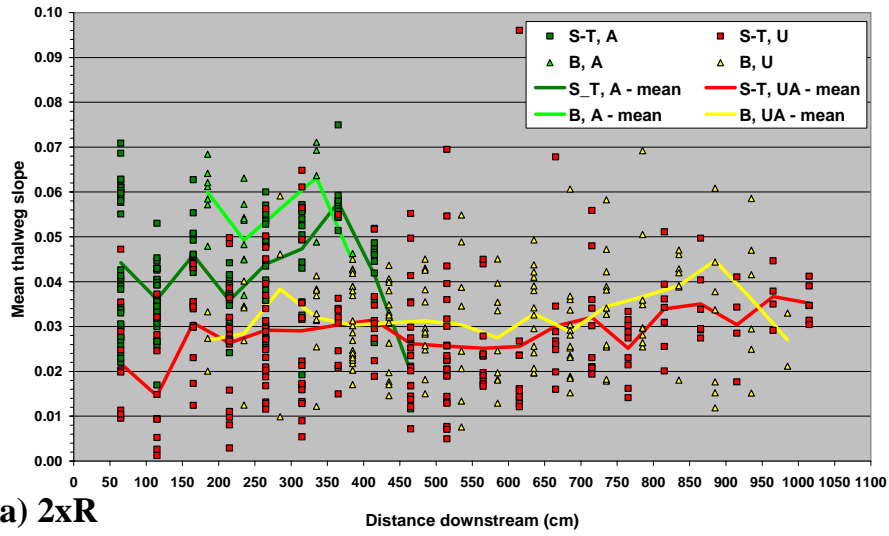
This probably occurred because the central and accelerated removal runs generally had a greater capacity to transport grains of armour-forming calibre out of the original delta area and to disperse them more widely throughout the prograding area of the reservoir than did the marginal runs, leading to an insufficient concentration, or a periodic exhaustion, of armour-forming grains in the downstream half of the original delta and the upstream part of the prograding delta.

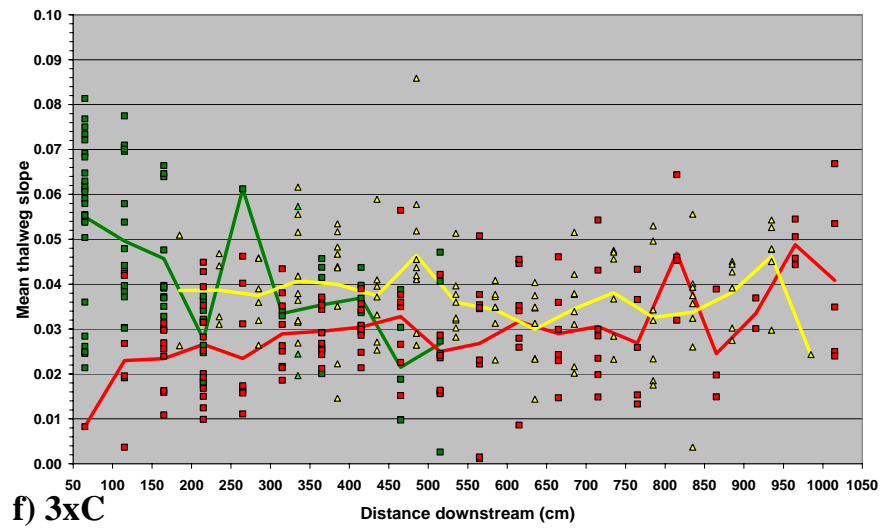
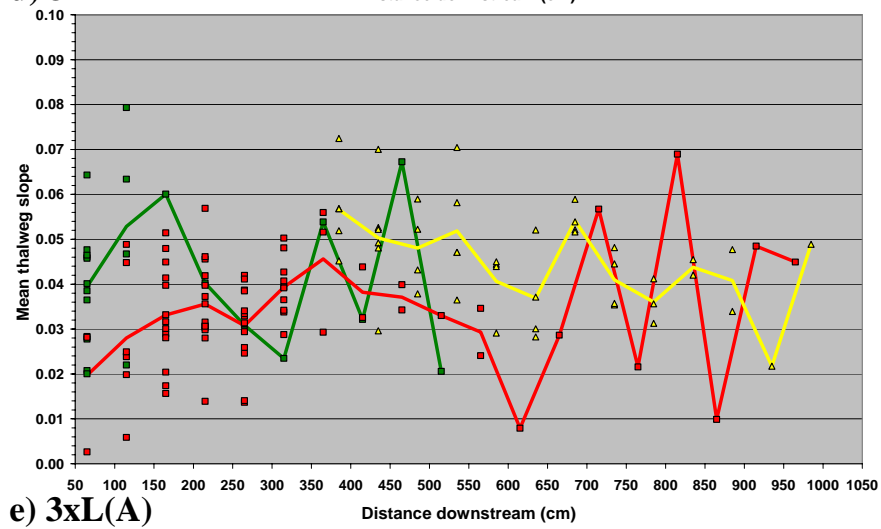
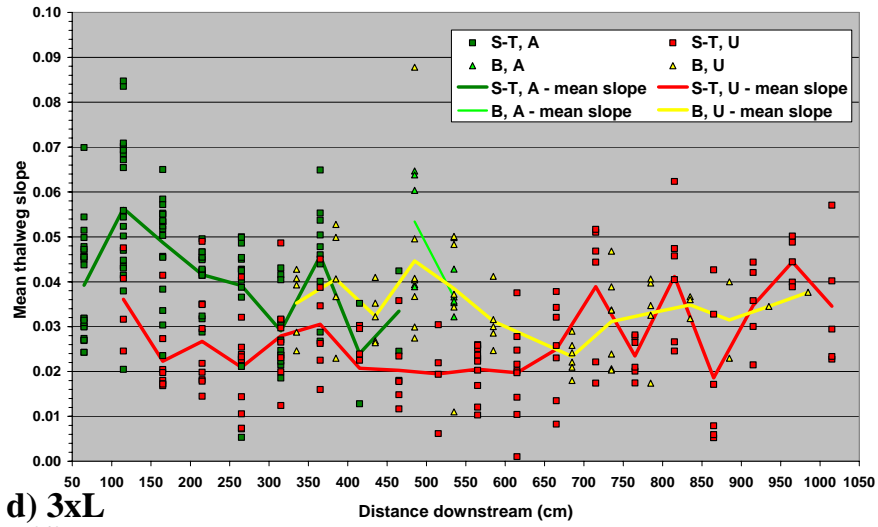
A second observation relating to the armour layer is that armoured reaches with both single-thread and braided planforms tended to have steeper mean thalweg slopes than their unarmoured counterparts (Figure 7.28). While there was some overlap, this distinction was most strongly developed in runs 2xR, 3xR, 1xL and 3xL over the entire original delta surface and the first 150 to 200 cm or so of the prograding delta while, in the central runs, and especially runs 6xC and 12xC (Figure 7.28g-h), it was restricted to the first 100-200 cm of the original delta surface. Runs 3xL(A) and 3xC (Figure 7.28e-f) appeared to be somewhat transitional between the two categories.

Run	Downstream limit of fully armoured 50-cm delta surface sections			
	Maximum section (cm)	Range (cm)	Majority of sections (cm)	Range (cm)
2xR	450-500		400-450	
3xR	550-600	450-600	350-400	350-450
1xL	500-550		500-550	
3xL	450-500	450-550	350-400	350-550
3xL(A)	500-550	-	100-150	-
3xC	500-550	-	200-250	-
6xC	200-250	200-400	100-150	100-150
12xC	350-400		100-150	
21xC	None	-	None	-

Table 7.4. Summary of downstream extents of armoured 50-cm delta surface sections.

The final, and perhaps most interesting, distinction lies in the relative proportion of single-thread and braided 50-cm reaches present in each run (Figure 7.29). Particularly noteworthy is the total proportion of single-thread versus braided reaches. A significantly greater proportion of the 50-cm reaches were single-thread in the marginal runs 3xR, 1xL and 3xL than in the four central runs, while runs 2xR and





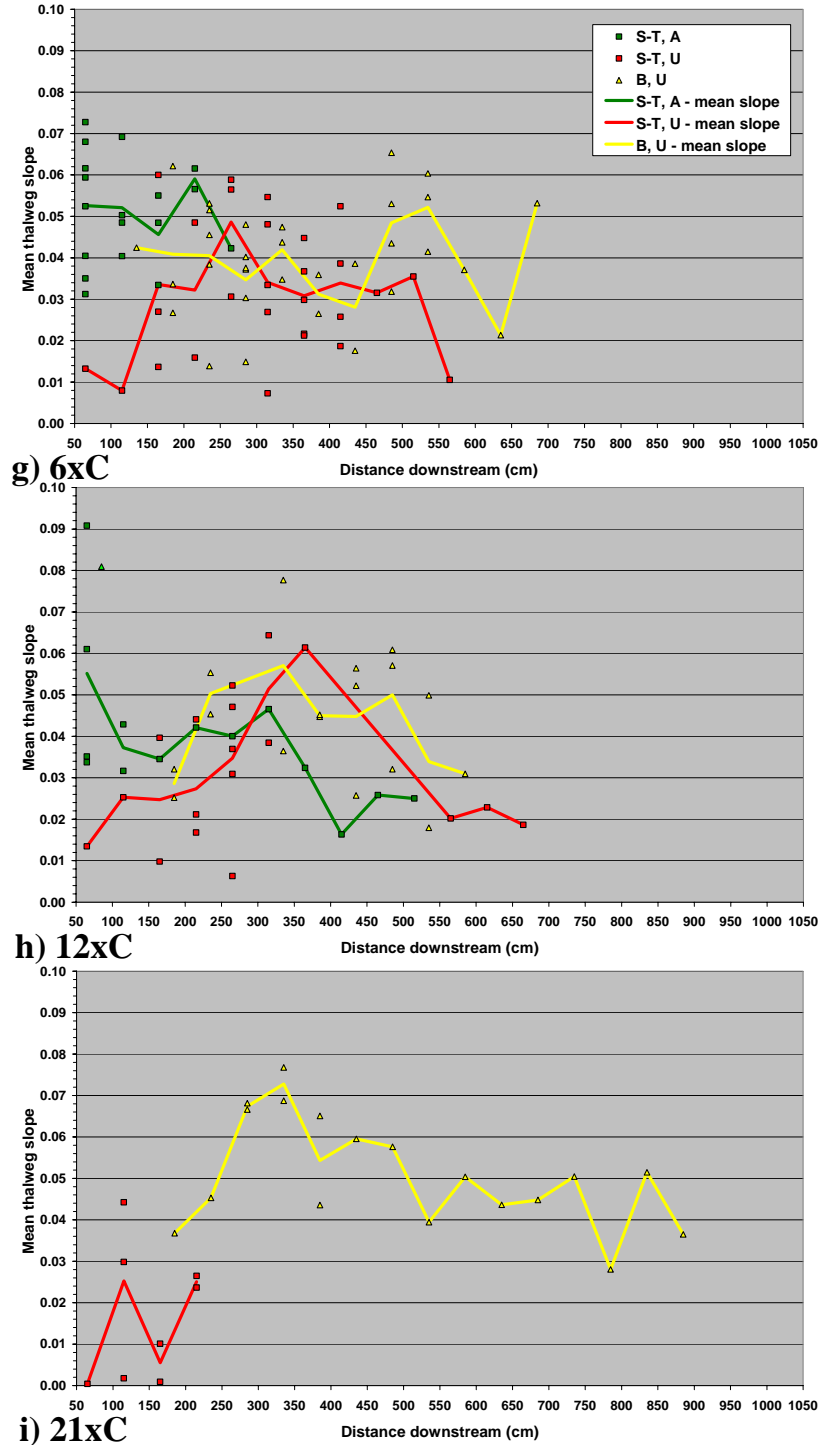


Figure 7.28. Distribution over the delta surface of armoured and unarmoured planform types as a function of mean thalweg slope for each 50-cm section of the delta surface. S-T = single-thread; B = braided; A = armoured; U = unarmoured.

3xL(A) appeared to be transitional. Almost the exact opposite is true for the total number of braided reaches. There were a larger number of braided reaches in the

central runs and run 3xL(A) than in runs 3xR, 1xL and 3xL, with run 2xR again being transitional between the two. Overall, a significantly larger proportion of the sections were single-thread (67%) than braided (24%), with 9% classified as 'Other'. This is consistent with observations from rivers in general, which show the single-thread, meandering planform to be predominant (Leopold, 1994).

Channel planform varies as a function of stream power and the grain size distribution of the channel boundary. Transitions from straight to meandering to braided usually occur as a result of a combination of increasing stream power and/or decreasing resistance to erosion of the channel boundary, while the intensity of braiding continues to increase with stream power above the meandering to braided threshold (Richards, 1982). Stream power per unit channel length is given by equation 3.6. Since $\rho_w g$, Q and the boundary grain size distribution were all constant in these experiments, planform should vary uniquely as a function of thalweg slope, which is a good approximation of the energy slope (Watson *et al.*, 1999).

The significantly greater proportion of braided reaches in the four central runs is thus explained by the fact that the larger magnitudes of drop in base level resulted in a higher energy delta surface system than that present in the marginal runs. The braided planform developed in response to the excess kinetic energy, dissipating it effectively as this configuration provides greater overall flow resistance than the equivalent single-thread channel (Richards, 1982).

Planform evolution and transitions between planform classes were extremely dynamic occurrences during the runs, taking place at different rates and with different frequencies in different parts of the delta surface. Consequently, the photographic observations, which are only snapshots in time of system behaviour, were not necessarily the most appropriate method for capturing this behaviour. Nevertheless the large numbers of observations (3,296 for all runs) on which Figure 7.29 is based provides a high degree of confidence in the accuracy of the results it presents.

In view of the above, there was reason to expect a greater distinction in the mean thalweg slopes between the single-thread and braided planforms than is apparent in Figure 7.28. With the exception of Run 21xC (Figure 7.28i) and the possible exceptions of the delta surface between about 300 and 600 cm in Runs 3xL, 3xC and 12xC (Figure 7.28d, f & h respectively), no clear distinction is apparent. This

may be due to the occurrence of chute-type features that developed in response to avulsions at various locations on the delta surface and to flow switching between multiple prograding lobes at the delta front, both of which shortened and steepened the channel over the delta surface and triggered further incision. It may also reflect the need to improve the thalweg-seeking algorithm, which would improve the accuracy of the calculated slopes.

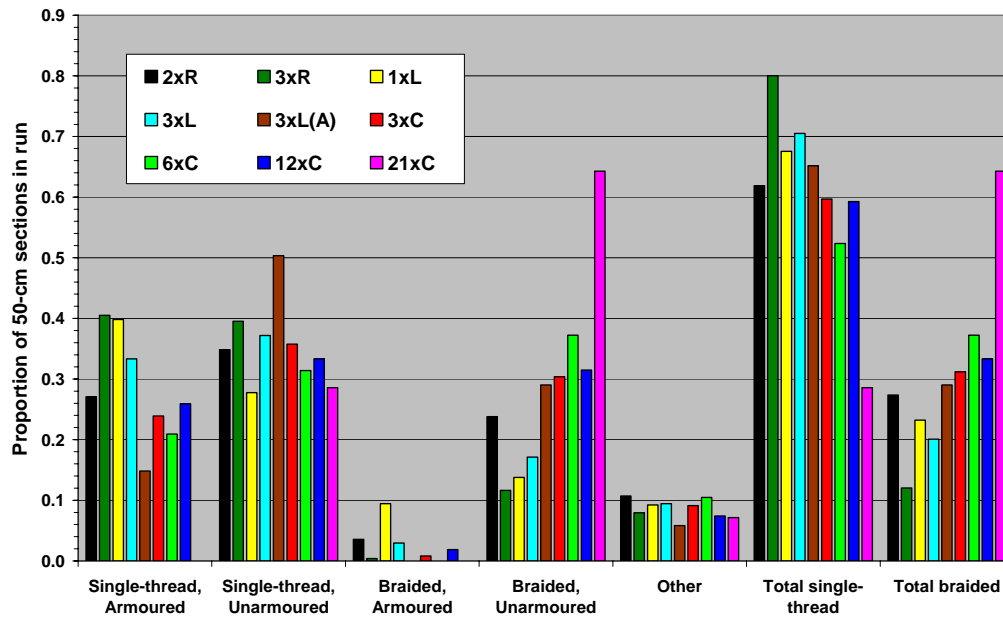


Figure 7.29. Frequency of occurrence of planform types.

7.7 Summary

The experimental results show clearly that the central runs eroded a greater proportion of the original delta at all stages of dam removal than the marginal runs (Figure 7.12). The bed elevation data show that channels in the marginal runs consistently incised to lower elevations than those in the central runs over the entire original delta surface during the whole dam removal phase (Figure 7.24). In contrast, laterally the central runs eroded a greater proportion of the original delta than the marginal runs, particularly the left marginal runs. During the central runs these factors combined to produce a greater rate of coarse sediment transport into the prograding reservoir area and thus a reduced controlling role for the armour layer in the original delta area, together with a higher frequency of braiding over the entire delta surface than occurred during the marginal runs.

Chapter 8 Discussion

8.1 Experimental limitations and scale effects

Before discussing the results presented in Chapter 7, it is necessary to consider the role that scale effects and a number of experimental limitations may have played in influencing the experimental results.

8.1.1 Experimental limitations

Perhaps most importantly, there was no experimental replication, which was not possible given the length of time required to complete each run (one month on average). Secondly, runs 6xC, 12xC and 21xC were only partially completed, which was also a function of time constraints. As well as running these three runs until the dam was fully removed, it would have been most instructive to perform a run 1xC, since this would then have encompassed the full range of magnitudes of baselevel drop from the central position. In turn, this would have provided a more complete frame of reference with which to examine the significance of the four marginal runs. Any extrapolation of the effects of runs 6xC and 12xC to a complete reservoir drawdown situation is thus purely hypothetical. Despite the lack of experimental replication, however, some confidence in the significance of the results can be taken from the fact that there are some very distinct differences in system behaviour between the marginal and central runs, which are expressed consistently by a number of different variables (Chapter 7).

All the runs were performed without bottomset deposits in the reservoir, so there is no indication of how these might have affected the patterns of delta erosion and progradation. The bottomsets were omitted because in the prototype they are composed almost entirely of silts and clays, which could not be scaled without using a lower density material (sections 4.3.3 and 5.3.1). The initial intention had been to perform a series of baseline runs without bottomsets and then to repeat one or two of these using lower-density coal dust for the bottomsets. This would have produced potentially useful qualitative information on the role of the bottomsets, but ultimately proved to be impossible given the aforementioned time constraints.

Possibly of greater significance, however, is the reduced space that was available at the upstream end of the model due to the presence of an adjacent model,

which resulted in the headbox having to be located very close to the upstream end of the model. During the 1994 drawdown experiment, the channel bed in Rica Canyon transitioned smoothly into the bed of the delta surface channels, which meant that there was a continuum of flow velocity from Rica Canyon into the reservoir. In the model, however, it was necessary to include a solid upstream end to the reservoir basin and to place the delivery channel at the top of this wall, which therefore introduced a drop between the channel and delta surface that became progressively larger as each run progressed (Figure 8.1). As the water entered the model it therefore experienced significant longitudinal deceleration and had to resume its flow over the delta surface from almost a standing start in the scour pool at the base of the drop. The net effect of this was that flow velocities, and therefore boundary shear stresses, in the upstream portions of the model were lower than they should have been, therefore reducing the flow's erosive capabilities. While this entrance effect was undesirable, it was consistent across the runs and its effect may therefore cancel itself out.

8.1.2 Scale effects

One of the assumptions underlying the experimental runs was that the model basin's geometry would transport and deposit the original delta sediment in a manner that was analogous to what would occur in the prototype. To help achieve this it was important that flow in the delta surface channels should be hydraulically similar to that of the 1994 drawdown experiment. Data from the temporary measuring station ELD2 (Figure 2.10) enabled the Reynolds and grain Reynolds numbers to be estimated for the downstream end of the prototype original delta surface (Table 8.1), which shows that the flow acting on the channel boundary as a whole and on individual sediment grains was fully turbulent according to most values cited in the literature (see sections 4.2.1 and 4.2.2 respectively). The same parameters were calculated for the model delta for two different flow situations: (i) during an armour-layer-breaking event in the upstream half of the original delta close to the start of run 1xL; and (ii) immediately following a drop in baselevel very close to the area of maximum disturbance (AMD) using data from run 2xR (Table 8.2).

The values for the Reynolds number show that the flow was fully turbulent according to most values cited in the literature (section 4.2.1), but most of the grain Reynolds numbers are close to the lower limits of published values (section 4.2.2), as

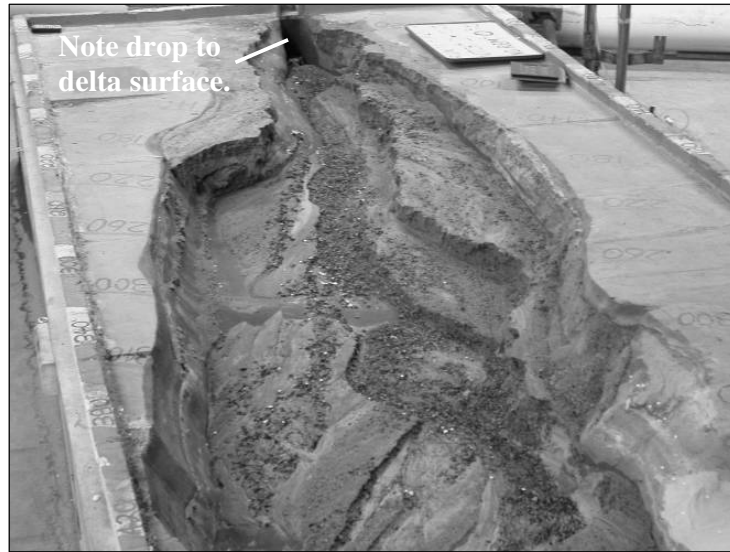


Figure 8.1. View looking upstream towards the end of run 3xC. Note the drop between the mouth of the delivery channel and the delta surface at the top of the photograph. Photograph courtesy of Corey Markfort.

Baselevel	Date (April 1994)	Reynolds number	Grain Reynolds number
Falling	10th	428,000	-
	12th	459,000	-
	13th	473,000	1,048
	15th	606,000	1,123
Constant	17th	833,000	187
	19th	966,000	498
	20th	849,000	681
	21st	795,000	154
	23rd	680,000	1,040
Rising	25th	574,000	-
	27th	576,000	-

Table 8.1. Reynolds and grain Reynolds numbers in one of the channels incising the Lake Mills delta surface during the 1994 drawdown experiment. Calculations based on data from the United States Geological Survey (2000).

Run	No. of dam pieces remaining	50-cm section (cm)	Mean flow velocity (m/s)	Discharge (m ³ /s)	Bed slope	Mean channel width (m)	Flow depth (m)	Reynolds number	Particle Reynolds number
1xL	17	70 - 100	0.32	0.00026	0.0405	0.123	0.0066	5,556	35.7
		100 - 150	0.31	0.00026	0.0402	0.123	0.0069	5,556	36.9
2xR	11	420 - 450	0.25	0.00026	0.0286	0.09	0.0116	7,593	44.4
		450 - 500	0.23	0.00026	0.1636	0.115	0.0098	5,942	214.2

Table 8.2. Estimated values of the Reynolds and grain Reynolds numbers during the experimental runs.

they were in the model's delivery channel for the entire sediment mixture (section 5.3.1). The final grain Reynolds number is a clear exception, comfortably exceeding the most frequently cited value of 70 needed to ensure full turbulence around the particle and falling well within the range of values that occurred during the period of constant baselevel during the 1994 drawdown experiment (Table 8.1). This value occurred following the removal of the 10th dam piece through the 50 cm section closest to the AMD, which was rapidly incising and whose slope was an order of magnitude greater than that of the next 50 cm section upstream (Table 8.2).

The values calculated in Table 8.2, which may or may not indicate fully turbulent flows, were taken from some of the more energetic periods of runs 1xL and 2xR. There were also long periods of these runs when slopes were less steep (Figure 7.27a&c), channels were wider and when the flow was almost certainly not fully turbulent. In the runs with larger magnitudes of baselevel drop, particularly the central runs, there was a greater proportion of steeper bed slopes than in the marginal runs (Figure 8.3) and probably a greater proportion of flows that were fully turbulent. Nevertheless, there were still long periods of time in which slopes were low, channels wide and flows almost certainly insufficiently turbulent.

In summary, it is likely that the flow conditions during the experiments ranged from fully turbulent, through semi-turbulent to hydraulically smooth, with a greater proportion of the flows falling in the latter two categories and thus allowing viscous effects to influence the rate of sediment transport, in particular of the finest sediments. On the other hand, during many of the periods of most dynamic delta surface activity, such as the rapid incision of the delta front or rapid erosion of large terrace deposits by relatively steep and narrow channels, it is likely that flows were close to or actually fully turbulent. It is thus probable that at least some of the total geomorphological work was performed under hydraulic and sediment-transporting conditions not dissimilar to those that would be likely to occur on the prototype delta surface. Furthermore, periods when the bed was heavily armoured and therefore rougher than a plane sand bed may have created turbulent flow (Chadwick and Morfett, 1998; Solari and Parker, 2000) (section 8.2.2.2).

A number of possible scale effects relate to the fact that all but the coarsest 1-2% of the model sediment was considerably coarser than required by the scaling calculations. Larger sediment grains are heavier and so require a greater shear stress

to entrain them, so it is possible that the erosion volumes presented in Chapter 7 underestimated the volumes that could have been eroded had a lower density modelling material been used. This scale effect could have been compounded by the reduced flow velocities at the upstream end of the model (section 8.1.1). These two effects may have been counteracted to a certain extent, however, by the possibility that there may have been a mobility reversal during sediment transport that resulted in greater amounts of sediments coarser than the geometric mean size being transported. This possibility is explored in greater detail in section 8.2.2.

Yet another possible scale effect related to excessively coarse model sediments, particularly relative to model discharge, is that they may have triggered an unrepresentatively high frequency of channel avulsion and planform change. Mass wasting events in the original delta frequently triggered channel avulsion and the formation of a braided planform where previously there had only been a single-thread planform. Because model discharge was correctly scaled, channel dimensions were a reasonably-scaled representation of what they would be on the prototype delta surface, since discharge is a key determinant of channel dimension. But the model sediments were considerably larger than required by the scaling calculations, which means that when sediment was delivered to the incising channels, it would more rapidly fill the available channel capacity than if it had been the correct size, thus leading to a greater ease and frequency with which the channel could avulse and switch from a single-thread to a braided planform. This does not mean that some of the braiding was not representative of reality, but that the frequency with which channel planform switched may have been a scale effect.

8.2 Volumetric response to baselevel fall

8.2.1 The role of the magnitude and rate of baselevel drop

It is not possible to completely disassociate the effects of the magnitude of baselevel drop from the effects of the basin boundary on erosion volumes during the dam removal phase of the experimental runs. Runs 1xL, 2xR, 3xL, 3xR, 6xC, 12xC and 21xC therefore cannot all be directly compared in order to make general statements about the effects of increasing the magnitude of baselevel drop on original delta erosion volumes. Subsets of these runs can be compared, however, in order to gain some useful insights.

Runs 1xL and 3xL eroded the same volume of sediment to within 0.5% of each other by the 12-piece equilibrium (Table 7.2). Similarly, runs 2xR and 3xR eroded the same volume of sediment to within 1.5% of each other by the 12-piece equilibrium (Table 7.2). For channels on the same side of the delta, the nature of the interactions between the incising channel and basin boundary were qualitatively very similar up to the 12-piece equilibrium, which indicates that these effects may have cancelled themselves out to a large extent.

Run 12xC eroded 4.4% more sediment than run 6xC by the 12-piece equilibrium. Following the second avulsions, which occurred from 4:55 minutes and 3:15 minutes onwards in the Run6xCCam1 and Run12xCCam1 movies respectively, the channel stabilised in the right half of the original delta area in run 6xC, where the sediment was less deep, and along the left basin boundary in run 12xC, where there was a greater depth of sediment that the channel was subsequently able to incise (section 7.3.3). Furthermore, the time lapse movies and Figures 7.26a-d clearly show that there was a greater amount of proximal and medial original delta terrace erosion by the 12-piece equilibrium in run 12xC than in run 6xC. There is thus some evidence to suggest that the magnitude of baselevel drop signal in the volume data for these two runs is significant, although the volume difference is not large and the effects of natural experimental variability cannot be ruled out. Clearly, experimental replication would have been useful in helping to determine the significance of this difference.

From the 12- to the 21-piece equilibriums, run 3xL eroded 6.5% more of the original delta than run 1xL, which suggests that a magnitude of baselevel drop signal was present. Run 2xR eroded 10% more of the original delta than run 3xR, but this was largely because run 3xR incised to the hard basin boundary and was unable to move laterally into the left terrace thereafter. It is not possible to say with any degree of certainty how runs 6xC and 12xC might have continued beyond the 12-piece equilibrium, although a possible response is hypothesised below.

The picture of system response described above would have benefited greatly from performing runs 6xC, 12xC and 21xC over complete dam removal cycles, from experimental replication, from a run 1xC, and from a run 3xC whose incremental baselevel drops were only performed once the system had stabilised following each previous drop. Together, these would have provided a much more comprehensive understanding of system behaviour. On balance, however, it is tentatively suggested

that hypothesis 1c (section 3.4) should be accepted, albeit in a slightly modified form.

The results of laboratory and field work cited in sections 3.3.1.1 and 3.3.1.2 consistently show that the degree of channel incision and widening decreases with increasing distance upstream from the AMD because of the presence of coarser sediments in the upstream reaches of the deposits being incised. This observation also holds for the results of this study. It was thus argued in Chapter 3 that a larger drop in baselevel would allow incision and channel widening to migrate further upstream, because the larger amount of stream power so introduced would more readily prevent or overcome the tendency of coarse sediments to form an armour layer, thus eroding a larger proportion of the delta deposit. The results presented in Chapter 7 for runs 6xC and 12xC show this to be the case, while the evidence from the central runs provides a more detailed understanding of why this occurs.

It took 90 minutes of model run time (24 seconds of the time lapse movies) for the reservoir water surface elevation to drop 16.8 cm, the equivalent of six removed dam pieces in runs 6xC, 12xC and 21xC. The time lapse movies for the three runs after 24 seconds show that the delta fronts prograded a very similar distance downstream. Following this drop, the system was allowed to equilibrate in run 6xC, during which time the delta front prograded to roughly 440 cm, at which point the next six dam pieces were removed. In contrast, the baselevel in run 12xC continued to drop, which meant that by the time the delta front in run 12xC had prograded to 440 cm, much of the potential energy generated by the removal of dam pieces 7-12 had already been delivered to the AMD while it was closer to the original delta area than in run 6xC. Similarly, by the time that the baselevel had dropped 33.6 cm after 180 minutes of model run time (48 seconds of the time lapse movies), the equivalent of 12 removed dam pieces, the delta fronts in runs 12xC and 21xC both prograded to about 480 cm. But while the system equilibrated in run 12xC, with the delta front eventually prograding to about 670 cm, by the time the delta front in run 21xC had prograded to 670 cm, most of the potential energy generated by the removal of dam pieces 13-21 had already been delivered to the AMD while it was closer to the original delta area than it would have been in run 12xC had the remaining nine dam pieces been removed. It should be noted that the delta front in run 12xC prograded to 440 cm after 40 seconds of movie time, which meant that the potential energy associated with the removal of dam pieces 11 and 12 was delivered to the delta system from a position

that was further downstream from the original delta area than the 6-piece equilibrium position of the prograding delta front in run 6xC. In other words, the potential energy associated with the removal of 10 dam pieces was introduced to the delta system in run 12xC, from a position closer to the original delta area than the potential energy associated with the removal of dam pieces 7 to twelve in run 6xC.

To summarise the above, by increasing the magnitude of the drop in baselevel, a greater amount of energy was delivered from a position closer to the original delta area than with a smaller magnitude of baselevel drop. For any dam removal whose reservoir-area river channel has the potential to develop an armoured bed, this is a highly significant finding, as the response of the channel bed and armour layer in this study shows. Over the 330-minute duration of run 21xC, no armour layer formed at or downstream of the 50 cm cross-section at any time (Figures 7.18j to 7.23j). In run 12xC, the armour layer began to form sometime between 90 and 210 minutes of run time at the 50 cm to 150 cm cross-sections (Figures 7.18i to 7.20i), while in run 6xC it began to form at the same cross-sections inside the first 90 minutes of run time (Figures 7.18h to 7.20h). This delay in the onset of armouring means that a larger amount of energy was able to erode the original delta for a greater length of time before having to overcome the effects of an armour layer.

According to the rationale presented above, run 6xC should have eroded more of the original delta than run 3xC by the 12-piece equilibrium, even though run 3xC was performed with an accelerated rate of dam removal, yet this was not the case (Figure 7.12). Run 3xC incised to a greater depth than run 6xC in the upstream half of the delta by the 12-piece equilibrium (Figure 7.25e) and this caused a greater degree of terrace erosion in the proximal and medial original delta (Figures 7.26a-d). Run 6xC incised the downstream half of the original delta more than run 3xC, but comparison of time lapse movies Run3xCCam1-4 and Run6xCCam1-3 show that much of this was against the left basin boundary. In addition, run 3xC moved to the right basin boundary in the upstream half of the original delta and incised a large amount very rapidly just before the end of the 12-piece equilibrium interval of run time.

In view of the preceding discussion and the results presented in Chapter 7, hypothesis 2c (section 3.4) should be rejected as it stands and replaced with a slightly modified version. Figure 7.14e for run 3xL(A) shows that if the relaxation interval

between periods of baselevel drop is sufficiently short, extremely high rates of sediment erosion can be generated that are comparable to those caused by much larger drops in baselevel (Figures 7.12; 7.14h-i). This means that hypothesis 2b should be accepted. If the relaxation time is too short, however, the plot for run 3xL(A) in Figure 7.12 shows that the maximum benefit in terms of total sediment eroded per increment of drop may not be realised and that the total volume eroded by the end of dam removal will be relatively small, at least when there are significant boundary effects. When there are fewer boundary effects, the relaxation time could be very short in order to make the overall dam removal as similar to a 21xC-type removal as possible. This suggests that there is an optimum rate at which the baselevel should be dropped, which strikes a balance between the need to maintain a high potential energy surface through the original delta area and the need for the channel to adjust laterally in order to maximise the erosion volume for the increment of drop. The optimum will be morphologically determined by the downstream extent of the armour layer reformation and is likely to vary from site to site as a function of discharge, deposit geometry and the quantity and availability of sediments of armour-forming calibre. The modified version of hypothesis 2c should thus read:

Hypothesis 2c

For a given magnitude of baselevel drop there exists an optimum rate of incremental drop, which, if applied over the course of the full dam removal, will cause the erosion of a greater total volume of sediment than the same magnitude of drop applied at a sub-optimal rate or by allowing the system to adjust completely to each incremental drop.

Hypothesis 2a should be rejected, because Figures 7.25 c&e and the time lapse movies for runs 3xC, 6xC and 12xC show that the delta front progrades slightly further downstream in the two latter runs. Hypothesis 1a should also be rejected, since the deltas in runs 6xC and 12xC both prograde almost exactly the same distance by the 12-piece equilibrium (see the Run6xCCam1-3 and Run12xCCam1-3 time lapse movies).

The differences between runs 6xC and 12xC described above suggest that the former eroded less of the original delta than the latter because the next increment of potential energy was introduced when the AMD was further away from the original delta than in run 12xC. This same reasoning explains why there should also be a

strong exponential decrease in the additional volume of sediment eroded as the magnitude of baselevel drop increases. This is explained as follows.

Run 6xC eroded less of the original delta than run 12xC by the 12-piece equilibrium, because the potential energy associated with the removal of the 7th to 12th dam pieces was introduced to the delta surface when the AMD was further away from the original delta than in run 12xC. This meant that a greater proportion of the potential energy was converted to kinetic energy and expended by the channel moving vertically and laterally over the *prograding* delta surface, as opposed to moving vertically and laterally within the *original* delta area. As the magnitude of baselevel drop increased, the delta front prograded further and more rapidly than with the next smaller magnitude of drop. The additional progradation of the distal delta front in run 12xC compared to run 6xC caused the AMD to move rapidly away from the original delta area while the baselevel was still falling, *i.e.* while potential energy was still being introduced into the system by the falling baselevel. In effect, the prograding portion of the delta increasingly acted as a buffer between the original delta and the AMD, so that the rate of erosion in the original delta area was reduced through a process of negative feedback. Eventually, therefore, it is hypothesized that a magnitude of baselevel drop is reached beyond which greater magnitudes of drop do not realize any significant further increases in the volume of the original delta eroded, because the additional kinetic energy is dissipated entirely by channel adjustments over the prograding delta topset or against the armour layer that would eventually form through the original delta area. The modified version of hypothesis 1c can thus be stated as follows:

Hypothesis 1c

The volume of original delta sediment eroded will increase with an increasing magnitude of baselevel drop, but only up to a certain point. Beyond this point, negative feedbacks will operate that effectively negate any further significant original delta erosion volumes.

It is therefore envisioned that there exists an optimum rate of smaller incremental baselevel drops (modified hypothesis 2c), which generates essentially the same volume of total original delta erosion as that attained by a slower rate of the

incremental removal of larger baselevel drops. This supposition should be tested further to investigate its validity.

The importance of the magnitude and rate of baselevel drop stem in part from the way in which they influence the degree of armouring and the amount of gravel transport through the original delta area. These dynamics will now be further discussed.

8.2.2 The role of armour layer dynamics

8.2.2.1 Bed Elevation Lowering Without Armour Layer Break-up (BELWALB)

A phenomenon termed Bed Elevation Lowering Without Armour Layer Break-up (BELWALB) was reported in Chapter 7 that, to the best of the author's knowledge, has not been reported elsewhere in the literature. It was also observed in the field during the drawdown experiment at Lake Mills in 1994 (Randle, Personal Communication, 2003). In the experiments reported herein, it seemed to occur at one point along a continuum of armour layer dynamics that could be categorised as ranging from (i) completely stable armour layer; (ii) BELWALB; (iii) partial armour layer break-up; to (iv) complete armour layer break-up.

One possible mechanism for the occurrence of this phenomenon was observed during the Run2xRCam1 movie from 04:28 to 04:30 minutes (section 7.3.1). As incision migrated upstream it lowered the channel bed elevation in the non-armoured or partially armoured reach immediately downstream from the fully armoured reach, to the extent that the downstream edge of the armour layer was destabilised, thus allowing a few gravel grains to roll forwards over a distance equivalent to a few gravel grain diameters. As they did so, the finer-grained sub-armour was temporarily exposed to lift and drag forces. Some of the finer sediments were entrained, which undermined the support for the next few pieces of gravel upstream and caused them to roll forwards a small amount and to settle at a slightly lower elevation, perhaps no more than one gravel grain diameter lower and one or two gravel grain diameters further downstream.

This phenomenon has potentially great morphological significance for two main reasons. Firstly, because the undermined gravel grain dropped to a lower elevation due solely to the force of gravity, if this then triggered a partial or complete

armour layer break-up, for example if the armour layer was close to a threshold of stability, then the actual initiation of motion may have occur at shear stresses lower than those that would normally be required to entrain gravel grains of that size in an armour layer. A similar effect was reported by Stewart (2006) for the role of knickpoints as the primary mechanism for reservoir erosion following two small dam removals in Oregon. Indeed, the occurrence of BELWALB may in fact simply be an example of a very small knickpoint. Secondly, if the drop in bed elevation does not trigger an armour layer break-up it will nevertheless alter the direction of the streamlines, perhaps only subtly, for some distance upstream and downstream. In turn, if a section of the bed, bank or terrace within this zone of adjustment was very close to a threshold of stability, the slight change in angle of attack of the current may have been sufficient to trigger a period of extensive erosion. This may have occurred following the episode of BELWALB described above (see also section 7.3.1 and 7.3.2).

If the mechanism proposed above for the occurrence of BELWALB is correct, then it has the potential to occur in any river where there is a transition between a gravel-bed and a sand-bed and an upstream-migrating knickpoint or knickzone. Its ability to initiate morphological work will probably depend on how much of the particular system is close to a threshold of instability. If a large portion of the system is close to such a threshold, then a potentially large amount of work could be performed due to the operation of positive feedbacks. If only a localised part of the system is close to a threshold of instability, then the effect of the BELWALB may be damped down due to negative feedback processes. This occurred on a number of occasions in the current experiments. Clearly, more work is required to examine this phenomenon and the range of conditions under which it might occur and under which it might lead to significant amounts of erosion.

8.2.2.2 Mobility reversal

The reduced presence of the armour layer in the central runs compared to the marginal runs was discussed in section 8.2.1. Two pieces of evidence suggest that this may have been at least partially due to a mobility reversal in sediment transport, which is the phenomenon in which coarser sediment grains are more readily transportable than finer grains of the same specific gravity (Solari and Parker, 2000). The first is that coarser sediment grains were frequently observed to be moving more

rapidly than finer grains over the none-armoured delta surface. This is exemplified in the movie footage on disc 7 entitled ‘Mobility Reversal’²⁶ The second is that model slopes over the entire delta surface, but particularly in the armoured reaches of the original delta area were frequently of the magnitude required for mobility reversal to occur according to the mechanism proposed by Solari and Parker (2000) (Figure 8.3).

Solari and Parker (2000) reviewed three existing hypotheses (viscous effects, flow blockage and bimodality) to explain mobility reversal and used data from a series of flume experiments, together with analytical reasoning to propose a fourth. The hypothesis of viscous effects states that mobility reversal will occur if flow is not fully rough and the mean size of the sediments being transported is sufficiently fine, since the finer sediments lie partially or completely within the viscous sub-layer, while the coarser particles are disproportionately subjected to the effects of flow turbulence. The dimensionless ratio k_s/δ_v is used to determine whether viscosity is responsible for any observed mobility reversal and it can be simply obtained from the particle Reynolds number, Re^* , using

$$\frac{k_s}{\delta_v} = \frac{Re^*}{11.6} \quad (8.1)$$

where k_s is related to a characteristic size of surface bed material by

$$k_s = n_k D_{90} \quad (8.2)$$

in which n_k is usually taken to be 2; δ_v is a measure of the depth of the viscous sub-layer obtained from

$$\delta_v = 11.6 \frac{\nu}{u^*} \quad (8.3)$$

in which ν = kinematic viscosity of water and u^* = shear velocity (Solari and Parker, 2000).

The hypothesis of flow blockage states that mobility reversal can occur when the flow is sufficiently shallow to allow the coarser particles to break the water surface, since this increases the drag force around the particle. The possibility of flow blockage causing mobility reversal is assessed using the ratio H/D_{90} , in which H =

²⁶ On disc 7, open the VIDEO_TS folder and double-click any of the .VOB files. Examples of mobility reversal can be seen from 38:08 – 39:00 minutes and from 41:50 – 43:00 minutes run time.

flow depth. Experiments in downstream fining showed that this value must be less than at least 3.5 in order for flow blockage to be considered a viable cause of mobility reversal (Solari and Parker, 2000).

The hypothesis of bimodality states that mobility reversal can occur when there is strong bimodality in the grain size distribution, such that the coarse grains can roll smoothly over a bed of much finer sediment grains. The degree of bimodality is assessed using the ratio $D_{coarse\ m} / D_{fine\ m}$, in which $D_{coarse\ m}$ is a characteristic size of the coarse fraction and $D_{fine\ m}$ is a characteristic size of the fine fraction.

Solari and Parker (2000) found that at bed slopes greater than about 2-3%, the coarsest sediment grains in a mixture were more mobile than some size fractions less than the geometric mean grain size, D_g , while with a slope of 7% or more, all grains coarser than D_g become more mobile than grains with a size of D_g or less. This occurred because at about 2%, the force of gravity acting directly on sediment grains was just sufficient to upset the balance between particle weight and hiding effects that usually make finer sediment grains slightly more entrainable than coarser grains. The more bed slope increased beyond the 2-3% threshold, the more this balance was destroyed and the greater the degree of mobility reversal.

Figure 8.2 shows the absence of bimodality in the modelling sediment mixtures, which therefore rules out this factor as a cause of the observed mobility reversal. The values of H / D_{90} in Table 8.3 fall within the range cited by Solari and Parker (2000) as being indicative of downstream fining, which means that flow blockage was also not the cause of the mobility reversal. The values of k_s/d_v for run 1xL are much greater than the value of 6.03 above which flow is considered to be hydraulically rough (Solari and Parker, 2000), which categorically shows that the flow was fully turbulent as a result of the coarse armour layer over which it was flowing, despite the particle Reynolds number indicating that the flow was very close to the lower end of what is normally considered to be hydraulically rough flow (Table 8.2). The ratio k_s/d_v was not calculated for run 2xR because the channel bed in the area indicated was unarmoured and therefore much finer than the D_{90} . To do so would have indicated fully rough flow due to grain coarseness, which was not the case. Viscosity was thus probably not the cause of mobility reversal when the channel bed was rough. For run 2xR, however, the ratio δ_v / D_{16} is a more appropriate measure of the effect of viscosity over the unarmoured bed. The values in Table 8.3 suggest that

viscosity could well have been responsible for some or all of the observed mobility reversal, by trapping the finer grains within the viscous layer and slowing the rate at which they were transported downstream.

The distribution of bed slopes from all 50 cm sections during all runs is shown in Figure 8.3, which shows that the majority of the slopes were capable of causing mobility reversal according to the mechanism proposed by Solari and Parker (2000). Furthermore, the central and accelerated removal runs had a slightly greater proportion of their slopes above the threshold required for mobility reversal according to this mechanism. This suggests that some of the increased entrainment of gravels from the original delta area during the central runs may have been caused by a mobility reversal triggered by the steeper bed slopes associated with the larger drops in baselevel.

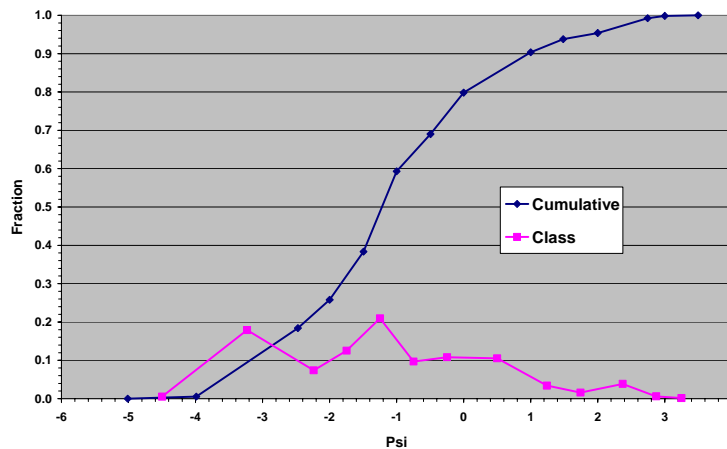


Figure 8.2. Model sediment mixture for run 6xC exemplifying lack of bimodality of the modelling sediment mixture.

Run	No. of dam pieces remaining	50-cm section (cm)	Bed slope	k_s/d_v	δ_v/D_{16}	H/D_{90}
1xL	17	70 - 100	0.0405	11.84	-	3.23
1xL	17	100 - 150	0.0402	12.03	-	3.36
2xR	11	420 - 450	0.0286	-	1.93	5.83
2xR	11	450 - 500	0.1636	-	0.88	4.91

Table 8.3. Dimensionless parameters used to assess cause of mobility reversal.

The values in Table 8.3 represent only a tiny proportion of the PTV

measurements that were taken. If and when a suitable means of processing the footage to automatically calculate flow velocities becomes available, then the hydraulic variables in Tables 8.2 and 8.3 can be calculated for a much greater range of conditions during the runs. As it stands, the data presented here are simply indicative of the types of behaviour that occurred during the runs; they do not show that such behaviour was the dominant type.

All but the coarsest 1-2% of the model's grain size distribution was significantly coarser than the distribution required by the scaling calculations. Because coarser sediments tend to form steeper slopes, it is possible that the bed slopes during the experimental runs were steeper than they would have been had a correctly-scaled size distribution been used. If, therefore, the coarser sediments resulted in a significant number of the 50 cm sections having slopes greater than the 2-3% slope threshold required for the onset of mobility reversal, then the occurrence, or frequency of occurrence, of this phenomenon in the model may represent the operation of a scale effect.

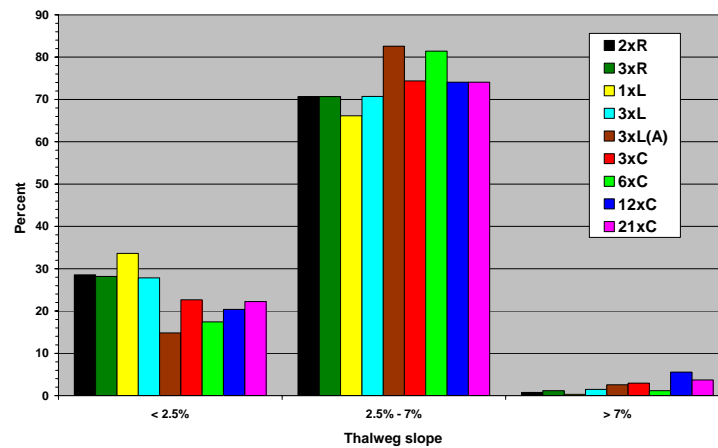


Figure 8.3. Distribution of bed slopes above and below the threshold for mobility reversal.

It is not unrealistic to expect that mobility reversal should occur during the removal of the prototype Elwha River dams, however, or of any other dams whose reservoirs impound coarse-grained sediments. In particular, if the magnitude of any single drop in baselevel is sufficiently great, or if the frequency of several smaller drops in baselevel is sufficiently high, such that the armour layer cannot fully extend downstream, then, for at least short periods of time until incision reduces them, bed slopes may be sufficiently high to allow mobility reversal to occur. Depending on the

length of time over which it could operate, mobility reversal could have significant impacts on the evolution of the armour layer and thus on the erosion of the entire deposit, as suggested by the results of the current experiments. Such a possibility merits more detailed investigation in future.

8.2.3 The role of basin geometry and flood flows

Because run 3xC was performed with an accelerated rate of dam removal, such that the system did not stabilise before the next incremental lowering of baselevel; because runs 3xL and 3xR were allowed to stabilise between each incremental baselevel drop; and because run 3xL(A) was performed with an accelerated rate of dam removal considerably greater than that of run 3xC, there is not one pair of runs in which the magnitude and rate of baselevel drop are the same in each run and which can thus be used to quantify the extent to which basin boundary effects modulated the amount of original delta erosion. Nevertheless, some distinct boundary effects are evident in the experimental results and these are discussed qualitatively below.

The way that boundary conditions affected the left and right marginal runs was described in detail in Chapter 7. The general tendency in the left marginal runs was for the left hand curvature of the basin boundary (Figure 8.5a, arrow D) to direct flow away from the main body of the original delta to the right of the channel, during both the dam removal and flood flow phases of the runs, as exemplified for run 1xL in (Figure 8.4a-d). The general tendency in the right marginal runs was for the channel to have a little more freedom to adjust laterally in the right half of the original delta up to the 12-piece equilibrium, thus eroding laterally a greater amount of the original delta than in the left marginal runs (Figure 7.26). From the 12- to the 21-piece equilibrium, however, the right marginal channels' ability to move laterally was greatly restricted, both by the armour layer and by the size of the left terraces. When the terraces experienced mass wasting, the large failure blocks introduced a significant degree of basal endpoint control to the channel. During the flood flows in run 3xR, however, there was significant erosion of the left terrace along the full length of the original delta (Figure 8.4d-h). This was due to the lack of erosion that occurred during the removal of the 13th to 21st dam pieces, as described in section 7.4; the straightening of

the channel through the centre of the original delta area; and the transverse slope of the basin's bed in this area (Figure 8.5).

The flood flows introduced the energy required by the channel to move away from the hard reservoir base, on which it had stabilised during the dam removal phase (Figure 8.5a, arrow A), and towards the topographic low along the left side of the original delta area (Figure 8.5a, arrow B). It was also able to move off the more gently sloping right reservoir wall (Figure 8.5a, arrow C) and over to the left side of the delta.

This channel movement during the run 3xR flood flows is probably no coincidence, since the pre-Glines Canyon Dam Elwha River channel is thought to have lain along the left side of the basin in the original delta area (Figure 5.1). Had flood flows been run following dam removal in run 2xR, it is likely that similar behaviour would have been observed, although perhaps with smaller erosion volumes, since more of the original delta had been eroded by the 21-piece equilibrium. This suggests that the natural tendency of delta surface channel(s) during dam removal will be to return to their pre-dam location, especially if this is in the topographically lowest point of the reservoir basin and there are no other topographical barriers to hinder migration.

Similar topographical steering of the river channel has been reported for a number of other alluvial channels. Coleman (1969) noted that the braided Brahmaputra River as it flows through Bangladesh has migrated steadily eastwards a distance of about 96 kilometres (60 miles) since the 1760s, due probably to faulting, and thus to inclination of the underlying solid geology. Alexander *et al.* (1994) found that parts of the Madison River in Montana had migrated laterally through parts of its floodplain due to tilting of the basin bed caused by an earthquake in 1959, while Nanson (1980) reported that the easterly migration of the Beatton River in British Columbia was caused by regional post-glacial isostatic tilting. Peakall *et al.* (2000) synthesised the results of several Holocene studies of lateral-tilt-induced channel migration to show that channels migrated laterally by avulsion in response to high rates of tilting, while they migrated laterally by progressive erosion of meander bends in response to lower rates of tilting. In run 3xR, the large left terrace in the original delta area precluded any chance of avulsion, but the magnitude of the cross-basin

slope and flood flows clearly combined to produce a certain stream power and certain rate of lateral channel movement.

The tendency for alluvial channels to migrate laterally due to geological tilting or cross-reservoir-basin slope is of general importance to the study of dam removal because it indicates that (Nanson, 1980)

‘the prediction of changes in channel position over time may depend not only on hydraulic and sedimentological variables, but also on factors that operate at a regional scale.’

In particular, if the reservoir sediment deposit is significantly wider than the channel, the volume of sediment eroded during and after dam removal has the potential to vary considerably depending on the point at which the incising channel intercepts the tilted surface and begins to be influenced by it. If the intercept is towards the up-tilt end of the sloping surface, as in the right marginal runs in these experiments, then the possibility exists that the channel will be able to migrate down-tilt, particularly during flood events when stream powers are higher and the channel has a greater capacity to erode large volumes of sediment. Conversely, if the intercept is at the down-tilt end of the slope, this possibility is eliminated. Furthermore, and all other factors being equal, it is reasonable to assume that a greater degree of cross-basin tilting should also result in a greater rate of sediment erosion and down-tilt migration, which clearly has important implications for sediment management and the magnitude of downstream impacts during and after dam removal, particularly when the greater magnitude of flood flows further amplifies the stream power associated with the tilt.

The model’s vertical distortion results in a cross-reservoir-basin tilt that is 3.79 times greater than in the prototype Lake Mills basin, which is much larger than the values reported in the literature in cases of lateral, down-tilt channel migration: Alexander *et al.* (1994) reported an earthquake-induced tilt of the Madison River floodplain of 0.00022, while Nanson (1980) reported an isostatic tilting of 0.0003 to 0.0004. This suggests that the *rate* at which the channel in run 3xR eroded leftwards may be a scale effect, but that the occurrence of down-tilt channel migration was a valid phenomenon.

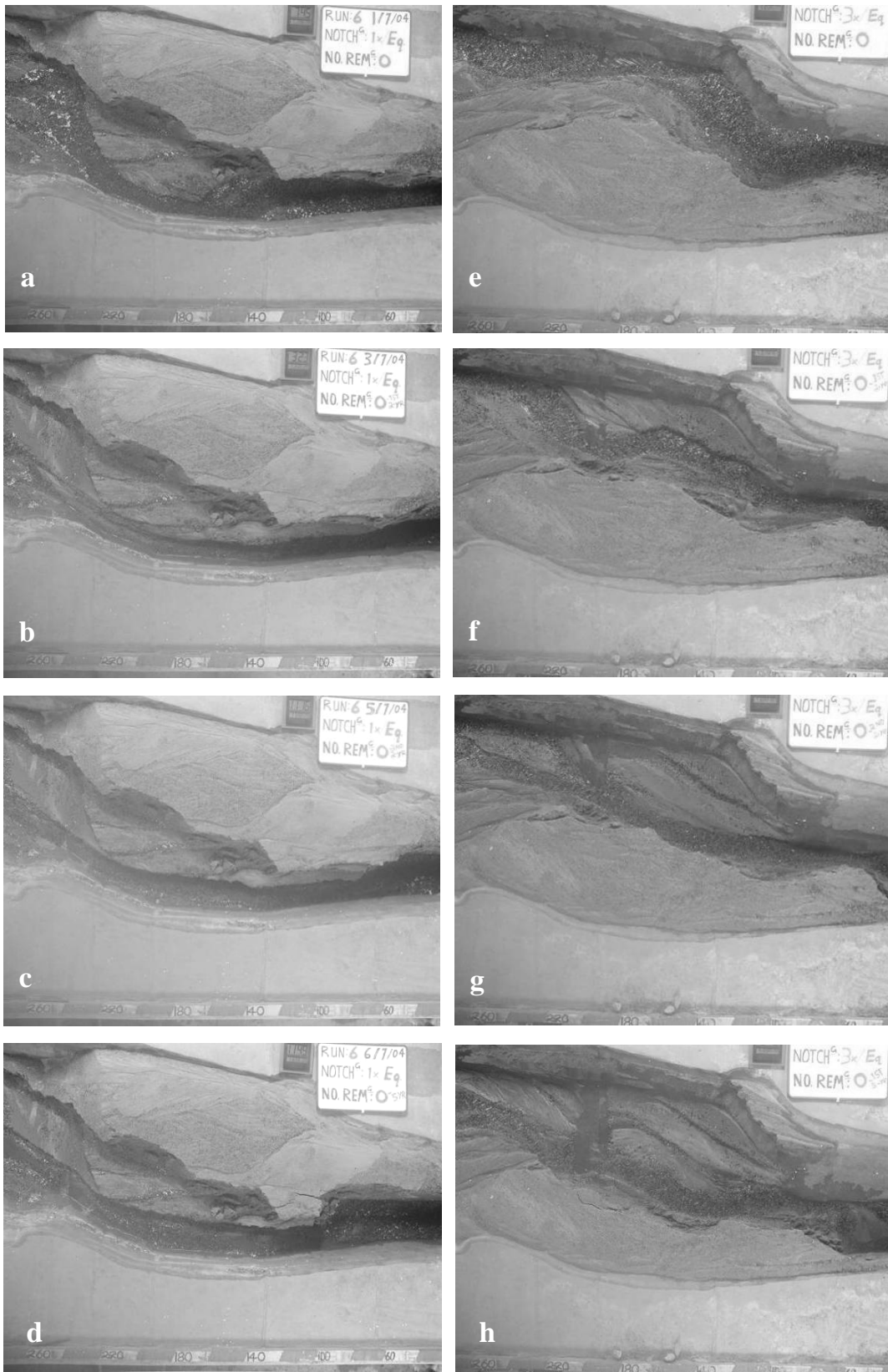


Figure 8.4. Original delta area in (a-d) run 1xL and (e-f) run 3xR at static equilibriums after (a & e) complete dam removal; (b & f) 1st two-year flow; (c & g) 2nd two-year flow; (d & h) five-year flow.

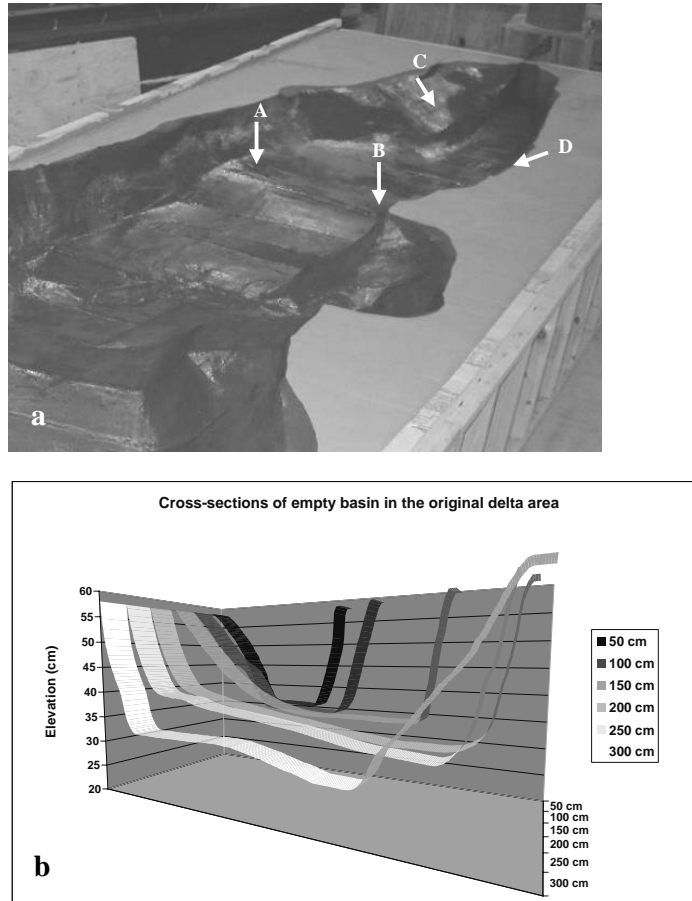


Figure 8.5. (a) View looking upstream at the empty basin in the original delta area. (b) Graphical representation of the original delta area, whose downstream extent is delimited by the arrows A and B in (a). Note the elevation difference between the streamwise right and left sides of the basin downstream from 150 cm. The maximum elevation difference (at the 200 cm cross-section) is about 8 cm.

8.3 Implications of the model results for removal of the prototype Glines Canyon Dam

Perhaps the key finding with regards to the sediment management objectives outlined in section 2.3.4 is that in order to maximize the distribution of original delta sediment throughout the entire reservoir area it is necessary to use a central pilot channel that will keep the incising and laterally moving channel away from the reservoir boundary for as long as possible. When the incising channel comes into contact with the reservoir boundary at or shortly after the start of dam removal, its ability to move laterally within the original delta area is restricted. This increases the chance that high, unstable terraces will remain in the original delta area.

In conjunction with a central pilot channel, the results suggest that the volume

of original delta sediment eroded will be maximised by maximising the magnitude of the incremental drop in base level. Such a magnitude of drop cannot practically be achieved with the chosen dam removal methodology, however, and it is doubtful that it could be achieved even if expensive engineering works were undertaken to install the gate facilities necessary to allow such rapid draining of the reservoir. In addition, the volumes of water released under such a scenario would probably pose a serious flood hazard. The results also suggest, however, that original delta erosion volumes comparable to those obtained using very large magnitude drops in baselevel can be achieved using much smaller increments of dam removal. This is encouraging from the practical point of view because it leads to the very real possibility that close to maximum volumes of original delta erosion can be obtained using incremental drops in baselevel that are obtainable in the prototype.

In turn, this suggests that it may be possible in the prototype to maximize the ratio of vegetation root-zone volume to overall reservoir sediment volume, thus maximizing the volume of sediment that is locked into short- to medium term storage within the reservoir area. But maximizing this ratio may result in much greater volumes of sediment entering the downstream system than if less of the original delta is eroded during the dam removal phase. This may occur because the greater the volume of sediment located in the downstream half of the reservoir by the end of dam removal, the shorter the distance it has to travel before entering the downstream system. Conversely, when larger volumes of sediment are maintained in the upstream half of the delta by the end of dam removal, a subsequent flood flow with a two-year recurrence interval will still mobilize significant proportions of delta material but, because this large influx of sediment leads to the formation of a braided planform, a greater proportion is deposited across much of the width of the middle and downstream reaches of the reservoir, which effectively act as a sediment trap, than is transported into the downstream system.

The possibility therefore arises that, while maximizing the volume of original delta material that is eroded will maximize the *potential* volume that can be stabilized by recolonizing vegetation, the *actual* volume that is stabilized may be somewhat less. At the very least, the results suggest that maximizing the volume of original delta eroded will lead to large volumes of the coarse fraction entering the downstream system in the latter stages of dam removal. How much sediment then actually remains

in the reservoir area after dam removal and over the period of time required for vegetation to begin providing significant protection against erosion, and especially against mass wasting, may be very sensitive to the timing of the first large flows following dam removal. If a large flow occurs before this protection has developed, then potentially very large volumes of sediment will be flushed into the downstream system. Every effort should therefore be made to ensure that vegetation is re-established as quickly as possible.

Chapter 9 Conclusions

This study has presented the results of a scaled physical modelling investigation of the proposed removal of the Glines Canyon Dam from the Elwha River in Washington, USA. There have been very few other laboratory investigations studying the effects of dam removal and, to the best of the author's knowledge, only one other scaled modelling investigation of a specific dam removal project, that of Marmot Dam on the Sandy River in Oregon (Grant, Personal Communication, 2007). While the site-specific nature of the study introduced a number of issues related to scale effects, experimental limitations and the number of variables influencing system behaviour, it revealed a number of important facets of system behaviour that might not otherwise have become apparent had the experiments been performed in a rectangular flume. These and the other experimental findings are summarised below, together with several suggestions for further investigations.

9.1 Summary of experimental results

The programme of experimental research was motivated by the uncertainty surrounding the behaviour of the coarse delta sediments in Lake Mills. Because of the coupled upstream-downstream nature of the response to dam removal outlined at the end of Chapter 1 and for the project-specific reasons described in Chapter 2, it was important to gain an understanding of the morphodynamical response of the reservoir delta to dam removal. At the outset, the principle variable to be investigated was primarily the influence of variations in the magnitude of incremental drops in reservoir water surface elevation and, secondarily, the effects of varying the rate of this drop in base level.

The results from the marginal runs did not show any magnitude of base level drop signal during the removal of the first 12 dam pieces, but runs 1xL and 3xL did display such a signal for the removal of the 13th to 21st dam pieces. The results from the central runs also suggest that there was a magnitude of base level drop signal in the original delta erosion volumes, but this signal was weaker than for the two left marginal runs, especially in relation to the large differences in incremental base level drop. This was thought to be caused by a negative feedback between the rate of original delta erosion, the rate of delta progradation and the ability of the effects of the

drop in base level to migrate upstream into the original delta area, and by the stabilising effects of the armour layer in the original delta area. It is hypothesised that the negative feedback may arise because of the lateral channel adjustments over the prograding delta surface, which acted to dissipate the excess energy through braiding and the development of a sinuous planform. If a full suite of central runs had been performed with magnitudes of drop ranging from one dam piece per increment of dam removed to 21 pieces per increment, this suggests that there may have been an exponential decrease in the volume of sediment eroded with increasing magnitudes of baselevel drop. In turn, this suggests that there may have been an optimum magnitude of base level drop beyond which no significant further increases in total erosion volume accrue. Without the full suite of central runs, it is not possible to state with any certainty which magnitude this may have been, but the relatively small difference in erosion volumes between runs 6xC and 12xC suggests that it may be close to the former.

The results from all runs showed clearly that the greatest volumes of original delta erosion occurred during central runs, when the incising channel was kept away from the basin boundary for as long as possible at the start of dam removal. Furthermore, the results from the marginal runs highlighted the great degree of influence that the asymmetrical reservoir basin boundary in the original delta area exerted on the trajectories of system evolution. In particular, the differences between the left and right marginal runs showed how a transverse slope through the original delta area could greatly affect the volumes of sediment eroded during floods, when the flows had sufficient power to completely break up the armour layer. The basin sloped from a higher elevation through the right half of the original delta area to a lower elevation through the left half, the path of the pre-dam thalweg. During run 3xR the flood flows' power and cross-basin tilt allowed the channel to very rapidly incise its bed and erode a substantial portion of the left terrace through the entire original delta area as it moved down-tilt towards the pre-dam thalweg. In runs 1xL and 3xL, the channel was already at the base of the tilted surface and this, together with the left hand curvature of the basin boundary, directed the bulk of the floods' erosive powers away from the right terrace deposits, which resulted in substantially smaller volumes of erosion for comparable flood flows. Although the effects of transverse slopes on lateral channel migration have been reported previously, their possible role in

influencing the response of reservoir sediments to dam removal has not been previously reported.

Two interesting phenomena relating to the armour layer were observed during the experiments. The first was referred to herein as Bed Elevation Lowering Without Armour Layer Break-up - BELWALB and, to the best of the author's knowledge, has not been reported elsewhere in the literature. The significance of BELWALB was that it was able to trigger periods of sometimes extensive geomorphological work without breaking up the armour layer, because of the alterations to streamlines that occurred as the bed changed shape. Incision and/or lateral adjustments were most likely to be triggered when the channel system was very close to a threshold of instability. The second phenomenon was mobility reversal, which has been observed in previous studies and whose causes have been investigated by Solari and Parker (2000). Some of the mobility reversal may have been caused by viscous effects and is therefore probably a scale effect, since viscous effects were unlikely to have been a feature of the 1994 drawdown experiment. Some of the mobility reversal may have been caused by bedslopes in excess of about 2-3%, however, which occurred throughout the entire delta surface and were shown to be a cause of mobility reversal by Solari and Parker (2000). This may also be a scale effect, since part of the steepness of the bedslopes may have been caused by the excessively coarse modelling material, but it is entirely possible that mobility reversal could occur in prototype dam removals, especially where large magnitude drops in base level can generate bed slopes in excess of 2-3%, at least for short periods of time. Mobility reversal increases the rate at which gravels are transported either further into the reservoir basin, where they can either be dispersed over or buried by the prograding delta, or concentrated to greatly extent the downstream limit of the armour layer.

Of particular concern to this study was the magnitude and rate at which sediment could enter the river system downstream from the dam, because of the potential for adverse impacts to human infrastructure and the aquatic community. In general, all full dam removal scenarios investigated in this study showed that the volumes of sediment entering the downstream channel during and immediately after dam removal will be substantial, ranging from about 37% of the total coarse load (run 3xL(A)) to 75% (run 3xC). Although there were a number of scale effects and experimental simplifications that precluded the erosion volumes being scaled up to

estimate possible prototype erosion volumes, if the proportions indicated are reasonable to within an order of magnitude, they suggest that the volumes of sediment entering the downstream channel will be far in excess of most normal sediment loads that would have occurred had the dams never been built.

The results of the central and marginal runs suggest that it is important to consider the possible downstream impacts over at least two different time scales. Here, a short-term time scale is defined as the period during and after dam removal, up to and including the first two-year flood, which is assumed to occur at any time between the end of dam removal and two-years after the end of dam removal. A medium- to long-term time scale is defined as any period of time longer than the short-term time scale.

The central run removal scenarios suggest that, in the short-term, the magnitudes and rates at which sediment enters the downstream channel will be very large, thus increasing the risk of adverse sediment-related impacts, perhaps despite the use of adaptive sediment management techniques. On the other hand, the results suggest that a central-run removal scenario would be the most effective in achieving the stated sediment management objectives (section 2.3.4). These objectives include leaving the remaining reservoir sediment deposits in a geotechnically-stable configuration, with relatively low relief and even topography, thus increasing the effectiveness with which they can be further stabilised by recolonizing vegetation. In turn, this suggests that the downstream sediment-related impacts over the medium to short-term would be quite small, since it would require a very large flood to entrain large quantities of sediment.

The marginal run removal scenarios suggest that, in the short-term, the magnitudes and rates at which sediment enters the downstream channel will be somewhat smaller than in the central runs, thus decreasing the risk of adverse sediment-related impacts and increasing the likelihood that adaptive management monitoring can prevent any serious consequences. On the other hand, the results of these runs suggest that there is an increased likelihood of leaving behind high and unstable terraces in the medium- to long-term that could be easily eroded by floods of even a moderate magnitude. There would thus be an increased risk of longer-term, lower intensity sediment-related impacts downstream. These scenarios would also be less likely to meet the sediment management objectives for the reservoir area. It

should be noted that the marginal runs were all performed with just a single-thread channel, while the drawdown experiment in 1994 proceeded with two main channels across the delta surface (Figure 2.10). The 1994 drawdown was only performed over a vertical distance of 5.5 metres, however, and it is highly likely that when the dam is removed and the drawdown is much greater, incision will migrate to the head of the proximal delta and allow one channel to capture all the flow, thus establishing conditions more similar to those in the model.

9.2 Wider implications

The results of this study show that it is possible for there to be an optimum magnitude and/or rate of baselevel drop signal for other dam removals, but possibly only for RPSF removals that fulfil certain criteria. The negative feedback hypothesis requires a sufficiently wide prograding delta surface over which the channel can exhibit significant lateral movements, both of cross-sectional width and planform. In turn, this implies that there may be a certain minimum ratio of channel width to reservoir width above which this mechanism does not operate, irrespective of whether the reservoir is long or short. This is in accordance with the observation of Annandale and Morris (1998), who note that in narrow reservoirs not much wider than channel width, most of the sediment will be eroded during reservoir flushing. According to this reasoning, then, a magnitude of baselevel drop signal should not be expected in RSF removals, because any extra lateral adjustments with increasing magnitudes of base level drop would by definition increase the volume of original delta erosion.

The second condition is that the channel bed over the surface of the eroding deposit probably needs to be able to form an armour layer, *i.e.* that the deposit is a mixture of sand and gravel/cobble, since this introduces a significant threshold of stability that requires a certain amount of energy to break through. In reservoirs whose deposit is mostly sand, experimental evidence suggests that the magnitude of erosion is likely to be similar along the full length of the deposit.

The role played by the pre-dam topography of the reservoir area in this study indicates that this factor is likely to be of importance in any dam removal study, be it an RSF or an RPSF removal and irrespective of the sediment management outcome being sought, since it has the ability to greatly enhance or hinder the process of delta erosion. Evidence beginning to emerge from the Marmot Dam modelling study

appears to support this finding, while data from the prototype removal, which took place in the summer of 2007, will provide further clarification (Grant, Personal Communication, 2007).

9.3 Further research

The research reported in this study has revealed a number of important relationships that appear to have significant effects on the rates and volumes at which sediment is eroded from the original delta area. A number of these factors may also be more widely applicable to other dam removal studies. A lack of experimental replication, scale effects and experimental simplifications means that more work should be carried to clarify the conditions under which the phenomena reported herein are likely to operate.

The hypothesised relationship between the ratio of channel width to reservoir width, magnitude of baselevel drop, grain size distribution and erosion volume should be further investigated. If the ability of the channel to adjust its planform does vary as described in Chapters 3 and 8, then this is an important relationship that needs to be understood, since it has important implications for sediment management. The research should first determine whether the hypothesised mechanism is valid and, if so, if there is a threshold value of the ratio above which it ceases to operate.

Experimental work should be undertaken to further understand the role played by BELWALB in the evolution of incising, gravel-bedded systems. BELWALB appears to operate at the threshold between stability and instability and, as such, it is an important step in understanding how armoured channel beds respond to disturbance, at least in an incising system. In some cases, it was the last adjustment that took place as upstream-migrating incision decayed below the point at which it could break-up the armour layer; in others it was the first adjustment that took place as positive feedbacks rapidly triggered large-scale incision and lateral channel movements. Work should focus first of all on identifying the conditions under which BEWALB is likely to develop. Secondly, it should examine precisely how it triggers morphological adjustments. Observations reported here suggest that it can do so by kick-starting the process of armour layer break up. It was also hypothesised that it may trigger adjustments by subtly altering the directions of streamlines, which in turn alter the distribution of boundary shear stresses. If the system is very close to a

threshold of instability, this may be sufficient to push the system across the threshold. This should be investigated.

Solari and Parker (2000, p.195) ‘predict with some confidence that the [mobility] reversal will indeed be observed in nature under the right conditions’. The results of the current study suggest that such conditions might include the removal of a dam whose reservoir impounds a mixture of sand and gravel. The results also suggest, however, that the occurrence of mobility reversal may have been due to scale effects. Work should be performed to see if the reversal can be replicated in conditions representative of those during dam removal and that are not affected by scale effects.

9.4 Concluding thoughts

Dam removal is increasingly being applied in the United States as a means of restoring degraded river systems. At present, the number of dams removed is a tiny fraction of the total number of dams in the country, but dam removal is entering the conscience of an increasing number of people, both environmental professionals and members of the public. Its viability as a management option is thus increasing apace and, as principally economic factors lead to decisions being made about what to do with old, or not so old, dams, removal will increasingly be applied as the most cost effective and environmentally beneficial option, although care will have to be exercised in dealing with contaminated sediments.

The world’s trend in large dam construction has closely mirrored that of the United States’ for construction of all dams (*cf.* Figures 1.1 and 1.2) and it will continue to do so as suitable sites for dam construction continue to diminish, although the time frame over which this will occur is unclear. It will be interesting to see if a global trend for dam removal similarly develops and mirrors that in the United States. If so, this is likely to happen first in the more economically developed countries and it may be some considerable time before it does so in less economically developed nations. Eventually, however, all countries with dams will be faced with the same issues of an ageing infrastructure currently being addressed in the United States and it is to be hoped that a greater body of understanding will exist and that predictive tools have been developed based on the U.S. experience to help these countries more easily manage these issues as and when they arise.

Three major confounding variables to a prediction of increased global dam removal are the effects of global population growth, socio-economical development and climate change. The first two will continue to place greater demands on the planet's freshwater resources over the coming decades (United Nations Environment Programme, 2000), while the effects of anthropogenic climate forcing will probably lead to an intensification of the hydrological cycle (Arnell, 1999b; 2003a; 2003b; Huntington, 2006). The effects of intensification will vary regionally and in some parts of the world they may counter the increasing water stress due to population growth and development, while in others they might exacerbate it (Arnell, 1999a; Vörösmarty *et al.*, 2000). The maintenance of existing dams and the construction of new ones will certainly be considered as options to address these pressures, although these are not always be the best options: there are less intrusive methods for managing floods and generating electricity, for example. For these to be more widely applied, however, there will need to be a paradigm shift in the thinking of many governments around the world, many of whom still have a 'build big' mentality or are beholden to special interests. Where decisions are taken to maintain the storage capacity of existing reservoirs, however, the results from dam removal studies such as this one may have a role to play, since the morphodynamical processes operating in the reservoir during dam removal may be similar to those that operate during reservoir flushing.

References

- Ackermann, F., 1978. Experimental investigation into the accuracy of contouring through digital terrain modelling. *Proceedings of the Digital Terrain Modelling Symposium*, St. Louis, pp. 165-192.
- Ackers, P., 1972. River regime: Research and Application. *Journal of the Institution of Water Engineers and Scientists*, 26: 257-275.
- Alexander, J., Bridge, J.S., Leeder, M.R., Collier, R.E.L. and Gawthorpe, R.L., 1994. Holocene meander-belt evolution in an active extensional basin, southwestern Montana. *Journal of Sedimentary Research Section B-Stratigraphy and Global Studies*, 64(4): 542-559.
- American Rivers, Friends of the Earth and Trout Unlimited, 1999. *Dam Removal Success Stories: Restoring Rivers through Selective Removal of Dams that don't make Sense*. American Rivers, Friends of the Earth, Trout Unlimited. 114 pp.
- American Rivers, 2004. *Rivers Unplugged*. Accessed at http://www.americanrivers.org/site/PageServer?pagename=AMR_content_1af3 on Tuesday 28 November 2006.
- Annandale, G.W. and Morris, G.L., 1998. Decommissioning of dams. In: G.L. Morris and J. Fan (Editors), *Reservoir Sedimentation Handbook: Design and Management of Dams, Reservoirs, and watersheds for Sustainable Use*. McGraw-Hill, New York, pp. 17.1-17.25.
- Antropovskiy, V.I., 1972. Criterial relations of types of channel processes. *Soviet Hydrology*, 11: 371-381.
- Apmann, R.P., 1972. Flow processes in open channel bends. *Journal of the Hydraulics Division, ASCE*, 98(HY5): 795-810.
- Arnell, N.W., 1999a. Climate change and global water resources. *Global Environmental Change*, 9, Supplement 1: S31-S49.
- Arnell, N.W., 1999b. The effect of climate change on hydrological regimes in Europe: a continental perspective. *Global Environmental Change*, 9(1): 5-23.
- Arnell, N.W., 2003a. Relative effects of multi-decadal climatic variability and changes in the mean and variability of climate due to global warming: future streamflows in Britain. *Journal of Hydrology*, 270: 195-213.
- Arnell, N.W., 2003b. Effects of IPCC SRES* emissions scenarios on river runoff: a global perspective. *Hydrology and Earth System Sciences*, 7(5): 619-641.
- ASCE, 1997. *Guidelines for Retirement of Dams and Hydroelectric Facilities*. American Society of Civil Engineers, New York, 222 pp.
- ASCE, 2000. *Hydraulic Modeling: Concepts and Practice*. ASCE Manuals and Reports on Engineering Practice, Manual 97, American Society of Civil Engineers, Reston, Virginia. 390 pp.
- ASCE Task Committee on Hydraulics Bank Mechanics and Modelling of River Width Adjustment, 1998. *River Width Adjustment. I: Processes and Mechanisms*. *Journal of Hydraulic Engineering-ASCE*, 124(9): 881-902.
- Ashmore, P.E., 1991a. How do gravel-bed rivers braid? *Canadian Journal of Earth Sciences*, 28: 326-341.
- Ashmore, P.E., 1991b. Channel morphology and bed load pulses in gravel-bed stream. *Geografiska Annaler*, 68: 361-371.
- Ashworth, P.J., Best, J.L., Leddy, J.O. and Geehan, G.W., 1994. The physical modelling of braided rivers and deposition of fine grained sediment. In: M.J. Kirkby (Editor), *Process Models and Theoretical Geomorphology*. Wiley, Chichester, pp. 115-139.

- Ashworth, P.J., Best, J.L. and Jones, M., 2004. Relationship between sediment supply and avulsion frequency in braided rivers. *Geology*, 32(1): 21-24.
- Assani, A.A. and Petit, F., 2004. Impact of hydroelectric power releases on the morphology and sedimentology of the bed of the Warche River (Belgium). *Earth Surface Processes and Landforms*, 29(2): 133-143.
- Atkinson, E., 1996. The Feasibility of Flushing Sediment from Reservoirs. Report OD 137, HR Wallingford, Wallingford.
- Bachtold, L.M., 1982. Destruction of Indian Fisheries and Impact to Indian Peoples. The Historic and Economic Value of Salmon and Steelhead to Treaty Fisheries in River Systems in Washington, Oregon and Idaho. A report to the Bureau of Indian Affairs. Meyer-Zangri Associates.
- Bagnold, R.A., 1960. Some aspects of the shape of river meanders. United States Geological Survey Professional Paper, 282E. 135-144 pp.
- Bagnold, R.A., 1966. An approach to the sediment transport problem from general physics. U.S. Geological Survey Professional Paper 422-I, United States Geological Survey. 1-37 pp.
- Bathurst, J.C., Thorne, C.R. and Hey, R.D., 1979. Secondary flow and shear stress at river bends. *Journal of the Hydraulics Division, ASCE*, 105(HY10): 1277-1294.
- Begin, Z.B., Meyer, D.F. and Schumm, S.A., 1980. Knickpoint migration due to baselevel lowering. *Journal of the Waterway Port Coastal and Ocean Division-ASCE*, 106(WW3): 369-388.
- Bennett, S.J., 1999. Effect of slope on the growth and migration of headcuts in rills. *Geomorphology*, 30(3): 273-290.
- Bennett, S.J., Alonso, C.V., Prasad, S.N. and Römken, M.J.M., 2000. Experiments on headcut growth and migration in concentrated flows typical of upland areas. *Water Resources Research*, 36(7): 1911-1922.
- Bennett, S.J. and Casali, J., 2001. Effect of initial step height on headcut development in upland concentrated flows. *Water Resources Research*, 37(5): 1475-1484.
- Berg, O.K., Arnekleiv, J.V. and Lohrmann, A., 2006. The influence of hydroelectric power generation on the body composition of juvenile Atlantic salmon. *River Research and Applications*, 22(DOI: 10.1002/rra.949): 993-1008.
- Bergstedt, L.C. and Bergersen, E.P., 1997. Health and movements of fish in response to sediment sluicing in the Wind River, Wyoming. *Canadian Journal of Fisheries and Aquatic Sciences*, 54: 312-319.
- Bettess, R., 1990. Survey of lightweight sediments for use in mobile-bed physical models. In: H.W. Shen (Editor), *Movable Bed Physical Models*. NATO ASI Series, Series C: Mathematical and Physical Sciences, Vol. 312. Kluwer Academic Publishers, Dordrecht, Netherlands, pp. 115-123.
- Bilby, R.E., Fransen, B.R. and Bisson, P.A., 1996. Incorporation of nitrogen and carbon from spawning coho salmon into the trophic system of small streams: Evidence from stable isotopes. *Canadian Journal of Fisheries and Aquatic Sciences*, 53(1): 164-173.
- Born, S.M., Genskow, K.D., Filbert, T.L., Hernandez-Mora, N., Keefer, M.L. and White, K.A., 1998. Socioeconomic and institutional dimensions of dam removals: The Wisconsin experience. *Environmental Management*, 22(3): 359-370.
- Bowman, M., 2002. Legal Perspectives on Dam Removal. *Bioscience*, 52(8): 739-747.

- Brandt, S.A., 2000a. Classification of geomorphological effects downstream of dams. *Catena*, 40: 374-401.
- Brandt, S.A., 2000b. Prediction of downstream geomorphological changes after dam construction: a stream power approach. *International Journal of Water Resources Development*, 16(3): 343-367.
- Brasington, J. and Smart, R.M.A., 2003. Close range digital photogrammetric analysis of experimental drainage basin evolution. *Earth Surface Processes and Landforms*, 28(10.1002/esp.479): 231-247.
- Bromley, J.C., 2003. Sutter Creek Sediment Transfer Study: The response of impounded sediment to a culvert replacement project on Sutter Creek, a tributary of Honey Grove Creek in the Alsea River Basin of the Central Oregon Coast Range. Unpublished report prepared for Benton County Public Works, Corvallis, OR. 96 pp.
- Bromley, J.C., Cantelli, A. and Wooster, J., Accepted for publication. Experimental research on reservoir sediment response following dam removal. ASCE Monograph on Sediment Dynamics Post Dam Removal. ASCE.
- Brookes, A., 1996. Floodplain Restoration and Rehabilitation. In: M.G. Anderson, D.E. Walling and P.D. Bates (Editors), *Floodplain Processes*. John Wiley & Sons Ltd., pp. 553-576.
- Brush, L.M. and Wolman, M.G., 1960. Knickpoint Behaviour in Noncohesive Material: A Laboratory Study. *Bulletin of the Geological Society of America*, 71: 59-74.
- Bryan, R.B., 1990. Knickpoint Evolution in Rillwash. In: R.B. Bryan (Editor), *Soil Erosion - Experiments and Models*, *Catena Supplement 17*. Cremlingen-Destedt, Germany, pp. 111-132.
- Buffington, J.M. and Montgomery, D.R., 1997. A systematic analysis of eight decades of incipient motion studies, with special reference to gravel-bedded rivers. *Water Resources Research*, 33(8): 1993-2029.
- Bunte, K. and Abt, S.R., 2001. Sampling Surface and Subsurface Particle-Size Distributions in Wadable Gravel- and Cobble-Bed Streams for Analyses in sediment Transport, Hydraulics, and Streambed Monitoring. General Technical Report, RMRS-GTR-74, United States Department of Agriculture, Forest Service, Rocky Mountain Research Station, Fort Collins, CO. 428 pp.
- Bureau of Reclamation, 1995a. Development of Flood Hydrographs. Elwha Technical Series PN-95-1, Department of the Interior, Pacific Northwest Region, Boise, Idaho. 88 pp.
- Bureau of Reclamation, 1995b. Lake Mills Geologic Section A-A', Drawing Number 1440-100-4, ACAD v12.
- Bureau of Reclamation, 1995c. Lake Mills Reservoir Site Preconstruction Topography - 1926, Drawing Number 1440-100-2, ACAD v12.
- Bureau of Reclamation, 1995d. Overview of Groundwater Conditions. Elwha Technical Series PN-95-3, U.S. Department of the Interior, Pacific Northwest Region, Boise, Idaho. 12 pp.
- Bureau of Reclamation, 1996a. Sediment Analysis and Modeling of the River Erosion Alternative. Elwha Technical Series PN-95-9, U.S. Department of the Interior Bureau of Reclamation Technical Service Center, Denver, CO and Pacific Northwest Regional Office, Boise, ID, Denver, CO. 157 pp.
- Bureau of Reclamation, 1996b. Removal of Elwha and Glines Canyon Dams. Elwha Technical Series PN-95-7, Department of the Interior, Bureau of Reclamation, Pacific Northwest Region, Boise, Idaho. 88 pp.

- Bureau of Reclamation, 1996c. Alluvium Distribution in the Elwha River Channel between Glines Canyon Dam and the Strait of Juan de Fuca, Washington. Elwha Technical Series PN-95-5, Department of the Interior, Bureau of Reclamation, Pacific Northwest Region, Boise, Idaho. 19 pp.
- Bureau of Reclamation, 1996a. Removal of Elwha and Glines Canyon Dams. Elwha Technical Series PN-95-7, Department of the Interior, Bureau of Reclamation, Pacific Northwest Region, Boise, Idaho. 88 (plus appendices) pp.
- Bureau of Reclamation, 1996b. Sediment Analysis and Modeling of the River Erosion Alternative. Elwha Technical Series PN-95-9, U.S. Department of the Interior Bureau of Reclamation Technical Service Center, Denver, CO and Pacific Northwest Regional Office, Boise, ID, Denver, CO. 157 pp.
- Bureau of Reclamation, 1997. Water Quality Analysis and Mitigation Measures. Elwha Technical Series PN-95-8, Department of the Interior, Pacific Northwest Region, Boise, Idaho. 105 pp.
- Butler, D.R. and Malanson, G.P., 2005. The geomorphic influences of beaver dams and failures of beaver dams. *Geomorphology*, 71(1-2): 48-60.
- Cairns Jr., J., 1991. The status of the theoretical and applied science of restoration ecology. *The Environmental Professional*, 13: 186-194.
- Camargo, J.A. and Voelz, N.J., 1998. Biotic and abiotic changes along the recovery gradient of two impounded rivers with different impoundment use. *Environmental Monitoring and Assessment*, 50(2): 143-158.
- Cantelli, A., Paola, C. and Parker, G., 2004. Experiments on upstream-migrating erosional narrowing and widening of an incisional channel caused by dam removal. *Water Resources Research*, 40, W03304, doi:10.1029/2003WR002940.
- Carlisle, B.H., 2005. Modelling the spatial distribution of DEM error. *Transactions in GIS*, 9(4): 521-540.
- Casagli, N., Rinaldi, M., Gargini, A. and Curini, A., 1999. Pore water pressure and streambank stability: results from a monitoring site on the Sieve River, Italy. *Earth Surface Processes and Landforms*, 24: 1095-1114.
- Chadwick, A. and Morfett, J., 1998. *Hydraulics in Civil and Environmental Engineering*. E & FN Spon, London and New York, 3rd Edition, 600 pp.
- Chanson, H., 1999. *The Hydraulics of Flow in Open Channels*. Arnold, London, First, 495 pp.
- Chorley, R.J., 1967. Models in Geomorphology. In: R.J. Chorley and P. Haggett (Editors), *Models in Geography*. Methuen, London, pp. 59-96.
- Clifford, N.J., 1993. Formation of Riffle Pool Sequences - Field Evidence for an Autogenetic Process. *Sedimentary Geology*, 85(1-4): 39-51.
- Cline, L.D., Short, R.A. and Ward, J.V., 1982. The Influence of Highway Construction on the Macroinvertebrates and Epilithic Algae of a High Mountain Stream. *Hydrobiologia*, 96(2): 149-159.
- Coleman, J.M., 1969. Brahmaputra River: Channel processes and sedimentation. *Sedimentary Geology*, 3: 129-239.
- Cui, Y.T., Braudrick, C., Dietrich, W.E., Cluer, B. and Parker, G., 2006a. Dam Removal Express Assessment Models (DREAM). Part 2: Sample runs/sensitivity tests. *Journal of Hydraulic Research*, 44(3): 308-323.
- Cui, Y.T., Parker, G., Braudrick, C., Dietrich, W.E. and Cluer, B., 2006b. Dam Removal Express Assessment Models (DREAM). Part 1: Model development and validation. *Journal of Hydraulic Research*, 44(3): 291-307.

- Culp, J.M., Wrona, F.J. and Davies, R.W., 1986. Response of Stream Benthos and Drift to Fine Sediment Deposition Versus Transport. *Canadian Journal of Zoology-Revue Canadienne De Zoologie*, 64(6): 1345-1351.
- Davies, T.R.H. and Sutherland, A.J., 1980. Resistance to flow past deformable boundaries. *Earth Surface Processes*, 5: 175-179.
- Davis, W.M., 1899. The geographical cycle. *Geographical Journal*, 14(5): 481-504.
- Dietrich, W.E., Kirchner, J.W., Ikeda, H. and Iseya, F., 1989. Sediment supply and the development of the coarse surface layer in gravel-bedded rivers. *Nature*, 340(6230): 215-217.
- Dietz, A.L., 1993. Alliances: The New Foundation for America's Ports and Waterways. In: M. Reuss (Editor), *Water Resources Policy in the United States: Policy, Practice, and Emerging Issues*. American Water Resources Association/Michigan State University Press, East Lansing, pp. 218-230.
- Doeg, T.J. and Koehn, J.D., 1994. Effects of Draining and Desilting a Small Weir on Downstream Fish and Macroinvertebrates. *Regulated Rivers-Research & Management*, 9(4): 263-277.
- Doyle, M.W., Harbor, J.M., Rich, C.F. and Spacie, A., 2000. Examining the effects of urbanization on streams using indicators of geomorphic stability. *Physical Geography*, 21(2): 155-181.
- Doyle, M.W., Stanley, E.H. and Harbor, J.M., 2002. Geomorphic analogies for assessing probable channel response to dam removal. *Journal of the American Water Resources Association*, 38(6): 1567-1579.
- Doyle, M.W., Stanley, E.H. and Harbor, J.M., 2003. Channel adjustments following two dam removals in Wisconsin. *Water Resources Research*, 39(1).
- Doyle, M.W., Stanley, E.H., Orr, C.H., Selle, A.R., Sethi, S.A. and Harbor, J.M., 2005. Stream ecosystem response to small dam removal: Lessons from the Heartland. *Geomorphology*, 71(1-2): 227-244.
- Dynesius, M. and Nilsson, C., 1994. Fragmentation and Flow Regulation of River Systems in the Northern Third of the World. *Science*, 266(5186): 753-762.
- Elwha River Fish Restoration Plan, 2003. Elwha River Fish Restoration Plan - Draft.
- Epple, R., 2000. Dam decommissioning: French pilot experiences and the European context. *European Rivers Network*. Accessed at http://www.rivernet.org/general/dams/decommissioning/decom3_e.htm on Wednesday 19th February 2003.
- Eshleman, J.A., Malhi, R.S. and Smith, D.G., 2003. Mitochondrial DNA studies of Native Americans: conceptions and misconceptions of the population prehistory of the Americas. *Evolutionary Anthropology*, 12: 7-18.
- Florsheim, J.L., Mount, J.F. and Rutten, L.T., 2001. Effect of baselevel change on floodplain and fan sediment storage and ephemeral tributary channel morphology, Navarro River, California. *Earth Surface Processes and Landforms*, 26(2): 219-232.
- Foster Wheeler Environmental Corporation, 2000. Environmental Assessment for the Interim Management Plan, Elwha River Ecosystem Restoration. Prepared for National Park Service, Port Angeles, WA, Bellevue, Washington. 63 pp.
- Friedkin, J.F., 1945. A laboratory study of the meandering of alluvial rivers. U.S. Army Corps of Engineers Waterways Experiment Station, Vicksburg, MS.
- Friedman, J.M., Osterkamp, W.R., Scott, M.L. and Auble, G.T., 1998. Downstream effects of dams on channel geometry and bottomland vegetation: regional patterns in the Great Plains. *Wetlands*, 18(4): 619-633.

- Galay, V.J., 1983. Causes of river bed degradation. *Water Resources Research*, 19: 1057-1090.
- Gardner, T.W., 1983. Experimental-Study of Knickpoint and Longitudinal Profile Evolution in Cohesive, Homogeneous Material. *Geological Society of America Bulletin*, 94(5): 664-672.
- Gayraud, S., Philippe, M. and Maridet, L., 2000. The response of benthic macroinvertebrates to artificial disturbance: drift or vertical movement in the gravel bed of two Sub-Alpine streams? *Archiv Fur Hydrobiologie*, 147(4): 431-446.
- Gilbert, G.K., 1917. Hydraulic-mining debris in the Sierra Nevada. United States Geological Survey Professional Paper 105, Washington, DC.
- Gomez, B., Banbury, K., Marden, M., Trustrum, N.A., Peacock, D.H. and Hoskin, P.J., 2003. Gully erosion and sediment production: Te Weraroa Stream, New Zealand. *Water Resources Research*, 39(7).
- Gore, J.A., Niemela, S., Resh, V.H. and Statzner, B., 1994. Near-Substrate Hydraulic Conditions under Artificial Floods from Peaking Hydropower Operation - a Preliminary-Analysis of Disturbance Intensity and Duration. *Regulated Rivers-Research & Management*, 9(1): 15-34.
- Graf, W.L., 1999. Dam nation: A geographic census of American dams and their large-scale hydrologic impacts. *Water Resources Research*, 35(4): 1305-1311.
- Grams, P.E. and Schmidt, J.C., 2005. Equilibrium or indeterminate? Where sediment budgets fail: Sediment mass balance and adjustment of channel form, Green River downstream from Flaming Gorge Dam, Utah and Colorado. *Geomorphology*, 71(1-2): 156-181.
- Grant, G.E., 2001. Dam removal: Panacea or Pandora for rivers? *Hydrological Processes*, 15: 1531-1532.
- Grant, G.E., Lewis, S.L. and Kast, P., 2002. Sediment mass balance for Cougar Reservoir sediment releases: Supplement to "Evaluation of fine sediment intrusion into salmon spawning gravels related to Cougar Reservoir sediment releases". Unpublished report prepared for Portland District Office, U.S. Army Corps of Engineers. Available online at <http://www.fsl.orst.edu/wpg/research/cougar.htm>, USDA Forest Service, Corvallis, Oregon. 9 pp.
- Gray, L.J. and Ward, J.V., 1982. Effects of Sediment Releases from a Reservoir on Stream Macroinvertebrates. *Hydrobiologia*, 96(2): 177-184.
- Gregory, D.I., 1983. Response of a meandering river to artificial modification. In: C.M. Elliott (Editor), *River Meandering*. ASCE, New Orleans, Louisiana, pp. 398-409.
- Gregory, K.J., Davis, R.J. and Downs, P.W., 1992. Identification of River Channel Change to Due to Urbanization. *Applied Geography*, 12(4): 299-318.
- Gregory, S.V., Swanson, F.J., McKee, W.A. and Cummins, K.W., 1991. An Ecosystem Perspective of Riparian Zones. *Bioscience*, 41(8): 540-551.
- Gregory, S.V., Li, H.W. and Li, J.L., 2002. The Conceptual Basis for Ecological Responses to Dam Removal. *Bioscience*, 52(8): 713-723.
- Grissinger, E.H., 1982. Bank erosion of cohesive materials. In: R.D. Hey, J.C. Bathurst and C.R. Thorne (Editors), *Gravel-bed Rivers*. Wiley, Chichester, pp. 273-287.
- Halsall, P., 2004. Byzantium: The Byzantine Studies Page. Accessed at <http://www.fordham.edu/halsall/byzantium/index.html> on Sunday 19 November 2006.

- Harvey, A.M., 2002. The role of base-level change in the dissection of alluvial fans: case studies from southeast Spain and Nevada. *Geomorphology*, 45(1-2): 67-87.
- Harvey, J.W. and Bencala, K.E., 1993. The effect of streambed topography on surface-subsurface water interactions in mountain catchments. *Water Resources Research*, 29(1): 89-98.
- Harvey, M.D. and Watson, C.C., 1986. Fluvial Processes and Morphological Thresholds in Incised Channel Restoration. *Water Resources Bulletin*, pp. 359-368.
- Hassan, M.A. and Klein, M., 2002. Fluvial adjustment of the Lower Jordan River to a drop in the Dead Sea level. *Geomorphology*, 45(1-2): 21-33.
- Hayes, S.K., Montgomery, D.R. and Newhall, C.G., 2001. Fluvial sediment transport and deposition following the 1991 eruption of Mount Pinatubo. *Geomorphology*, 45: 211-224.
- Heinz Center, 2002. Dam Removal: Science and Decision Making. The H. John Heinz III Center for Science, Economics and the Environment, Washington, D.C., 221 pp.
- Heinz Centre, 2002. Dam Removal: Science and Decision Making. The H. John Heinz III Center for Science, Economics and the Environment, Washington, D.C., 221 pp.
- Hey, R.D., 1975. Response of Alluvial Channels to River Regulation, Proceedings of the Second World Congress, International Water Resources Association. International Water Resources Association, New Delhi, V, pp. 183-188.
- Hey, R.D. and Thorne, C.R., 1975. Secondary flows in river channels. *Area*, 7: 191-195.
- Hey, R.D., 1979. Dynamic process-response model of river channel development. *Earth Surface Processes*, 4: 59-72.
- Hey, R.D., 1988. Mathematical models of channel morphology. In: M.G. Anderson (Editor), *Modelling Geomorphological Systems*. Wiley, Chichester, pp. 99-125.
- Hickin, E.J., 1974. The development of meanders in natural river channels. *American Journal of Science*, 274: 414-442.
- Hickin, E.J. and Nanson, G.C., 1975. The character of channel migration on the Beaton River, northeast British Columbia, Canada. *Geological Society of America Bulletin*, 86: 487-494.
- Higgins, R.J., Pickup, G. and Cloke, P.S., 1987. Estimating the transport and deposition of mining waste at Ok Tedi. In: C.R. Thorne, J.C. Bathurst and R.D. Hey (Editors), *Sediment transport in gravel-bed rivers*. John Wiley and Sons Ltd., Chichester, pp. 949-975.
- Hogg, I.D. and Norris, R.H., 1991. Effects of Runoff from Land Clearing and Urban-Development on the Distribution and Abundance of Macroinvertebrates in Pool Areas of a River. *Australian Journal of Marine and Freshwater Research*, 42(5): 507-518.
- Holland, W.N. and Pickup, G., 1976. Flume study of knickpoint development in stratified sediment. *Geological Society of America Bulletin*, 87: 76-82.
- Hosey and Associates, 1988. Elwha Project FERC No. 2683, Glines project FERC No. 588, Response to Request for Additional Information of May 28, 1987, Appendix 5, Sediment Transport, Channel and Beach Morphology. James River II, Inc. 32 pp.

- Hosey and Associates Engineering Company, 1990. Response to August 15 1989 Request for Additional Information, Schedule A, Items 1-5, Distribution and Composition of Sediments Stored in Lake Aldwell and Lake Mills and Sediment Transport Characteristics. Elwha Project FERC No. 2683, Gline project FERC No. 588. Prepared for James River II, Inc., Seattle, Washington. 64 pp.
- Howard, A.D., Keetch, M.E. and Vincent, C.L., 1970. Topological and geometrical properties of braided streams. *Water Resources Research*, 6(6): 1674-1688.
- Huntington, T.G., 2006. Evidence for intensification of the global water cycle: Review and synthesis. *Journal of Hydrology*, 319: 83-95.
- Ippen, A.T. and Drinker, P.A., 1962. Boundary shear stresses in curved trapezoidal channels. *Journal of the Hydraulics Division, ASCE*, 88: 143-179.
- James, L.A., 1991. Incision and morphological evolution of an alluvial channel recovering from hydraulic mining sediment. *Bulletin of the Geological Society of America*, 103: 723-736.
- Janda, R.J., Meyer, D.F. and Childers, D., 1984. Sedimentation and geomorphic changes during and following the 1980-1983 eruptions of Mount St. Helens, Washington (2). *Sabo*, 37(3): 5-18.
- Johnson, S.E. and Graber, B.E., 2002. Enlisting the Social Sciences in Decisions About Dam Removal. *Bioscience*, 52(8): 731-738.
- Junk, W.J., Bayley, P.B. and Sparks, R.E., 1989. The Flood Pulse Concept in River-Floodplain Systems. In: D.P. Dodge (Editor), *Proceedings of the International Large River Symposium*. Canadian Special Publication of Fisheries and Aquatic Sciences, Department of Fisheries and Oceans, Ottawa, Ontario, Canada, Toronto, Ontario, 106, pp. 110-127.
- Kandiah, A., 1974. *Fundamental Aspects of Surface Erosion of Cohesive Soil*. Unpublished Unpublished Ph.D. Thesis, University of California, Davis, CA.
- Keller, E.A. and Melhorn, W., 1973. Bedforms and fluvial processes in alluvial stream channels: selected observations. In: M. Morisawa (Editor), *Fluvial Geomorphology*. Publications in Geomorphology, Binghampton, pp. 253-283.
- Knighton, A.D., 1989. River adjustment to changes in sediment load: the effects of tin mining on the Ringarooma River, Tasmania, 1875-1984. *Earth Surface Processes and Landforms*, 14: 333-359.
- Knighton, A.D., 1991. Channel Bed Adjustment Along Mine-Affected Rivers of Northeast Tasmania. *Geomorphology*, 4(3-4): 205-219.
- Knighton, A.D., 1998. *Fluvial forms and processes: A new perspective*. Arnold, London, 383 pp.
- Knuuti, K., 2001. Assessing the geomorphic effects of instream gravel mining on the Mad River, Humboldt County, California, *Proceedings of the Seventh Federal Interagency Sedimentation Conference*, Reno, Nevada, 2, pp. XI73-XI80.
- Kondratiev, N., Popov, I. and Snishchenko, B., 1982. *Foundations of Hydromorphological Theory of Fluvial Processes (In Russian)*. Gidrometeoizdat, Leningrad.
- Lane, S.N., Chandler, J.H. and Richards, K.S., 1994. Developments in Monitoring and Modeling Small-Scale River Bed Topography. *Earth Surface Processes and Landforms*, 19(4): 349-368.
- Lane, S.N., 1998. The Use of Digital Terrain Modelling in the Understanding of Dynamic River Channel Systems. In: S.N. Lane, K. Richards and J. Chandler (Editors), *Landform Monitoring, Modelling and Analysis*. John Wiley & Sons, Chichester, pp. 311-342.

- Lane, S.N., James, T.D. and Crowell, M.D., 2000. Application of digital photogrammetry to complex topography for geomorphological research. *Photogrammetric Record*, 16(95): 793-821.
- LaTray, D.A. and Stein, O.R., 1997. Headcut Advance in Stratified Soils. *Environmental and Coastal Hydraulics: Protecting the Aquatic habitat*. ASCE, New York, pp. 1245-1249.
- Leopold, L.B. and Wolman, M.G., 1957. River channel patterns - braided, meandering and straight. U.S. Geological Survey Professional Paper, 422-H, U.S. Geological Survey. 84 pp.
- Leopold, L.B., Bagnold, R.A., Wolman, M.G. and Brush, L.M., 1960. Flow resistance in sinuous or irregular channels. United States Geological Survey Professional Paper, 282D. 111-135 pp.
- Leopold, L.B. and Wolman, M.G., 1960. River Meanders. *Bulletin of the Geological Society of America*, 71: 769-794.
- Leopold, L.B. and Langbein, W.B., 1962. The concept of entropy in landscape evolution. U.S. Geological Survey Professional Paper, 500-A, United States Geological Survey. 20 pp.
- Leopold, L.B., Wolman, M.G. and Miller, J.P., 1964. *Fluvial Processes in Geomorphology*. Freeman, San Francisco, 552 pp.
- Leopold, L.B., 1994. *A View of the River*. Harvard University Press, Cambridge, MA, 298 pp.
- Lisle, T.E., 1982. Effects of Aggradation and Degradation on Riffle-Pool Morphology in Natural Gravel Channels, Northwestern California. *Water Resources Research*, 18(6): 1643-1651.
- Lisle, T.E. and Hilton, S., 1999. Fine bed material in pools of natural gravel bed channels. *Water Resources Research*, 35(4): 1291-1304.
- Lisle, T.E., Cui, Y., Parker, G., Pizzuto, J. and Dodd, A.M., 2001. The dominance of dispersion in the evolution of bed material waves in gravel-bed rivers. *Earth Surface Processes and Landforms*, 26: 1409-1420.
- Lisle, T.E., Submitted. The evolution of sediment waves influenced by varying transport capacity in heterogeneous rivers. *Gravel-Bed Rivers VI*.
- Long, B.D., 1993. Water Resources Development at a Crossroads. In: M. Reuss (Editor), *Water Resources Policy in the United States: Policy, Practice, and Emerging Issues*. American Water Resources Association / Michigan State University Press, East Lansing, pp. 258-263.
- Lyons, J.K., Pucherelli, M.J. and Clark, R.C., 1992. Sediment Transport and Channel Characteristics of a Sand-Bed Portion of the Green River Below Flaming Gorge Dam, Utah, USA. *Regulated Rivers-Research & Management*, 7(3): 219-232.
- Madej, M.A. and Ozaki, V., 1996. Channel response to sediment wave propagation and movement, Redwood Creek, California, USA. *Earth Surface Processes and Landforms*, 21(10): 911-927.
- Magilligan, F.J. and Nislow, K.H., 2001. Long-term changes in regional hydrologic regime following impoundment in a humid-climate watershed. *Journal of the American Water Resources Association*, 37: 1557-1570.
- Magilligan, F.J., Nislow, K.H. and Graber, B.E., 2003. Scale-independent assessment of discharge reduction and riparian disconnectivity following flow regulation by dams. *Geology*, 31(7): 569-572.
- Magilligan, F.J. and Nislow, K.H., 2005. Changes in hydrologic regime by dams. *Geomorphology*, 71(1-2): 61-78.

- Mann, D.M., 1993. Political Science: The Past and Future of Water Resources Policy and Management. In: M. Reuss (Editor), *Water Resources Policy in the United States: Policy, Practice, and Emerging Issues*. American Water Resources Association / Michigan State University Press, East Lansing, Michigan, pp. 55-65.
- Matthaei, C.D., Peacock, K.A. and Townsend, C.R., 1999. Scour and fill patterns in a New Zealand stream and potential implications for invertebrate refugia. *Freshwater Biology*, 42(1): 41-57.
- McClelland, W.T. and Brusven, M.A., 1980. Effects of sedimentation on the Behaviour and Distribution of Riffle Insects in a Laboratory Stream. *Aquatic Insects*, 2(3): 161-169.
- McCuen, R.H. and Levy, B.S., 2000. Evaluation of peak discharge transposition. *Journal of Hydrologic Engineering*: 278-279.
- McCullagh, M.J., 1998. Quality, Use and Visualisation in Terrain Modelling. In: S.N. Lane, K. Richards and J. Chandler (Editors), *Landform Monitoring, Modelling and Analysis*. John Wiley & Sons, Chichester, pp. 95-117.
- McCully, P., 2001. *Silenced Rivers : The Ecology and Politics of Large Dams*. Zed Books Ltd, London, 350 pp.
- Meffe, G.K., 1984. Effects of Abiotic Disturbance on Coexistence of Predator-Prey Fish Species. *Ecology*, 65(5): 1525-1534.
- Meyer, P.A., Lichtkoppler, R., Hamilton, R.B., Borda, C.L., Harpman, D.A. and Engel, P.M., 1995. *Elwha River Restoration Project: Economic Analysis, Final Technical Report*. U.S. Bureau of Reclamation, The National Park Service, The Lower Elwha S'Klallam Tribe, Davis, California. 63 pp.
- Milne, J.A., 1982. Bedforms and bend-arc spacings of some coarse-bedload channels in upland Britain. *Earth Surface Processes and Landforms*, 7: 227-240.
- Milne, J.A. and Sear, D.A., 1997. Modelling river channel topography using GIS. *International Journal of Geographical Information Science*, 11(5): 499-519.
- Montgomery, D.R., 1994. Road Surface Drainage, Channel Initiation, and Slope Instability. *Water Resources Research*, 30(6): 1925-1932.
- Montgomery, D.R., Panfil, M.S. and Hayes, S.K., 1999. Channel-bed mobility response to extreme sediment loading at Mount Pinatubo. *Geology*, 27(3): 271-274.
- Moreton, D., Ashworth, P.J. and Best, J.L., 2002. The physical scale modelling of braided alluvial architecture and estimation of subsurface permeability. *Basin Research*, 14(3): 265-287.
- Morris, G.L. and Fan, J., 1998. *Reservoir Sedimentation Handbook: Design and Management of Dams, Reservoirs, and Watersheds for Sustainable Use*. McGraw-Hill, New York, 1st.
- Nanson, G.C., 1980. A regional trend to meander migration. *Journal of Geology*, 88: 100-108.
- National Park Service, 1995. *Elwha River Ecosystem Restoration, Final Environmental Impact Statement, Olympic National Park*. National Park Service. 674 pp.
- National Park Service, 1996. *Elwha River Ecosystem Restoration Implementation: Draft Environmental Impact Statement (April)*. National Park Service. 483 pp.
- National Park Service, 2005. *Final Supplement to the Final Environmental Impact Statement, Elwha River Ecosystem, Restoration Implementation*. United States Department of the Interior, National Park Service. 336 pp.

- National Research Council, 1992. Restoration of Aquatic Ecosystems: Science, Technology, and Public Policy. National Research Council, Washington, D.C., National Academy Press. 552 pp.
- National Research Council, 1996. Upstream: Salmon and Society in the Pacific Northwest. National Academy Press, Washington D.C., First Edition, 452 pp.
- Natural Resources Conservation Service, 2000. A Report to Congress on Aging Watershed Infrastructure. United States Department of Agriculture, Natural Resources Conservation Service. 15 pp.
- Noble, C.A. and Palmquist, R.C., 1968. Meander growth in artificially straightened streams. *Iowa Academy of Science Proceedings*, 75: 234-242.
- Novak, P. and Cábélka, J., 1981. Models in Hydraulic Engineering - Physical Principles and Design Applications. Pitman, Boston, 459 pp.
- Nuttall, P.M., 1972. The effects of sand deposition upon the macroinvertebrate fauna of the River Camel, Cornwall. *Freshwater Biology*, 2: 181-186.
- Nuttall, P.M. and Bielby, G.H., 1973. The effects of China-clay wastes on stream invertebrates. *Environmental Pollution*, 5: 77-86.
- Otteson, B., 2004. Keyence LK500 Laser Carriage User Manual. St. Anthony Falls Laboratory, National Centre for Earth-surface Dynamics, Minneapolis, MN. 12 pp.
- Packman, A.I. and MacKay, J.S., 2003. Interplay of stream-subsurface exchange, clay particle deposition, and streambed evolution. *Water Resources Research*, 39(4).
- Packman, A.I. and Salehin, M., 2003. Relative roles of stream flow and sedimentary conditions in controlling hyporheic exchange. *Hydrobiologia*, 494(1-3): 291-297.
- Palmer, M.A., Hakenkamp, C.C. and Nelson-Baker, K., 1997. Ecological heterogeneity in streams: Why variance matters. *Journal of the North American Benthological Society*, 16(1): 189-202.
- Paola, C., 2000. Quantitative models of sedimentary basin filling. *Sedimentology*, 47: 121-178.
- Parker, G., Klingeman, P.C. and McLean, D.G., 1982. Bedload and Size Distribution in Paved Gravel-Bed Streams. *Journal of the Hydraulics Division-ASCE*, 108(4): 544-571.
- Peakall, J., Ashworth, P.J. and Best, J.L., 1996. Physical modelling in fluvial geomorphology: Principles, applications and unresolved issues. In: C.E. Thorn (Editor), *The Scientific Nature of Geomorphology: Proceedings of the 27th Binghampton Symposium in Geomorphology*. John Wiley and Sons Ltd., pp. 221-253.
- Peakall, J. and Warburton, J., 1996. Surface tension in small hydraulic models - the significance of the Weber number. *The Journal of Hydrology (New Zealand)*, 35(2): 199-212.
- Peckarsky, B.L., Cooper, S.D. and McIntosh, A.R., 1997. Extrapolating from individual behavior to populations and communities in streams. *Journal of the North American Benthological Society*, 16(2): 375-390.
- Pejchar, L. and Warner, K., 2001. A river might run through it again: criteria for consideration of dam removal, and interim lessons from California. *Environmental Management*, 28(5): 561-575.
- Petts, G.E., 1979. Complex response of river channel morphology subsequent to reservoir construction. *Progress in Physical Geography*, 3: 329-362.

- Petts, G.E. and Lewin, J., 1979. Physical effects of reservoirs on river systems. In: G.E. Hollis (Editor), *Man's impact on the hydrological cycle in the United Kingdom*, pp. 79-92.
- Petts, G.E., 1982. Channel changes in regulated rivers. In: B.H. Adlam, C.R. Fenn and L. Morris (Editors), *Papers in Earth Studies, Lovatt Lectures*, Worcester. Geo Books, Norwich, pp. 117-142.
- Petts, G.E. and Pratts, J.D., 1983. Channel changes following reservoir construction on a lowland river. *Catena*, 10: 77-85.
- Petts, G.E., 1984a. Sedimentation within a Regulated River. *Earth Surface Processes and Landforms*, 9(2): 125-134.
- Petts, G.E., 1984b. *Impounded Rivers: Perspectives for Ecological Management*. John Wiley & Sons, New York.
- Petz-Glechner, R., Patzner, R.A. and Jagsch, A., 2001. Effects of suspended solids from reservoir flushing on some tissues of rainbow trouts (*Oncorhynchus mykiss*): A qualitative study, *Verhandlungen der Gesellschaft für Ichthyologie*, Berlin, 2, pp. 131-141.
- Phillips, J.D., 2003. Toledo Bend reservoir and geomorphic response in the lower Sabine River. *River Research and Applications*, 19(2): 137-159.
- Phillips, J.D., Slattery, M.C. and Musselman, Z.A., 2005. Channel adjustments of the lower Trinity River, Texas, downstream of Livingston Dam. *Earth Surface Processes and Landforms*, 30(11): 1419-1439.
- Pizzuto, J., 2002. Effects of Dam Removal on River Form and Process. *BioScience*, 52(8): 683-691.
- Poff, N.L. and Ward, J.V., 1989. Implications of Streamflow Variability and Predictability for Lotic Community Structure - a Regional Analysis of Streamflow Patterns. *Canadian Journal of Fisheries and Aquatic Sciences*, 46(10): 1805-1818.
- Poff, N.L., Allan, J.D., Bain, M.B., Karr, J.R., Prestegard, K.L., Richter, B.D., Sparks, R.E. and Stromberg, J.C., 1997. The natural flow regime: A paradigm for conservation and restoration of river ecosystems. *Bioscience*, 47(11): 769-784.
- Pohl, M.M., 2002. Bringing down our dams: Trends in American dam removal rationales. *Journal of the American Water Resources Association*, 38(6): 1511-1519.
- Pohl, M.M., 2004. Channel Bed Mobility Downstream from the Elwha Dams, Washington. *The Professional Geographer*, 56(3): 422 - 431.
- Power, M.E., Dietrich, W.E. and Finlay, J.C., 1996. Dams and downstream aquatic biodiversity: Potential food web consequences of hydrologic and geomorphic change. *Environmental Management*, 20(6): 887-895.
- Quraishy, M.S., 1944. The origin of curves in rivers. *Current Science*, 13: 36-39.
- Randle, T.J., 2003. Dam removal and sediment management. In: W.L. Graf (Editor), *Dam Removal Research, Status and Prospects: Proceedings of the Heinz Center's Dam Removal Research Workshop, October 23-24, 2002*. The H. John Heinz III Center for Science, Economics and the Environment, Washington, D.C., pp. 81-104.
- Rathburn, S.L. and Wohl, E.E., 2001. One-dimensional sediment transport modeling of pool recovery along a mountain channel after a reservoir sediment release. *Regulated Rivers-Research & Management*, 17: 251-273.
- Rathburn, S.L. and Wohl, E.E., 2003a. Sedimentation hazards downstream from reservoirs. In: W.L. Graf (Editor), *Dam Removal Research, Status and*

- Prospects: Proceedings of the Heinz Center's Dam Removal Research Workshop, October 23-24, 2002. The H. John Heinz III Center for Science, Economics and the Environment, Washington, D.C., pp. 105-118.
- Rathburn, S.L. and Wohl, E.E., 2003b. Predicting fine sediment dynamics along a pool-riffle mountain channel. *Geomorphology*, 55: 111-124.
- Reid, I., Laronne, J.B. and Powell, D.M., 1999. Impact of major climate change on coarse-grained river sedimentation: a speculative assessment based on measured flux. In: A.G. Brown and T.A. Quine (Editors), *Fluvial Processes and Environmental Change*. John Wiley and Sons Ltd, pp. 105-115.
- Reisner, M., 1993. *Cadillac Desert: The American West and its Disappearing Water*. Penguin, 582 pp.
- Renwick, W.H., 1992. Equilibrium, disequilibrium and nonequilibrium landforms in the landscape. *Geomorphology*, 5: 265-276.
- Renwick, W.H., Smith, S.V., Bartley, J.D. and Buddemeier, R.W., 2005. The role of impoundments in the sediment budget of the conterminous United States. *Geomorphology*, 71(1-2): 99-111.
- Rhoads, B.L. and Thorn, C.E. (Editors), 1996. *The Scientific Nature of Geomorphology*. John Wiley and Sons, Chichester. 496 pp.
- Richards, C. and Bacon, K.L., 1994. Influence of Fine Sediment on Macroinvertebrate Colonization of Surface and Hyporheic Stream Substrates. *Great Basin Naturalist*, 54(2): 106-113.
- Richards, K.S., 1976. The morphology of riffle-pool sequences. *Earth Surface Processes*, 1: 71-88.
- Richards, K.S., 1978. Simulation of flow geometry in a riffle-pool stream. *Earth Surface Processes*, 3: 345-354.
- Richards, K.S., 1982. *Rivers: Form and Process in Alluvial Channels*. Methuen, London, 358 pp.
- Richardson, W.R. and Thorne, C.R., 2001. Multiple thread flow and channel bifurcation in a braided river: Brahmaputra-Jamuna River, Bangladesh. *Geomorphology*, 38(3-4): 185-196.
- River Alliance of Wisconsin, 2006. International Dam Removal Information. Accessed at <http://www.wisconsinrivers.org/index.php?page=content&mode=view&id=9#Global> on Tuesday 28 November 2006.
- Robinson, K.M. and Hanson, G.J., 1995. Large-Scale Headcut Erosion Testing. *Transactions of the Asae*, 38(2): 429-434.
- Robinson, K.M. and Cook, K.R., 1998. Stress measurement upstream of an overfall. *Transactions of the ASAE*, 41(4): 1019-1024.
- Rubey, W.W., 1933. Equilibrium conditions in debris-laden streams, 14th Annual Meeting, *Transactions of the American Geophysical Union*, pp. 479-505.
- Sarakinos, H. and Johnson, S.E., 2003. Social perspectives on dam removal. In: W.L. Graf (Editor), *Dam Removal Research, Status and Prospects: Proceedings of the Heinz Centre's Dam Removal Research Workshop, October 23-24, 2002*. The H. John Heinz III Centre for Science, Economics and the Environment, Washington, D.C., pp. 40-55.
- Savat, J., 1976. Discharge velocities and total erosion of a calcareous loess: a comparison between pluvial and terminal runoff. *Revue de Geomorphologie Dynamique*, 25: 113-122.

- Schmidt, J.C., Grams, P.E. and Webb, R.H., 1995. Comparison of the Magnitude of Erosion Along Two Large Regulated Rivers. *Water Resources Bulletin*, 31(4): 617-631.
- Schnitter, N.J., 1994. *A History of Dams: The Useful Pyramids*. Balkema Publishers, Rotterdam, The Netherlands, 282 pp.
- Schumm, S.A. and Lichty, R.W., 1965. Time, Space and Causality in Geomorphology. *American Journal of Science*, 263: 110-119.
- Schumm, S.A. and Khan, H.R., 1972. Experimental study of channel pattern. *Bulletin of the Geological Society of America*, 83: 1755-1770.
- Schumm, S.A., 1973. Geomorphic thresholds and complex response of drainage systems. In: M. Morisawa (Editor), *Fluvial Geomorphology*. New York State University, Binghamton, NY, pp. 299-310.
- Schumm, S.A., 1976. Episodic erosion: a modification of the geomorphic cycle. In: W.N. Melhorn and R.C. Flemal (Editors), *Theories of Landform Development, Publications in Geomorphology*. State University of New York, Binghamton, N.Y., pp. 69-85.
- Schumm, S.A., 1977. *The Fluvial System*. The Blackburn Press, 338 pp.
- Schumm, S.A., Harvey, M.D. and Watson, C.C., 1984. *Incised Channels: Morphology, Dynamics and Control*, 1. Water Resources Publications, Littleton, Colorado, 200 pp.
- Schumm, S.A., Mosley, M.P. and Weaver, W.E., 1987. *Experimental Fluvial Geomorphology*. John Wiley, New York, 413 pp.
- Sear, D.A., 1994. Viewpoint: river restoration and geomorphology. *Aquatic Conservation: Marine and Freshwater Ecosystems*, 4: 169-177.
- Servizi, J.A. and Martens, D.W., 1992. Sublethal responses of coho salmon (*Oncorhynchus kisutch*) to suspended sediments. *Canadian Journal of Fisheries and Aquatic Sciences*, 49: 1389-1395.
- Shields Jr., F.D., Simon, A. and Steffen, L., 2000. Reservoir effects on downstream river channel migration. *Environmental Conservation*, 27(1): 54-66.
- Simon, A. and Hupp, C.R., 1986. Channel evolution in modified Tennessee, *Proceedings of the 4th Federal Interagency Sedimentation Conference*. U.S. Government Printing Office, Washington D.C., Las Vegas, Nevada, pp. 5.71-5.82.
- Simon, A., 1989. A model of channel response in disturbed alluvial channels. *Earth Surface Processes and Landforms*, 14: 11-26.
- Simon, A., 1992. Energy, Time, and Channel Evolution in Catastrophically Disturbed Fluvial Systems. *Geomorphology*, 5(3-5): 345-372.
- Simon, A., 1994. *Gradation Processes and Channel Evolution in Modified West Tennessee Streams: Process, Response and Form*. U.S. Geological Survey Professional Paper, 1470, U.S. Geological Survey. 84 pp.
- Simon, A. and Thorne, C.R., 1996. Channel adjustment of an unstable coarse-grained stream: Opposing trends of boundary and critical shear stress, and the applicability of extremal hypotheses. *Earth Surface Processes and Landforms*, 21(2): 155-180.
- Simon, A. and Darby, S.E., 1999. The Nature and Significance of Incised River Channels. In: S.E. Darby and A. Simon (Editors), *Incised River Channels: Processes, Forms, Engineering and Management*. John Wiley and Sons Ltd, Chichester, pp. 3-18.
- Simon, A., Curini, A., Darby, S.E. and Langendoen, E.J., 2000. Bank and near-bank processes in an incised channel. *Geomorphology*, 35(3-4): 193-217.

- Simon, A. and Thomas, R.E., 2002. Processes and forms of an unstable alluvial system with resistant, cohesive streambeds. *Earth Surface Processes and Landforms*, 27(7): 699-718.
- Simon, A. and Rinaldi, M., 2006. Disturbance, stream incision, and channel evolution: The roles of excess transport capacity and boundary materials in controlling channel response. *Geomorphology*, 79(3-4): 361-383.
- Simons, D.B. and Li, R.M., 1982. Sediment Problems Associated with Dam Removal - Muskegon River, Michigan. *Engineering Analysis of Fluvial Systems*.
- Siska, P.P. and Hung, I.-K., 2001. Assessment of Kriging Accuracy in the GIS Environment, 21st Annual ESRI International User Conference, San Diego, CA. ESRI, San Diego, CA, pp. 6.
- Slattery, M.C. and Bryan, R.B., 1992. Hydraulic Conditions for Rill Incision under Simulated Rainfall - a Laboratory Experiment. *Earth Surface Processes and Landforms*, 17(2): 127-146.
- Smith, N.A.F., 1971. *A History of Dams*. Citadel Press, Secaucus, New Jersey, 279 pp.
- Soar, P.J. and Thorne, C.R., 2001. Channel restoration design for meandering rivers. ERDC/CHL CR-01-1, U.S. Army Corps of Engineers, Vicksburg, MS. 456 pp.
- Solari, L. and Parker, G., 2000. The curious case of mobility reversal in sediment mixtures. *Journal of Hydraulic Engineering-ASCE*, 126(3): 185-197.
- St. Louis, V.L., Kelly, C.A., Duchemin, E., Rudd, J.W.M. and Rosenberg, D.M., 2000. Reservoir Surfaces as Sources of Greenhouse Gases to the Atmosphere: A Global Estimate. *BioScience (American Institute of Biological Sciences)*, 50(9): 766-775.
- Stanley, E.H., Luebke, M.A., Doyle, M.W. and Marshall, D.W., 2002. Short-term changes in channel form and macro invertebrate communities following low-head dam removal. *Journal of the North American Benthological Society*, 21(1): 172-187.
- Stanley, E.H. and Doyle, M.W., 2003. Trading off: the Ecological Effects of Dam Removal. *Frontiers in Ecology and the Environment*, 1(1): 15-22.
- Stein, O.R., Alonso, C.V. and Julien, P.Y., 1993. Mechanics of Jet Scour Downstream of a Headcut. *Journal of Hydraulic Research*, 31(6): 723-738.
- Stein, O.R. and Julien, P.Y., 1993. Criterion Delineating the Mode of Headcut Migration. *Journal of Hydraulic Engineering-ASCE*, 119(1): 37-50.
- Steinberg, B., 1993. The Federal Perspective. In: M. Reuss (Editor), *Water Resources Policy in the United States: Policy, Practice, and Emerging Issues*. American Water Resources Association / Michigan State University Press, East Lansing, pp. 264-273.
- Stewart, G., Glasmann, J.R., Grant, G.E., Lewis, S. and Ninneman, J., 2002. Evaluation of fine sediment intrusion into salmon spawning gravels related to Cougar Reservoir sediment releases. Unpublished report prepared for the Portland District Office, U.S. Army Corps of Engineers, Oregon State University, Corvallis, Oregon. 30 pp.
- Stewart, G., 2006. Patterns and Processes of Sediment Transport following Sediment-filled Dam Removal in Gravel Bed Rivers. Unpublished PhD Thesis, Oregon State University, Corvallis, OR, 100 pp.
- Sweka, J.A. and Hartman, K.J., 2001. Influence of turbidity on brook trout reactive distance and foraging success. *Transactions of the American Fisheries Society*, 130(1): 138-146.

- Taxpayers for Common Sense, Save Our Wild Salmon, Republicans for Environmental Protection, Pacific Coast Federation of Fishermen's Associations, Institute for Fisheries Research, Northwest Sportfishing Industry Association, NW Energy Coalition and Rivers, A., 2006. Revenue Stream: An Economic Analysis of the Costs and Benefits of Removing the Four Dams on the Lower Snake River. 24 pp.
- Thomas, R.E., 2006. Flow processes and channel change in sand-bedded braided rivers. Unpublished PhD Thesis, University of Leeds, 295 pp.
- Thoms, M.C., Southwell, M. and McGinness, H.M., 2005. Floodplain-river ecosystems: Fragmentation and water resources development. *Geomorphology*, 71(1-2): 126-138.
- Thorne, C.R. and Tovey, N.K., 1981. Stability of Composite River Banks. *Earth Surface Processes and Landforms*, 6(5): 469-484.
- Thorne, C.R., 1982. Processes and mechanisms of river bank erosion. In: R.D. Hey, J.C. Bathurst and C.R. Thorne (Editors), *Gravel-Bed Rivers*. John Wiley & Sons, Inc., Chichester, U.K., pp. 227-271.
- Thorne, C.R., Russell, A.P.G. and Alam, M.K., 1993. Planform pattern and channel evolution of the Brahmaputra River, Bangladesh. In: J.L. Best and C.S. Bristow (Editors), *Braided Rivers*. Geological Society Special Publication No. 75, pp. 257-276.
- Thorne, C.R., 1998. *Stream Reconnaissance Guidebook: Geomorphological Investigation and Analysis of River Channels*. John Wiley and Sons, Chichester, UK, 127 pp.
- Tiffany, J.B. and Nelson, G.A., 1939. Studies of meandering model-streams. *Transactions of the American Geophysical Union*, 20: 644-649.
- Townsend, C.R., Scarsbrook, M.R. and Doledec, S., 1997. The intermediate disturbance hypothesis, refugia, and biodiversity in streams. *Limnology and Oceanography*, 42(5): 938-949.
- Triangle Associates, 2004. *Technical Workshop on Nearshore Restoration in the Central Strait of Juan de Fuca*. Triangle Associates, Inc. 141 pp.
- United Nations Environment Programme, 2000. *Global Environment Outlook 2000*. Report accessed online at <http://www.unep.org/geo2000/english/index.htm> on 27 February 2006, United Nations Environment Programme.
- United States Army Corps of Engineers, 1999b. *Cougar Reservoir Water Temperature Control Project, Supplemental Biological Assessment*. Portland District, U.S. Army Corps of Engineers, Portland, Oregon. 60 pp.
- United States Congress, 1992. *Elwha River Ecosystem and Fisheries Restoration Act (Public Law 102-495)*.
- United States Geological Survey, 2000. *Hydrological Data Collected During the 1994 Lake Mills Drawdown Experiment, Elwha River, Washington*. Water-Resources Investigations Report, 99-4215, U.S. Geological Survey, Tacoma, WA. 115 pp.
- USACE NID, 2000. *U.S. Army Corps of Engineers National Inventory of Dams*. Accessed at <http://crunch.tec.army.mil/nid/webpages/nid.cfm>
- Van Heijst, M.W.I.M. and Postma, G., 2001. Fluvial response to sea-level change: a quantitative analogue, experimental approach. *Basin Research*, 13(3): 269-292.
- Van Heijst, M.W.I.M., Postma, G., Meijer, X.D., Snow, J.N. and Anderson, J.B., 2001. *Quantitative analogue flume-model study of river-shelf systems:*

- principles and verification exemplified by the Late Quaternary Colorado river-delta evolution. *Basin Research*, 13(3): 243-268.
- Vinson, M.R., 2001. Long-term dynamics of an invertebrate assemblage downstream from a large dam. *Ecological Applications*, 11(3): 711-730.
- Vörösmarty, C.J., Green, P., Salisbury, J. and Lammers, R.B., 2000. Global water resources: vulnerability from climate change and population growth. *Science*, 289(5477): 284-288.
- Ward, R.C. and Robinson, M., 1990. *Principles of Hydrology*, Third Edition, 365 pp.
- Watson, C.C., Biedenbarn, D.S. and Thorne, C.R., 1999. *Demonstration Erosion Control Project Design Manual - Draft*. U.S. Army Corps of Engineers, Engineer Research and Development Center.
- Wemple, B.C., Jones, J.A. and Grant, G.E., 1996. Channel network extension by logging roads in two basins, western Cascades, Oregon. *Water Resources Bulletin*, 32(6): 1195-1207.
- Wemple, B.C., Swanson, F.J. and Jones, J.A., 2001. Forest roads and geomorphic process interactions, Cascade Range, Oregon. *Earth Surface Processes and Landforms*, 26(2): 191-204.
- Whipple, K.X., Parker, G., Paola, C. and Mohrig, D., 1998. Channel dynamics, sediment transport, and the slope of alluvial fans: Experimental study. *Journal of Geology*, 106(6): 677-693.
- Whitelaw, E. and MacMullan, E., 2002. A Framework for Estimating the Costs and Benefits of Dam Removal. *Bioscience*, 52(8): 724-730.
- Wik, S.J., 1995. Reservoir Drawdown - Case-Study in Flow Changes to Potentially Improve Fisheries. *Journal of Energy Engineering-Asce*, 121(2): 89-96.
- Williams, G.P. and Wolman, M.G., 1984. Downstream effects of dams on alluvial rivers. U.S. Geological Survey Professional Paper 1286. 83 pp.
- Winter, B.D., Reisenbichler, R. and Schreiner, E., 2000. *The Importance of Marine-Derived Nutrients For Ecosystem Health and Productive Fisheries*. 41 pp.
- Wise, S.M., 1998a. Digital Terrain Models - Traps for the Unwary, Third International Conference on GeoComputation, University of Bristol, United Kingdom, pp. 15-22.
- Wise, S.M., 1998b. The Effect of GIS Interpolation Errors on the Use of Digital Elevation Models in Geomorphology. In: S.N. Lane, K. Richards and J. Chandler (Editors), *Landform Monitoring, Modelling and Analysis*. John Wiley & Sons, Chichester, pp. 139-164.
- Wohl, E.E., 2000. *Mountain Rivers*. Water Resources Monograph, Volume 14. American Geophysical Union Press, Washington, D.C., 320 pp.
- Wohl, E.E. and Cenderelli, D.A., 2000. Sediment deposition and transport patterns following a reservoir sediment release. *Water Resources Research*, 36(1): 319-333.
- Wolman, M.G. and Brush, L.M., 1961. Factors Controlling the Size and Shape of Stream Channels in Coarse, Non-Cohesive Sands. U.S. Geological Survey Professional Paper, U.S. Geological Survey Professional Paper 282G. 183-210 pp.
- Wong, M., Cantelli, A., Paola, C. and Parker, G., 2004. Erosional narrowing after dam removal: Theory and numerical model, River Restoration Symposium - ASCE-EWRI Congress, Salt Lake City, Utah, pp. 10.
- Wood, A.L., Simon, A., Downs, P.W. and Thorne, C.R., 2001. Bank-toe processes in incised channels: the role of apparent cohesion in the entrainment of failed bank materials. *Hydrological Processes*, 15(1): 39-61.

- Wooster, J., Larsen, E.W. and Mount, J.F., Submitted. A Flume Study Investigating the Erosional Responses Following Dam Removal. Submitted to Earth Surface Processes and Landforms.
- World Commission on Dams, 2000. Dams and Development: A New Framework for Decision-Making. World Commission on Dams. Published by Earthscan, London. 404 pp.
- Xu, K., Milliman, J.D., Yang, Z. and Wang, H., 2006. Yangtze sediment decline partly from Three Gorges Dam. EOS, 87(19): 185 & 190.
- Yalin, M.S., 1971a. Theory of Hydraulic Models. MacMillan, London, 266 pp.
- Yalin, M.S., 1971b. On the formation of dunes and meanders, Proceedings of the 14th International Congress of the Hydraulic Research Association, Paris, 3, C13, pp. 1-8.
- Yalin, M.S., 1992. River Mechanics. Pergamon, Oxford, 219 pp.
- Yang, C.T., 1996. Sediment Transport - Theory and Practice. McGraw-Hill, New York, First, 396 pp.
- Zhang, G., 1995. An experimental study on the form of headwater erosion in a reservoir, Sixth International Symposium on River Sedimentation, New Delhi, India, pp. 843-851.

Appendix A A Chronology of Dams

The following chronology has been modified and expanded from the one presented by Schnitter (1994) and lists the important dams, inventions, publications and developments that enabled the art and science of dam building to develop, together with random interesting statistics and facts related to the history of dams. The place names are as they are today, and not what they may have been at the time mentioned.

- >3,000 B.C.** World's oldest dams possibly built in Armenia but supporting data provided by Agakhanian (1985; cited in Schnitter, 1994) are unclear and inconsistent.
- 3,000 B.C.** The World's oldest dams (five gravity dams) for which concrete evidence exists were built in northern Jordan to supply town of Jawa with water. One was 5.5 m high.
- 2,600 B.C.** The Sadd-al-Kafara was an embankment dam built in Egypt for flood protection and/or water supply to a quarry (Smith, 1971). It was 14 m high with a crest length of 113 m.
- 2,500 B.C.** Check dams (gravity type) were built for water and soil conservation in Baluchistan, what is now the border area between Iran and Pakistan, possibly marking the first time dams had been used for such a purpose. Larger dams up to about 20 m high were used for water storage.
- 1,800 B.C.** A large reservoir in the Faiyûm depression in Egypt is filled with water from the 340 km-long Yûsuf branch of the River Nile. As rebuilt in the 3rd century B.C. the dam was 8,000 m long, 7 m high and impounded a reservoir of 275 million m³.
- 1,500 B.C.** The Sabeans completely dam the River Danah in Yemen for the first time.
- C. 13th B.C.** Mycenaean diversion and storage dams are built in Greece to supply irrigation water. Dam heights ranged from 2-4 m, lengths from 200-2,500 m and reservoir capacity from 2-24 million m³.
- 1,260 B.C.** The Kofini diversion embankment was built in Greece to protect the city of Tiryns from the floods of the Lakissa River. It is 10 m high, 100 m long and is still in use today.

- 950 B.C.** Solomon's 'Pool of Shiloah' reservoir built in the Tyropoeon Ravine to store water from the Gihon Spring in order to supply Jerusalem.
- 730 B.C.** Achaz's Probatika Dam (13 m high, 40 m long) was built in the Rephaïm Valley, also to supply Jerusalem. This structure made use of water intakes at multiple elevations.
- 703 B.C.** First of the Assyrian King Sennacherib's dams built at Kisiri (or Qayin) to divert water from the Khosr River into a 15 km-long canal to supply the then Iraqi capital city of Niniveh.
- C.7th-8th B.C.** A number of storage reservoirs were built on the Engusner and Doni Rivers to store snowmelt runoff to supply the city of Van (then Tuşpa), the capital of the Kingdom of Urartu in southeastern Turkey. They stored an estimated 100 million m³ of water.
- 700 B.C.** Construction of the Purron earth embankment, by early farming communities that pre-dated the later and more famous Latin American civilizations, is begun at the southern end of the Tehuacan Valley, 260 km southeast of Mexico City in central Mexico. This is the oldest known structure in Mesoamerica²⁷. Initial dam height was 3 m but an additional 4 m was added in about 600 B.C. The dam was 400 m long at this point and impounded 1.4 million m³. In about 200 A.D. the dam was raised to 18 m, had a volume of 370,000 m³ and impounded a reservoir with a 5.1 million m³ storage capacity.
- 581 B.C.** The oldest known reservoir in China is the Anfengtang (or Shao) Reservoir and Embankment northwest of Shanghai (Pinyin). It was built on the Huai River from alternating layers of straw and earth, impounds 100 million m³ of water and is still in use today. Six other diversion weirs were built between this time and the break up of ancient China in 317 A.D.
- 510 B.C.** Start of Sabean gravity dam at Marib in Yemen. Final dimensions may have been about 700 m long and up to 20 m high, with a storage capacity of about 30 million m³, or 15% of the river's annual flow.
- C. 5th B.C.** A diversion weir for irrigation was built near Xoxocotlan about 370 km southeast of Mexico City. The dam was 10 m high, 40 m long and 40 m thick.
- 453 B.C.** The oldest known Chinese diversion weir was built at Zhiboqu (see 219 B.C.)
- 370 B.C.** The first of many large storage reservoirs was built at Panda in Sri Lanka by the Singhalese Dynasty of kings. It had a storage capacity of 9 million m³. These large reservoirs supplemented the large number of much smaller village reservoirs that had been built by farming communities to store the large volumes of winter runoff.
- 275 B.C.** The largest Meroitic reservoir for water supply was impounded by the Musawwarat Embankment in northern Sudan.

²⁷ Here defined as stretching from the southwestern United States in the north to the northern portion of South America.

- 221 B.C. – 317 A.D.** Several storage reservoirs for flood control and irrigation were built following the unification of China in 221 B.C. These included structures at Honxi, Maren, Aijin, Lian, Jian and Dongqian.
- 219 B.C.** The 3.9-m high Tianping diversion weir was built on the Xiang River in southern China to divert water into navigation canals (see 453 B.C.).
- C. 2nd B.C.** A 14-m high and 43-m long rockfill flood control dam was built to divert flash floods away from the Nabatean capital of Petra in Jordan.
The Nabateans also built many check dams to retain eroded soil and runoff. 17,000 such structures were built in a 130 km² area, thus increasing the area of arable land from about 0.5 to 7.5 km². These dams were typically 1.8-2.0 m high, 40-50 m long and 2.0-2.5 m high.
- C. 1st B.C.** Two of the three reservoirs referred to as ‘Solomon Pools’ were built 11 km southwest of Jerusalem and stored about 85,000 m³ and 90,000 m³ of water.
- C. 1st B.C.** The Asid (or Adraa) Dam was built about 100 km south of Sana by the Himyar Kingdom in Yemen. The structure was a gravity dam that utilised a 2.3-m thick vertical sand drain that was used to keep the downstream half of the dam dry and free of uplift forces. The same technology is used in modern embankment dams.
- ca. C. 1st A.D** The Romans may have been the first to use buttresses instead of embankments on the downstream faces of their lower and shorter dams.
- 60 A.D.** The 40-m high Subiaco Dam was built by the Emperor Nero as an ornamental feature for his villa. This was one of the earliest dams built by the Romans and, together with two other structures upstream and downstream, was one of only three dams ever built in Italy by them. The Subiaco Dam was also the highest ever Roman dam.
- ca. 130** The Proserpina Dam was built by the Romans near Mérida in Spain and is still in use today (Smith, 1971). Sometime after this, the Romans built the Cornalbo Dam to the northeast of Mérida. The dam was 24 m high and had a volume of 70,000 m³ making it both the tallest and largest Roman dam outside Italy. It impounded a reservoir of 10 million m³. The most important feature of this dam is its upstream wall, which slopes downwards at an angle of 1:1.5. The dam was thus able to utilise the weight of the water pressing down on this face to help prevent it from sliding.
- 140** The 65 km-long and 4-m high Jian (or Jin) embankment was built in central China to provide irrigation water.
- C. 2nd** Many Roman embankment dams were built on the Iberian Peninsula.
- 250-650** The Zapotecs (Mexico) used small storage dams in gullies as part of their domestic water supply system to the town of Monte Alban.
- 270** Four Roman bridge-weirs were built in south western Iran by captured Roman soldiers during the reign of the Sassanian king Shapur I. They range from 3-4 m high and 170-900 m long.

- 284** A large, concrete Roman gravity dam was built at Homs, north of Damascus in Syria. The dam was 7 m high, 2,000 m long, 14 m and 6.6 m wide at the base and crest respectively and impounded a reservoir of about 90 million m³.
- ca. C. 3rd** Possibly the world's first true arch dam was built for water supply by the Romans in the Vallon de Baume, near Saint-Rémy in south eastern France. The dam was 12 m high, 18 m long, 3.9 m wide at the base and had a curvature radius of about 14 m. Although the Romans used the arch frequently in their construction work (its use in construction was developed by the Etruscans (Smith, 1971)), they did so only very rarely in their dam building.
- ca. C. 3rd** The 5.6-m high and 320-m long Esparragalejo Dam built by the Romans north west of Mérida in south western Spain was the first multiple-arch buttress dam ever built.
- 290** The Minneriya Reservoir on the Mahaweli River in Sri Lanka is expanded to hold 136 million m³ of water.
- C. 3rd - 7th** Small storage dams are used by the Zapotec Civilization in Mexico.
- C. 4th – 8th** Following the unification of Japan in about 300 AD, about 80 dams over 8 m high were built, many of which were used to provide irrigation water for rice paddies.
- 380** The Sayama Embankment was built 20 km south of Osaka in Japan. It is 8 m high and 900 m long and still exists.
- 460** The Paskanda Ulpotha Dam in Sri Lanka was raised to a record height (for an embankment) of 34 m, which was not exceeded until 1675.
- 514-515** During the division of China, the 32-m high and about 4,000-m long Fushan Embankment was built on the Huai River in central China in order to flood an upstream enemy embankment. Four months later the dam was overtopped and breached, releasing the entire reservoir's capacity of 10 billion m³ of water and killing over 10,000 people.
- C. 6th** The Byzantine Emperor Justinian I built several flood control dams in south eastern Turkey.
- 600-900** A large number of domestic water supply reservoirs were built by the Mayas in Tikal, Guatemala. These included a 14-m high and 83-m long embankment dam built in 700 that impounded the 50,000-m³ Palace Reservoir at Tikal in Guatemala.
- C. 7th – 8th** About 18 gravity dams were built by the Arabs near Mecca and Medina in Saudi Arabia.
- C. 8th – 10th** Following their invasion of Spain in 711, the Muslims reactivated many Roman irrigation works, which possibly included diversion weirs, as well as building nine diversion weirs themselves in the 10th century. These weirs either had stepped or gently sloping downstream faces to help to dissipate flow energy.
- C. 9th/10th** The invention of the cam in Western Europe allowed a diversification in the use of water wheels. At the same time, water wheels were moved

away from the rivers and hazards such of floods, floating ice and debris. Water thus had to be diverted away from the rivers and this led to the construction of diversion weirs that were frequently amplified into storage reservoirs. The first such dams were wooden lattices in-filled with earth and rock (*i.e.* crib dams), later replaced by earth embankments and, rarely, masonry structures.

- ca. 800** Earliest date that Native North Americans begin building small dams for irrigation and domestic water supply (Smith, 1971).
- 970** Muslims from Yemen build the Parada Weir on the Segura River upstream from Murcia in Spain. The weir is up to 8 m high, about 300 m long and was built with rubble masonry set in limestone mortar.
- C. 10th** The local Bujid rulers build a series of irrigation and power dams on the Kur River to the east of Shiraz in southern Iran. The Amir and Feizabad dams powered 30 and 22 water wheels respectively. Water was directed out of a nozzle at the base of vertical shafts and against a paddle wheel that was connected to the grindstone.
- 1037** The 9.1-m high and 16 km-long Veeranam Embankment was built in southern India, marking the start of a dam-building boom there that lasted until the 16th century under a variety of Hindu (Pallava, Chola, Vijayanagara) and Muslim (Sultanate of Delhi) dynasties.
- c. 1100** Anasazi irrigation and domestic water supply reservoir built in southern Colorado and northern New Mexico.
- 1170** The Topa Reservoir in Sri Lanka was enlarged by the Singhalese King Parakrama Bahu to create his samudra or ‘sea’, which had a volume of 102 million m³. The embankment built to impound the ‘sea’ was 15 m high, 13.6 km long and had a volume of 4.6 million m³, which made it the largest embankment ever built until the construction of the Gatun Dam in Panama in 1912.
- ca. 1180** The first fish pond for which data are available is built at Kilburn, 90 km south of Newcastle in England. It was a 7-m high and 55-m long embankment dam.
- ca. C.12th - 1648** Thousands of dual use mill dams and fish ponds were built around Europe, mostly by cities, monasteries and nobles to help generate income. They were important sources of food, particularly during times of war. The construction of dams (mostly earth embankments) for this purpose ended during the 30-years war from 1618-1648. Individual reservoirs contained as much as 20 million m³ of water.
- 1213** The 17.1-m high Ramappa Embankment was built in southern India and impounded a reservoir of 153 million m³, which was a record to date for southern India.
- 1272** The Máchovo Dam and fish pond, 60 km north of Prague in the Czech Republic, was the first of numerous such ponds built in Bohemia. It was 9 m high and impounded 5.5 million m³ of water.
- c. 1300** The first arch dam since Roman times was built by the Mongolians at Kebar in central Iran. It was 26 m high, 55 m long, 9m wide at the base

- and 6 m wide at the crest. The middle 21 m of the structure was curved with a radius of 35 m.
- 1350** The 60 m-high Kurit arch dam was built in central Iran by the Mongolians. Following its heightening to 64 m in about 1850 it was the world's tallest dam until the early years of the 20th century.
- 1384** The 17-m high Almansa curved, gravity dam was built in south eastern Spain with a radius of curvature of 31 m. This may reflect the influence of Mongolian arch-dam construction techniques spreading from Iran (see *c.*1300) into Spain. This spread of knowledge would have been facilitated by the fact that both Iran and Spain were then under Muslim rule (although Spain was gradually re-conquered by the Christians over the period 1031-1492). A new feature at this dam was a large bottom outlet (3 m²) used for flushing sediment reservoir.
- C. 15th** The 16-km long Nezahualcoyotl Dam was built in Lake Texcoco to the west of the Aztec capital of Tenochtitlan (now Mexico City).
- C. 15th – 16th** About 700 fish ponds were built in Bohemia in the Czech Republic, covering an area of about 1,800 km². Their embankments were built from sandy clay placed in compacted layers 0.15-0.2 m thick.
- 1404** The 4-m high Greifen (formerly Geyer) Embankment was built to the southeast of Leipzig in Germany and was the first dam used to power water wheels in mines.
- 1430** 9- and 6-km long dikes were built in Lake Texcoco around Tenochtitlan (now Mexico City) to provide road access to the city.
- 1492** The Jordán Dam was the oldest known structure (embankment) for the supply of fresh running water built in Europe since Roman times. It was built near Tabor in southern Bohemia in the Czech Republic using the same technology as the Bohemian fish ponds (see C. 15th – 16th). It is 18 m high, 300 m long and impounds 3 million m³.
- C. 16th** The Spanish Conquistadors, particularly the clergy in the first instance, brought European dam-building knowledge to the Americas, such as the use of curved bridges for aqueducts, masonry to build the structures and the use of water wheels for power. These supplemented the pre-existing dam-building knowledge of the indigenous people.
- 1500** The 19-m high Castellar buttress storage dam was built in south western Spain. Three water wheels were powered in the same fashion as those on the Kur River in Iran (see C. 10th).
- c.* 1520** The first transfer of European dam-building technology to India took place when one of the last kings of the Vijayanagara Dynasty consulted the Portuguese engineer Joao de la Ponta when building a reservoir to supply his new city of Nagalpara.
- 1530** The Italian architect Baldassare Peruzzi proposes the idea that a dam with an upstream-sloping face will be more stable due to the weight of water pressing down on this surface (see *ca.* 130 and 1735).
- 1547** The bishop Jan Skála (writing under the pseudonym Dubravius) published 'Five books on Fish Ponds', which describes the Bohemian

- experience of pisciculture and building fish ponds (see 1272 and C.15th – 16th). It was the first book containing information on dam building. Originally written in Latin, it was soon reprinted in English, German and Polish, thus enabling its contents to be more widely disseminated.
- 1548/1550** A 12 m-high gravity dam was built to impound the 221 million m³ Yuriria irrigation reservoir in a volcanic crater 230 km north west of Mexico City.
- 1558** The 9-m high Berthelsdorf Dam, 85 km southeast of Leipzig in the German Ore Mountains, was the first earth embankment to be built with an impervious clay core.
- 1560** The Belgrade (Büyük) gravity dam was the first masonry water supply dam built for Istanbul in Turkey, where most of the other early European water supply dams were also built, since Roman times. It was 15 m high, 85 m long and impounded 1.3 million m³.
- 1573-1621** An network of about 30 reservoirs, impounded by gravity dams, was built by the Spanish near Potosí in Bolivia, 415 km south east of La Pax. The reservoirs impounded a total of about 6 million m³ and were used to power 132 silver ore grinding mills.
- 1575** The construction of the 23-m high Hussain Dam in Hyderabad, with an earth-backed masonry wall, may be a further example of Portuguese influence in India, since this design had never before been used in eastern Asia but had been used by the Romans.
- 1578** The 13 billion m³ Hongze Reservoir was built in central China and was the world's largest storage capacity until the Hoover Dam was built in 1936, which impounded about three times as much water. The Hongze Embankment was initially about 30 km long but was eventually increased to over 67 km long.
- 1594** The 46 m-high Tibi curved gravity dam was built during the reign of Philip II in south eastern Spain. Its volume exceeded 36,000 m³ of rubble masonry.
- C. 17th** An explosion of canal building in northern Europe lead to many dams and reservoirs being built towards the end of the 17th century to ensure a steady supply of water.
- 1600** Another early book containing information about dam building, entitled 'Certaine Experiments concerning Fish and Fruite', was written by John Taverner, the Surveyor General of the King's Woods south of the River Trent in England. The dam-building recommendations are identical to those of Dubravius (see 1547).
- 1612** The first 5 m of the Pontalto arched flood control dam were built on the Fersina Creek in South Tirol in Austria, to protect the town of Trento from flooding. The dam was raised to 17 m in 1752 and to 40 m in order to keep up with reservoir siltation, which meant that it was now also a sediment retention dam.

- 1632** The Charles River near Boston, Massachusetts was first dammed. Over the next 250 years, two dozen dams were built out of wood and/or stone on the 127-km river to provide water power.
- 1640** The first true arch dam (no gravity component) since Roman times was built in Europe by Joanes del Temple at Elche in south eastern Spain. The dam was 23 m high, 75 m long, 9 m and 13.5 m wide at the crest and base respectively (ratio = 0.58), with a curvature radius of 62 m.
- 1675** The St. Ferréol navigation embankment was built 50 km south east of Toulouse in France to supply the Languedoc Canal with water, making it the first such dam. It is 36 m high, 780 m long and impounds a reservoir of 6.7 million m³. It was the world's highest embankment dam at the time.
- 1685** The system of recreational lakes in the gardens of the Palace of Versailles, near Paris in France was completed. In total, about 20 reservoirs impound nearly 8 million m³ of water, making it the largest dam network ever built for purely recreational purposes (see 60 AD).
- 1695** The Joux Verte arch dam 30 km south east of Lausanne in Switzerland was the first fluming dam built out of masonry. Its bottom outlet was 3.5 m wide x 1.7 m high = 5.95 m² and could be opened instantly, thus providing the necessary discharge to flush (flume) logs downstream.
- 1723** The 6.5-m high and 209-m long Yekaterinburg crib dam was the first mining dam built in western Siberia. It powered 50 water wheels.
- 1735** Five small multiple-arch buttress dams were built by Pedro Villareal de Berriz near Bilbao in north western Spain. These were the first multiple-arch structures built since the Roman Esparragalejo Dam (see *ca.* C. 3rd). They also utilised the upstream-sloping upstream face to help stabilise the structures (see 1530 and 1795).
- C. 18th** Ornamental lakes became popular with the land-owning classes in Great Britain. Lancelot 'Capability' Brown may have built over 40 such lakes, all of them impounded by earth embankments up to 7 m high, with puddled clay²⁸ linings on their upstream faces.
- 1741** The hydraulic engineer John Grundy claimed to be the first engineer in Great Britain to use puddled clay to build the impervious core of embankment dams. This technique was used in all future major embankment dams in Britain (see also 1558).
- c. 1750-1760** The four buttress dams built near Aguascalientes in central Mexico represented the first appearance of the Roman-developed buttress dam in the Americas (see *ca.* C. 1st A.D). The construction of the 24-m high San Blas Dam in about 1750 was a world record for the type.
- 1765** The 11-m high and 150-m long San Antonio Dam, built 150 km northwest of Mexico City, was the world's first triangular gravity dam, built 100 years before this structure was rationally designed in France (see 1853).

²⁸ Puddled clay was made by mixing clay with water and then compacting it (Schnitter, 1994).

- 1776** The French engineer Charles Coulomb published his paper describing the importance of cohesive forces and internal friction on the stability of cohesive soils.
- c. 1780** The 100,000-m³ Zmeinogorsk Embankment in the Altay Mountains, was the largest Russian water-power supply dam built for mining.
- 1787** Construction started on the 87 m-high Gasco navigation dam on the Guadarrama River near Madrid, which would have supplied a trans-Iberian canal linking the Atlantic Ocean to the Mediterranean Sea. Construction stopped at 56 m and the dam was never used.
- 1795** The wheelwright Oliver Evans published ‘The Young Mill-Wright and Miller’s Guide’ in America, which describes the use of stone-filled crib and log dams to help generate water power. The timber dams described had upstream-sloping faces to help stabilise them (see 1735). The book also states that masonry dams should have curved upstream faces.
- 1797** The 11-m high Blackbrook Embankment was one of the first navigation dams built in Great Britain.
- 1804** The 12-m high Mir Alam (Meer Allum) multiple-arch dam was built by Henry Russle (Royal Engineers) to supply Hyderabad in central India with water. The dam contained 21 semi-circular arches with spans up to 51 m. This was unprecedented at the time and was not surpassed for a further 120 years.
- 1820-1930** About 260 embankment dams over 15 m high were built in Britain and a further 80 in India, Pakistan and Bangladesh, based entirely on empirically-gained experience. There was much standardization of the embankment dam-building technique by the British during this period, which may explain why only four failures occurred.
- 1824** The 21-m high Glencourse Embankment to the south of Edinburgh, designed by Thomas Telford, was the first major water supply dam built in Britain.
- 1826** The first textbook on sediment control in mountain rivers was published by the South Tirolean Josef Duile. One of the methods described is the use of check dams (see 1612).
- 1831** Lieutenant-colonel John By of the British Royal Engineers built the 19-m high Jones Falls arch dam in Ontario, Canada. The dam had an almost constant width of 44% of its height and, for an arch dam, an unprecedented crest length-height ratio of 5.6.
- 1840** The Entwistle Embankment near Manchester in England was raised to 38 m, making it the world’s highest embankment dam until 1882.
- 1840** The Frenchman Alexandre Collin developed Coulomb’s work to identify the circular shape of slides in clayey soils and also the importance of water content on cohesive soil strength (see 1776).
- ca. 1850-1930** Of about 380 U.S. embankment dams built over 15 m high, about 9% failed. While this record is poor, it benefited dam construction in the long run since the failures were well reported in the American technical literature and therefore lessons were learned.

- 1852** The 21.9-m high South Fork Embankment in Pennsylvania, USA, was the first to use loose rockfill. This construction technique went on to be used around the world.
- 1853** Following a series of developments in the stress analysis of structures, Augustin Torterne de Sazilly (French Corps of Bridge and Highway Engineers) published his paper showing that a triangular cross-section with a vertical upstream face is the most stable configuration for gravity dams. (See 1866).
- 1853** Commodore Matthew C. Perry forced Japan to open its boundaries to westerners, following which Japan adopted western technology, including that for dam building, with great success.
- 1854** The 43-m high Zola Dam in France was the first arch dam to be designed using methods of stress analysis. The cylinder formula was used, which analyses the ability of individual arches in a stack of arches to resist the weight of water at a given depth (see 1889).
- 1856** The 16-m high Parramatta thin arch dam was built in Australia with a crest length-height ratio of 4.3 and a base width-height ratio of 0.29.
- 1866** The 60 m-high Gouffre d'Enfer gravity dam, built near St. Etienne in France for flood control, was the first structure designed and built using the stable triangular cross-section (see 1853).
- 1869** Hydraulic fill was used for the first time to line the downstream face of the 32-m high Temescal Dam in California, USA. The dam was designed by Anthony Chabot to supply Oakland with water.
- 1872** Concrete was used in dam construction for the first time since the Romans, in the 24-m high Boyds Corner (New York, USA) and the 21-m high Pérolles (Switzerland) gravity dams.
- 1881** The first concrete arch dam in Great Britain was built at Abbeystead in England to supply Lancaster with water. It is 20 m high.
- 1882** The 42 m-high Upper Barden Embankment built near Manchester in England and designed by Alexander Binnie, set a new record for the type and remained Britain's highest until World War II.
- 1884** The Big Bear Valley arch dam was built in California with a record crest slenderness of 105²⁹.
- 1886** The 49 m-high Lower Otay Dam built in California was the first pure rockfill dam (see 1852). Built with a central steel core to make it impermeable, it was the world's largest embankment dam.
- 1889** The crown cantilever analysis of arch dams was developed by Hubert Vischer and Luther Wagoner. This considers the interactions between the different sections of the arched dam in distributing the load imposed by the water, in contrast to the cylinder method (see 1854).
- 1892** The French engineer René Féret published data showing the importance of the water-cement ratio on concrete strength.

²⁹ Crest slenderness is the ratio of radius of curvature to thickness.

- 1903** The world's first reinforced concrete, flat-slab buttress dam was built at Theresa in New York, USA to a height of 3 m.
- 1908** The first reinforced concrete, multiple arch dam was built at Hume Lake in California, USA, to create a fluming reservoir (see 1695). The dam is 21 m high and used just 1,700 m³ of concrete, about 10% of that required for the equivalent gravity dam.
- 1910** The Pathfinder and Buffalo Bill (Shoshone) arch dams were the first to be designed using the crown cantilever method. They were 65 m and 99 m high respectively, which were records at the time (see 1889).
- 1914** The 51-m high Salmon Creek Dam in south eastern Alaska, designed by Lars Jorgensen, was the world's first variable-radius arch dam. This design is more economical than other arches and is particularly well suited to high and large hydropower dams. The design of arch dams was refined in the U.S. through empirical observation and physical modelling up to shortly after World War II. Their construction in the U.S. after the war declined temporarily until the 1960s but increased in Europe, particularly in Italy, France and Switzerland (see 1957).
- 1915** The U.S. Bureau of Reclamation's Arrowrock concrete gravity dam was built near Boise in Idaho to a record height for the type of 105 m. It used elaborate drainage and impermeabilization techniques, which perhaps marked the development of a complete understanding of the need to negate uplift forces in order to ensure gravity dam stability.
- 1922** World's first documented dam removal occurs in the United States (Pohl, 2002).
- 1925** A series of research developments culminated with the publication of Terzaghi's 'Principles of Soil Mechanics'. This, together with the establishment of the relationship between soil water content and compaction by Ralph Proctor in 1933 and the mechanization of embankment dam-building techniques, formed the basis for the worldwide explosion of the construction of increasingly large embankment dams after World War II (see 1976, 1980).
- 1928** The 35-m high Carranza contiguous buttress dam, built in Mexico for irrigation, was one of the first such dams. The design involves a thickening of the buttress head in the upstream direction so that the heads join together, thus eliminating the need for slabs or arches between them and making the dam more economical to build.
- 1928** The International Commission on Large Dams (ICOLD) was created in Paris. Its international meetings and numerous publications greatly facilitates the spread and standardisation of dam-building technology.
- 1936** The 221 m-high and 379-m long Boulder or Hoover concrete gravity dam was built on the Colorado River, USA. It was 60% higher than any existing dam, had a volume of 2.486 million m³ (2.5 times larger than any existing dam) and impounded a world record 38.55 billion m³ of water.

- 1942** The 168-m high, 1,272-m long Grand Coulee concrete gravity multipurpose dam was built on the Columbia River in Washington, USA. It had a world record volume of 7.45 million m³.
- 1948** The 83 m-high Escaba flat-slab buttress dam built in Argentina was the tallest such dam built.
- 1957** The 250 m-high Mauvoisin variable-radius arch dam is the most noteworthy example of this type built in Switzerland.
- 1961** The Grand Dixence concrete gravity dam was built in Switzerland to a record height for the type of 285 m. Its volume is 5.957 million m³.
- 1968** The 214 m-high D. Johnson multiple-arch dam was built on the Manicouagan River, Canada and impounds 141.9 billion m³ of water.
- 1976** The main Tarbela Embankment was built in Pakistan, for irrigation and power generation, with a record volume of 105.6 million m³.
- 1976** The Grand Teton Dam on the Teton River, Idaho, U.S.A. fails, effectively ending the construction of large dams by the U.S. Bureau of Reclamation (Thorne, Written Communication, 2007).
- 1980** The Inguri variable-radius arch dam was built near Tbilisi in Georgia. It is 272 m high, 680 m long and has a volume of 3.96 million m³ of concrete, all of which were records for a variable-radius arch dam.
- 1980** The 58 million-m³ Nurek Embankment was built in Tajikistan for irrigation and power generation to a type record height of 300 m.
- 1983** The Itaipu Dam was built on the Brazil-Paraguay border to a record height of 196 m for a contiguous buttress dam. It also set a record for hydro-electric power generation, with a capacity of 12,600 MW.
- 1983** The 245-m high, 1,066-m long Sayano concrete gravity dam was built near Novosibirsk in Russia with a record volume of 9.075 million m³.
- 1984** The Lhano (Tucuruí) gravity dam in Brazil was built with a world record spillway capacity of 110,000 m³/s.
- 2000** The World Commission on Dams published its landmark report on 'Dams and Development'. Written by stakeholders both for and against the construction of large dams, it highlights the benefits and adverse consequences of large dam construction.
- 2006** China completes construction of the main wall of the Three Gorges Dam, a 185-m high, 2,309-m long concrete gravity structure on the Yangtze River. With a generating capacity of 18,200 MW it is the world's largest hydroelectric plant (<http://news.bbc.co.uk/2/hi/asia-pacific/5000092.stm>).

Appendix B Arc Macro Language (AML) Script for the Cut-fill Analysis

B.1. Overview of the AML

The following is an example of the AML used to perform the cut-fill analysis in ARC/INFO Workstation. In each filename, 'r4' refers to Run 4, while the five digits that follow denote the run time in minutes: 00030 thus represents the delta surface after 30 minutes of run time. Lines preceded by '/' are not executed by ARC-Info and are used to provide a description of the code that follows. The following is a detailed explanation of the commands used in the AML and of their importance to the results of the cut-fill analysis. The information presented below has been compiled and edited from the ARC/INFO help files (version 5.1.2600.2180).

The AML is designed to run from the GRID prompt. GRID is a raster-based (cell-based) geoprocessing toolbox that is integrated with ARC/INFO. GRID accurately portray continuous surfaces by dividing space into discrete units called cells and provides a range of tools for both simple and complex grid-cell analyses. GRID is one of four data structures available in ARC/INFO, the other three being vector, network and TIN. Each of these data structures provides a means of accurately storing certain types of geographical information that the others cannot do so accurately. For instance, a boundary of some kind is a precise linear feature that can only be represented using a vector data structure – a series of GRID cells would only be able to approximate the boundary.

Prior to running the AML, the *x, y, z* coordinate files for every delta surface of every run were converted from the dBASE IV (*.dbf) format into ArcGIS shapefiles (*.shp) using a Python script (Appendix C). The shapefile is the basic input file for such coordinate data.

B.2 AML for cut-fill analysis

/* Create point coverages

arc SHAPEARC r400000.shp r400000 point
arc BUILD r400000 point

arc SHAPEARC r400030.shp r400030 point
arc BUILD r400030 point

/* Create tins

arc CREATETIN r400000tin
COVER r400000 point Z 1
end

arc CREATETIN r400030tin
COVER r400030 point Z 1
end

/* Create lattices

arc TINLATTICE r400000tin r400000lat linear
~
~
~
0.1

arc TINLATTICE r400030tin r400030lat linear
~
~
~
0.1

/* create polygons

arc LATTICEPOLY r400000lat r400000tmp1 NODATA
arc CLEAN r400000tmp1 r400000tmp1 # 0.001 poly
arc RESELECT r400000tmp1 r400000tmp2 poly
res data-code = 1
~
n
n
arc kill r400000tmp1 all

arc LATTICEPOLY r400030lat r400030tmp1 NODATA
arc CLEAN r400030tmp1 r400030tmp1 # 0.001 poly
arc RESELECT r400030tmp1 r400030tmp2 poly
res data-code = 1
~
n
n
arc KILL r400030tmp1 all

/* Intersect

arc INTERSECT r400000tmp2 r400030tmp2 r4000030x POLY 0.001

arc CLEAN r4000030x r4000030x # 0.001 poly
arc BUILD r4000030x poly

arc KILL r400000tmp2 all
arc KILL r400030tmp2 all

arc SHAPEARC 525.shp 525 poly

arc CLEAN 525 525 # 0.001 poly
arc BUILD 525 poly

arc INTERSECT r4000030x 525 r4000030C POLY 0.001

arc CLEAN r4000030C r4000030C # 0.001 poly
arc BUILD r4000030C poly

arc KILL r4000030x all
arc KILL 525 all

/* Gridclip, lattice resample, cut and fill

GRIDCLIP r400000lat r400000tmp COVER r4000030C
arc LATTICERESAMPLE r400000tmp r400000clat

~

~

~

0.1

GRIDCLIP r400030lat r400030tmp COVER r4000030C
arc LATTICERESAMPLE r400030tmp r400030clat

~

~

~

0.1

arc CUTFILL r400000clat r400030clat r4000030v r4000030W

arc KILL r400000lat all
arc KILL r400000tmp all
arc KILL r400000clat all
arc KILL r400030lat all
arc KILL r400030tmp all
arc KILL r400030clat all

B.3. Discussion of the AML commands

In the following sections, the AML is broken down into subsections and presented, along with the syntax for each command, in order to explain the role of each section of code. In the presentation of the syntax for the commands, arguments enclosed by <> are necessary, while those enclosed by { } are optional.

B.3.1. Create coverages

```
arc SHAPEARC r400000.shp r400000 point  
arc BUILD r400000 point
```

A coverage simply represents a set of geographical features within a given area. In this case, the coverages are the delta surface topography at each time step. A coverage supports the georelational model, *i.e.* it contains both the spatial (location – in this case the *x* and *y* coordinates) and attribute (descriptive – in this case the elevation) data for geographic features. ARC/INFO supports point, line and polygon coverages.

Syntax

```
SHAPEARC <in_shape_file> <out_cover> {out_subclass} {DEFAULT|DEFINE}  
BUILD <cover> {POLY | LINE | POINT | NODE | ANNO.<subclass>}
```

The SHAPEARC command converts the input shapefile into an ARC/INFO point coverage, as specified by the last command on the first line, while the BUILD command creates the feature attribute table, in this case a Point Attribute Table (PAT), for the coverage. (See also the discussion of the CLEAN command in section B.3.4.).

B.3.2. Create tins

```
arc CREATETIN r400000tin  
COVER r400000 point Z 1  
end
```

TIN is ARC/INFO's surface modelling package and is used to create, store, analyze and display surface information. Surfaces are composed of a potentially infinite number of points that could be measured but, since it is impossible to measure all of them, some method for sampling the surface is required that selects the most important points to enable a surface model that approximates the real surface to be built. The three methods most commonly used to approximate a real surface are

contours, regularly spaced (in both the x and y directions) sample points (DEMs), and irregularly spaced sample points. The latter is used to create a Triangulated Irregular Network (TIN). Because of the sampling resolution of the delta surface together with the use of additional cross-sections to tie down topographical details (section 5.5.1), the individual data points are located more or less optimally in terms of their ability to provide an accurate representation of the real surface. This makes it possible for a TIN to accurately represent a surface with fewer points, *i.e.* more efficiently, than the other two data models and so it is the most appropriate one to use here. It should be noted, however, that the TIN data model will provide poor results if important areas of the surface are under-sampled.

Syntax

```
CREATETIN <out_tin> {weed_tolerance} {proximal_tolerance} {z_factor} {bnd_cover | xmin ymin
xmax ymax} {device}
COVER <in_cover> {POINT | LINE | POLY} {spot_item | spot_value} {sftype_item | sftype}
{density_interval} {logical_expression | select_file} {weed_tolerance}
```

The CREATETIN command is used to create a TIN with the name indicated using the point coverage specified by the COVER subcommand. ‘Z’ is the name of the numeric item in the point coverage’s feature attribute table that contains the elevation data (the spot_item), while ‘1’ denotes the fact that all the features – the sftype - contributing to the TIN are mass points, *i.e.* points derived from any combination of point, line or polygon coverages (but in this case only a point coverage).

B.3.3. Create lattices

```
arc TINLATTICE r400000tin r400000lat linear
~
~
~
0.1
```

A lattice is just one way of representing a surface, which can also be represented using a TIN or a grid, but it is the most accurate for performing surface calculations, hence the need to convert the TIN to a lattice (Milne and Sear, 1997). A lattice represents a surface using a series of points (called mesh points) that are spaced equidistant apart in the x and y directions. Each mesh point contains the z value of that location. z values for locations between mesh points are estimated by interpolating from the values of neighbouring mesh points. The lattice will represent

the tin in a rectangular area called the minimum bounding rectangle, so some mesh points will fall outside the area occupied by the model basin and these are given the NODATA value (equal to -9999). (Note: a lattice and a grid are similar but different. Both use the same data model, but while a lattice represents a surface value as a single mesh point at the centre of a cell, a grid represents the same value as a square area such that all locations within the cell have the same value. A lattice is thus the point representation of a grid).

Syntax

```
TINLATTICE <in_tin> <out_lattice> {LINEAR | QUINTIC} {z_factor} {FLOAT | INT}  
-  
-  
-  
-
```

The TINLATTICE command is used to convert the named input TIN to the named output lattice using linear interpolation. TINLATTICE is one of four methods of surface resampling available in the TIN software package. Resampling is the process whereby the *z* value of the surface is calculated at regularly spaced intervals. In this case, the surface was changed from the irregularly-spaced vertices of the triangular faces of the TIN to the regularly-spaced mesh points of a lattice using the LINEAR interpolation algorithm to generate the elevation values for the new mesh points. The LINEAR (as opposed to the QUINTIC) interpolator is the default option and is the most appropriate for this data set because the delta surface at each time step was systematically sampled to include all the significant topographical features (defined as local maxima and minima, inflection points and breaklines). The high density of points in the cross-sectional direction (spaced at 0.5 cm intervals) ensured that the topographical changes from channel bed to bank face to bank top were recorded in great detail, while the regular (5 cm) longitudinal spacing, with additional cross-sections where necessary, ensured that all changes in bank line direction (breaklines were not specifically measured), bed features, failure blocks, and the shape of the delta front were accurately recorded.

Some loss of information occurs when converting a TIN to a lattice, but several steps were taken to ensure that this was minimized. First, wherever lattice mesh points coincide with TIN vertices, they preserve the precise elevation values of the vertices by using the FLOAT option. (This is the default setting for this option and is not shown in the code). Second, the higher the resolution of the output lattice,

generally, the more closely it will represent the input TIN. Thus, while the x (cross-sectional) and y (longitudinal) resolution of the input TIN is 0.5 cm and 5 cm respectively, the x and y resolution of the output lattice was 0.1 cm, as specified by the last line of the TINLATTICE section of code. (The first and second tildes indicate that the bottom left (origin) and top right corners respectively of the output lattice have the same coordinates as those of the input TIN, while the third tilde indicates that the resolution of the output lattice will be set explicitly by the user). The $\{z_factor\}$ is used to change the z -units of the out-lattice to some other units of measure. The default value is zero.

B.3.4. Create polygons

In order for the cut-fill calculation to be performed, the two lattices involved must be coincident; that is, they must have a common origin, they must have the same number of points in the x and y directions, and the distance between the points in both directions must be the same. If these conditions are not met, CUTFILL stops execution. Making the lattices coincident is a multi-step process. First, each lattice is converted to a polygon coverage.

```
arc LATTICEPOLY r400000lat r400000tmp1 NODATA
arc CLEAN r400000tmp1 r400000tmp1 # 0.001 poly
arc RESELECT r400000tmp1 r400000tmp2 poly
res data-code = 1
~
n
n
arc KILL r400000tmp1 all
```

Syntax

```
LATTICEPOLY <in_lattice> <out_cover> <SLOPE | ASPECT | RANGE | NODATA | BOX |
EXTENT> {lookup_table} {z_factor}
```

The LATTICEPOLY command converts the input lattice into the output polygon coverage indicated. The NODATA option classifies the input lattice mesh points into two classes of polygons: those with valid z values, *i.e.* with a real elevation, and those with the NODATA value. Mesh points with valid data are assigned a DATA-CODE of 1, while NODATA mesh points are assigned a DATA-CODE of 0. Polygon areas are calculated on the basis that mesh points lay in the centre of their polygon, so polygons representing mesh points on the edges of the

lattice extend beyond the edge of the minimum bounding rectangle by one half of the mesh-point spacing.

Syntax

```
CLEAN <in_cover> {out_cover} {dangle_length} {fuzzy_tolerance} {POLY | LINE}
```

A polygon is made up of arcs which define the boundary and a label point which links the polygon feature to an attribute record in the Polygon Attribute Table (PAT). Each arc is composed of a line with nodes at each end. ARC/INFO stores polygons topologically as a list of arcs and a label that make up each polygon. This is important to remember when creating and editing polygons because the list must be rebuilt whenever the arcs that define a polygon change. When a new polygon coverage is created, the CLEAN command is used to build polygon topology for the first time. It generates a coverage with correct polygon topology by editing and correcting geometric coordinate errors, assembling arcs into polygons and creating the PAT. Sometimes, one or more of the arcs forming the polygon's boundary extend further than they should and part of their length and their end node is left 'dangling' away from the body of the polygon. The {dangle_length} argument specifies the minimum acceptable length. In this case, '#' denotes the default value of zero (units of measurement). Arc nodes do not always snap together when the polygon is being created and the {fuzzy_tolerance} argument denotes the distance within which nodes, if they are not connected, will be snapped together. In this case the value is set to 0.001 cm. Use of fuzzy tolerance moves slightly the polygon's vertices, thus altering the coordinates of that point, although in this case by only a very small amount. The {POLY} argument simply specifies that a polygon (as opposed to a LINE) topology is being built.

The CLEAN command is very similar to the BUILD command, since it also defines coverage topology. But whereas CLEAN uses a fuzzy tolerance when processing coverages BUILD does not, which means that CLEAN can detect and create intersections but that BUILD cannot. However, since BUILD does not use a fuzzy tolerance, the coordinates will not be adjusted while topology is being built. Also, only CLEAN can be used to build topology for the first time.

Syntax

```
RESELECT <in_cover> <out_cover> {in_feature_class} {selection_file} {out_feature_class}  
Subcommand
```

-

-
-

RESELECT extracts selected features from an input coverage and stores them in the output coverage, which is then rebuilt. At the start of RESELECT, all features are in the selected set but, since no {selection_file} is specified, it must be specified which features of the input coverage are to be retained. Thus, since LATTICEPOLY created polygons for both the areas that have real elevation data and for those classified as NODATA (outside the model's physical boundary), 'res data-code = 1' selects only the former (where 'res' is the subcommand for RESELECT). The first tilde simply denotes the necessary carriage return following the entry of the subcommand, while the two subsequent n's indicate 'no', to the two questions of do you want to re-enter the subcommand or enter a new subcommand? RESELECT will now proceed. The KILL command simply deletes all components of the file indicated, that is no longer required, in order to free up disc space.

B.3.5. Intersect

```
arc INTERSECT r400000tmp2 r400030tmp2 r4000030x POLY 0.001
arc CLEAN r4000030x r4000030x # 0.001 poly
arc BUILD r4000030x poly
```

```
arc KILL r400000tmp2 all
arc KILL r400030tmp2 all
```

```
arc SHAPEARC 525.shp 525 poly
arc CLEAN 525 525 # 0.001 poly
arc BUILD 525 poly
```

```
arc INTERSECT r4000030x 525 r4000030C POLY 0.001
arc CLEAN r4000030C r4000030C # 0.001 poly
arc BUILD r4000030C poly
```

```
arc KILL r4000030x all
arc KILL 525 all
```

The second step in making the two lattices coincident is to intersect the two polygons to produce a new polygon coverage that contains only the model and sediment surface area occupied jointly by the two input polygons. Thirdly, this polygon coverage is intersected with a polygon coverage that represents only the delta surface topset area and the areas occupied by and immediately around the foreset and

bottomset surfaces. This polygon was created manually before executing the code by digitizing the required area from the tins of the time intervals involved.

The second intersection is necessary because it eliminates as much of the model basin from the cut-fill calculation as possible (while still leaving sufficient basin area to account for the maximum possible delta surface elevations and downstream extent of sediment progradation for all cut-fill calculations). This minimizes the proportions of the reported sediment cut and fill volumes that are actually due to small discrepancies between the shape of the model basin at the two time intervals. These discrepancies arise because the number and location of additional cross-sections varies between time intervals, thus causing the shape of the basin as represented by the point data, and thus the TIN, to vary slightly. The result of the second intersection is thus a polygon coverage that covers the full extent of both delta surfaces with as little as possible of the surrounding model basin area.

Syntax

```
INTERSECT <in_cover> <intersect_cover> <out_cover> {POLY | LINE | POINT} {fuzzy_tolerance}  
{JOIN | NOJOIN}
```

The INTERSECT command is used to calculate the geometric intersection of the input and intersect coverages, with only those features in the area common to both coverages being preserved in the output coverage. The {POLY} argument is the default and specifies that two polygons are being intersected, while the {fuzzy_tolerance} argument specifies the minimum distance between coordinates in the output coverage and is set to 0.001 cm (it cannot be set to zero). Finally, the {JOIN | NOJOIN} argument specifies whether all items in both the <in_cover> and <intersect_cover> PATs will be combined into the output PAT. JOIN indicates that they will be and is the default option used unless NOJOIN is specified. The purpose of the CLEAN, BUILD and KILL commands is as described elsewhere.

B.3.6. Gridclip, lattice resample and cut & fill

```
GRIDCLIP r400000lat r400000tmp COVER r4000030C  
arc LATTICERESAMPLE r400000tmp r400000clat  
~  
~  
~  
0.1  
GRIDCLIP r400030lat r400030tmp COVER r4000030C
```

```

arc LATTICERESAMPLE r400030tmp r400030clat
~
~
~
0.1
arc CUTFILL r400000clat r400030clat r4000030v r4000030W

```

The next step in making the two lattices coincident is to clip both of them using the final polygon coverage obtained in section (A.3.5.) so that they occupy exactly the same area. Each clipped lattice is then resampled to make them coincident and, finally, the cut-fill calculation is carried out.

Syntax

```
GRIDCLIP <in_grid> <out_grid> {* | COVER <clip_cover> | BOX <xmin ymin xmax ymax>}
```

GRIDCLIP clips the input grid using the <clip_cover> polygon specified by the COVER command, which in this case is the final polygon created in section B.3.5. All lattice mesh points that fall outside the area of the <clip_cover> polygon are assigned the NODATA value, while the lattice is clipped to the exact size of the <clip_cover> polygon boundary.

Syntax

```

LATTICERESAMPLE <in_lattice> <out_lattice> {z_factor}
-
-
-
-

```

Following the GRIDCLIP operation, the two lattices to be used in the CUTFILL calculation now occupy exactly the same area, but they may not be coincident, *i.e.* their origins and mesh points may not be aligned and the mesh point spacing may not be the same in the x and y directions. This is corrected using the LATTICERESAMPLE command, which is another of the four methods of surface resampling available in the TIN software package (see also discussion of TINLATTICE in section B.3.3.). The first tilde indicates that the x_{min} , y_{min} of each clipped lattice is to be used as the origin, while the second tilde indicates that the x_{max} , y_{max} each clipped lattice is to be used as the top right-hand corner, thus making these two corners coincident in both lattices. The third tilde indicates that the mesh point spacing will be set explicitly by the user in the fifth line – 0.1 cm in this case. The {z_factor} is used to change the z-units of the out-lattice to some other units

of measure. The default value is zero. LATTICERESAMPLE uses bilinear interpolation, which computes the output mesh point value from the values of the four nearest input mesh points, based on the weighted distance to these points.

Syntax

CUTFILL <before_lattice> <after_lattice> <out_lattice> <out_cover> {z_factor}

The output lattice is created by subtracting the <after_lattice> from the <before_lattice>. The mesh point z values in <out_lattice> represent the net change in the surface z values following the cut-and-fill operation, with negative z values indicating regions of the <before_lattice> that have been filled and positive values indicating cuts. Areas and volumes are calculated on the basis that the mesh points lay in the centre of each calculation area, so output polygons representing mesh points lying on the edges of the input lattices extend one half of the mesh point spacing beyond the lattice extents. The formula for calculating the volumetric change at each lattice point is,

$$\text{Volume} = \text{polygon area} \times \Delta Z, \quad \text{where } \Delta Z = Z_{\text{before}} - Z_{\text{after}} \quad (\text{B.1})$$

The <out_cover> has an associated INFO data file named <out_cover>.CF. The file has one record of summary statistics about the cut-and-fill areas and volumes. A positive BALANCE_VOL value in the <out_cover>.CF file indicates that sediment has been deposited, while a negative value indicates that erosion has occurred. The <out_cover>.CF were exported into *.dbf format for processing and analysis in Excel using the relevant tools in ArcCatalogue.

Appendix C Thalweg Extraction Macros

The following macros were written to extract the thalweg x , y , z , coordinates from a *.dbf Excel file, in which the x , y , z , coordinates are located in the first three columns of the worksheet with the headings X, Y and Z in the first row. The macros require a destination worksheet entitled "EB2_Thalweg.xls" (which can be changed as needed), with the cell A3 selected in that sheet. Text in green and preceded by an apostrophe provides a description of the following section of code and is not executed when the macro is run.

Option Explicit

'USThalX is a variable containing the X coordinate of the Thalweg immediately upstream

'from the profile currently being evaluated.

Dim USThalX As Double, rgS As Range

Dim PrevVal As Double

Dim MinZStart As Range, MinZFinal As Range

Dim LeftCell As Range, RightCell As Range

Dim Lower As Double, Upper As Double

Dim fName As String

Sub Batch_Thalweg()

'The 4 procedures here together extract the Thalweg points from each X,Y,Z coordinate file.

'Create a list of all the files in the folder and all subfolders.

Dim fs As FileSearch

Dim I As Integer

Set fs = Application.FileSearch

With fs

```

        .LookIn =
"C:\ElwhaRiverProject\Physical_modelling\Data_analysis\Laser_Data\Long_Profiles\
Empty Basin"
        .SearchSubFolders = True
        .Filename = "*.dbf"
        .Execute
    End With

    'Pass each file in the list in turn to the Select_Profile procedure.
    For I = 1 To fs.FoundFiles.Count
        Call Select_Profile(fs.FoundFiles(I))
    Next I
End Sub

```

```

Sub Select_Profile(Filename As String)

```

```

    'Open the file passed to the procedure by the Batch-Thalweg procedure
    Application.ScreenUpdating = False
    Workbooks.Open Filename:=Filename
    fName = ActiveWorkbook.Name

```

```

    'Select Column B that contains the Y-coordinate data
    Set rgS = Worksheets(1).Range("B2:B65536")
    rgS.Select

```

```

    'Check to see whether cell B2 contains the value 0. If so, the FindMinZzero
procedure

```

```

    'is called.
    If ActiveCell.Value <> 500 Then
        If ActiveCell.Value = 0 Or ActiveCell.Value = 20 _
            Or ActiveCell.Value = 15 Then
            Call FindMinZzero

```

```

    'If FindMinZzero was called, control is now passed back to the Select_Profile
procedure

```

```

    'and the USThalX variable is given the value of the ActiveCell in the Thalweg
'spreadsheet.
    USThalX = ActiveCell.Value
    ActiveCell.Offset(1, 0).Select
    Windows(fName).Activate
    ActiveCell.Offset(0, -1).Select

```

```

    'The ActiveCell then scrolls down to the last Y=0 cell.
    Do Until ActiveCell.Offset(1, 0).Value > ActiveCell.Value
        ActiveCell.Offset(1, 0).Select
    Loop
    End If

```

```

    'The first non-zero Y coordinate / first Y coordinate of the next non-zero profile is

```

'selected and the FindMinZnonzero procedure called.

```
Do
  ActiveCell.Offset(1, 0).Select
  Call FindMinZnonzero(UStalX)
  ActiveCell.Offset(1, 0).Select
  Windows(fName).Activate
  ActiveCell.Offset(0, -1).Select
  Do While ActiveCell.Offset(1, 0).Value = ActiveCell.Value
    ActiveCell.Offset(1, 0).Select
  Loop
Loop While Not IsEmpty(ActiveCell.Offset(1, 0))
ActiveCell.Offset(1, 0).Select
End If
```

'If cell B2 doesn't contain a 0 it is one of the ...Z.dbf files and its first Y value
'will be 500, which can be ignored, since this Thalweg point will already have been
'extracted.

```
If ActiveCell.Value = 500 Then
  Do While ActiveCell.Offset(1, 0).Value = ActiveCell.Value
    ActiveCell.Offset(1, 0).Select
  Loop
```

'All post-500 cm Thalweg points are then extracted from fName.

```
Do
  ActiveCell.Offset(1, 0).Select
  Call FindMinZnonzero(UStalX)
  UStalX = ActiveCell.Value
  ActiveCell.Offset(1, 0).Select
  Windows(fName).Activate
  ActiveCell.Offset(0, -1).Select
  Do While ActiveCell.Offset(1, 0).Value = ActiveCell.Value
    ActiveCell.Offset(1, 0).Select
  Loop
Loop While Not IsEmpty(ActiveCell.Offset(1, 0))
End If
```

'Once all the X,Y,Z coordinates in the file have been evaluated the filename and the
'column headings X, Y & Z are inserted at the top of the list of pasted coordinates

in

```
'the 'Thalweg' sheet.
Windows("EB2_Thalweg.xls").Activate
If ActiveCell.Offset(-1, 1).Value <> 500 Then
  ActiveCell.Offset(-1, 0).Select
  ActiveCell.End(xlUp).Select
  ActiveCell.Offset(-2, 0).Select
  ActiveCell.Value = fName
  ActiveCell.Offset(1, 0).Select
  ActiveCell.Value = "X"
  ActiveCell.Offset(0, 1).Select
  ActiveCell.Value = "Y"
```

```

ActiveCell.Offset(0, 1).Select
ActiveCell.Value = "Z"
ActiveCell.Offset(1, 2).Select
End If

```

```

Windows(fName).Activate
ActiveWorkbook.Close SaveChanges:=False

```

```
End Sub
```

```
Sub FindMinZzero()
```

```

Application.ScreenUpdating = False
Set MinZFinal = ActiveCell.Offset(0, 1) 'i.e. MinZFinal = cell C2

```

```

'Evaluate the X and Z coordinates for each Y coordinate
Do While ActiveCell.Value = ActiveCell.Offset(1, 0).Value
  Select Case ActiveCell.Offset(1, 1).Value
    Case Is < ActiveCell.Offset(0, 1).Value
      If ActiveCell.Offset(1, 1).Value <= MinZFinal.Value Then
        Set MinZFinal = ActiveCell.Offset(1, 1)
        ActiveCell.Offset(1, 0).Select
      Else: End If
      If ActiveCell.Offset(1, 1).Value > MinZFinal.Value Then
        ActiveCell.Offset(1, 0).Select
      Else: End If
    Case Is = ActiveCell.Offset(0, 1).Value
      If ActiveCell.Offset(1, 1).Value <= MinZFinal.Value Then
        Set MinZFinal = ActiveCell.Offset(1, 1)
        ActiveCell.Offset(1, 0).Select
      Else: End If
      If ActiveCell.Offset(1, 1).Value > MinZFinal.Value Then
        ActiveCell.Offset(1, 0).Select
      Else: End If
    Case Is > ActiveCell.Offset(0, 1).Value
      ActiveCell.Offset(1, 0).Select
  End Select
Loop

```

```

'Select the cell containing the smallest Z value that is within the acceptable range of
'X coordinate values
MinZFinal.Select

```

```

'Copy all contiguous cells in the row containing MinZFinal and paste them into the
'Thalweg' worksheet
Set LeftCell = Cells(ActiveCell.Row, 1)
Set RightCell = Cells(ActiveCell.Row, 256)

```

```

If IsEmpty(LeftCell) Then Set LeftCell = LeftCell.End _
(xlToRight)

```

```

If IsEmpty(RightCell) Then Set RightCell = RightCell.End _
(xlToLeft)
If LeftCell.Column = 256 And RightCell.Column = 1 Then _
ActiveCell.Select Else Range(LeftCell, RightCell).Copy

```

```

Windows("EB2_Thalweg.xls").Activate
ActiveSheet.Paste

```

```

End Sub 'Control passes back to the 'Select_Profile' procedure

```

```

Sub FindMinZnonzero(ByVal USThalXpassed)

```

```

Application.ScreenUpdating = False
Set MinZStart = ActiveCell.Offset(0, 1)
Set MinZFinal = ActiveCell.Offset(0, 1)

```

```

'Set the range of X coordinate values from which the Z coordinate can be chosen
Lower = USThalXpassed - 8.4
Upper = USThalXpassed + 8.4

```

```

'Evaluate the X and Z coordinates for each Y coordinate

```

```

Do While ActiveCell.Value = ActiveCell.Offset(1, 0).Value

```

```

Select Case ActiveCell.Offset(1, 1).Value

```

```

Case Is < ActiveCell.Offset(0, 1).Value

```

```

If ActiveCell.Offset(1, 1).Value <= MinZFinal.Value And _
ActiveCell.Offset(1, -1).Value >= Lower And _
ActiveCell.Offset(1, -1).Value <= Upper Then
Set MinZFinal = ActiveCell.Offset(1, 1)
ActiveCell.Offset(1, 0).Select

```

```

Else: End If

```

```

If ActiveCell.Offset(1, 1).Value <= MinZFinal.Value And _
ActiveCell.Offset(1, -1).Value < Lower Or _
ActiveCell.Offset(1, -1).Value > Upper Then
ActiveCell.Offset(1, 0).Select

```

```

End If

```

```

If ActiveCell.Offset(1, 1).Value > MinZFinal.Value And _
ActiveCell.Offset(1, -1).Value >= Lower And _
ActiveCell.Offset(1, -1).Value <= Upper Then
ActiveCell.Offset(1, 0).Select

```

```

Else: End If

```

```

If ActiveCell.Offset(1, 1).Value > MinZFinal.Value And _
ActiveCell.Offset(1, -1).Value < Lower Or _
ActiveCell.Offset(1, -1).Value > Upper Then
ActiveCell.Offset(1, 0).Select

```

```

End If

```

```

Case Is = ActiveCell.Offset(0, 1).Value

```

```

If ActiveCell.Offset(1, 1).Value < MinZFinal.Value And _
ActiveCell.Offset(1, -1).Value >= Lower And _
ActiveCell.Offset(1, -1).Value <= Upper Then

```

```

        Set MinZFinal = ActiveCell.Offset(1, 1)
        ActiveCell.Offset(1, 0).Select
    Else: End If
    If ActiveCell.Offset(1, 1).Value = MinZFinal.Value And _
        ActiveCell.Offset(1, -1).Value >= Lower And _
        ActiveCell.Offset(1, -1).Value <= Upper Then
        ActiveCell.Offset(1, 0).Select
    Else: End If
    If ActiveCell.Offset(1, 1).Value <= MinZFinal.Value And _
        ActiveCell.Offset(1, -1).Value < Lower Or _
        ActiveCell.Offset(1, -1).Value > Upper Then
        ActiveCell.Offset(1, 0).Select
    End If
    If ActiveCell.Offset(1, 1).Value > MinZFinal.Value Then
        ActiveCell.Offset(1, 0).Select
    Else: End If
    Case Is > ActiveCell.Offset(0, 1).Value
    If ActiveCell.Offset(1, 1).Value <= MinZFinal.Value And _
        ActiveCell.Offset(1, -1).Value >= Lower And _
        ActiveCell.Offset(1, -1).Value <= Upper Then
        Set MinZFinal = ActiveCell.Offset(1, 1)
        ActiveCell.Offset(1, 0).Select
    Else: End If
    If ActiveCell.Offset(1, 1).Value <= MinZFinal.Value And _
        ActiveCell.Offset(1, -1).Value < Lower Or _
        ActiveCell.Offset(1, -1).Value > Upper Then
        ActiveCell.Offset(1, 0).Select
    End If
    If ActiveCell.Offset(1, 1).Value > MinZFinal.Value And _
        ActiveCell.Offset(1, -1).Value >= Lower And _
        ActiveCell.Offset(1, -1).Value <= Upper Then
        ActiveCell.Offset(1, 0).Select
    Else: End If
    If ActiveCell.Offset(1, 1).Value > MinZFinal.Value And _
        ActiveCell.Offset(1, -1).Value < Lower Or _
        ActiveCell.Offset(1, -1).Value > Upper Then
        ActiveCell.Offset(1, 0).Select
    End If
End Select

```

'MsgBox "MinZFinal =" & MinZFinal

Loop

'If the Thalweg point is still the maximum possible value of Z for the profile, then
'the entire profile must be re-searched, but this time without the restriction of the
'plus or minus 8.4 cm criteria for the X coordinate. This will allow the full profile
'to be searched for the lowest possible value of Z.

If MinZFinal = MinZStart Then

'Scroll back up to the start of the current profile

Do Until ActiveCell.Offset(-1, 0).Value < ActiveCell.Value

```

ActiveCell.Offset(-1, 0).Select
Loop

'Re-evaluate the X and Z coordinates for each Y coordinate
Do While ActiveCell.Value = ActiveCell.Offset(1, 0).Value
  Select Case ActiveCell.Offset(1, 1).Value
    Case Is < ActiveCell.Offset(0, 1).Value
      If ActiveCell.Offset(1, 1).Value <= MinZFinal.Value Then
        Set MinZFinal = ActiveCell.Offset(1, 1)
      Else: End If
      ActiveCell.Offset(1, 0).Select
    Case Is = ActiveCell.Offset(0, 1).Value
      If ActiveCell.Offset(1, 1).Value < MinZFinal.Value Then
        Set MinZFinal = ActiveCell.Offset(1, 1)
      Else: End If
      ActiveCell.Offset(1, 0).Select
    Case Is > ActiveCell.Offset(0, 1).Value
      If ActiveCell.Offset(1, 1).Value <= MinZFinal.Value Then
        Set MinZFinal = ActiveCell.Offset(1, 1)
      Else: End If
      ActiveCell.Offset(1, 0).Select
  End Select
Loop

'If all values in the profile are the same, then don't select any profile and
'move on to the next one.
If MinZFinal = MinZStart Then
  Windows("EB2_Thalweg.xls").Activate
  ActiveCell.Offset(-1, 0).Select
  USThalX = ActiveCell.Value
  Windows(fName).Activate
  ActiveCell.Offset(0, 1).Select
  Windows("EB2_Thalweg.xls").Activate
  Exit Sub
End If
End If

'Select the cell containing the smallest Z value that is within the acceptable range
'of X coordinate values
MinZFinal.Select

'Copy all contiguous cells in the row containing MinZFinal and paste them into the
'Thalweg' worksheet.
Set LeftCell = Cells(ActiveCell.Row, 1)
Set RightCell = Cells(ActiveCell.Row, 256)

If IsEmpty(LeftCell) Then Set LeftCell = LeftCell.End _
(xlToRight)
If IsEmpty(RightCell) Then Set RightCell = RightCell.End _
(xlToLeft)

```

```
If LeftCell.Column = 256 And RightCell.Column = 1 Then _  
    ActiveCell.Select Else Range(LeftCell, RightCell).Copy  
  
Windows("EB2_Thalweg.xls").Activate  
ActiveSheet.Paste  
USThalX = ActiveCell.Value  
  
End Sub 'Control passes back to the 'Select_Profile' procedure
```